LEABHARLANN CHOLÁISTE NA TRÍONÓIDE, BAILE ÁTHA CLIATH | TRINITY COLLEGE LIBRARY DUBLIN
Ollscoil Átha Cliath | The University of Dublin

Terms and Conditions of Use of Digitised Theses from Trinity College Library Dublin

Copyright statement

All material supplied by Trinity College Library is protected by copyright (under the Copyright and Related Rights Act, 2000 as amended) and other relevant Intellectual Property Rights. By accessing and using a Digitised Thesis from Trinity College Library you acknowledge that all Intellectual Property Rights in any Works supplied are the sole and exclusive property of the copyright and/or other IPR holder. Specific copyright holders may not be explicitly identified. Use of materials from other sources within a thesis should not be construed as a claim over them.

A non-exclusive, non-transferable licence is hereby granted to those using or reproducing, in whole or in part, the material for valid purposes, providing the copyright owners are acknowledged using the normal conventions. Where specific permission to use material is required, this is identified and such permission must be sought from the copyright holder or agency cited.

Liability statement

By using a Digitised Thesis, I accept that Trinity College Dublin bears no legal responsibility for the accuracy, legality or comprehensiveness of materials contained within the thesis, and that Trinity College Dublin accepts no liability for indirect, consequential, or incidental, damages or losses arising from use of the thesis for whatever reason. Information located in a thesis may be subject to specific use constraints, details of which may not be explicitly described. It is the responsibility of potential and actual users to be aware of such constraints and to abide by them. By making use of material from a digitised thesis, you accept these copyright and disclaimer provisions. Where it is brought to the attention of Trinity College Library that there may be a breach of copyright or other restraint, it is the policy to withdraw or take down access to a thesis while the issue is being resolved.

Access Agreement

By using a Digitised Thesis from Trinity College Library you are bound by the following Terms & Conditions. Please read them carefully.

I have read and I understand the following statement: All material supplied via a Digitised Thesis from Trinity College Library is protected by copyright and other intellectual property rights, and duplication or sale of all or part of any of a thesis is not permitted, except that material may be duplicated by you for your research use or for educational purposes in electronic or print form providing the copyright owners are acknowledged using the normal conventions. You must obtain permission for any other use. Electronic or print copies may not be offered, whether for sale or otherwise to anyone. This copy has been supplied on the understanding that it is copyright material and that no quotation from the thesis may be published without proper acknowledgement.

MESOZOIC-TERTIARY TECTONICS OF SE IRELAND AND GENETIC LINK TO OFFSHORE EXTENSIONAL BASINS

Volume 1 of 3

By

Michael J. M. Cunningham

Submitted to the University of Dublin for the degree Doctor of Philosophy

November 2000

TRINITY COLLEGE
20 MAR 2001
LIBRARY DUBLIN
THESIS
6320.1

DECLARATION.

This thesis is entirely my own work, except where stated. It has not been submitted to this or any other university. All references are duly acknowledged. I agree that the Library of Trinity College, Dublin may lend it on request.

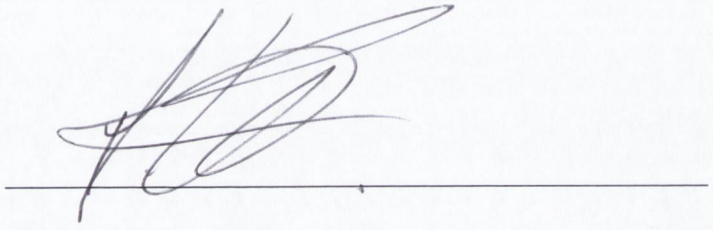

Summary of thesis

This work shows that Mesozoic-Tertiary tectonics in Central-East and SE Ireland is more significant than previously recognised. A review of the existing geological and geophysical literature and structural mapping around the coastline of Dublin Bay identified important brittle shear zones. The lack of polygonisation and strained quartz grains in thin-section implies that these structures are post-Hercynian.

The analysis of seismic, well logs, bathymetry and aeromagnetic data of the offshore Mesozoic Kish Bank basin showed that NNW-SSE compression and ENE-WSW extension was compatible with the geometry and kinematics of the youngest brittle structures that cut onshore outcrop at Sorrento Point (Co. Dublin). Regional correlation with both the Ulster and Lough Neagh-Larne basins showed that the most deformed structures (near Blackrock) were compatible with an Early Tertiary age whereas the younger structures are probably of Late Tertiary in age. The correlation was based on independent structural work on the Antrim basalts, and apatite fission track and vitrinite reflectance studies of the Irish Sea region, which indicates substantial post-Liassic erosion. Seismic evidence showed a previously unrecognised palaeo-channel flowing west from the Kish basin, possibly from the postulated Irish Sea dome. The channel comes onshore and corresponds with a topographic low.

Statistical analysis of digital terrain models and geology, using ARC/INFO GIS software, shows that the landscape of the Wicklow and Blackstairs Mountains is compatible with recent Tertiary tectonic stresses. Furthermore, the results of detailed studies of slope, relief and hydrology with lithological control shows that differential weathering has not played a significant role in shaping the present-day landscape of SE Ireland. The main control has been recent Neogene tectonics. This study led to the discovery of previously unknown Tertiary structures, which are compatible with regional studies. A LANDSAT lineament analysis supported the conclusions of the topographic studies.

The analysis of an apatite fission track (AFT) data-set down the spine of the Wicklow Mountains permitted quantification of denudation and tectonic uplift values, and the recognition of 4 previously unknown cooling (uplift?) events in the Wicklow-Blackstairs Mountains, with the Tullow Lowlands experiencing subsidence. The cooling events occur in the Triassic to Mid Jurassic, Early Cretaceous, Early Tertiary and Late Tertiary.

Utilising an extensive AFT database for all of Ireland it was shown that these events have regional significance, except in the Central Midland's plain. Modelled thermal histories of the apatite fission track samples facilitated quantification of sediment discharge and mass balancing with deposition in the Atlantic Seaboard basins.

Using high quality aeromagnetic, seismic lines and well logs for the Porcupine basin, it was shown that these onshore denudation events correlate with offshore unconformities and major periods of clastic influx into the basin. However, the total preserved volume of Tertiary sediment in the Porcupine basin is far greater than the total amount being eroded from Ireland, implying that the hinterland was of greater extent.

The transform model has been modified to account for the results of this work, which is based on structural observation, topographic and geomorphological studies of SE Ireland, high quality seismics in the Porcupine, seismics and high resolution aeromagnetics in the Kish basin, and an AFT database. Two stress systems are identified as mentioned earlier. The Early Tertiary (Palaeogene) is more regional than the Late Tertiary (Neogene) model which produced local block faulting.

Acknowledgements

I wish to thank my supervisor Professor Adrian Phillips for his immense dedication and commitment to my thesis (and of course being patient with me). I am also indebted to the tremendous assistance and friendship of Doctor Alex Densmore, who has been my second supervisor. I also wish to express my gratitude and appreciation to Professor Philip Allen for allowing me to use the TULIP apatite fission track data, and for his ideas and inspiration which helped motivate me towards the end. I also acknowledge the constructive discussions I had over the past 4 years with Professor George Sevastopulo. I also enjoyed the useful discussions and comments from Doctor Andrea Cozzi, Doctor Joe Galewsky, and Doctor Kerry Gallagher. I also wish to thank Doctor John Graham, Doctor Ian Sanders, Doctor Patrick Wise Jackson, Professor Geoff Clayton, Professor Chris Stillman, and Doctor Pete Coxon for their support.

My project was funded by Total Oil Marine and I am grateful to them and particularly Tony Rochester and Olivier Wattez for their help and assistance and giving me data for the Porcupine basin. I am also grateful to Dr. Peter Croker at the Department of Marine (Petroleum Affairs Division) for giving me access to well-logs, reports and for supplying me with seismic lines and bathymetric data for the Kish Bank basin. I also received considerable assistance from Peter Readman and Brian O'Reilly at the Dublin Institute for Advance Studies for which I am grateful. I also wish to thank Cathy Norman and Colm Murphy at World Geoscience (now Fugro Airborne Surveys) for giving me a high resolution aeromagnetic data-set for the Kish Bank basin. Deepak Inamder at the Geological Survey of Ireland assisted me with digital onshore aeromagnetic data and I am grateful to him for this. I received considerable help from Dr. Martin Critchley at ERA with statistical analyses of lineament data for which I am grateful. I also acknowledge the help of Doctor David Naylor who allowed me to use some of his hand-drawn well-logs for the Porcupine basin. Many thanks to Eric Lazzaretti for scanning in these logs and the drawings he did in Adobe Illustrator. My thesis would have been more difficult without the spirited help and assistance of Declan Burke, Neil Kearney, Frank

Hendron and Stephen, especially for looking after my books and gear during my time in London. I also thank Joann Layng for her professionalism and assistance.

Last but not least, I wish to thank all my post-graduate friends and colleagues past and present for such a great time over the past 4 years. In particular, I wish to thank Brian MacSharry for all his help and understanding, thanks it is appreciated. I also want to thank Stuart Bennett for our constructive discussions on Tertiary tectonics and other interesting matters. Many thanks to Mags Duncan and Jeff Lord for their moral support during the early days of my project, when things were going a bit pear-shaped. Thank you Niamh for all the interesting drunken laughter. Thanks to Jamie and Gerry for always keeping me on my toes with their light entertainment and jokes. I also wish to thank my TULIP friends, Cristina Solla, Ric Pasquali, and Sarah Taylor. Many thanks to Jonathan Leather, John Malone and Paulo Fernandes for getting me pulled over by the police. I'm grateful to Gemma Cryan for her understanding and help during my write-up. I also enjoyed the friendships and encouragement of Kerstin, Pete, Phonsie Duncan, Kay, Jackie J, Jackie C, Becky, John Murray, Niall, Clare and Kate. And of course, I'm forever indebted to Dolly for keeping up my strength with breakfasts, bananas, short-bread and her delicious cakes. And apologies to anyone who I have forgotten to mention.

This thesis is dedicated to my mum and dad and my brothers John and Bernard.

MESOZOIC-TERTIARY TECTONICS OF SE IRELAND AND GENETIC LINK TO OFFSHORE EXTENSIONAL BASINS

VOLUME 1

Title Page
Declaration
Summary
Acknowledgements
Dedication
Abstract (loose)

Chapter 1 – Previous Work and Introduction

1.1	Introduction	1
1.2	Occurrences of Mesozoic-Tertiary Deposits	1
1.2.1	Mesozoic Geological History of NE Ireland	2
1.2.2	Tertiary Igneous Activity in NE Ireland	4
1.2.3	Kingscourt Half-Graben	5
1.2.4	Wexford Outlier	6
1.2.5	Ballydeenlea Cretaceous Outlier	6
1.2.6	Other Mesozoic-Tertiary Deposits	7
1.2.7	Implications – Mesozoic-Tertiary Tectonics	8
1.2.7.1	Present-Day Landscape	8
1.2.7.2	Denudation Events	10
1.3	Offshore Stratigraphic Record	10
1.3.1	Irish Sea Region	11
1.3.2	Northern Flanks	12
1.3.3	Celtic Sea Basins	12

1.3.4	Porcupine Basin	13
1.3.5	Slyne/Erris Troughs and Donegal Basin	14
1.3.6	Rockall-Hatton Troughs	15
1.3.7	Implications	15
1.3.7.1	Extensional Events	15
1.3.7.2	Inversion Events	16
1.4	Working Hypothesis	18
1.4.1	Basic Theory – Transform Fault Zones (TFZ)	19
1.4.2	Reactivation of Fractures	19
1.4.3	Transpression/Transtension	20
1.4.4	Structural Template	21
1.5	Dextral Transform Hypothesis	21
1.5.1	Scope of Thesis	22

Chapter 2 –Transform Model - Central-East Ireland

2.1	Introduction and Summary	23
2.1.1	Materials and Methods – Desk Study	23
2.2	Geology – Study Area	26
2.2.1	Basement	26
2.2.2	Lower Palaeozoic	27
2.2.3	Leinster Batholith	28
2.2.4	Carboniferous Rocks	29
2.2.5	Quaternary	31
2.2.6	Mesozoic-Tertiary Tectonism	31
2.3	Faults and Warm Springs	32

2.4	Digital Elevation Models – Topography	33
2.5	Thickness of Overburden	33
2.6	Elevation of Bedrock	34
2.7	Potential Mesozoic-Tertiary Pull-Apart Basin (?)	34
2.7.1	Locality – Newcastle (Co. Dublin)	35
2.7.2	Previous Survey/Drill Program	35
2.7.3	Geology of Survey Area	36
2.7.4	Boreholes	36
2.7.5	Resistivity of Lower Layer	36
2.7.6	Modelled Thickness of Overburden	37
2.7.7	Interpretation and Implications	37
2.8	Regional Geophysics	38
2.8.1	Aeromagnetics	38
2.8.2	Bouguer Gravity Anomaly	39
2.8.3	Low Bouguer Anomalies in the Central Midlands plain	40
2.8.4	Geophysical Models	40
2.8.5	Relationship of Warm Springs/Faults and Thick Overburden Section	41
2.9	Implications	42

Chapter 3 – Structural Work in Dublin Bay Area

3.1	Introduction	43
3.1.1	Aims and Objectives	43
3.2	Structures on the Northern Margin of the Leinster Batholith	44

3.2.1	Previous Work	45
3.3	Structural Observation and Interpretation	46
3.3.1	Sigmoidal Foliation	46
3.3.2	S-C Fabrics	47
3.3.3	Tectonic Fish	47
3.3.4	Fault Rocks	48
3.3.5	Slickensides, Slip-Fibre Lineations and Chatter Marks	49
3.3.6	Offset Markers and Sigmoidal Veins	50
3.3.7	Sigmoidal Drag Fold	50
3.3.8	Magmatic Lineation	50
3.4	Macroscopic Scale – Shear Zones	51
3.4.1	Semi-Ductile Sinistral Normal NW-SE Shear Zones	51
3.4.2	Semi-Brittle Reverse Dextral WNW-ESE Shear Zones	51
3.4.3	Brittle-Ductile Normal Sinistral N-S Shear Zones	52
3.4.4	Brittle to Semi-Ductile Normal Dextral NW-SE Shear Zones	53
3.5	Microscopic Scale – Deformation Mechanisms	53
3.5.1	Blackrock Breccia	53
3.5.2	Seapoint Breccia-Cataclasite	54
3.5.3	Shear Zone – Locality 3 (Killiney Bay)	54
3.5.4	Non-sheared Granite – Locality 2 (Sandycove)	55
3.5.5	Implications	55
3.6	Relative Chronology of Field Structures	57
3.7	Model	57
3.8	Howth Peninsula	58
3.8.1	Balscadden Fault	58

3.9	Structure at Balscadden Bay	59
3.9.1	Stratigraphy	60
3.9.2	Cleavage and Stylolites	60
3.9.3	Intersection Lineation	61
3.9.4	Slickensides and Minor Fault	61
3.9.5	Veins	61
3.9.6	Folds	62
3.9.7	Progressive Dextral Shear	63
3.10	NNW Strand of Southern Boundary Fault (SBF)	64
3.10.1	Major Growth Fault	64
3.10.2	Minor Faults	64
3.10.3	Slump Features and Porphyroclasts	65
3.10.4	Veins	65
3.10.5	Folds	65
3.10.6	Kinematic Indicator	65
3.11	Implications for Dextral Transform Hypothesis	66
3.12	Limitations	67

Chapter 4 - Structural Analyses of Kish Bank Basin and Regional Correlation

4.1	Introduction and summary	68
4.1.1	Aims and Objectives	69
4.1.2	Methods	69
4.1.3	Previous Work	76
4.1.4	Regional Setting	78
4.2	Geology and structure of the Kish Bank basin	79

4.3	Stratigraphy	80
4.3.1	Well 33/22-1 – Pre-rift and basement geology	80
4.3.2	Wells 33/21-1 & 33/17-1 – Syn-rift deposits	81
4.3.2.1	Permo-Triassic facies	82
4.3.2.2	Onshore lithological correlation with the Kingscourt outlier	83
4.3.3	Post/Syn-rift Liassic rocks (?)	83
4.3.4	Post-Liassic preservation	85
4.4	Structure	86
4.4.1	Codling fault zone	86
4.4.2	TRIST-92-21	86
4.4.3	Bathymetrical expression	87
4.4.4	Implications	87
4.4.5	Bathymetrical Features – faults (?)	88
4.5	Onshore-Offshore Correlation of Dalkey and Bray Fault Zones	90
4.5.1	Line AIR-78-61	91
4.5.2	Line AIR-78-62	91
4.5.3	Line AIR-78-63	92
4.5.4	Line AIR-78-64	93
4.5.5	Palaeo-channel (?)	93
4.5.6	Discussion of implications	94
4.6	Aeromagnetic survey – structural implications	95
4.6.1	Total magnetic intensity (reduced-to-pole [RTP])	95
4.6.2	First horizontal derivative of total magnetic intensity	96
4.6.2	High frequency – pseudo-depth slice 1, 2 and 3	97
4.6.4	Low frequency – pseudo-depth slice 4	99
4.6.5	Azimuth images – pseudo-depth slice 2 to 4	100
4.6.6	Implications	101
4.7	Post-Liassic history – Regional Correlation	102

4.7.1	Kish Bank basin	102
4.7.2	Irish Sea region – Integrated AFT and VR data	103
4.7.3	Other lines of evidence	105
4.7.4	VR studies in the Kish basin and adjacent area	105
4.8	Discussion	107
4.8.1	Age of NW-SE compression and NE-SW extension palaeostress	107
4.8.2	Age of NNW-SSE compression and ENE-WSW extension palaeostress	108
4.9	Implications	109

Chapter 5 - Topographic Analyses of SE Ireland

5.1	Introduction	110
5.1.1	Methods and Materials	111
5.1.2	Concepts	114
5.1.3	Regional Setting and Previous Work	115
5.1.4	Scope of Chapter	119
5.2	Topography – Mechanisms & Processes	119
5.2.1	Bedrock Structures	120
5.2.2	Climatic Fluctuations	121
5.2.3	Elevation Histograms	121
5.2.3.1	Leinster Mountain Chain & Tullow Lowland	122
5.2.4	Preliminary Interpretation	122
5.3	Areas of Study	123
5.4	Vartry Area	123
5.4.1	Elevation	124

5.4.2	Elevation Profiles	124
5.4.3	Bedrock Structures	125
5.4.4	Bouguer Gravity Anomaly	126
5.4.5	Metamorphic Aureole	126
5.4.6	Elevation – Ribband Group & Aureole	127
5.4.7	Elevation of Bray Group – Quartzites & Greywackes	128
5.4.8	Elevation – Northern Pluton	129
5.4.9	Elevation – Other Igneous Rocks	129
5.4.10	Slope	130
5.4.10.1	Slope & Elevation	131
5.4.11	Slope & Geology	132
5.4.11.1	Bray Group (Greywacke and Quartzite)	132
5.4.11.2	Ribband Group	133
5.4.11.3	Northern Pluton	134
5.4.11.4	Hypsometry – Differences & Similarities of Slope Distributions	134
5.4.12	Relief	135
5.4.12.1	Bray Group & Quartzite	136
5.4.12.2	Ribband Group & Aureole	137
5.4.13.3	Northern Pluton	137
5.4.13.4	Standard Deviation and Skewness	138
5.4.14	Fluvial Geomorphology	138
5.4.14.1	Vartry Surface	138
5.4.14.2	Vartry Escarpment and Knickpoints	139
5.4.14.3	Discussion	139
5.4.14.4	Conclusions	142
5.5	Bunclody Area	143
5.5.1	Elevation	143
5.5.2	Preliminary Interpretation	144
5.5.3	Elevation Profiles	144
5.5.4	Bedrock Structures	145

5.5.5	Bouguer Gravity Anomaly	146
5.5.6	Metamorphic Aureole	146
5.5.7	Ribband Group & Aureole	146
5.5.8	Tullow Pluton	148
5.5.9	Blackstairs Pluton	148
5.5.10	Other Igneous Rocks	149
5.5.11	Slope	149
5.5.11.1	Slope and Elevation	149
5.5.12	Slope and Geology	151
5.5.12.1	Tullow Pluton	151
5.5.12.2	Blackstairs Pluton	151
5.5.12.3	Ribband Group & Aureole	152
5.5.12.4	East Carlow Deformation Zone (ECDZ)	152
5.5.12.5	Hypsometry – Differences & Similarities of Slope Distribution	153
5.5.13	Relief	155
5.5.13.1	Ribband Group & Aureole	155
5.5.13.2	Tullow Pluton	156
5.5.13.3	Blackstairs Pluton	156
5.5.13.4	Influence of Structure – East Carlow Deformation Zone	157
5.5.14	Fluvial Geomorphology	157
5.5.15	Discussion	158
5.5.16	Conclusions	161
5.6	Glen of Imail Area	162
5.6.1	Elevation Histogram	162
5.6.2	Preliminary Interpretation	162
5.6.3	Elevation Profiles	163
5.6.4	Bedrock Structures	164
5.6.5	Bouguer Gravity Anomaly	164
5.6.6	Metamorphic Aureole	165
5.6.7	Ribband Group & Aureole	165

5.6.8	Tullow Pluton & Kilcullen Group	166
5.6.9	Lugnaquillia Pluton	166
5.6.10	Northern Pluton	167
5.6.11	Other Igneous Rocks	167
5.6.12	Slope	167
5.6.12.1	Slope and Elevation	168
5.6.13	Slope and Geology	169
5.6.13.1	Ribband Group & Aureole	169
5.6.13.2	Tullow Pluton	169
5.6.13.3	Kilcullen Group	170
5.6.13.4	Lugnaquillia Pluton	170
5.6.13.5	Northern Pluton	170
5.6.13.6	Hypsometry – Differences & Similarities of Slope Distributions	171
5.6.14	Relief	172
5.6.14.1	Ribband Group & Aureole	172
5.6.14.2	Tullow Pluton	173
5.6.14.3	Kilcullen Group	173
5.6.14.4	Lugnaquillia Pluton	173
5.6.14.5	Northern Pluton	174
5.6.15	Geomorphology	174
5.6.15.1	Glen of Imail Basin	175
5.6.15.2	Baltinglass Escarpment	175
5.6.17	Conclusions	177
5.7	Discussion of Conclusions	177

Chapter 6 – LANDSAT™ Lineament Analysis

6.1	Introduction	179
6.1.1	Methods and Materials	179

6.1.2	Previous Study	181
6.2	Regional LANDSAT Coverage of SE Ireland	182
6.2.1	WNW-ESE to NW-SE Lineaments	182
6.2.2	Hue Intensity Saturation (HIS)	184
6.2.3	Principal Components Analysis	185
6.2.4	Direction Filtered Images	185
6.3	Statistical Analysis of Lineaments	186
6.3.1	Rose Diagram	186
6.3.2	Entropy	187
6.3.3	Intersection Density	188
6.3.4	Length Density	189
6.3.5	Lineament Spacing	189
6.3.6	Interpretation	190
6.4	Vartry Area	190
6.4.1	Lineament Capture and Interpretation	191
6.4.2	Conclusions	192
6.5	Bunclody Area	192
6.5.1	Lineament Capture and Interpretation	193
6.5.2	Conclusions	193
6.6	Glen of Imail Area	194
6.6.1	Lineament Capture and Interpretation	194
6.6.2	Conclusions	195
6.7	Discussion of Conclusions	195

Chapter 7 - AFT Study of the Leinster Mountain Chain

7.1	Introduction and Summary	197
7.1.1	Aims	197
7.1.2	Apatite Fission Track Method	198
7.2	Interpreting AFT Data	202
7.3	AFT Samples – TULIP Database for Leinster Mountain Chain	204
7.3.1	Wicklow Massif – Geological Profile and AFT Samples	205
7.3.2	Fossilised PAZ Profiles	206
7.3.2.1	Regional	206
7.3.2.2	Geological Profile – Elevation/Central Age	207
7.3.3	Boomerang Plots – Leinster Mountain chain	208
7.3.3.1	Regional	208
7.3.3.2	Geological Profile – Age/MTL	209
7.3.4	AFT Profiles – Evidence for Faulting	209
7.3.4.1	Track-Length Distributions	211
7.4	Thermal Modelling	212
7.4.1	Hercynian Thermal Event	213
7.4.2	Time of Cooling from Maximum AFT Palaeotemperatures	213
7.5	Denudation Estimates	215
7.5.1	Estimate of Tertiary Palaeogeothermal Gradients	216
7.6	Estimates of Tectonic Uplift	217
7.6.1	Interpretations	219
7.7	Summary of Conclusions	221

Chapter 8 - Regional Implications of Models for SE Ireland

8.1	Introduction and Summary	223
8.1.1	Aims and Objectives	223
8.1.2	Methods and Materials	223
8.2	Tertiary Stress Models of SE Ireland	224
8.2.1	Regional Implications	225
8.3	AFT Analysis – A Test	226
8.3.1	Methodology	227
8.3.2	Results	228
8.3.3	Central Age – Observation & Interpretation	229
8.3.4	MTL – Observations & Interpretation	231
8.3.5	Partial Annealing Zone	232
8.3.6	Palaeotemperatures during Early Tertiary	235
8.3.7	Major Periods of Cooling	236
8.4	Porcupine Basin	237
8.4.1	Methods and Materials	238
8.4.2	Structure & Stratigraphy	239
8.4.2.1	Pre-Rift Rocks	240
8.4.2.2	Syn-Rift Rocks	240
8.4.2.3	Post-Rift Thermal Subsidence	242
8.4.2.4	Tertiary Rocks	244
8.4.2.5	Palaeogene Deltaic Complexes	245
8.4.3	Late Palaeogene-Neogene Unconformities	245
8.4.3.1	Syn-Sedimentary Slumps	245
8.4.4	Magnetic Basement	246
8.4.5	Two-Way Travel Time Maps	246
8.4.6	Seismic Reflection Lines	247

8.5 Tertiary – Sediment Budget 250
8.5.1 Denudation Efflux 250
8.5.2 Cenozoic Sediment – Porcupine Basin 252

8.6 Palaeotopography Reconstruction 253
8.6.1 Reconstruction of Tectonics – Boundary Conditions 254
8.6.2 Isostacy & Eustacy 255
8.6.3 Palaeotopography & Palaeobathymetry 255

Chapter 9 – Summary of Conclusions

9.1 Introduction 256
9.2 Dextral Transform Hypothesis 256
9.3 Offshore Correlation 258
9.4 Onshore Correlation with Geomorphology 259
9.5 AFT Results – SE Ireland 261
9.6 Regional Implications 261
9.7 Sediment Budget Analysis 262
9.8 Geodynamics 262

Further Work 263

References 265

List of Tables

Table 4.1 Irish National Grid Projection 72
Table 5.1 Correlation Matrix of relief, slope & elevation (Vartry area) 131

Table 5.2 Correlation Matrix of relief, slope & elevation (Bunclody area) 150
Table 5.3 Correlation Matrix of relief, slope & elevation (Glen of Imail area) 168
Table 6.1 Lineaments and known faults (Leinster Mountain chain) 182
Table 7.1 TULIP AFT samples for SE Ireland 204
Table 7.2 Denudation and Uplift values – modelled AFT data 218
Table 7.3 Tectonic uplift for samples forming fossilised PAZ profile 220
Table 8.1 Details of wells for Porcupine basin 238

VOLUME 2

Title Page

List of Figures

Chapter 1

Figure 1.1:- Simplified Mesozoic-Tertiary map of Ireland.
Figure 1.2:- Map showing major faults in the north of the Irish landmass.
Figure 1.3:- Map of Kingscourt outlier.
Figure 1.4:- Map of Wexford outlier.
Figure 1.5:- Simplified geology map and topography of Ireland.
Figure 1.6:- Map of Ireland and offshore Mesozoic-Tertiary basins.
Figure 1.7:- Free air gravity map of the Celtic and central-southern Irish Sea regions.
Figure 1.8:- Map of Porcupine basin.
Figure 1.9:- Map of offshore wells.
Figure 1.10:- Bathymetry of the continental shelf and abyssal plain, west of Ireland.
Figure 1.11:- Free air gravity map of NE Atlantic.
Figure 1.12:- Simple diagram of Mohr circle.
Figure 1.13:- Block diagram of transpression.

Figure 1.14:- Conceptual model of strike-slip faults with pronounced curvature.
Figure 1.15:- Bouguer gravity anomaly map of Ireland.
Figure 1.16:- Dextral transform model.

Chapter 2

Figure 2.1:- Map showing towns and lines of communication in the area of study.
Figure 2.2:- Principal of the very low frequency (VLF) method.
Figure 2.3a,b:- Simplified solid geology and structure map of study area.
Figure 2.4:- Map of known faults.
Figure 2.5:- Two maps showing known warm springs in the area of study.
Figure 2.6:- Graphs showing temperature measurements.
Figure 2.7:- Contoured map of elevation of study area.
Figure 2.8:- Map showing borehole database.
Figure 2.9:- Map showing interpolated thickness of overburden in study area.
Figure 2.10:- Thick overburden sections near the town of Kinnegad (Co. Meath).
Figure 2.11:- Map showing bedrock elevation.
Figure 2.12:- Composition of cored overburden material, south of Newcastle (Co. Dublin).
Figure 2.13:- Solid geology map of VLF-R survey area.
Figure 2.14a:- Modelled thicknesses of overburden from VLF-R measurements.
Figure 2.14b:- Modelled resistivity values of the lower layer.
Figure 2.15:- Aeromagnetic map of study area (GSI).
Figure 2.16:- Bouguer anomaly contours.
Figure 2.17:- Map showing occurrence of small Bouguer anomalies in Central Midlands.
Figure 2.18a,b:- Maps of Bouguer gravity and magnetic anomaly.

Chapter 3

Figure 3.1:- Location map of structural areas.

Figure 3.2:- Key structural localities along the northern margin of the Leinster batholith.
Figure 3.3:- Rose diagrams of structural elements.
Figure 3.4:- Location of structures at locality 1.
Figure 3.5:- Map of magmatic foliation.
Figure 3.6:- Location map of thin-section studies.
Figure 3.7:- Summary map of structures at locality 2 (Sandycove).
Figure 3.8:- Summary map of structures at locality 1 (Blackrock-Seapoint).
Figure 3.9:- Summary map of structures at locality 3 (Sorrento-Killiney).
Figure 3.10:- Deformation map of quartz showing strength envelope.
Figure 3.11:- Palaeostress reconstructions .
Figure 3.12:- Regional geology of the Howth peninsula.
Figure 3.13:- Summary of structure at Balscadden bay, Howth.
Figure 3.14:- Extensional jog on Southern Boundary fault.

Chapter 4

Figure 4.1:- Map of the pre-Tertiary geology of the Kish Bank basin.
Figure 4.2:- Map of seismic database.
Figure 4.3:- Principal of CDP stacking.
Figure 4.4:- Principal of diffraction.
Figure 4.5:- The gravity trend in the Kish Bank basin.
Figure 4.6:- Structural interpretation of unmigrated WINCH4A line.
Figure 4.7:- Map showing locations of Mesozoic basins in the Irish Sea region.
Figure 4.8:- Free-air anomaly map of the Irish Sea region.
Figure 4.9:- Well stratigraphy of Kish basin.
Figure 4.10:- Small section of the WNW-ESE trending TRIST-92-14 line.
Figure 4.11:- Map of onshore-offshore pre-Tertiary geology.
Figure 4.12:- Correlation of Kish basin with Kingscourt.
Figure 4.13:- Geoseismic interpretation over Bray Fault zone.
Figure 4.14:- Mesozoic-Tertiary rocks in the Ulster basin.

Figure 4.15:- N-S seismic line interpreted by Corcoran & Clayton (1999).
Figure 4.16:- Small section of the SW-NE trending TRIST-92-21 line.
Figure 4.17:- Contoured bathymetry map over the Kish basin.
Figure 4.18:- Bathymetry of Irish sea.
Figure 4.19:- Three video stills of the Codling fault.
Figure 4.20:- Pre-Tertiary geology map with seismic lines.
Figure 4.21:- Line AIR 78-61, Kish basin.
Figure 4.22:- Line AIR 78-62, Kish basin.
Figure 4.23:- Line AIR 78-63 shows small positive flower structure.
Figure 4.24:- Line AIR 78-64 shows basement offset.
Figure 4.25:- Line AIR 78-66 shows palaeo-channel.
Figure 4.26:- Line AIR 78-53.
Figure 4.27:- Map showing extent of palaeo-channel, based on seismic evidence.
Figure 4.28:- Contour map of magnetic frequency.
Figure 4.29:- Total Magnetic Intensity (Reduced-to-Pole) image for the Kish Bank basin.
Figure 4.30:- RTP image over Kish Basin, created by World Geoscience.
Figure 4.31:- Image is the first horizontal (non-directional) derivative.
Figure 4.32:- Pseudo-depth slice of aeromagnetic anomaly.
Figure 4.33:- Pseudo-depth slice two.
Figure 4.34:- Pseudo-depth slice three.
Figure 4.35:- Principal of log-power spectrum and Fourier analysis.
Figure 4.36:- Pseudo-Depth Slice 4.
Figure 4.37:- Azimuth 4 is a derivative of pseudo-depth slice 4.
Figure 4.38:- NW trending lineament in Kish basin.
Figure 4.39:- Azimuth 3 highlights shallow magnetic lineament.
Figure 4.40:- Azimuth 3 image.
Figure 4.41:- Azimuth 2 image.
Figure 4.42:- Azimuth 2 displays the smallest signal-to-noise ratio.
Figure 4.43:- Location Map of wells showing estimates of exhumation.
Figure 4.44:- Structural Correlation of Lough Neagh and Kish basin.
Figure 4.45:- Modified geological and structural maps of Kish basin.

Chapter 5

Figure 5.1:- Shaded-relief topographic image of SE Ireland.

Figure 5.2:- Location of areas of geomorphic and tectonic interest.

Figure 5.3:- Simple geological map of SE Ireland with topography.

Figure 5.4:- Regional 1milligal Bouguer gravity anomaly map.

Figure 5.5:- Map of plutons and geology of study areas.

Figure 5.6:- Geological map of the Northern and Upper Liffey Valley plutons.

Figure 5.7:- Geological map of the Lugnaquillia pluton.

Figure 5.8:- Geological map of the Tullow pluton.

Figure 5.9:- Geological map of the Blackstairs pluton.

Figure 5.10:- Theoretical slope profiles.

Figure 5.11a:- Elevation histogram for the Leinster Mountain chain.

Figure 5.11b:- Elevation histogram of Wicklow Massif.

Figure 5.12:- Digital elevation model and elevation histogram for the Vartry area.

Figure 5.13:- Bouguer gravity map of Vartry area of study.

Figure 5.14:- Shaded relief topographic image of the Vartry study area.

Figure 5.15a,b,c:- Statistical graphs showing the relationship between elevation and rock.

Figure 5.16:- Solid bedrock geology map of Vartry area.

Figure 5.17:- NW illuminated hillshade looking NNE.

Figure 5.18:- Slope image of Vartry area.

Figure 5.19a,b,c:- Statistical graphs of slope and elevation in the Vartry area.

Figure 5.20:- Graph showing the frequency of slopes in the area.

Figure 5.21a,b:- Histogram of slopes.

Figure 5.22:- Graph showing slope skewness based on lithology.

Figure 5.23a,b:- Graph showing slope characteristics of the main lithological types.

Figure 5.24a,b:- Histogram of slope type on Quartzites.

Figure 5.25a,b:- Histogram and cumulative frequency of slope type on Ribband Group.

Figure 5.26a,b:- Histogram and cumulative frequency of slope type on aureole rocks.

Figure 5.27a,b:- Histogram and cumulative frequency of slope on Northern pluton.

Figure 5.28:- Graph of normalised slope distribution for the main lithologies (Vartry).

Figure 5.29a,b:- Relief images of the Vartry area.
Figure 5.30a,b,c:- Descriptive statistical graphs of rock and relief.
Figure 5.31a,b,c,d,e:- Relief histograms for the main lithologies in the Vartry area.
Figure 5.32:- Image illustrating the main aspect in the Vartry area.
Figure 5.33:- Fluvial geomorphology.
Figure 5.34:- River profiles crossing the Vartry escarpment.
Figure 5.35:- Topographic image of the Vartry area looking west.
Figure 5.36a,b,c:- NW-SE geological, slope and relief profiles of the Vartry area.
Figure 5.37:- Model for Vartry area.
Figure 5.38:- DEM and elevation histogram for the Bunclody area of study.
Figure 5.39:- Shaded relief topographic image of the Bunclody study area.
Figure 5.40:- Solid bedrock geology map.
Figure 5.41:- Bouguer gravity anomaly of the Bunclody area.
Figure 5.42a,b,c:- Statistical graphs of slope and elevation in the Bunclody area.
Figure 5.43:- Slope image of Bunclody area.
Figure 5.44a,b,c:- Statistical graphs showing slopes on main lithological types.
Figure 5.45:- Graph showing the frequency of slopes in the area.
Figure 5.46a,b:- Histogram and cumulative frequency of slope type on Tullow rock.
Figure 5.47a,b:- Statistical graphs of slope and lithology in the Bunclody area.
Figure 5.48a,b:- Histogram and cumulative frequency of slope type for Blackstairs rocks.
Figure 5.49:- Graph showing slope skewness based on lithology.
Figure 5.50a:- Histogram and cumulative frequency of slope type for aureole rocks.
Figure 5.51a,b:- Histogram and cumulative frequency of slope type for aureole.
Figure 5.52a:- Histogram and cumulative frequency of slope type for Ribband Group.
Figure 5.53a,b:- Histogram and cumulative frequency of slope type for all rocks.
Figure 5.54:- Graph of normalised slope distribution for the main lithologies (Bunclody).
Figure 5.55a,b:- Relief images of the Bunclody area.
Figure 5.56a,b,c:- Descriptive statistical graphs between various rock type and relief.
Figure 5.57a,b,c,d,e:- Relief histograms for the main lithologies.
Figure 5.58:- Shaded relief topographic image of the Bunclody area.
Figure 5.59a,b:- Two topographic relief images of the Bunclody area.

Figure 5.60:- Sketch showing extent of Lower Carboniferous unconformity.

Figure 5.61a,b,c:- WNW-ESE geological, slope and relief profiles of the Bunclody area.

Figure 5.62:- Hillshaded image of the Nore and Barrow Rivers.

Figure 5.63:- Model for Bunclody area.

Figure 5.64:- DEM and histogram for the Glen of Imail area of study.

Figure 5.65:- Topographic relief image of the Glen of Imail area looking ~ W.

Figure 5.66:- Solid bedrock geology map.

Figure 5.67:- Bouguer gravity anomaly map of the Glen of Imail area.

Figure 5.68:- Shaded relief topographic image of the Glen of Imail.

Figure 5.69a,b,c:- Statistical graphs between lithology and elevation.

Figure 5.70:- Slope image of Glen of Imail area.

Figure 5.71a,b,c:- Statistical graphs of slope and elevation in the Glen of Imail area.

Figure 5.72a,b,c:- Histogram and cumulative frequencies of the Ribband Group.

Figure 5.73a,b:- Statistical graphs of slope and lithology in the Glen of Imail area.

Figure 5.74:- Graph of skewness for slope distribution of rock type.

Figure 5.75a:- Histogram and cumulative frequencies for Tullow rocks.

Figure 5.76a:- Histogram and cumulative frequencies of rocks of the Kilcullen Group.

Figure 5.77a:- Histogram and cumulative frequencies of the Lugnaquillia plutonic rocks.

Figure 5.78a:- Histogram and cumulative frequencies of the Northern pluton.

Figure 5.79a,b:- Graph of normalised slope distribution for the main lithologies (Glen of Imail).

Figure 5.80a,b:- Relief images of the Glen of Imail area.

Figure 5.81a,b,c:- Descriptive statistical graphs of rock type and relief.

Figure 5.82a,b:- Relief histograms for the Ribband Group and aureole.

Figure 5.83:- Relief histogram of the Tullow pluton.

Figure 5.84:- Relief histograms for the Kilcullen Group.

Figure 5.85:- Relief histograms for the Lugnaquillia pluton.

Figure 5.86:- Relief histograms for the Northern pluton.

Figure 5.87a,b:- Fluvial geomorphology.

Figure 5.88a:- NNE-SSW geological, slope and relief profiles of the Glen of Imail area.

Figure 5.89:- Model for Glen of Imail area.

VOLUME 3

Title Page

Chapter 6

Figure 6.1:- Regional LANDSAT draped over DEM.

Figure 6.2:- Corine image and lineaments.

Figure 6.3:- Regional HIS image.

Figure 6.4:- Regional LANDSAT lineament.

Figure 6.5:- Regional rose-diagram.

Figure 6.6:- Sub-cell rose diagram and faults.

Figure 6.7:- Entropy and faults.

Figure 6.8:- Intersection density and faults.

Figure 6.9:- Length density and faults.

Figure 6.10:- Lineament spacing and faults.

Figure 6.11a:- Landsat of Vartry area.

Figure 6.11b:- Landsat & DEM – facing NE.

Figure 6.11c:- Landsat & DEM – facing W.

Figure 6.12a:- Principal components analysis – Vartry area.

Figure 6.12b:- NE-SW spatial filter – Vartry area.

Figure 6.12c:- NW-SE spatial filter – Vartry area.

Figure 6.12d:- N-S spatial filter – Vartry area.

Figure 6.13a:- Landsat lineament.

Figure 6.13b:- Sub-Rose diagrams with faults – Vartry.

Figure 6.14:- Lineament direction, faults, geology – Vartry.

Figure 6.15a:- Landsat of Bunclody area.

Figure 6.15b:- Landsat & DEM – facing NNE.

Figure 6.15c:- Landsat & DEM – facing N.

Figure 6.16a:- Principal components analysis - Bunclody area.

Figure 6.16b:- NE-SW spatial filter - Bunclody area.

Figure 6.16c:- NW-SE spatial filter - Bunclody area.

Figure 6.16d:- N-S spatial filter - Bunclody area.

Figure 6.17a:- Landsat lineament - Bunclody area.

Figure 6.17b:- Sub-cell rose diagram with faults – Bunclody.

Figure 6.18:- Lineament direction, faults, geology – Bunclody.

Figure 6.19a:- Landsat of Glen of Imail area.

Figure 6.19b:- Landsat & DEM – facing NNE.

Figure 6.19c:- Landsat & DEM – facing N.

Figure 6.20a:- Principal components analysis – Glen of Imail.

Figure 6.20b:- NE-SW spatial filter – Glen of Imail.

Figure 6.20c:- NW-SE spatial filter – Glen of Imail.

Figure 6.20d:- N-S spatial filter – Glen of Imail.

Figure 6.21a:- Landsat lineament – Glen of Imail.

Figure 6.21b:- Rose diagram with faults – Glen of Imail.

Figure 6.22:- Lineament direction, faults, geology – Glen of Imail.

Chapter 7

Figure 7.1:- Diagram showing four simple thermal histories.

Figure 7.2:- Simple diagram showing concept of an exhumed partial annealing zone (PAZ).

Figure 7.3:- Map showing location of TULIP AFT samples.

Figure 7.4a,b:- Plots of AFT 'Central Age', 'Elevation' and MTL.

Figure 7.5:- Topographic image of the Wicklow Massif.

Figure 7.6:- Geological profile with AFT samples.

Figure 7.7:- Plot of central age against elevation.

Figure 7.8a,b:- Maps of a) vitrinite reflectance and b) derived palaeotemperature.

Figure 7.9:- Thermal modelling of AFT profile samples.

Figure 7.10:- Map showing AFT study of Keeley *et al.,* (1993) in SE Ireland.

Figure 7.11:- Profile showing modelled values of Tertiary denudation.

Chapter 8

Figure 8.1:- TULIP AFT database.

Figure 8.2:- Conceptual Model of Horsetail terminations.

Figure 8.3a,b:- Maps of Ireland showing a) AFT central age, and b) MTL.

Figure 8.4:- Plot of Elevation against AFT Central Age for Connemara.

Figure 8.5a,b:- Thermal modelled histories of TULIP samples.

Figure 8.6:- Duration that AFT samples were in the PAZ.

Figure 8.7:- Early Tertiary palaeotemperatures.

Figure 8.8a,b:- Denudation for Triassic to upper Lower Jurassic.

Figure 8.9:- Denudation for Early Cretaceous.

Figure 8.10:- Denudation for Palaeogene.

Figure 8.11:- Denudation for Neogene.

Figure 8.12:- Regional map of Porcupine basin and adjacent areas.

Figure 8.13:- Location map of seismic lines and wells.

Figure 8.14:- Regional E-W geoseismic interpretation showing typical steer's head profile.

Figure 8.15:- Tertiary isopach map of the Main Porcupine basin.

Figure 8.16:- Aeromagnetic anomaly map of the Porcupine basin.

Figure 8.17:- Fault styles in Porcupine Basin.

Figure 8.18:- Total Tertiary denudation based on AFT modelling.

Figure 8.19a,b:- Denudation rate and volumetric discharge for Ireland since the Triassic.

Figure 8.20:- DEM of Ireland at 1km cell resolution.

Figure 8.21:- Palaeotopography without eustacy.

Figure 8.22:- Palaeotopography with eustacy.

List of Plates

Chapter 1

Plate 1.1:- Tertiary Basalts overlying karstified Cretaceous surface.

Chapter 3

Plate 3.1:- View of Dalkey Quarry (facing NNW).

Plate 3.2:- Breccia on coast (Blackrock).

Plate 3.3:-Sigmoidal deformation of shear plane.

Plate 3.4:- S-C fabrics – locality 3 (Killiney Bay).

Plate 3.5:- Dextral reverse fish – locality 2 (semi-vertical face, viewed from NE).

Plate 3.6:- Reverse fish – locality 1.

Plate 3.7:- Tectonic fish with component of dextral shear (low vorticity, locality 2, near Bullock Harbour).

Plate 3.8:- Foliation and 'fish' – locality 2.

Plate 3.9:- Fault breccia-cataclasite – locality 1 (Seapoint).

Plate 3.10:- Slickenlines – locality 2 (Sandycove).

Plate 3.11:- Pegmatite sill intruding granite (locality 2).

Plate 3.12:- Sigmoidal drag fold (locality 1).

Plate 3.13:- Sandycove coastal exposures.

Plate 3.14:- Locality 2 (viewed from the east).

Plate 3.15:- Sandycove storm-drain and forty-foot bathing area.

Plate 3.16:- Dextral WNW-ESE shear plane (locality 1).

Plate 3.17:- WNW-ESE shear zone (viewed down line of transport).

Plate 3.18:- NW-SE dextral shear zone (locality 3, Sorrento Point).

Plate 3.19a,b:- Thin-section of Blackrock breccia; a) quartz showing undulose extinction and polygonisation of the margins, b) fine-grained ground-mass (XPL).

Plate 3.20a,b:- Thin-section of Seapoint cataclasite showing secondary muscovite that has been smeared between foliation planes (XPL).

Plate 3.21a,b:- Thin section (XPL) and meso-scale at Killiney Bay (locality 3). a) Micro-plate of shear zone (horizontal) and b) meso-scale of secondary mica growth.

Plate 3.22:- Thin section (XPL) of non-sheared granite showing unstrained quartz polygon.

Plate 3.23:- Balscadden fault scarp (viewed from the west) truncating wind-gap.

Plate 3.24:- Balscadden Fault breccia.

Plate 3.25:- Balscadden Fault breccia showing reddened quartz grains.

Plate 3.26:- Thin section (XPL) of Balscadden fault breccia – quartz grains show undulose extinction on margins.

Plate 3.27:- Evidence for Tertiary weathering surface.

Plate 3.29:- Apparent offset of calcite vein evident from orthogonal stylolite.

Plate 3.30:- Strain softened matrix cut by late-stage (post-Hercynian) reddened calcite vein.

Plate 3.31:- Dextral reverse en-echelon calcite veins, cut by Hercynian stylolites.

Plate 3.32:- Strand of Southern Boundary Fault (near Rathcoole – N7 Cork road).

Plate 3.33a,b:- Clasts of Silurian greywacke in Carboniferous limestone.

Plate 3.34:- Profile of Hercynian open folds with wavelength of ~2-3m.

Plate 3.35:- Thin section of kinematic indictor taken from fault plane.

Chapter 5

Plate 5.1:- Pie-chart of Northern Pluton (Vartry area).

Plate 5.2:- Pie-chart of Northern Pluton (Glen of Imail area).

Plate 5.3:- Pie-chart of Lugnaquillia Pluton (Glen of Imail area).

Plate 5.4:- Pie-chart of Tullow Pluton (Bunclody area).

Plate 5.5:- Pie-chart of Tullow Pluton (Glen of Imail area).

Plate 5.6:- Pie-chart of Blackstairs Pluton (Bunclody area).

Plate 5.7:- Pie-chart of Ribband Group (Bunclody area).

Plate 5.6:- Pie-chart of Ribband Group (Vartry area).

Plate 5.9:- Pie-chart of Ribband Group (Glen of Imail area).

Plate 5.10:- Pie-chart of Bray Group (Vartry area).

Plate 5.11:- Pie-chart of Kilcullen Group (Glen of Imail area).

Plate 5.12:- Lithological correlation of three study areas.

Appendices

Appendix 1:- Model - Reactivation of Pre-existing fractures.

Appendix 2:- Structural Observations (Dalkey Quarry, Co. Dublin).

Appendix 3:- Outline of geology of SE Ireland with proportions of rock type in the Vartry, Bunclody and Glen of Imail areas of study.

Appendix 4:- Track-Length Distribution Histograms. 1μm bins for track lengths.

Appendix 5:- Time-Temperature profiles of TULIP AFT samples for SE Ireland.

Appendix 6:- TULIP AFT Database.

Appendix 7:- Well-logs for the Porcupine basin.

Appendix 8:- Seismic Reflection lines (Porcupine basin).

Appendix 9:- Two-way time maps of Porcupine basin.

VOLUME 2

Title Page

List of Figures

Chapter 1

Figure 1.1:- Simplified Mesozoic-Tertiary map of Ireland.

Figure 1.2:- Map showing major faults in the north of the Irish landmass.

Figure 1.3:- Map of Kingscourt outlier.

Figure 1.4:- Map of Wexford outlier.

Figure 1.5:- Simplified geology map and topography of Ireland.

Figure 1.6:- Map of Ireland and offshore Mesozoic-Tertiary basins.

Figure 1.7:- Free air gravity map of the Celtic and central-southern Irish Sea regions.

Figure 1.8:- Map of Porcupine basin.

Figure 1.9:- Map of offshore wells.

Figure 1.10:- Bathymetry of the continental shelf and abyssal plain, west of Ireland.

Figure 1.11:- Free air gravity map of NE Atlantic.

Figure 1.12:- Simple diagram of Mohr circle.

Figure 1.13:- Block diagram of transpression.

Figure 1.14:- Conceptual model of strike-slip faults with pronounced curvature.

Figure 1.15:- Bouguer gravity anomaly map of Ireland.

Figure 1.16:- Dextral transform model.

Chapter 2

Figure 2.1:- Map showing towns and lines of communication in the area of study.

Figure 2.2:- Principal of the very low frequency (VLF) method.

Figure 2.3a,b:- Simplified solid geology and structure map of study area.

Figure 2.4:- Map of known faults.

Figure 2.5:- Two maps showing known warm springs in the area of study.

Figure 2.6:- Graphs showing temperature measurements.
Figure 2.7:- Contoured map of elevation of study area.
Figure 2.8:- Map showing borehole database.
Figure 2.9:- Map showing interpolated thickness of overburden in study area.
Figure 2.10:- Thick overburden sections near the town of Kinnegad (Co. Meath).
Figure 2.11:- Map showing bedrock elevation.
Figure 2.12:- Composition of cored overburden material, south of Newcastle (Co. Dublin).
Figure 2.13:- Solid geology map of VLF-R survey area.
Figure 2.14a:- Modelled thicknesses of overburden from VLF-R measurements.
Figure 2.14b:- Modelled resistivity values of the lower layer.
Figure 2.15:- Aeromagnetic map of study area (GSI).
Figure 2.16:- Bouguer anomaly contours.
Figure 2.17:- Map showing occurrence of small Bouguer anomalies in Central Midlands.
Figure 2.18a,b:- Maps of Bouguer gravity and magnetic anomaly.

Chapter 3

Figure 3.1:- Location map of structural areas.
Figure 3.2:- Key structural localities along the northern margin of the Leinster batholith.
Figure 3.3:- Rose diagrams of structural elements.
Figure 3.4:- Location of structures at locality 1.
Figure 3.5:- Map of magmatic foliation.
Figure 3.6:- Location map of thin-section studies.
Figure 3.7:- Summary map of structures at locality 2 (Sandycove).
Figure 3.8:- Summary map of structures at locality 1 (Blackrock-Seapoint).
Figure 3.9:- Summary map of structures at locality 3 (Sorrento-Killiney).
Figure 3.10:- Deformation map of quartz showing strength envelope.
Figure 3.11:- Palaeostress reconstructions .
Figure 3.12:- Regional geology of the Howth peninsula.

Figure 3.13:- Summary of structure at Balscadden bay, Howth.
Figure 3.14:- Extensional jog on Southern Boundary fault.

Chapter 4

Figure 4.1:- Map of the pre-Tertiary geology of the Kish Bank basin.
Figure 4.2:- Map of seismic database.
Figure 4.3:- Principal of CDP stacking.
Figure 4.4:- Principal of diffraction.
Figure 4.5:- The gravity trend in the Kish Bank basin.
Figure 4.6:- Structural interpretation of unmigrated WINCH4A line.
Figure 4.7:- Map showing locations of Mesozoic basins in the Irish Sea region.
Figure 4.8:- Free-air anomaly map of the Irish Sea region.
Figure 4.9:- Well stratigraphy of Kish basin.
Figure 4.10:- Small section of the WNW-ESE trending TRIST-92-14 line.
Figure 4.11:- Map of onshore-offshore pre-Tertiary geology.
Figure 4.12:- Correlation of Kish basin with Kingscourt.
Figure 4.13:- Geoseismic interpretation over Bray Fault zone.
Figure 4.14:- Mesozoic-Tertiary rocks in the Ulster basin.
Figure 4.15:- N-S seismic line interpreted by Corcoran & Clayton (1999).
Figure 4.16:- Small section of the SW-NE trending TRIST-92-21 line.
Figure 4.17:- Contoured bathymetry map over the Kish basin.
Figure 4.18:- Bathymetry of Irish sea.
Figure 4.19:- Three video stills of the Codling fault.
Figure 4.20:- Pre-Tertiary geology map with seismic lines.
Figure 4.21:- Line AIR 78-61, Kish basin.
Figure 4.22:- Line AIR 78-62, Kish basin.
Figure 4.23:- Line AIR 78-63 shows small positive flower structure.
Figure 4.24:- Line AIR 78-64 shows basement offset.
Figure 4.25:- Line AIR 78-66 shows palaeo-channel.
Figure 4.26:- Line AIR 78-53.
Figure 4.27:- Map showing extent of palaeo-channel, based on seismic evidence.

Figure 4.28:- Contour map of magnetic frequency.
Figure 4.29:- Total Magnetic Intensity (Reduced-to-Pole) image for the Kish Bank basin.
Figure 4.30:- RTP image over Kish Basin, created by World Geoscience.
Figure 4.31:- Image is the first horizontal (non-directional) derivative.
Figure 4.32:- Pseudo-depth slice of aeromagnetic anomaly.
Figure 4.33:- Pseudo-depth slice two.
Figure 4.34:- Pseudo-depth slice three.
Figure 4.35:- Principal of log-power spectrum and Fourier analysis.
Figure 4.36:- Pseudo-Depth Slice 4.
Figure 4.37:- Azimuth 4 is a derivative of pseudo-depth slice 4.
Figure 4.38:- NW trending lineament in Kish basin.
Figure 4.39:- Azimuth 3 highlights shallow magnetic lineament.
Figure 4.40:- Azimuth 3 image.
Figure 4.41:- Azimuth 2 image.
Figure 4.42:- Azimuth 2 displays the smallest signal-to-noise ratio.
Figure 4.43:- Location Map of wells showing estimates of exhumation.
Figure 4.44:- Structural Correlation of Lough Neagh and Kish basin.
Figure 4.45:- Modified geological and structural maps of Kish basin.

Chapter 5

Figure 5.1:- Shaded-relief topographic image of SE Ireland.
Figure 5.2:- Location of areas of geomorphic and tectonic interest.
Figure 5.3:- Simple geological map of SE Ireland with topography.
Figure 5.4:- Regional 1milligal Bouguer gravity anomaly map.
Figure 5.5:- Map of plutons and geology of study areas.
Figure 5.6:- Geological map of the Northern and Upper Liffey Valley plutons.
Figure 5.7:- Geological map of the Lugnaquillia pluton.
Figure 5.8:- Geological map of the Tullow pluton.
Figure 5.9:- Geological map of the Blackstairs pluton.
Figure 5.10:- Theoretical slope profiles.

Figure 5.11a:- Elevation histogram for the Leinster Mountain chain.

Figure 5.11b:- Elevation histogram of Wicklow Massif.

Figure 5.12:- Digital elevation model and elevation histogram for the Vartry area.

Figure 5.13:- Bouguer gravity map of Vartry area of study.

Figure 5.14:- Shaded relief topographic image of the Vartry study area.

Figure 5.15a,b,c:- Statistical graphs showing the relationship between elevation and rock.

Figure 5.16:- Solid bedrock geology map of Vartry area.

Figure 5.17:- NW illuminated hillshade looking NNE.

Figure 5.18:- Slope image of Vartry area.

Figure 5.19a,b,c:- Statistical graphs of slope and elevation in the Vartry area.

Figure 5.20:- Graph showing the frequency of slopes in the area.

Figure 5.21a,b:- Histogram of slopes.

Figure 5.22:- Graph showing slope skewness based on lithology.

Figure 5.23a,b:- Graph showing slope characteristics of the main lithological types.

Figure 5.24a,b:- Histogram of slope type on Quartzites.

Figure 5.25a,b:- Histogram and cumulative frequency of slope type on Ribband Group.

Figure 5.26a,b:- Histogram and cumulative frequency of slope type on aureole rocks.

Figure 5.27a,b:- Histogram and cumulative frequency of slope on Northern pluton.

Figure 5.28:- Graph of normalised slope distribution for the main lithologies (Vartry).

Figure 5.29a,b:- Relief images of the Vartry area.

Figure 5.30a,b,c:- Descriptive statistical graphs of rock and relief.

Figure 5.31a,b,c,d,e:- Relief histograms for the main lithologies in the Vartry area.

Figure 5.32:- Image illustrating the main aspect in the Vartry area.

Figure 5.33:- Fluvial geomorphology.

Figure 5.34:- River profiles crossing the Vartry escarpment.

Figure 5.35:- Topographic image of the Vartry area looking west.

Figure 5.36a,b,c:- NW-SE geological, slope and relief profiles of the Vartry area.

Figure 5.37:- Model for Vartry area.

Figure 5.38:- DEM and elevation histogram for the Bunclody area of study.

Figure 5.39:- Shaded relief topographic image of the Bunclody study area.

Figure 5.40:- Solid bedrock geology map.

Figure 5.41:- Bouguer gravity anomaly of the Bunclody area.
Figure 5.42a,b,c:- Statistical graphs of slope and elevation in the Bunclody area.
Figure 5.43:- Slope image of Bunclody area.
Figure 5.44a,b,c:- Statistical graphs showing slopes on main lithological types.
Figure 5.45:- Graph showing the frequency of slopes in the area.
Figure 5.46a,b:- Histogram and cumulative frequency of slope type on Tullow rock.
Figure 5.47a,b:- Statistical graphs of slope and lithology in the Bunclody area.
Figure 5.48a,b:- Histogram and cumulative frequency of slope type for Blackstairs rocks.
Figure 5.49:- Graph showing slope skewness based on lithology.
Figure 5.50a:- Histogram and cumulative frequency of slope type for aureole rocks.
Figure 5.51a,b:- Histogram and cumulative frequency of slope type for aureole.
Figure 5.52a:- Histogram and cumulative frequency of slope type for Ribband Group.
Figure 5.53a,b:- Histogram and cumulative frequency of slope type for all rocks.
Figure 5.54:- Graph of normalised slope distribution for the main lithologies (Bunclody).
Figure 5.55a,b:- Relief images of the Bunclody area.
Figure 5.56a,b,c:- Descriptive statistical graphs between various rock type and relief.
Figure 5.57a,b,c,d,e:- Relief histograms for the main lithologies.
Figure 5.58:- Shaded relief topographic image of the Bunclody area.
Figure 5.59a,b:- Two topographic relief images of the Bunclody area.
Figure 5.60:- Sketch showing extent of Lower Carboniferous unconformity.
Figure 5.61a,b,c:- WNW-ESE geological, slope and relief profiles of the Bunclody area.
Figure 5.62:- Hillshaded image of the Nore and Barrow Rivers.
Figure 5.63:- Model for Bunclody area.
Figure 5.64:- DEM and histogram for the Glen of Imail area of study.
Figure 5.65:- Topographic relief image of the Glen of Imail area looking ~ W.
Figure 5.66:- Solid bedrock geology map.
Figure 5.67:- Bouguer gravity anomaly map of the Glen of Imail area.
Figure 5.68:- Shaded relief topographic image of the Glen of Imail.
Figure 5.69a,b,c:- Statistical graphs between lithology and elevation.
Figure 5.70:- Slope image of Glen of Imail area.

Figure 5.71a,b,c:- Statistical graphs of slope and elevation in the Glen of Imail area.
Figure 5.72a,b,c:- Histogram and cumulative frequencies of the Ribband Group.
Figure 5.73a,b:- Statistical graphs of slope and lithology in the Glen of Imail area.
Figure 5.74:- Graph of skewness for slope distribution of rock type.
Figure 5.75a:- Histogram and cumulative frequencies for Tullow rocks.
Figure 5.76a:- Histogram and cumulative frequencies of rocks of the Kilcullen Group.
Figure 5.77a:- Histogram and cumulative frequencies of the Lugnaquillia plutonic rocks.
Figure 5.78a:- Histogram and cumulative frequencies of the Northern pluton.
Figure 5.79a,b:- Graph of normalised slope distribution for the main lithologies (Glen of Imail).
Figure 5.80a,b:- Relief images of the Glen of Imail area.
Figure 5.81a,b,c:- Descriptive statistical graphs of rock type and relief.
Figure 5.82a,b:- Relief histograms for the Ribband Group and aureole.
Figure 5.83:- Relief histogram of the Tullow pluton.
Figure 5.84:- Relief histograms for the Kilcullen Group.
Figure 5.85:- Relief histograms for the Lugnaquillia pluton.
Figure 5.86:- Relief histograms for the Northern pluton.
Figure 5.87a,b:- Fluvial geomorphology.
Figure 5.88a:- NNE-SSW geological, slope and relief profiles of the Glen of Imail area.
Figure 5.89:- Model for Glen of Imail area.

VOLUME 3

Title Page

Chapter 6

Figure 6.1:- Regional LANDSAT draped over DEM.

Figure 6.2:- Corine image and lineaments.

Figure 6.3:- Regional HIS image.

Figure 6.4:- Regional LANDSAT lineament.

Figure 6.5:- Regional rose-diagram.

Figure 6.6:- Sub-cell rose diagram and faults.

Figure 6.7:- Entropy and faults.

Figure 6.8:- Intersection density and faults.

Figure 6.9:- Length density and faults.

Figure 6.10:- Lineament spacing and faults.

Figure 6.11a:- Landsat of Vartry area.

Figure 6.11b:- Landsat & DEM – facing NE.

Figure 6.11c:- Landsat & DEM – facing W.

Figure 6.12a:- Principal components analysis – Vartry area.

Figure 6.12b:- NE-SW spatial filter – Vartry area.

Figure 6.12c:- NW-SE spatial filter – Vartry area.

Figure 6.12d:- N-S spatial filter – Vartry area.

Figure 6.13a:- Landsat lineament.

Figure 6.13b:- Sub-Rose diagrams with faults – Vartry.

Figure 6.14:- Lineament direction, faults, geology – Vartry.

Figure 6.15a:- Landsat of Bunclody area.

Figure 6.15b:- Landsat & DEM – facing NNE.

Figure 6.15c:- Landsat & DEM – facing N.

Figure 6.16a:- Principal components analysis - Bunclody area.

Figure 6.16b:- NE-SW spatial filter - Bunclody area.

Figure 6.16c:- NW-SE spatial filter - Bunclody area.
Figure 6.16d:- N-S spatial filter - Bunclody area.
Figure 6.17a:- Landsat lineament - Bunclody area.
Figure 6.17b:- Sub-cell rose diagram with faults – Bunclody.
Figure 6.18:- Lineament direction, faults, geology – Bunclody.
Figure 6.19a:- Landsat of Glen of Imail area.
Figure 6.19b:- Landsat & DEM – facing NNE.
Figure 6.19c:- Landsat & DEM – facing N.
Figure 6.20a:- Principal components analysis – Glen of Imail.
Figure 6.20b:- NE-SW spatial filter – Glen of Imail.
Figure 6.20c:- NW-SE spatial filter – Glen of Imail.
Figure 6.20d:- N-S spatial filter – Glen of Imail.
Figure 6.21a:- Landsat lineament – Glen of Imail.
Figure 6.21b:- Rose diagram with faults – Glen of Imail.
Figure 6.22:- Lineament direction, faults, geology – Glen of Imail.

Chapter 7

Figure 7.1:- Diagram showing four simple thermal histories.
Figure 7.2:- Simple diagram showing concept of an exhumed partial annealing zone (PAZ).
Figure 7.3:- Map showing location of TULIP AFT samples.
Figure 7.4a,b:- Plots of AFT 'Central Age', 'Elevation' and MTL.
Figure 7.5:- Topographic image of the Wicklow Massif.
Figure 7.6:- Geological profile with AFT samples.
Figure 7.7:- Plot of central age against elevation.
Figure 7.8a,b:- Maps of a) vitrinite reflectance and b) derived palaeotemperature.
Figure 7.9:- Thermal modelling of AFT profile samples.
Figure 7.10:- Map showing AFT study of Keeley *et al.*, (1993) in SE Ireland.
Figure 7.11:- Profile showing modelled values of Tertiary denudation.

Chapter 8

Figure 8.1:- TULIP AFT database.

Figure 8.2:- Conceptual Model of Horsetail terminations.

Figure 8.3a,b:- Maps of Ireland showing a) AFT central age, and b) MTL.

Figure 8.4:- Plot of Elevation against AFT Central Age for Connemara.

Figure 8.5a,b:- Thermal modelled histories of TULIP samples.

Figure 8.6:- Duration that AFT samples were in the PAZ.

Figure 8.7:- Early Tertiary palaeotemperatures.

Figure 8.8a,b:- Denudation for Triassic to upper Lower Jurassic.

Figure 8.9:- Denudation for Early Cretaceous.

Figure 8.10:- Denudation for Palaeogene.

Figure 8.11:- Denudation for Neogene.

Figure 8.12:- Regional map of Porcupine basin and adjacent areas.

Figure 8.13:- Location map of seismic lines and wells.

Figure 8.14:- Regional E-W geoseismic interpretation showing typical steer's head profile.

Figure 8.15:- Tertiary isopach map of the Main Porcupine basin.

Figure 8.16:- Aeromagnetic anomaly map of the Porcupine basin.

Figure 8.17:- Fault styles in Porcupine Basin.

Figure 8.18:- Total Tertiary denudation based on AFT modelling.

Figure 8.19a,b:- Denudation rate and volumetric discharge for Ireland since the Triassic.

Figure 8.20:- DEM of Ireland at 1km cell resolution.

Figure 8.21:- Palaeotopography without eustacy.

Figure 8.22:- Palaeotopography with eustacy.

List of Plates

Chapter 1

Plate 1.1:- Tertiary Basalts overlying karstified Cretaceous surface.

Chapter 3

Plate 3.1:- View of Dalkey Quarry (facing NNW).

Plate 3.2:- Breccia on coast (Blackrock).

Plate 3.3:-Sigmoidal deformation of shear plane.

Plate 3.4:- S-C fabrics – locality 3 (Killiney Bay).

Plate 3.5:- Dextral reverse fish – locality 2 (semi-vertical face, viewed from NE).

Plate 3.6:- Reverse fish – locality 1.

Plate 3.7:- Tectonic fish with component of dextral shear (low vorticity, locality 2, near Bullock Harbour).

Plate 3.8:- Foliation and 'fish' – locality 2.

Plate 3.9:- Fault breccia-cataclasite – locality 1 (Seapoint).

Plate 3.10:- Slickenlines – locality 2 (Sandycove).

Plate 3.11:- Pegmatite sill intruding granite (locality 2).

Plate 3.12:- Sigmoidal drag fold (locality 1).

Plate 3.13:- Sandycove coastal exposures.

Plate 3.14:- Locality 2 (viewed from the east).

Plate 3.15:- Sandycove storm-drain and forty-foot bathing area.

Plate 3.16:- Dextral WNW-ESE shear plane (locality 1).

Plate 3.17:- WNW-ESE shear zone (viewed down line of transport).

Plate 3.18:- NW-SE dextral shear zone (locality 3, Sorrento Point).

Plate 3.19a,b:- Thin-section of Blackrock breccia; a) quartz showing undulose extinction and polygonisation of the margins, b) fine-grained ground-mass (XPL).

Plate 3.20a,b:- Thin-section of Seapoint cataclasite showing secondary muscovite that has been smeared between foliation planes (XPL).

Plate 3.21a,b:- Thin section (XPL) and meso-scale at Killiney Bay (locality 3). a) micro-plate of shear zone (horizontal) and b) meso-scale of secondary mica growth.

Plate 3.22:- Thin section (XPL) of non-sheared granite showing unstrained quartz polygon.

Plate 3.23:- Balscadden fault scarp (viewed from the west) truncating wind-gap.

Plate 3.24:- Balscadden Fault breccia.

Plate 3.25:- Balscadden Fault breccia showing reddened quartz grains.

Plate 3.26:- Thin section (XPL) of Balscadden fault breccia – quartz grains show undulose extinction on margins.

Plate 3.27:- Evidence for Tertiary weathering surface.

Plate 3.29:- Apparent offset of calcite vein evident from orthogonal stylolite.

Plate 3.30:- Strain softened matrix cut by late-stage (post-Hercynian) reddened calcite vein.

Plate 3.31:- Dextral reverse en-echelon calcite veins, cut by Hercynian stylolites.

Plate 3.32:- Strand of Southern Boundary Fault (near Rathcoole – N7 Cork road).

Plate 3.33a,b:- Clasts of Silurian greywacke in Carboniferous limestone.

Plate 3.34:- Profile of Hercynian open folds with wavelength of ~2-3m.

Plate 3.35:- Thin section of kinematic indictor taken from fault plane.

Chapter 5

Plate 5.1:- Pie-chart of Northern Pluton (Vartry area).

Plate 5.2:- Pie-chart of Northern Pluton (Glen of Imail area).

Plate 5.3:- Pie-chart of Lugnaquillia Pluton (Glen of Imail area).

Plate 5.4:- Pie-chart of Tullow Pluton (Bunclody area).

Plate 5.5:- Pie-chart of Tullow Pluton (Glen of Imail area).

Plate 5.6:- Pie-chart of Blackstairs Pluton (Bunclody area).

Plate 5.7:- Pie-chart of Ribband Group (Bunclody area).

Plate 5.6:- Pie-chart of Ribband Group (Vartry area).

Plate 5.9:- Pie-chart of Ribband Group (Glen of Imail area).

Plate 5.10:- Pie-chart of Bray Group (Vartry area).
Plate 5.11:- Pie-chart of Kilcullen Group (Glen of Imail area).
Plate 5.12:- Lithological correlation of three study areas.

Appendices

Appendix 1:- Model - Reactivation of Pre-existing fractures.
Appendix 2:- Structural Observations (Dalkey Quarry, Co. Dublin).
Appendix 3:- Outline of geology of SE Ireland with proportions of rock type in the Vartry, Bunclody and Glen of Imail areas of study.
Appendix 4:- Track-Length Distribution Histograms. 1μm bins for track lengths.
Appendix 5:- Time-Temperature profiles of TULIP AFT samples for SE Ireland.
Appendix 6:- TULIP AFT Database.
Appendix 7:- Well-logs for the Porcupine basin.
Appendix 8:- Seismic Reflection lines (Porcupine basin).
Appendix 9:- Two-way time maps of Porcupine basin.

CHAPTER 1 – PREVIOUS WORK AND INTRODUCTION

1.1 Introduction

The original aim of this thesis was to evaluate the tectonic and economic significance of potential Mesozoic-Tertiary transform fault zones and the genetic link to offshore extensional basins. This was based on a working hypothesis proposed by Professor Adrian Phillips, which won my scholarship funding from Total Oil Marine plc. But, it became evident that the aim needed to be modified to include an analysis of Mesozoic and, particularly, Tertiary tectonism in SE Ireland. This was subsequently broadened to include the entire Irish landmass and adjacent continental shelf.

1.2 Occurrences of Mesozoic-Tertiary Deposits

In mainland Ireland, there is a general absence of Mesozoic-Tertiary deposits (figure 1.1). The general accepted view is that this is due to significant tectonic uplift and exhumation of the north-western European continental margin (e.g., Bray *et al,* 1992; Brodie & White, 1995; Bulat & Stoker, 1987; Clift *et al.,* 1998; Green, 1989; Green *et al.,* 1993; Hillis, 1992; Hillis, 1995; Japsen, 1997; Menpes & Hillis, 1995; Rohrman *et al.*, 1995; Rohrman & van der Beek, 1996; White, 1988; White & Lovell, 1997) during both Palaeogene and Neogene times. Much of our knowledge of Mesozoic-Tertiary deformation onshore is based on the displacement of Triassic to Cretaceous sequences, Palaeocene basaltic flows and Oligocene sequences in NE Ireland (George, 1967; Parnell *et al.*, 1988; Naylor, 1992; Geoffroy *et al.,* 1996). There is also a considerable literature on the tectonic and sedimentological evolution of Mesozoic-Tertiary basins offshore (e.g. Cook, 1987; Jenner, 1981; Naylor & Anstey, 1987; Roberts, 1989; Shannon, 1991a; Naylor, 1992; Shannon *et al.,* 1993; O'Driscoll *et al.,* 1995; Shannon *et al.,* 1995; Vermeulen *et al.,* 1999; Vogt, 1995). However, to-date there have been very few attempts to structurally correlate both onshore and offshore areas together for the Mesozoic-Tertiary era (Keeley, 1995, Naylor, 1992, Shannon *et al.*, 1993).

The vast majority of Mesozoic-Tertiary rocks in Ireland occur in the Ulster basin (figure 1.1). These rocks have been preserved under thick piles of Tertiary lava flows, which

erupted from Icelandic-type fissures (Wilson, 1972; Naylor, 1992). Slightly younger Tertiary intrusive centres of Mourne, Carlingford and Slieve Gullion (Counties Down and Armagh) cut, and are cut by, the NW-SE trending dyke swarms (e.g. Meighan *et al.,* 1999). These dyke swarms represent the remnants of fissures, which once fed hot molten lava over the eroded Mesozoic landscape of NE Ireland.

Few other Mesozoic deposits occur outside this region. Notable exceptions include the Kingscourt half-graben in Co. Cavan (Jackson, 1965; Gardiner & Visscher, 1971) and the Wexford Outlier in Co. Wexford (Clayton *et al.,* 1986). The only known occurrence of Cretaceous strata outside the region is the Ballydeenlea chalk outlier in Co. Kerry (section 1.2.5). This deposit has been dated as Campanian in age, based on foraminiferal evidence (Barr, 1966; Walsh, 1966; Evans & Clayton, 1998). In addition Upper Jurassic to Lower Cretaceous clays occur near Carrick-on-Suir, County Kilkenny (Higgs and Jones, 1998), and reddened Middle Jurassic clays occur at Cloyne, south County Cork (Higgs & Beese, 1986). There are also many other small deposits of clays and sands of known and presumed Tertiary age in Central and Southern Ireland (Wynne, 1857; Davies, 1970; Mitchell, 1980; Beese *et al.,* 1983; Higgs & Beese, 1986; Coxon & Flegg, 1987; Naylor, 1992).

1.2.1 Mesozoic Geological History of NE Ireland

The main outcrop of Mesozoic-Tertiary rocks onshore Ireland is located in the Ulster basin (UB), NE Ireland. The UB has an aerial extent of approximately 6,000km^2 and is made up of 2 onshore sub-basins. The basin extends offshore and correlates with the North Channel basin (Naylor, 1992). The main onshore part is composed of the Rathlin Trough and Lough Neagh-Larne basin, which is subsequently composed of smaller sub-basins.

The Rathlin Trough is bounded by the Foyle and Tow Valley faults to the NW and SE respectively (figure 1.2). The Lough Neagh-Larne basin (LNLB) is separated from the Rathlin Trough, to the north, by the Dalradian Highland Border Ridge (HBR) which abuts against the Sixmilewater fault (western extension of the Southern Uplands fault) to the south (Kerr, 1987; McCaffrey & McCann, 1992).

The basin fill ranges in age from Permian to Oligocene (George, 1967; Reid, 1971; Wilson, 1972; Fletcher, 1977; Thompson, 1979; Wilkinson *et al.,* 1980; Penn, 1981; Illing & Griffith, 1986; Smith, 1986; McCann, 1988; Parnell *et al.,* 1989; McCann, 1990; McCaffrey & McCann, 1992). Deep boreholes drilled at Magilligan and Port More encountered 2km of Mesozoic strata in the Rathlin Trough and 3km of post-Carboniferous strata in the LNLB (Wilson, 1972; Thompson, 1979; McCann, 1988, 1990). Two other wells, to-date, have been drilled in the centre of the basin (Newmill-1 and Larne-2) to a depth of 1,981m and 2,880m respectively (Penn, 1981; McCann, 1990). Both wells failed to penetrate the full Permian section.

In the Lough Neagh-Larne basin, the Triassic sandstones and marls of the Sherwood Sandstone Group overstep Permian carbonates northwards and onlap the HBR. These are conformably overlain by the Mercia Mudstone Group, which consists primarily of mudstones and subordinate evaporite successions (Naylor, 1992). Deposition was interrupted in Mid-Liassic times by up an uplift event (Hall *et al.*,1984; McCaffrey & McCann, 1992; Naylor, 1992). This event left thick but variable lower Liassic sequences, with the overlying Hibernian Greensand Formation, which locally contains reworked Mid-to-Late Jurassic fossils (Wilson, 1972; McCann, 1988, 1990).

Deposition resumed in Mid-to-Late Cretaceous times with a major transgression commencing at the beginning of the Senonian stage (McCaffrey & McCann, 1992). This led to the complete submergence of the HBR by the late Santonian times (Naylor, 1992). From early Cenomanian to early Maastrichtian, two main facies developed, the Hibernian Greensand and Ulster White Limestone Formations. Locally, these facies are lateral equivalents (Reid, 1971; Fletcher, 1977; Naylor, 1992). The maximum thickness of the Ulster White limestone is estimated at 120m and occurs in the Ballycastle area of the Rathlin Trough (Naylor, 1992). A major regression then commenced in the latest Cretaceous and continued until earliest Tertiary times. This hiatus spanned approximately 8Myr and differential erosion led to the establishment of karst topography, which was subsequently covered by Palaeocene lava flows (plate 1.1).

1.2.2 Tertiary Igneous Activity in NE Ireland

Thick lava piles, associated with the Palaeogene evolution of the opening of the North Atlantic, spilled out of fissures and volcanic centres (Dewey & Windley, 1988; Dicken, 1988; Mussett *et al.,* 1988; Roberts, 1989; Ziegler, 1989; Shannon, 1991a; Brodie & White, 1995; Geoffroy *et al.,* 1996; Clift *et al.,* 1998). Three main units have been distinguished and the presence of lateritic alteration at the top of each unit is evidence for a significant period of quiescence before emplacement of each pile (Wilson, 1972). The lavas belong to the tholeiitic magma series and have a maximum present-day thickness of about c.500m. Published ages range from c.61Ma to c.58Ma and recent SHRIMP dating of zircons give ages of c.58.4±0.7Ma for the Tardee Rhyolite complex, and c.58Ma for the interbasaltic formation (Dicken, 1988; Meighan *et al.,* 1999). Late-faulting of the Antrim Plateau lavas occurred on reactivated NE-SW and NNE-SSW major faults (Kerr, 1987; Geoffroy *et al.,* 1996; Naylor, 1992). For example, the Tow Valley fault displaces Tertiary lavas, and isoclinal folding of basalts along splays of this fault has been reported from Rathlin Island (Wilson & Robbie, 1966).

At the top of the lava piles, the basalts were subjected to chemical weathering under tropical climatic environments during Early Tertiary times. Boreholes in the Lough Neagh region have proven a 300+m thick succession of interbedded lithomarge, pyroclastics and lacustrine deposits, which are interpreted as Oligocene in age (Parnell *et al.,* 1986). Subsequent reactivation of basement faults produced transtension and subsidence of the Lough Neagh region (George, 1967; Parnell *et al.,* 1986). Freshwater lacustrine environments were then established, and produced thick accumulations of siliciclastic and lignitic deposits, known as the Lough Neagh Group (Griffith *et al.,* 1987; the Lough Neagh Clays) and have been dated Oligocene (Chattian) in age (Wilkinson *et al.,* 1980). The area was then subjected to NNW-SSE horizontal compression and ENE-WSE horizontal extension (Geoffroy *et al.,* 1996; chapter 3). This produced gentle warping and erosion of the Lough Neagh Group. The contemporary section is preserved in the footwall of major NE faults downthrowing to the south. Likewise, the Oligocene aged lignite deposits at Ballymoney are preserved in dilational beds from the NW side of the Tow Valley Fault (figure 1.2).

Tertiary aged plutons include the Mourne, Slieve Gullion and Carlingford complexes of Counties Armagh, Down and Louth respectively (figure 1.1). Radiometric dating of the Mourne mountains gives a date of c.56Ma based on Rb-Sr WR (Meighan *et al.*, 1988) and Ar-Ar (Gibson *et al.,* 1995) and recent U/Pb zircon ages come out at c.55.5±1.1Ma (Meighan *et al.*, 1999). The Slieve Gullion central complex gives a Rb-Sr WR age of c.57.6±1.0Ma and a SHRIMP age of c.56.5±1.3Ma. Therefore, the Mourne and Slieve Gullion complexes were probably emplaced contemporaneously. These Tertiary granites appear to be 2-3Myr younger than the Antrim basalts, although there are no apparent crosscutting relationships. Since these granites have cooled below the respective radiometric closure temperatures at depths of c.3km in the upper crust, there has evidently been very significant unroofing (c.50mMy^{-1} time-averaged) to their present-day elevation of ~800m maximum (chapter 8).

1.2.3 Kingscourt Half-Graben

The Kingscourt outlier is a small extensional half-graben, of approximately 100km^2 in extent (figure 1.3). The stratigraphy has been correlated with other extensional basins (chapter 4) of the Irish Sea region (Naylor *et al.,* 1993). Much of our understanding of the stratigraphy of the deposit is derived from boreholes. The outlier is unconformable with the synclinally folded Upper Carboniferous rocks and has been preserved within a N-S trending half-graben structure, which is down-faulted on the west against Lower Palaeozoic strata (Jackson, 1965).

The outlier is associated with a low bouguer gravity anomaly of 13Mgal (Young, 1976), with a steep gradient over the main N-S fault, with gravity values falling to the regional background value of 20Mgal, 1km west of the main N-S fault. The anomaly is smaller than expected from the volume of sedimentary fill estimated from boreholes. This is attributed to high-density Tertiary igneous rocks, which are offsetting the negative contributions from the sediments (Young, 1976).

Tournasian limestone-shales rest unconformably on Lower Palaeozoic slates. Viséan strata and overlapping Namurian shales and sandstones continue the succession, with the latter outcropping on the west. The two main formations recognised are the Kingscourt Gypsum Formation and the younger Kingscourt Sandstone Formation. The

former comprises a basal conglomeratic sequence overlain by red and grey mudstone and gypsum cycles (Naylor 1992). This apparently passes up, conformably, into the Kingscourt Sandstone Formation, which consists of a basal sequence of red siltstone overlain by red and grey fine-grained sandstone.

The graben has a fill of approximately 550m of Permo-Triassic transitional marine-continental red-beds. Both palynological and sedimentological evidence from the Permo-Triassic sequence indicates a marine-continental transitional sedimentary tract. Gardiner & Visscher (1971) suggested that the marine conditions persisted during the deposition of Permian sequences, which gave way to an arid, continental environment in the succeeding Triassic.

Later periods of differential erosion probably removed the missing predictive post-rift sequence (based on the McKenzie (1978) stretching model). This erosion also cuts out part of the syn-rift package (chapter 8). For example, a palaeokarst surface developed over Permian gypsum is overlain by highly weathered Tertiary basaltic lavas flows (Simms, 1998).

1.2.4 Wexford Outlier

The Wexford outlier is located in the extreme SE of the country, just west of the Pre-Cambrian Rosslare complex (figure 1.4). The outlier is not exposed, however boreholes have proven more than 200m of Permo-Triassic conglomerate and red beds (Killag Formation). This formation rests on Westphalian, Namurian, and Dinantian limestones in different boreholes (Clayton *et al.,* 1986), indicating significant post-Namurian to pre-Permian differential erosion. Preservation of the outlier was controlled by the reactivation of a major Caledonian trending NE-SW fault system (chapter 8).

1.2.5 Ballydeenlea Cretaceous Outlier

The Ballydeenlea outlier is located in the Gweestin valley about 6 miles north of the town of Killarney (figure 1.1). Walsh (1966) originally described the deposit as a breccia mass of shale fragments which contain a prominent matrix of fossiliferous Cretaceous chalk with small pieces of flint. The chalk is a hard white compact

limestone, similar to the Ulster White Limestone (Co. Antrim). The angular fragments of mudstone and shale appear to be derived locally from the adjacent Namurian sediments. The margins of the outlier are not exposed. However, geophysical surveys, outcrop, and borehole data provide evidence to suggest that the deposit is no larger than 150m in diameter. Boreholes drilled in 1994 reached a maximum of 98m, and failed to penetrate the base of the breccia. Although, the ratio of chalk to clay matrix decreases with depth, and all chalk was absent >41m below the surface level (Evans & Clayton, 1998).

Walsh (1966) suggested that the outlier was a karstic collapse body and George (1967) proposed that the deposit was a synclinal remnant of a greater extensive chalk cover. Recent work by Evans & Clayton (1998) hypothesise that the outlier is the remnant of a suite of sediments which were deposited at the foot of an active submarine fault scarp during Campanian times. Based on vitrinite reflectance profiles and Early Tertiary geothermal gradients of 80-90°C km^{-1}, Evans & Clayton (1998) show that the deposit attained a maximum burial depth of 1 to 1.5km, indicating a subsequent period of exhumation and/or surface uplift during the Tertiary. However, the Early Tertiary palaeogeothermal gradient they use is probably too high (chapter 8).

1.2.6 Other Mesozoic-Tertiary Deposits

The small Mesozoic-Tertiary deposits shown on figure 1.1 are based on a map compiled by Naylor (1992) of documented occurrences. More deposits have been discovered since Naylor's paper and an updated map is currently in press (Jones, pers. comm. 1999). Most of the deposits are less then $1km^2$ and range in composition from silicified clays to unconsolidated sands/gravels and lignite. The majority appear to have been preserved in karst/solution cavities as a direct result either of fault-related or solution-related subsidence within the predominantly Carboniferous limestone bedrock. For example, Upper Jurassic to Lower Cretaceous marginal marine clays near Carrick-on-Suir, County Kilkenny (Higgs & Jones, 1998) and Middle Jurassic non-marine reddened clays at Cloyne, S Co. Cork (Higgs & Beese, 1986).

In addition, Coxon & Coxon (1998) have documented evidence for late Pliocene deposits in Co. Galway, based on palynological dating. The organic sediments occur in depressions within the limestone surface, over an area of at least $3km^2$. This may therefore represent a Late Pliocene land surface indicating that there was little subsequent erosion during Quaternary glaciation.

The occurrence of karstic cave passages and pinnacles along pre-existing joints in the Ulster White Limestone (Simms, 1998), show that it was well cemented and fractured before the eruption of ashes and lavas of the Antrim Lava Group. This was most likely achieved by burial under a pile of Maastrichtian and possibly Lower Palaeocene sediment, subsequently removed by dissolution and erosion.

1.2.7 Implications - Mesozoic-Tertiary Tectonics

From the fragmentary stratigraphic record of Mesozoic-Tertiary rocks, it appears that Ireland has experienced combinations of surface uplift, exhumation and/or periods of non-deposition post-Hercynian times (Bulat & Stoker, 1987; White, 1988; Hillis, 1992; Green *et al.*, 1993; Rohrman *et al.*, 1995; Rohrman & van der Beek, 1996; Japsen, 1997; White & Lovell, 1997; Clift *et al.*, 1998). In the Ulster basin, post-Permian gaps in the record include the (1) upper-Lias to lower-Mid Cretaceous, (2) Late Cretaceous to Early Palaeocene, (3) Late Eocene to Middle Oligocene, and (4) the Miocene to Quaternary.

1.2.7.1 Present-Day Landscape

The occurrences of Mesozoic, and to a lesser extent, Tertiary deposits in the Ulster basin, Kingscourt, Wexford and Ballydeenlea outliers, and the numerous other small Mesozoic-Tertiary deposits scattered over the length and breadth of Ireland, have produced lively debate about Mesozoic-Tertiary palaeogeography. George (1967) and Mitchell (1980) stressed the importance of Tertiary tectonism, which they believe played a major role in shaping much of the present-day landscape in Ireland. Dewey & McKerrow (1968) and Davies (1970) showed that the drainage in the Conemmara and Leinster areas respectively bears little resemblance to the geological structure, and

therefore, implies that the rivers have been superimposed from a younger, eroded cover (chapter 5) on to older crystalline basement rocks.

On the other hand, many authors believe that the present-day landscape (figure 1.5) is a fossilised palaeotopography inherited from the Hercynian orogeny (McCaffrey & McCann, 1992; Naylor, 1992). Naylor (1992) postulated that Ireland has most likely been positive during Permo-Triassic times. This evidence was based on the lack of reddened weathering surfaces on the underlying Carboniferous surfaces (e.g. which occurs at Kingscourt), and the fact that most of the onshore deposits are associated with major faults. But, if significant denudation of Permo-Triassic strata did occur, it is equally feasible that any reddened surfaces were removed by erosion.

The Late Cretaceous was a time of maximum global sea-level with average levels estimated to be 220m (Haq *et al.,* 1987) to 300m (Vail *et al.,* 1977) higher than present-day values. The probability that much of the Irish Plain was blanketed by a variable Late Cretaceous chalk cover is an acceptable assumption to most authors (e.g. George, 1967; Mitchell, 1980; Naylor, 1992; Cope, 1994, 1998). However, the extent to which the chalk onlapped and overstepped positive massifs is highly conjectural. Nevertheless, the wide occurrence of pieces of flint in glacial deposits across Ireland lends credence to the idea of a former, extensive chalk cover blanketing most of the country. Similarly, Lower Palaeozoic roof pendants are still present on parts of the of the Leinster batholith, e.g. on Lugnaquillia, the highest mountain in the region (chapter 5). This is probably due to an earlier Mesozoic protective cover of Jurassic and Cretaceous strata which has subsequently been eroded during the Tertiary (e.g. Davies, 1970).

The geological map of Ireland gives a first order impression of the time-integrated denudation of Ireland since the end of the Palaeozoic (figure 1.5). Crystalline and metasedimentary basement of Dalradian and Lower Palaeozoic rocks have emerged from a regional Carboniferous cover in the NW of Ireland from Donegal to County Galway. In SE Ireland, the Leinster Massif is composed of Caledonian granites intruded into Lower Palaeozoic metasediments. This massif was partially unroofed in the Late Devonian to provide detritus for the Munster basin, and again in the Late Triassic to Mid Jurassic to feed basins in the Celtic Sea. The form of the present-day topography

also strongly suggests uplift during the Tertiary, e.g. the local presence of schist roof pendants on the Lugnaquillia pluton (chapter 5) demonstrates that the pluton is currently exposed close to its upper surface. The highest topography occurs around the periphery of the island. With the exception of the Mourne Mountains, the oldest rocks underlie these elevated areas.

1.2.7.2 Denudation Events

Published AFT modelled results are consistent with episodes of cooling and denudation during two intervals: Late Cretaceous to Early Tertiary, and Miocene to present (Green *et al.*, 1993; McCulloch, 1993, Keeley *et al.*, 1993; McCulloch, 1994; Green *et al.*, 1999). Recent work by the "Tertiary Uplift of Ireland Project" (TULIP) at the Geology Departments of Trinity College Dublin, and Imperial College London, confirm that an early Tertiary cooling event has occurred over much of Ireland.

Supportive evidence of significant Tertiary erosion is deduced from the analyses of vitrinite reflectance, spore coloration, and sonic velocity studies (Keeley, 1995; Corcoran & Clayton, 1999; Rowley and White 1998; Allen *et al.* 1999). These datasets have been interpreted to show that southern and eastern Ireland and the Irish Sea region have experienced between 0.5km and 2km of post-Carboniferous denudation. For example, spore coloration data from a small onshore outcrop of Middle Jurassic Colbond clay (near Cork) and the adjacent Carboniferous rocks, indicate that ~2km of section is missing (Roberts, 1989). Additionally, Evans & Clayton (1998) estimate that c.1km of section is missing from the Ballydeenlea outlier.

1.3 Offshore Stratigraphic Record

As noted earlier, direct observation of Mesozoic-Tertiary tectonics onshore in Ireland is severely hampered (see Naylor, 1992, for references) by the limited occurrence of suitably aged rocks. Consequently, our understanding of onshore Mesozoic-Tertiary tectonics for much of the country is currently lacking. This is in marked contrast to the offshore areas (figure 1.6) which frame mainland Ireland, where a large literature exists on the Mesozoic-Tertiary geological history.

1.3.1 Irish Sea Region

The Irish Sea region consists of many fault-controlled half-grabens, filled with 3-5km of Permian to Lower Jurassic sediments (Shannon, 1991a) that extend down the length of the Irish Sea (figure 1.6). The basins are bounded by mainly NE-SW and NW-SE faults, which produce strong gravity lineaments (figure 1.7). The mainly syn-rift stratigraphy consists of Permo-Triassic terrestrial clastic sequences (Shannon, 1991a; Naylor, 1992). Stretching factors for the Permo-Triassic extension event, based on the McKenzie (1978) model, display relatively low β values between c. 1.1 to 1.3 (Brodie & White, 1995).

In the Kish Bank basin, seismic interpretations from well data suggests the presence of over 3km of Permo-Triassic rocks (Jenner, 1981; Broughan *et al.,* 1989; Naylor *et al.,* 1993). Liassic rocks have been sampled from the seabed at the northern margin of the basin. Broughan *et al.,* (1989) suggested that there may be as much as 2.7km of Liassic section preserved in the hangingwall of the Bray Fault zone of the Kish basin (chapter 4). The Mochras borehole on the Welsh coast encountered 1.3km of Liassic sequences in the Cardigan Bay basin (Woodland, 1971). Seabed coring on the flank of the St George's Channel basins also encountered Liassic shales and limestones (Whittington *et al.,* 1981).

The Liassic sequences in the Irish Sea region and Ulster basin are uniformly fine-grained and thin-bedded, suggesting quiet marine conditions persisted throughout the Early Jurassic (Naylor, 1992). The Middle Jurassic appears to be absent in most of the Irish Sea basins, with the exception of the Cardigan Bay basin, where drilling encountered about 760m of Middle Jurassic mudstone with subordinate limestone beds conformable with an almost complete lower Lias succession (Barr *et al.,* 1981).

There are no known occurrences of Cretaceous rocks in the Irish Sea basins, with one notable exception. Over 1km of Upper Cretaceous rocks unconformably succeed Lower Cretaceous rocks in the western part of the Bristol Channel basin. However, these thin eastwards and are completely absent in the eastern part of the basin (Shannon, 1991a; Naylor, 1992).

1.3.2 Northern Flanks

The Rathlin basin forms the offshore extension of the Ulster basin and extends along a Caledonian trend northeastwards towards Kintyre (Scotland). The preserved stratigraphy consists of thick continental Triassic sequences overlain by a marine transgressive Rhaetian package. But, Mid to Upper Jurassic and Cretaceous sediments are generally absent (McCaffrey & McCann, 1992). However, a thin basal layer of sand and chalk unconformably overlies eroded Mesozoic and older rocks. This sequence correlates with the Hibernian Greensand and Ulster White Limestone of the onshore Ulster basin and demonstrates a pre-Late Cretaceous erosional event. The subsequent removal of much of this chalk layer records Tertiary denudation.

1.3.3 Celtic Sea Basins

The Celtic Sea region is underlain by several discrete rift basins (Tucker & Arter, 1987; Rowell, 1995) and includes the North Celtic Sea (largest), the South Celtic Sea and the Bristol Channel basins. These pass northeast into the Irish Sea and St George's Channel basins, and to the SW the Fastnet and Goban Spur basins.

Cretaceous chalk subcrops over much of the present-day sea floor (Naylor & Shannon, 1982). Gravity gradients and fault patterns, derived from seismic studies, show a general NE-SW Caledonian trend (figures 1.6 & 1.7). A subordinate NW-SE trend also exists and may represent present-day active structures, similar to the Codling Fault (figure 1.7), or they may represent relic transform fault zones (Petrie *et al.,* 1989; O'Reilly *et al.,* 1991).

In general, Triassic rocks are unconformable with Palaeozoic basement. A thick but variable Lower-to-Middle Jurassic section (Millson, 1987) unconformably overlies Triassic sequences. However, this unconformity is restricted to the margins of the basin and dies out towards the centre of the basin. Upper Jurassic lacustrine sequences occur on the northern margin of the North Celtic Sea basin (Millson, 1987).

The Lower Cretaceous rocks are divisible into a lower continental sandy section that gives way to a marine sand and shale sequence. Deposition of chalk began in

Cenomanian times and reaches thicknesses of over 1km (Naylor & Shannon 1982). These rocks conformably overlie Jurassic sequences in the centre of the basin. Subordinate amounts of Tertiary sediment are restricted to an elongate outcrop in the eastern part of the North Celtic Sea basin, and attain a maximum thickness of about 800m (Naylor, 1992). Major inversion along WSW-ENE structures also caused unconformities in the central portion of the North Celtic Sea basin (Tucker & Arter, 1987; Murdoch *et al.*, 1995; Menpes & Hillis, 1995) during the post-Maastrichtian to pre-Middle Eocene interval.

1.3.4 Porcupine Basin

The main depocentre of the west coast of Ireland is the Porcupine basin. The northern part of the basin lies approximately 150km west of Ireland, has an average width of about 100km, and extends over 300km to the south (figure 1.8). It is asymmetrically divided in two by an E-W ridge at latitude 53°N and comprises the Northern Porcupine basin (NPB) in the north and the much larger Main Porcupine basin (MPB) to the south. Bathymetric depths range from <500m in the NPB to depths >2,700m in the MPB. An ESE trending break in the gravity and magnetic data, at 51°30N and through the basin at approximately 51°N, is known as the Clare lineament (figures 1.8 & 1.11) and is postulated as a predecessor of the Charlie Gibbs Fracture Zone (Naylor & Shannon, 1982).

The basin has approximately 10km of post-Carboniferous sediments in the centre, thinning to about 2km on the margins (Naylor & Anstey, 1987; Croker & Shannon 1995). Triassic to Cretaceous syn-rift deposits is unconformable with a mainly eroded upper Palaeozoic surface. The syn-rift package is onlapped and overstepped by post-rift thick Upper Cretaceous chalks, which are ~1km thick along the basin axis of the MPB. This passes up into a more or less continuous package of Palaeocene to Pliocene sediments (Naylor & Anstey, 1987) in the MPB. However there is a stratigraphic break at the top of the Upper Cretaceous chalks in the NPB (chapter 8)

1.3.5 Slyne/Erris Troughs and Donegal Basin

To the north of the Porcupine basin, the Slyne and Erris troughs and the Donegal basin form a chain of relatively complex, narrow sedimentary depocentres which run nearly parallel to the Irish coast (figure 1.6). In the Slyne Trough, well 27/13-1 (figure 1.9) has proven thick shallow marine and estuarine sequences of Middle Jurassic age (Trueblood, 1992). The Slyne Trough consists of three sub-basins, which are separated from each other by a variety of tectonic structures. Much of the Jurassic section in the Slyne Trough appears to be preserved. Scotchman & Thomas (1995) have used apatite fission track data and vitrinite reflectance profiles to model an approximate uplift and erosion event, with a maximum of 1.6km of rock being removed, and inferred timing of 80-60Ma (Campanian-Danian).

The Erris and Donegal basins (figure 1.6) are still relatively unexplored with only two wells having been drilled by Amoco in each basin (Tate & Dobson, 1989). Well 19/5-1 was drilled in the Erris Trough (figure 1.9) and encountered 288m of Permo-Triassic continental sequences resting conformably on an evaporitic Upper Permian sequence. Well 12/13-1A was drilled in the Donegal basin (figure 1.9) encountering 655m of Permo-Triassic sequences. A Liassic section was also encountered in both wells, but the upper parts of the Liassic are missing and are unconformably overlain by Cretaceous and/or Tertiary sequences (Tate & Dobson, 1989; Naylor, 1992). Both areas are believed to have experienced a similar history to the Slyne trough during the Jurassic (Trueblood, 1992). But, an erosional event during the Early Cretaceous has stripped away the upper Liassic sequences from both the Erris Trough and Donegal basin (Trueblood & Morton, 1991). It has been suggested that the location of these basins may be related to reactivation of splays from the Great Glen Fault zone (e.g. Naylor & Shannon, 1982; Ziegler, 1982; Shannon, 1991a).

The Early Tertiary unconformity that is apparent in the North Porcupine and Ulster basins, is not recognised in these basins. However, it is likely that a major unconformity exists beneath the Mio-Pliocene due to a Neogene uplift event of the NW flanks of Ireland and the adjacent continental shelf (Stoker *et al.* in press).

1.3.6 Rockall-Hatton Troughs

The Rockall-Hatton Troughs are situated NW of the Slyne-Erris troughs at the edge of the continental margin (figure 1.6) and is ~200km wide (Roberts 1989) with water depths >2km (figure 1.10). The Rockall Trough underwent significant extension during rift phases in the Jurassic, the Cretaceous and probably the Permo-Triassic. The Hatton basin, however, experienced less rifting in the Jurassic and Cretaceous. The Rockall-Hatton troughs have not been drilled in the Irish sector, but Shannon *et al.,* (1995) suggested that the troughs may contain up to 6km of Upper Palaeozoic to Tertiary aged rocks. Well 132/15-1 in the British sector penetrated Lower Cretaceous sediments resting with a pronounced angular unconformity on crystalline basement (Musgrove & Mitchener, 1996) and demonstrates that the flanks of the Rockall Trough have experienced considerable erosion prior to Early Cretaceous onlap. Seismic refraction models demonstrate an asymmetric crustal profile in the Rockall Trough (Roberts *et al.,* 1988; Makris *et al.,* 1991) and implies that the basins were probably formed by the transtensional reactivation of deep-rooted Caledonian structures.

1.3.7 Implications

The development of Ireland's offshore basins was largely a consequence of episodic extension (in the context of Pangean rifting) of the North Atlantic (Roberts, 1989; Shannon, 1991a; Rowell, 1995). Caledonian basement structure and possibly Hercynian structural fabrics primarily controlled extension. These inherited structures would have played a major role during subsequent inversion events, particularly in the Irish and Celtic Sea regions (chapter 4), aiding denudation of section. These offshore events would most likely have reactivated similar structures onshore particularly during periods of cooling as indicated by AFT analysis (chapters 7 & 8).

1.3.7.1 Extensional Events

Deep seismic profiles indicate moderate stretching with little significant attenuation of the continental crust under the Irish Sea region (Shannon, 1991a). The crust beneath the Slyne-Erris-Donegal troughs has also experienced minimum crustal attenuation (Makris *et al.,* 1990). This is similar underneath basement highs in the Celtic Sea region

(Shannon, 1991b), although, significant thinning has occurred under depocentres, e.g. the crust is estimated to be about 30km thick beneath basement highs and as thin as 19km under the North Celtic Sea basin (McGeary *et al.,* 1987). Seismic and gravity models show a stretched and thinned continental crust beneath the Rockall trough (Smyth, 1989). In the Porcupine basin, deep seismic profiles have imaged the Moho and show that the continental crust has been considerably thinned in the south of the MPB with thicknesses <10km (Naylor & Shannon, 1982).

Two main episodes of post-Carboniferous rifting are recognised in the basins of the west of Ireland and the Celtic Sea region. Rifting occurred during Triassic, and Late Jurassic to Early Cretaceous times (Shannon, 1991a), though, rifting occurred in the Porcupine slightly earlier than the Celtic Sea region. Each event is associated with a thermal subsidence phase. In the Irish Sea region, only the Triassic-rifting event is recorded. It is possible that a second rifting event also occurred but subsequent uplift and erosion has removed the syn- and post-rift strata, and cut down as far as the syn-rift package of the first rifting event (chapter 4).

1.3.7.2 Inversion Events

According to the lithospheric stretching model (McKenzie, 1978; Jarvis & McKenzie, 1980), periods of syn-rift stretching are usually followed by an exponentially decreasing post rift or thermal subsidence phase. This appears to be in agreement with the post-rift phases of Permo-Triassic and Late Jurassic extension (Glennie, 1990) which have been documented in the North Sea (Brodie & White, 1995), and other extensional basins throughout NW Europe (Ziegler, 1982). But, fault controlled Permo-Triassic sedimentary rocks, which outcrop near the sea-bed such as in the Kish Bank basin, and at onshore outcrops at Kingscourt, are missing this predicted post-rift subsidence (Jenner, 1981; Naylor & Anstey, 1987; Shannon, 1991a; Naylor, 1992; Shannon *et al.,* 1993; O'Driscoll *et al.,* 1995; Shannon *et al.,* 1995; Vermeulen *et al.,* 1999; Vogt, 1995; Corcoran & Clayton, 1999). Therefore, it is most likely that these basins must have subsided after the main Permo-Triassic rifting phase, and subsequently the post-rift sedimentation has been removed (chapter 4).

Whether or not a second rifting event occurred in the Irish Sea region is highly speculative. However, seismic reflection profiles indicate that the post-rift sequences from the Triassic event are missing (chapter 4). Based on maturation profiles, between 1.5km (Corcoran & Clayton, 1999) and 3km (Jenner, 1981) of section has been eroded from the southern margin of the Kish Bank basin (chapter 4). Therefore, major inversion must have occurred in the Irish Sea region post-Liassic times (Lewis *et al.,* 1992; Cope, 1994; Brodie & White, 1995). Sonic velocity studies (Turner & Phillip, 1998) from compacted sediments in the Irish Sea basins, and apatite fission track samples from drilled wells (Lewis *et al.,* 1992; Green *et al.,* 1993; Green *et al.,* 1997; Green *et al.,* 1999) provide supportive evidence for significant periods of Tertiary cooling and hence exhumation (chapter 4).

Major Mesozoic and Tertiary inversion events are also documented for the Celtic Sea basins (Tucker & Arter, 1987; Menpes & Hills, 1995; Murdoch *et al.,* 1995). The first inversion event occurred during the Mid-to-Late Jurassic and may correlate with the same unconformity in the Ulster basin. The unconformity has been attributed to uplift related to Mid-Cimmerian tectonism (Naylor & Shannon, 1982). In the North Celtic Sea basin, a regional uplift event occurred during the Palaeocene. A second event with basin doming and fault reversal is believed to have occurred during the Oligo-Miocene. Exhumation of Cretaceous chalk is estimated to be as much as 1.1km (Tucker & Arter, 1987; Murdoch *et al.,* 1995). Erosion was most severe in the eastern part of the North Celtic Sea basin where the Cretaceous rocks have been completely removed (Menpes & Hillis, 1995; Murphy *et al.*, 1995).

Minor inversion has been documented for the Atlantic seaboard basins. Rotated fault blocks near the margins of the Porcupine basin are truncated and onlapped by Lower Cretaceous sediments (the Base Cretaeceous Unconformity – BCU). The BCU is probably associated with the initiation of sea-floor spreading in the North Central Atlantic. The unconformity is subsequently offset by faults suggesting extension during the Cenozoic opening of the North Atlantic Ocean (chapter 8).

In the Main Porcupine basin, there is little stratigraphic break at the base of the Tertiary with a more or less continuous succession of Palaeocene to Pliocene sediments (Naylor & Anstey, 1987). However, in the North Porcupine basin there is a stratigraphic break at

the top of the Upper Cretaceous chalks (Tate, 1993; chapter 8), corresponding to that seen in onshore sections in the Ulster basin. In general, the Porcupine basin has subsided due to thermal relaxation during the Tertiary with the deposition of thick Cenozoic sediments. This is supported by AFT data from well 26/28-1 which shows that all samples are presently at their maximum post-depositional burial temperatures (McCulloch, 1993).

Roberts (1989) noted that an antiformal structure in the Porcupine basin of Late Cretaceous-Early Tertiary age which lies directly above Upper Jurassic-Lower Tertiary fault rotated blocks. The age of the inversion can be bracketed between the Eocene and Miocene, e.g. deformation of an Eocene reflector is on-lapped by Miocene strata. Uplift and compressional deformation during Oligocene times is observed in the basins of the southern Main Porcupine, Fastnet, and Goban Spur, consistent with similar structures observed in the western English Channel (Cook, 1987; Roberts, 1989). A pulse of Plio-Pleistocene fan sedimentation and slope propagation in the Rockall Trough also argues for significant denudation and sediment mobilisation (Stoker, 1997) at this time.

In sum, thick Cretaceous chalk exists in the Celtic Sea basins, but to-date, none appear to exist in the Irish Sea basins, with the notable exception of the western part of the Bristol Channel basin (Shannon, 1991b; Naylor, 1992). Thick Mesozoic and Tertiary deposits also occur in the basins of the west of Ireland (see Croker & Shannon, 1995 for references). Therefore, establishing the tectonic and sedimentary framework of these offshore basins during Mesozoic-Tertiary times may facilitate an understanding of how these processes may be manifested onshore.

1.4 Working Hypothesis

The premise, which provided the starting point for this research, is a dextral transform hypothesis (section 1.5). This hypothesis predicts that onshore fracture patterns acted as transforms to offshore extensional basin-bounding faults. Hence, based on the kinematics of the transform system, a change in orientation of the onshore fractures and/or structural fabrics facilitates predictions about the location of areas that would have evolved under conditions of transpression or transtension. Hence, the basic theory of the working transpression model is the reactivation of old Caledonian/Hercynian

fractures. The kinematics depends on orientation and strike swings of these ancient faults. The driving mechanism envisaged is a divergent tectonic setting coupled with plume-head processes (chapter 9).

1.4.1 Basic Theory - Transform Fault Zones (TFZ)

Modern-day extension along the Mid-Atlantic ridge shows that ridges and transform faults lie along the family of great and small circles respectively (figure 1.11). In contrast with oceanic lithosphere, however, the continental lithosphere contains many ancient lines of weakness. This is due to differences in thickness, strength, and a greater, complex and protracted geological history than in oceanic crust. Therefore, continental TFZs deviate from the oceanic TFZ model, and may reactivate suitably oriented fractures.

An example of the complex nature of a continental TFZ can be illustrated by examining the present-day active San Andreas Fault zone. This fault zone developed in Miocene times as the Farallon plate was being partially subducted underneath the North American Plate (NAP), and the Murray Transform fault intersected the trench at c.29Ma (Stewart, 1978), the boundary of the NAP. This resulted in a section of the northwest moving Pacific Plate to come into contact with the NAP. Thus, the sense of movement on the American Plate boundary changed from convergent to a strike-slip transtensional fault zone along an existing fracture network. If such a fracture system did not exist for inheritance, then the fault zone would probably have developed at the transition from continental to oceanic lithosphere on the continental margin, where the crust is weakest (Beck, 1986; Nicholson, 1986).

1.4.2 Reactivation of Fractures

Quantitative experiments have proven that an already fractured rock possesses low tensile and cohesive strength (Davies & Reynolds, 1996). Therefore, rocks may preferentially fail along suitably oriented pre-existing fractures (Appendix 1). Hence, Mesozoic-Tertiary reactivation of basement structures in Ireland would primarily depend on the magnitude of the deviatoric stresses, and the orientation of the fractures to the stress eigenvector (figure 1.12).

1.4.3 Transpression/Transtension

Harland (1971) was the first worker to conceptually describe transpression and transtension, related to oblique relative motions of plates, producing the segmentation and partitioning of oblique plate boundaries into discrete deformational domains. Sanderson & Marchini (1984) derived a succinct mathematical model of Harland's original ideas where they specifically considered constant-volume homogeneous deformation in a vertical zone that was laterally confined and had a fixed basal surface. They developed a scheme in which bulk finite transpressional deformation can be factorised into 2 separate plane-strain components, one a pure shear and the other a simple shear. Transpression is considered as a wrench or transcurrent shear accompanied by horizontal compression and vertical extension along the shear plane (figure 1.13).

Many workers have applied this model to complex continental transform fault zones to facilitate the visualisation of non-coaxial three-dimensional strains, in which the superposition of incremental amounts of strain can be used to model deformation paths and interpret structures in transpressional zones. However, Jones *et al.*, (1997) relaxed the boundary condition of constant-volume. This model permits lateral extrusion of material out of the system and applied this modified model to explain the geometry of structures observed along the Troodos-Mamonia suture zone of SW Cyprus, and to explain mid-Devonian upper crustal deformation in central Scotland.

The curvature of reactivated faults, imposed by existing lithospheric weaknesses, can give rise to alternate zones of convergence and divergence, where the fault geometry causes blocks on either side of the fault to be compressed (transpression) or extended (transtension). For example, the Transverse Ranges of California developed along a portion of the San Andreas Transform Fault Zone, which strikes more westerly than the general NW trend. This produced oblique strike motion resulting in a component of horizontal compression and transpressional uplift (vertical extension), creating relatively high, rugged relief (Cox & Hart, 1986). When curvature is pronounced on a fault, or where one fault terminates and side-steps to a parallel adjacent fault, the curved zone or area separating the ends of the faults will be thrown into a state of tension or compression. Likewise, fractures can be initiated by reactivation of suitably oriented

fabrics, and where there is a change in strike, these fractures will terminate as horsetail structures (figure 1.14).

1.4.4 Structural Template

In Ireland, there is an array of pre-existing fractures inherited from previous deformation events including the Grenville, Grampian, Caledonian, and Hercynian orogenic cycles (O'Reilly *et al.,* 1996). These can be depicted on gravity survey maps. Many gravity maps for Ireland have been produced by the Dublin Institute for Advanced Studies (DIAS) and are useful for revealing large-scale lineaments (figure 1.15) that can be related to geological structures (Readman *et al.,* 1995; Readman et al., 1997).

Rock density tends to increase with depth, therefore, anticlinal folds will generally bring older more, denser rocks to the surface, and synclinal folds will do the opposite (chapter 2). Faults will also bring together rocks of differing densities. The shaded gravity (figure 1.15) and geological relief (figure 1.5) maps highlight the dominant NE-SW (and to a lesser extent, NW-SE) structural grain in Ireland. A subordinate E-W trend occurs in the Munster basin area, and around the northern margin of the Leinster Massif and along the west coast. The gravity lineaments are probably reflecting a combination of Moho depth and major structural discontinuity in the upper crust. It is this structural fabric which is most likely to take up the strain and act as transforms to offshore extension and potentially result in vertical block transpression (chapter 5), i.e. faults acting as transforms and inversion structures, accommodating periods of strike-slip and epeirogenic uplift.

1.5 Dextral Transform Hypothesis

As noted in the introduction, the original aim of this thesis was to test the working dextral transform hypothesis, proposed by W.E.A.Phillips (pers. comm. 1997). Figure 1.16 shows this model with dextral transforms crossing the onshore landmass, linking the extensional basins of the Porcupine with the Irish Sea. This model also shows that the Leinster and Welsh Massifs are uplifted rift margins related to E-W extension in the southern Irish Sea region during Mesozoic-Tertiary times. The northern termination of

this rift system, in the Dublin region, implies that there have been E-W trending dextral transform faults. This coincides with a regional E-W Caledonian-Hercynian structural grain as already mentioned. However, where this strike orients to a less favourable trend then it is likely that the faults will produce transpression or transtension.

1.5.1 Scope of Thesis

Therefore, the original aim of this thesis is to test the TFZ hypothesis by reviewing all the existing literature (chapter 2). Structural mapping on potential transforms was conducted (chapter 3). An onshore-offshore correlation with the Mesozoic Kish Bank basin (chapter 4), and regional correlation with the Irish Sea region and the Lough Neagh-Larne basin was then carried out, based on the results of the structural study. Onshore correlation with the proposed uplifted rift margin, the Leinster Massif, and the identification of a later stress system subsequently led to a broadening of the project aims. This included topographic (chapter 5), LANDSAT lineament (chapter 6) and AFT analysis (chapter 7) of the structural and geomorphological development of SE Ireland during the Tertiary. The regional implications of this are finally addressed using AFT analysis for the entire Irish landmass and offshore correlation with the Porcupine basin (chapter 8) and the major conclusions of the thesis are summarised in chapter 9.

CHAPTER 2 –TRANSFORM MODEL - CENTRAL-EAST IRELAND

2.1 Introduction and Summary

The main aim of this section is to test the transform hypothesis by evaluating the lines of evidence for potential Mesozoic-Tertiary fault zones in Central-East Ireland. The results of a deskstudy show that the presence of relatively warm geothermal springs and anomalously thick unconsolidated deposits appear to be associated with faults. The spatial pattern can be explained by the dextral hypothesis in that transpression and transtension is predicted to occur on NE and NW trending faults respectively. In many cases, both transpression and transtension can occur on a single fault that displays pronounced curvature, e.g. the Southern Boundary fault (SBF). The VLF-R survey shows that the thick deposits may represent pull-apart basins.

2.1.1 Materials and Methods – Desk Study

The area of study encompasses a region of about 4,500km^2 and extends from the town of Balbriggan in the NE to the town of Killeigh in the SW (figure 2.1). A number of large faults traverse this area and are ideal candidates for testing the dextral hypothesis (figure 2.3). The initial desk-study concentrated on compiling all existing data into a Geographical Information System (GIS; using ESRI's ArcView and ArcInfo software) and the compilation of a series of new geo-datasets. Overlaying combinations of all these geo-datasets proved useful for interpreting the spatial patterns between different features. The main aim was to identify areas at the ends of dilation zones, e.g. evaluating the evidence for small pull-apart basins and the occurrence of warm-springs.

Digital Elevation Models & Spatial Grids

In section 2.4, the topography of the study area is analysed by using two spliced together digital elevation models (DEM). Much of the area comprises a DEM (obtained free of charge from the United States Geological Survey) with a spatial resolution of 200m.

However, in the SE of the study area, the DEM has a spatial resolution of 50m and was purchased, under license, from the Irish Ordnance Survey.

In section 2.5, the location of over 3,178 boreholes (GSI, Navan Resources) in the study area were compiled into a GIS point coverage and interpolated onto a continuous grid. This method determines output cell values using a linearly weighted combination of a set of sample points. The weight is a function of inverse distance. The input of sample points was limited to 12, using the nearest neighbour method. The power parameter in the IDW interpolation controls the significance of the surrounding points upon the interpolated value, a higher power resulting in a smaller influence from distant points. The power used in the interpolation of the contours was 2. The output value for a cell using IDW is limited to the range of values used to interpolate, that is, the maximum and minimum values are constrained by the original boreholes. Since the IDW is a weighted distance average, the average cannot be greater than the highest or less than the lowest input (Watson & Philip, 1985). The resulting surface is the best estimate of what quantity is on the actual surface for each location. However, this method will tend to smooth out potential discontinuities in the original data.

In section 2.6, the elevation of bedrock is computed by subtracting the interpolated spatial grid of 'thickness of overburden' from the DEM (of 200m spatial resolution).

Very Low Frequency-Resistivity (VLF-R)

In section 2.7, the results of a VLF-R survey are discussed. This method takes advantage of electromagnetic radiation generated in the low frequency band of 15-25kHz by powerful radio transmitters used in long-range communications and navigational systems. At large distances from the source of transmission the electromagnetic field is planar. The magnetic component (**H**) is horizontal and the electric component (**E**) is perpendicular to this and to the direction of propagation (figure 2.2). A conductor that strikes in the direction of the transmitter (located in England and Norway) is cut by the magnetic vector. This induces eddy currents that produce a secondary electromagnetic field. The Geonics EM16R

measures the ratio of the phase angle between the electric and magnetic fields of this wave (figure 2.2).

The VLF-R method assumes a two-layer geometry and the phase angle will normally be <45°. The EM16R measures only 2 pieces of information, the apparent resistivity and the phase angle. In this situation there are 3 unknown quantities, the apparent resistivity of both layer 1 (ρ_1) and layer 2 (ρ_2), and thickness of overburden. Therefore, one piece of information is missing. If a phase angle of 45° exists anywhere in the mapped area, the apparent resistivity of this reading may be assumed to represent the true resistivity of the overburden. This can subsequently be plugged in as the third piece of information for interpreting the thickness of overburden and bedrock resistivity.

Alternatively, 'vertical electrical sounding' values for the upper layer may be directly measured for the top layer (or, if available, utilising previous resistivity data, e.g. Reynolds (1980) has shown that the average resistivity values in Ireland range between 100-300Ωm). In this study, resistivity of the overburden (ρ_1) was modelled using both the 100Ωm and 300Ωm values. By trial and error, it was assumed that the overburden in the Newcastle area was closer to the 300Ωm value.

Aeromagnetic & Gravity

In section 2.8, the interpretation of aeromagnetic and gravity maps are assessed. The data utilised for the aeromagnetic survey was obtained in 1979. The flight line direction was NNW and the tie line direction was ENE. The NNW lines are at a spacing of 1km, and the tie-lines are 10 kilometres apart. Station measurements are at approximately 60 metres (Max & Inamder, 1983). Gravity measurements for Ireland were taken over a number of years by DIAS and the Geological Survey of Northern Ireland (e.g. Murphy, 1952, 1974; Carruthers *et al.,* 1987). The data coverage is approximately 4.2 stations per $10km^2$ and the accuracy is estimated to be generally better than 0.2mGal.

The aeromagnetic data were obtained in digital format from the Geological Survey of Ireland (Deepak Inamder). A 1-mgal bouguer gravity contour map (Dublin Institute of

Advanced Studies) was also digitised. The interpolation of both geo-datasets, to form spatial grids, was conducted using ESRI's Triangulated Irregular Network (TIN) method. The TIN method is useful for modelling irregularly spaced points by using a series of triangles. The denser the points the smaller the triangles and vice versa. Hillshading TIN surfaces is also useful for highlighting the main trends, and the intensity of illumination gives an impression of the horizontal rate of change. For example, a large flattish triangle would represent an area where there is little change in the gravity/magnetic field.

2.2 Geology – Study Area

In this section, evidence for Mesozoic-Tertiary transform fault zones is being assessed despite the fact that the youngest rocks in the area of study are Namurian in age. Hence, the lack of stratigraphical resolution requires models for testing, and, in this case, the dextral transform hypothesis as outlined in chapter 1. The model predicts that pre-existing fractures may have reactivated during Mesozoic-Tertiary times. Therefore, a brief outline of the geological history (figure 2.3) is necessary to facilitate an understanding of how the movements may manifest themselves in the geomorphology and hydrology of the area.

2.2.1 Basement

Basement rocks only outcrop in the NW of the Central Midlands plain but occur as fragments in volcanic rocks, near the centre of the plain (Strogen, 1973). These rocks are Pre-Cambrian granulitic gneiss and form basement north of the Iapetus suture zone. To the south of the suture, basement rocks are mostly of amphibolite facies (Kennan *et al.*, 1979; Brown & Williams, 1985). The depth to Pre-Cambrian basement underneath the Central Midlands plain is estimated to be ~4km. This figure is derived from the interpretation of a regional NE-SW seismic profile where a *Vp* (velocity of propagating seismic waves) of c.6km sec^{-1} has been interpreted as representing Pre-Cambrian gneiss (Jacob *et al.*, 1985).

2.2.2 Lower Palaeozoic

Lower Palaeozoic rocks in the study area form part of the Leinster Massif (Brück *et al.*, 1974) and the oldest metasedimentary rocks occur east of the Leinster batholith, namely the Lower-Middle Cambrian aged Bray Group. Lower Palaeozoic rocks also outcrop on the Howth peninsula (chapter 3) and at Portrane and Lambay.

During Devonian times (Phillips *et al.*, 1976), rocks of the Bray Group were thrusted to the NW over the slightly younger Tremadoc to Llanvirn aged Ribband Group. The Ribband Group rocks occur on both sides of the batholith and are in fault contact with the younger Llandovery-Ludlow Kilcullen Group to the west. (The geology of these rocks is described in chapter 5.) Lower Palaeozoic inliers also occur within the Midlands plain. These include the Chair of Kildare and the Sion Hill inliers. The Chair of Kildare is a small NE trending inlier of 11km by 1.5km. The inlier is thrusted over Carboniferous limestones on the northwestern margin (the Kilmeage fault) and the southeastern margin is unconformably overlain with Old Red Sandstone (ORS) conglomerates and sandstones. The sequences consist of shales of Llanvirn age overlain by andesitic lavas and tuffs of Caradoc age with a cap of Ashgill limestone and shale (Parkes & Palmer, 1974). The Sion Hill inlier occurs in the NW of the study area. This relatively small inlier consists of Silurian greywackes, which are unconformably overlain by thin sequences of Late Devonian to Early Carboniferous terrestrial ORS. At Portrane and Lambay, north of Dublin, Caradoc andesites and tuffs are overlain by Ashgill shales and limestones. These rocks pass up into Silurian greywackes.

Structure

As figure 2.3b shows, Central Ireland is divided by the ~NE-SW trending Iapetus suture, where an abrupt change of structural style in the Lower Palaeozoic rocks is evident (Phillips, et al., 1976). The strike of Caledonian folds and cleavage is E-W near the east coast in the Dublin Bay area. South and west of Dublin, the strike changes to NE-SW. This trend demarcates an important structural boundary.

2.2.3 Leinster Batholith

The Leinster batholith is ~1500km^2 (chapter 5) and is composed of five more or less simultaneously emplaced dome-like units (Brindley, 1973), with the "Northern" and smaller "Upper Liffey Valley" plutons located in the area of study. The composition is predominantly adamellite (Brindley, 1973) and the margins are concordant with the schistosity in the Lower Palaeozoic country rocks (chapter 5). It is believed that this reflects a general syn-tectonic NE-SW grain, which exerted strong control on the emplacement of the batholith, along Caledonian sinistral shear zones. However, more recent work shows that parts of the batholith were emplaced in a regional sinistral extensional regime parallel to the pluton as a series of south-east dipping sheets (M.J.O'Mahony pers. comm. 1999). O'Connor and Brück (1978) obtained a Rb-Sr whole rock isochron age of 404 ±24Ma from the northern margin of the batholith. In view of the uncertainties in interpreting this 'age', there is a need for U-Pb method to be used with abraded zircon crystals.

Emplacement of the batholith produced both a structural and thermal aureole in the Lower Palaeozoic country rocks (chapter 5). The thermal aureole varies in width from 0.5 to 3km. The main contact metamorphic minerals are andalusite, staurolite, almandine-spessartite and biotite (Stillman *et al.*, 1978). The structural aureole extends for approximately 5km from the granite contact (Brück & Reeves, 1976). The sequence of deformation events shows that the emplacement of the batholith post-dates the development of D1 structures, as it truncates a suite of cleaved dolerite dykes (Brindley, 1956), near the town of Tallaght (Co. Dublin). However, the batholith has been affected by a second Caledonian deformation (D2) phase, which is manifested in the form of WNW trending cleavage with minor intrafolial folds (F2). The SE margin of the batholith is also deformed by the East Carlow Deformation zone (McArdle & Kennedy, 1985), which was synchronous with granite intrusion (chapter 5).

2.2.4 Carboniferous Rocks

Lower Carboniferous (Dinantian) sequences were deposited on an angular unconformity with Lower Palaeozoic rocks. A Carboniferous marine transgression moved northwards over the area during the Dinantian period. At this time, Ireland lay close to the equator. Variable basal Carboniferous transgressive sequences unconformably overlie a Devonian alluvial peneplain (Sevastopulo, 1981). These rocks are of early Courceyan age and include basal sandstones grading up into limestone and shaley calcareous mudstone (chapter 3). This gives way in the late Courceyan to the deposition and formation of Waulsortian mudbank limestones. Marine conditions persisted through the Chadian to Brigantian stages with the deposition of dark basinal limestones and shales, although shallow water limestones and ramp sequences occur towards basement highs.

Asbian aged limestone turbidites occur close to the Southern Boundary fault (SBF), which is in contact with the Leinster Massif. The turbidites contain fragments of limestone and their orientation indicates northward movement down a palaeoslope into a depocentre, namely the Dublin basin (Nolan, 1986). Against the SBF, blocks of granite (Montgomery, 1864-67; Ball 1888) and Silurian basement (chapter 3) occur within the basin, indicating that the fault was syn-depositional during Lower Carboniferous times. A series of smaller, interconnected basins developed with north-dipping faults dominant in the south and south-dipping faults in the north (Johnston *et al.,* 1995).

During the Late Carboniferous (Silesian), the deposition of turbidite facies of Namurian sediments occurred. The rocks consist of basinal shales, limestones and thin sandstones, conformable with the underlying Dinantian sequences (Sevastopulo, 1981) and are preserved in the NE part of the area of study (near the town of Trim).

Carboniferous aged volcanics occur in the Central Midlands plain, the most prominent of which occurs towards the SW of the study area (figure 2.3), Croghan Hill (Co.Offally). The main texture and composition of the rocks are coarse vitric tuffs and ankaramite lavas. Volcanic clasts also occur in the adjacent carbonate rocks, which exhibit geochemical

affinity with the main body and are Arundian in age. In addition, many thin and very fine-grained tuff bands have been encountered within the Lower Carboniferous rocks in boreholes (Counties Meath, Westmeath and Longford).

Structure

Local tectonism in the Dublin basin occurred during the late Chadian-early Arundian and early Brigantian stages, shown by low angle unconformities recognised at Lane (Co. Dublin), and at Newcastle (Co. Dublin), which lies towards the SE of the study area. The unconformity cuts down into older Courceyan and Chadian horizons (Nolan, 1986). The basin was subsequently inverted during Hercynian (Late Carboniferous-Early Permian) times. The rocks have endured a relatively high degree of deformation for an area so far north of the Hercynian front (Sevastopulo, 1981).

The pronounced swing in the structural orientation of folds is apparent (figure 2.3). The fold axes trend ~ENE-WSW, near the coast, but change to a regional NE-SW trend ~5km inland. The intensity of folding is also highest where the fold axes are ~ENE-WSW. Nolan (1986) suggested this strike swing is due to a clockwise rotation of σ_1, which has a NW-SE orientation inland and rotates to a ~N-S orientation towards the coast. However, this change in strike can also be observed in Caledonian rocks where Hercynian deformation is minimal (W.E.A. Phillips, pers. comm. 2000), therefore, it is likely that this strike swing is structurally controlled.

The close parallelism of Hercynian and Caledonian strike indicates that reactivation of Caledonian structures such as shear zones occurred during Hercynian deformation with the reactivation of basement fractures producing dextral transpression on post-Dinantian ENE shears. These shears attain widths of several kilometres and are characterised by en-echelon vein arrays and anticlockwise transection of folds by weak stylolitic cleavages (chapter 3). Conjugate NNE sinistral faults and shear zones are consistent with a NNW-SSE maximum horizontal compression, which is in harmony with regional tectonic reconstructions (Ziegler, 1988). To the south and west of the study area, this simple pattern is complicated by rigid basement blocks, which have experienced very little deformation.

Some of these blocks are up to 50km across (the Nenagh block) and are bounded by corridors of shear zone deformation (Sanderson *et al.,* 1980; Coller, 1984).

2.2.5 Quaternary

Much of the study area is now blanketed by a thick but variable Quaternary glacial cover of poorly drained tills. These deposits were formed during the Midlandian glaciation (c.50,000-10,000 BP) and are dominated by moraines, kettle holes, eskers and kames. The glacial landforms are believed to be the product of two interstadials and three stadials (Mitchell, 1977). In the SE of the study area, the NW flanks of the Wicklow Mountains forms the southern limit of the Late Midlandian ice (Farrington & Mitchell, 1973; Synge, 1979; Cohen, 1979). The landforms in this area are the products of a large glacial lake (McNabe, 1985), Lake Blessington (24km by 5km). The Blessington moraines accumulated in a high energy, ice-marginal delta environment with delta progradation and coarsening-up glaciolacustrine sediments. In the Liffey Valley, extensive terraces formed as the ice margin wasted up-valley (McNabe, 1985). Kame and kettle sequences and eskers also occur in the study area (Warren, 1985).

2.2.6 Mesozoic-Tertiary Tectonism

As illustrated in chapter 1, tectonic processes (onshore and offshore) have effected areas of Mesozoic-Tertiary rocks. As a corollary, the Central Midlands plain have also probably experienced similar deviatoric stresses. Unfortunately, the youngest rocks are of Namurian age. In addition, the very low relief of the region and subsequent glacial deposits inhibit direct observation of the bedrock morphology and the dating of fault gouge.

The implication of the dextral hypothesis is that faults have been reactivated as transforms. As figure 2.3 shows, the southern boundary fault is of considerable length (~100km including possible correlation westwards). The fault extends from Dublin bay in the NE of the study area, and the orientation is ~NE-SW to ENE-WSW. This changes to an ~E-W trend ~25km west, near the town of Newcastle (Co. Dublin). The fault then side-steps in a

right lateral sense and continues ~20km westwards on a WNW-ESE trend. The tip-line of the original strand of the fault terminates with horse-splays, just SW of Newcastle (figure 2.3). Therefore, the dextral model would predict this area as being an extensional 'jog' with the formation of a possible pull-apart basin.

2.3 Faults and Warm Springs

The Geological Survey of Ireland (GSI) and "Chevron Mineral Corporation of Ireland and Ivernia West plc" solid bedrock 1:100,000 series geology maps (sheets 16 & 15 respectively) were used for digitising and compiling a GIS line coverage of mapped faults in the study area. The recognition of known faults on GSI solid geology maps is mainly based on sporadic outcrops from coastal sections, quarries, road-cuttings, and indirect observations from boreholes and geophysics (as mentioned in the introduction). The main trend of faults in the study area is NE-SW and, to a lesser extent, NW-SE (figure 2.4). There are also a series of NNW trending faults, e.g., NW Dublin and SW of Newcastle (Co. Dublin) which show associated warm springs and thick overburden sections.

The location of warm springs in Leinster were compiled into a GIS database. In total, Minerex Limited (1981) documented eighteen warm springs. The vast majority of the springs are located in Counties Dublin, Kildare, and Meath (figure 2.5). The notable exceptions being well 1017W in County Laois and five warm springs in the Province of Munster. Two additional springs were added in this study, including the Trinity College Dublin (TCD) and Newcastle springs (W.E.A.Phillips pers.comm., 1998).

During the period of May 1981 to January 1983, Minerex Limited (Burdon & Burns, 1983) recorded regular observations of warm springs. Cold springs of ambient temperature were also monitored as benchmarks for comparison with the warm springs. As figure 2.6 shows, the average temperature drop for 13 warm springs was 0.48°C from summer 1981 to winter 1981/82, and the average rise was 0.29°C from winter 1981/82 to summer 1983. The average fall in temperature for all 16 warm springs was 0.71°C from summer 1982 to the first three months of the winter of 1983.

The seasonal variation of the temperatures of warm springs is a function of ambient temperature (figure 2.6a). However, many of the springs were warmer than the ambient temperature (Bordon & Burns, 1983) during all seasons, and show very small deviation from their mean temperature (figure 2.6c). Therefore, much of the heat must be a function of deep ground water circulation and heat flow through fracture systems. As figure 2.5 shows, many of the warm springs are associated with known faults, e.g. wells 1002W, 1003W, 1004W, 1005W, 1007W, 1009W, 1013W, 1015W and the Newcastle well. It is highly likely that the 7 other wells are also closely associated with, hitherto, unidentified fracture systems. Hence, warm springs may be a good proxy indicator for identifying relatively young, reactivated fracture systems. This is because the fractured rock would increase permeability and permit the flow of water to deep levels in the upper crust.

2.4 Digital Elevation Models - Topography

Much of the Central Midlands is an area of relatively low elevation and is on average ~50m above sea level (asl), with the exception of the high ground of the Wicklow Mountains (Leinster Massif) to the SE (chapter 5) of the study area. West and N of the mountains, the landscape is of gently rolling and low-lying relief (figure 2.7) with the small exception of Croghan Hill, which reaches a maximum height of ~231m asl. The highest ground in the Leinster Massif is the Lugnaquillia Mountain, which attains a maximum height of 925m (chapter 5). However, in the study area, the Kippure Mountain forms the highest elevation at 742m. The topography of the Leinster Massif is discussed in great length in chapter 5 and will not be considered further in this section. In essence, the area of study is of low elevation and relief, with bedrock features masked and subdued by a variable but continuous blanket of glacial deposits. Therefore, tectonic structures cannot be generally inferred from the form of the landscape.

2.5 Thickness of Overburden

The location of over 3,178 boreholes (data courtesy of the GSI, Navan Resources, Noranda Ltd) in the study area were compiled into a GIS point coverage (figure 2.8) and interpolated

onto a continuous grid. As figure 2.8 shows, there is a large area in the NE and SE with no borehole coverage therefore the interpolation (figure 2.9) or contouring of overburden thickness in these areas has little meaning. In the vicinity of Dublin City and in the SW of the study area, there is dense borehole coverage. Hence, the interpolation in these areas gives a fairly sound representation of sub-surface bedrock morphology.

The average thickness of overburden in the study area, based on the borehole coverage, is 11m with a standard deviation of 8.5m (figure 2.9). Notwithstanding, there are numerous small areas, of about 2 to 10km^2 in extent, with anomalously thick sections of overburden. One particular area (borehole PN-3576-1) about 5km NW of Kinnegad (figure 2.10), penetrated an overburden section 163m thick. However, the boreholes surrounding PN-3576-1 display sections of thickness that are, on average, less than 20m. Therefore, it is likely that PN-3576-1 borehole penetrated a swallow hole in the limestone bedrock, which is typical of karstified areas, such as the Central Midlands plain (Drew, 1982).

2.6 Bedrock of Elevation

Subtracting the overburden and topographical DEM grids produces a bedrock elevation surface (figure 2.11). At Newcastle (Co. Dublin), the elevation in one borehole (CN-NC-08) is below sea level (figure 2.11). In areas where there is dense borehole coverage, and assuming that the topography approximates that deduced from drilling and geophysical data, then it is clear that the underlying bedrock forms a very irregular surface.

2.7 Potential Mesozoic-Tertiary Pull-Apart Basin (?)

Based on the evaluation of all the above evidence coupled with a substantial deskstudy and model predictions, areas of particular interest were selected to test the possibility of the existence of small pull-apart basins. The main purpose was to gather more detailed information on a local scale and to assess whether or not such areas are the products of Mesozoic-Tertiary tectonics. This included the identification of potential pull-apart basins as targets for Very Low Frequency-Resistivity (VLF-R) surveying.

2.7.1 Locality – Newcastle (County Dublin)

A VLF-R pilot survey was undertaken near the village of Newcastle (Co. Dublin) using the Geonics EM16R equipment. The aim of the VLF-R survey was to see whether or not this area was a pull-apart basin as would be predicted by the dextral model. The locality was selected on the following criteria:

(1) thick overburden sequences encountered in boreholes (see below);
(2) occurrence of warm spring;
(3) the strike swing and apparent right-lateral step of a potential transform fault (southern boundary fault);
(4) previous borehole (e.g. CN-NC-08) and geophysical work (Aquitaine Mining (Ireland) Ltd and CSA);
(5) Rothery & Phillips (1983) previously suggested the area may represent the termination of a transform fault zone;
(6) the relatively small extent of the area and easy access.

2.7.2 Previous Survey/Drill Program

Drew (1982) and Jones & Hurley (1983) have previously interpreted a drilling program and geophysical survey of a linear feature in the Newcastle area. Boreholes penetrated a geochemically anomalous linear feature that trends approximately WNW-ESE between Lower Palaeozoic basement and Carboniferous carbonates. The channel appears to continue to the west of Newcastle, and to the east the feature swings towards the SE and appears to terminate. Thick glacial overburden overlies chemically weathered bedrock in the area (figure 2.12). The boreholes and geophysical data were insufficient for Drew (1982) to propose a unifying model to explain the timing and formation of the feature. However, he suggested that the feature might be a karstic channel that has preferentially exploited tectonic weaknesses.

2.7.3 Geology of Survey Area

In the S of the survey area, the underlying sequences are Silurian rocks of the Carrighill Formation (figure 2.13). These rocks are composed of calcareous greywackes, siltstones and shales, and form the footwall rocks of an E-W trending fault, which downthrows the Carboniferous strata to the north. These Carboniferous rocks are known as the Ballysteen Formation and are Courceyan in age. The deposits consist of fossiliferous dark-grey muddy limestones and form the footwall rocks of another sub-parallel E-W fault, which likewise downthrows to the N. These two faults are approximately 500m apart. The hangingwall rocks of this second fault are the Calp Formation, which form dark-grey-to-black basinal limestones with subordinate intercalations of shale (Chadian to Brigantian). They are cross-cut by a series of NW trending faults which were discovered by previous VLF-R, IP and resistivity surveys carried out by Noranda Exploration Ltd .

2.7.4 Boreholes

There are 13 boreholes in the area of interest, exhibiting a wide range of overburden sequences (figures 2.12 & 2.13). The thickest overburden sections are located over the Ballysteen Formation with an average thickness of 48m and the thickest section of 101m was penetrated by well CN-NC-08. Observation of the drill logs shows that much of the section is residual material derived from chemical and physical weathering. The one well in the survey area, CN-NC-04, which penetrated the Lower Palaeozoic (Carrighill Formation), recorded a thickness of section of 36m, suggesting the feature may extend towards the SE. This suggests that the feature may not be a karstic channel, i.e. because rocks of the Carrighill Formation are mostly argillaceous and therefore not susceptible to chemical dissolution.

2.7.5 Resistivity of Lower Layer

Figure 2.14 shows the results of a VLF-R survey just south of Newcastle. Assuming that the lower layer is bedrock, then the following observations of modelled values can be

illustrated. The Lower Palaeozoic rocks show consistent resistivity values (figure 2.14b), with an average of 10,240Ωm. Values for the Ballysteen Formation range from 1,000Ωm to 4,000Ωm, with an average of 2,478Ωm. These values are significantly less than those obtained from the basinal limestone to the north. The resistivity values of these rocks are much greater and range from 1,500 to 30,000Ωm. Three of the stations N of the main fault range from 1,500 to 6,000Ωm, whereas the rest of the stations further N have resistivity values ranging from 4,000 to 30,000Ωm (with the exception of one station which has a value of 1,250Ωm). Therefore, it is likely that there is a fault between these two areas, and there may also be another fault in the far N of the survey area (1,250 to 4,000Ωm). Hence, these values may be an indicator of heavily fractured bedrock, which would probably increase permeability and hence groundwater movements, thus reducing the resistivity of the bedrock.

2.7.6 Modelled Thickness of Overburden

The average thickness of overburden for the Lower Palaeozoic rocks is 4m, with the notable exception of the 150m value (figure 2.14a). This may imply that the 4m value is actually over the linear feature, in which case, the fault contact between the Carboniferous and the Lower Palaeozoic may be further to the S. The overburden thickness on average for the Ballysteen and Calp Formations are estimated to be 15m and 13m respectively. The 100m reading in the north of the survey area is discarded due to proximity of electrical sheep fencing, and hence may have adversely affected the result.

2.7.7 Interpretation and Implications

The linear feature is located mainly between the two main E-W faults. In the E, it appears to swing SE over the Lower Palaeozoics. The modelled thicknesses of overburden show little correlation with the boreholes, although this may in part be due to the depth of the water table. Well logs show that the overburden material is layered. The top layer is mainly glacial deposit, which overlies residual weathered (physical and chemical) material (figure 2.12). Hence, it is likely that the second resistivity layer is at the interface between

these two layers and not bedrock. The weathered overburden also contains high amounts of metallic minerals such as galena, which may also adversely affect the VLF-R results. Therefore, based on the ambiguity of the results from the pilot survey and the many other variables that can influence the VLF measurements, it was decided to discontinue the VLF-R work as a method of testing the dextral hypothesis.

2.8 Regional Geophysics

The regional geophysics is useful for detecting major basement structures. This is interpreted below in light of the dextral hypothesis implications.

2.8.1 Aeromagnetics

In the study area, the magnetic values (population of 68,571) vary from –100nanoTesla (nT) to 9784nT with a mean of 8689nT (standard deviation of 438.8nT). These values represent total magnetic intensity, and the numbers are purely relative to the survey area (figure 2.15). The highest values are located towards the NW of the study area, albeit with smaller areas of high values in the W, associated with volcanics. The lowest values are located in the Dublin Bay area and are related to the Leinster batholith, to the immediate SE (figure 2.16). The main trend in the E of the study area is ~E-W but this changes to a ~NE-SW trend ~5km W of the coast. This resembles the orientation pattern of fold axes (section 2.2), which argues against the notion (Nolan, 1986) that the structural grain is a Hercynian feature.

The magnetic values represent deep basement structure. Depths to the magnetic basement have been estimated from a power spectrum analysis (Brown & Brock, 1983). The depths calculated are c.4km, which is within the 6.0km/sec seismic refractor of Jacob *et al.*, (1985). Locally, the Ordovician volcanic rocks of the Kildare-Portrane axis are picked out. Therefore, the magnetic trend probably represents Pre-Cambrian basement. There is little magnetic variation across the Namurian rocks and this may reflect a uniform thickness and/or low magnetite content. It is likely that the Namurian rocks are of sufficient

thickness to depress the Pre-Cambrian basement to the extent of masking deep, basement structural discontinuities.

2.8.2 Bouguer Gravity Anomaly

The Bouguer gravity anomaly in the study area ranges from −10mGal to 29mGal (population of 1,308,827), with a mean of 9.5mGal (standard deviation of 6.85mgal). The gravity contour map is depicting the long wavelength, representing deep structure (figure 2.16). The low values correlate with the Leinster batholith and the highs with shallow basement brought towards the surface by folding, i.e. the NE-SW anticline, located in the east of the study area, between the Howth peninsula to the south and the town of Rush, to the north. A small gravity low, trending ~NNE and of ~54km^2 in extent, occurs on the NW side of the Leinster batholith between the towns of Rathcoole and Tallaght. This probably represents a finger of protruding granite.

In similar fashion to the magnetic trends and structural fold axes, there is an obvious swing in the gravity field from an ~E-W trend near the coast to a more regional ~NE-SW trend about 5km west. Strong gravity gradients occur in the east where contours show close spacing (figure 2.16). The steepest gradients are associated with the low-density granites of the Leinster batholith and a postulated high-density body on the eastern flanks (Murphy 1989) that underlies the metasediments of the Bray and Ribband Groups. In the NE of the study area, the gravity contours also show relatively close spacing with steep gradients between the anticline to the S and the Balbriggan block to the N. There are a number of Ordovician volcanic centres between these areas i.e., Portrane, the Chair of Kildare, and Lambay Island. Hence, the positive ridge probably reflects Ordovician basic volcanic rocks and Pre-Cambrian basement in the core of a major Caledonian anticline. There is little change in the gravity values between the towns of Enfield and Trim, which is underlain by Namurian turbidite sequences. This indicates that these rocks are fairly uniform in thickness and are probably well compacted.

The NE-SW trend to the SW, between Tyrells Pass and the town of Kinnegad, represents a relative low and is associated with a syncline on geological maps (figure 2.15). This is most likely because the slightly younger rocks may have experienced relatively less compaction due to lithostatic load. All things being equal, this will increase porosity, and thus reduce the overall density of the rocks in comparison with more compacted sequences, which form cores of major anticlines, i.e. the Kildare anticline. Unconsolidated sediments, i.e. near the town of Kinnegad, Co. Meath (figure 2.16), may also therefore contribute to the low.

2.8.3 Low Bouguer Anomalies in the Central Midlands plain

During a regional gravity survey, Murphy (1962) noticed some unusually low Bouguer gravity values in Counties Westmeath, Offaly and Meath (figure 2.17). He re-surveyed the areas with a tighter spacing of stations and discovered a series of intense anomalies of ~1km^2 extent. All of the anomalies were negative, with the lowest value of –6.4mGal being recorded, and gradients of up to 9mGal km^{-1}. Furthermore, the majority of the anomalies are aligned on a NE-SW azimuth, which are ~115km in length. The anomalies were modelled using Bott & Smith's (1958) theorem and concluded that each anomaly had a mass of 0.3gm cm^{-3}. Murphy (1962) attributed the cause of the anomalies to solution cavities in the underlying limestone bedrock, which he speculated to be filled with water or rock debris and/or gravels and of hydrothermal origin. This appears to be the case at Kinnegad and may represent either a karstic depression, a small pull-apart basin or a buried river channel.

2.8.4 Geophysical Models

As noted above, Murphy (1950, 1952, 1962) was the first to discover the presence of NE-SW trending, long wavelength gravity and magnetic anomalies, and the numerous small Bouguer anomalies in the Central Midland's plain. Brown & Williams (1985) and Williams & Brown (1986) interpreted these NE-SW trending anomalies as horsts of Ordovician volcanic rocks (highs) beneath the intervening grabens, filled with Upper

Palaeozoic sediments (lows). They postulated that the late Caledonian NE-SW trending folds have substantial volumes of volcanic rocks in the cores, which were exposed during Devonian peneplanation. Differential subsidence then occurred during Dinantian times, which lead to relatively thick deposition of Carboniferous aged carbonates in the troughs. The occurrence of strong gradients and faulting at the edges of the geophysical ridges and troughs is cited as further evidence for this, and the geodynamics controlling the formation of these features was the Caledonian orogeny, and subsequent subsidence which they attributed to Hercynian plate-margin processes. Woodham & Barton (1992) produced a series of second vertical derivative gravity maps which they believe are in harmony with Williams & Brown's (1986) interpretation. In addition, exploration drilling has confirmed the ridge and trough geometry of the Carboniferous in the Irish Midlands (Andrews, 1992). However, as Johnston *et al.* (1995) pointed out, some of the Lower Palaeozoic inliers do not match this interpretation of Williams & Brown (1986), nor do the thickness, form and variation of the upper Palaeozoic rocks.

2.8.5 Relationship of Warm Springs/Faults and Thick Overburden Section

As figure 2.18a & 2.18b show, wells 1004W, 1009W, 1010W, 1012W, 1013W, 1014W, 1015W, 1016W, align sub-parallel, and near coincident, with the axis of the Kildare anticline. All warm springs, with the exception of the Newcastle and 1013W well, follow an ENE (in the east) to NE azimuth and follow the trend of both a gravity high and magnetic ridge. The magnetic values surrounding the wells increase from S to N along a similar trend. However, this overall increase may simply reflect depth to magnetic basement.

Similar patterns are evident further W with springs aligned along both gravity highs and lows and magnetic ridges and troughs. For example, wells 1002W, 1003W and 1011W, and wells 1005W and 1006W (near the town of Enfield) follow the trace of a magnetic trough and ridge respectively. Notable exceptions are wells 1007W and 1008W, which appear to be on a NNW trend. This coincides with a NNW gravity and weaker NNW

magnetic lineament. It represents a break from the strong NE-trending highs and lows and coincides with the western margin of the Namurian outlier.

2.9 Implications

This section has outlined features that may be the product of the dextral hypothesis. Faults that are oriented NE-SW and NW-SE will produce transpression and transtension. In N Dublin, there are a number of closely spaced NNW-SSE trending faults with relatively thick sections of overburden and the occurrence of two warm springs. This may be due to the change in regional strike from E-W to a less favourable NE-SW orientation, and hence, may coincide with the termination of a transform fault producing dilation and classic horse-tail structures. Likewise, at Newcastle (Co. Dublin) there is an ENE-WSW feature, where warms spring and thick overburden occurs. This coincides with a right-step on the southern boundary fault, where the trend changes from ~E-W to ENE-WSW. The Kinnegad locality may also represent a similar feature but data are sparser in this area.

These features may relate to small extensional 'bridges' or pull-aparts where the curvature of the transform is pronounced. Unfortunately, the results of the preliminary VLF-R survey were not encouraging. The association of the warm springs with faults, however, does suggest potentially recent movements on these fractures. Furthermore, the apparent coincidence of the warm springs with the NE-SW trending basin and trough geometry of the Midlands plain (section 2.8) may be due to terminations of fractures meeting unfavourable orientations in the bedrock, i.e. warm springs may be due to en-echelon horse-tail structures.

To conclude this chapter, the results obtained from testing of the dextral hypothesis are encouraging but also equivocal and highly circumstantial. The model requires further testing and in particular structural control. This is tackled in chapter 3 by looking at structures and kinematics in the Caledonian Leinster granite, adjacent the SBF.

CHAPTER 3 – STRUCTURAL WORK IN DUBLIN BAY AREA

3.1 Introduction

Structural work in the Dublin bay area provides evidence of two post-Devonian stress systems. The models account for apparent 'late' brittle fractures, which cut the northern margin of the Leinster batholith, faulting on the Howth peninsula, and an extensional jog on the southern boundary fault. Deformational mechanisms are consistent with brittle, cataclastic deformation that generally conforms to the predictions of the dextral transform hypothesis.

3.1.1 Aims & Objectives

The introduction and desk study from chapters 1 and 2 highlighted the merit of the dextral transform hypothesis. The main aim of this chapter is to test the hypothesis by analysis of structural features exposed in the Dublin Bay coastal area (figure 3.1). Key test areas for potential Mesozoic-Tertiary deformation were selected due to reasonable outcrop and position in respect to the Mesozoic outlier of the offshore Kish Bank basin (chapter 4).

The Southern Boundary fault (SBF), a potential Mesozoic-Tertiary transform, extends from the NW margin of the Leinster batholith at Blackrock, bringing limestones of the Dublin basin down to the north. As it is traced westwards, the fault swings from ENE-WSW to an E-W to WNW-ESE orientation, over a distance of ~30km. West of Dublin a temporary road section exposed a strand of the fault, where it side-steps in a right lateral sense, between the towns of Rathcoole and Newcastle, Co. Dublin. As the fault changes orientation to the WNW, one of the strands of the SBF continues ~E-W for ~5km and terminates, with a series of closely spaced NW-SE 'horse splays' (chapter 2). The temporary exposure provided an opportunity for direct observation and study of fault kinematics.

The Balscadden fault on the Howth peninsula shows similar characteristics to the SBF, although on a much smaller scale. The fault is ~2km in length and traverses the

peninsula, with limestone forming the footwall rock to the north. Topographically, the Cambrian rocks of the Bray Group to the east produce relatively moderate relief, in comparison with the flat terrain underlain by Carboniferous rocks to the west (chapter 5). As figure 2.3 showed, a number of closely spaced NNW-SSE faults occur in the NW of the city of Dublin and are associated with warm-springs and thick overburden sections. Therefore, a prediction of the model is that the Balscadden fault swings to an ~E-W direction south of the peninsula. A change in strike of the structural grain to the west leads to the fault terminating with horse-tail dilation zones and hence the occurrence of warm springs (chapter 2).

Most of the structures addressed in this chapter are traditionally regarded as the products of Hercynian deformation. Therefore, one of the main aims is to map these structural elements and to see if their features and kinematics are compatible with the dextral transform hypothesis. The timing of structural events is a major limitation and is discussed in more detail in chapter 4 and subsequent chapters.

3.2 Structures on the Northern Margin of the Leinster Batholith

Structural mapping of shear fabrics along the northern margin of the Leinster granite were recorded on to a base map scale of 1:5,000 (Dun Laoghaire Corporation, 1990). At key localities however, the scale was increased by an order of magnitude, to facilitate the detailed mapping of fabrics and structural relationships. These key areas are located along a section of coastline that extends from the fault contact between the Carboniferous and the Leinster batholith, near Blackrock, and the Lower Palaeozoic country rock contact at Killiney Bay (figure 3.2). With the exception of Dalkey quarry (plate 3.1), all sections occur below the high water level. The orientation of structures were measured and recorded in a field note-book and mapped on to both field and office sheets. Detailed mapping at these localities reveals four sets of shear zones that cut the granite. Each shear zone set has been distinguished and classified, based on geometry, deformational style, kinematics, overprinting relationships, and stress-strain models. Additionally, thin-section analysis was undertaken to facilitate the identification of deformational mechanisms.

This section first outlines the results of previous research in this area and is followed with a detailed description of structural observation and interpretation of mapped structures. Micro-structural work addresses the deformational mechanisms. The final part details various stress-strain models to account for the observed structures and presents evidence to suggest that the age of these models is post-Hercynian.

3.2.1 Previous Work

The Leinster batholith was first mapped in detail by the Geological Survey of Ireland and published on one inch to the mile sheets during the middle of the last century. The batholith was subsequently described by Jukes & Du Noyer (1861, 1869), Hull (1880), and Lamplugh *et al.,* (1903). The petrography was first described by Sollas (1889, 1895), and later by Smithson (1928, 1932). Since the 1950s, detailed field work and petrographic analysis over much of the batholith was conducted by geologists from University College Dublin, e.g. Brindley (1954a, 1954b, 1956, 1957) and Brindley *et al.* (1973). Field mapping to a scale of 1:10,560 and isotopic age dating of the Leinster batholith was carried out by Brück (1968), Brück (1974) and Brück & O'Connor (1977, 1981) and O'Connor & Brück (1978).

Brindley (1954) recognised three important phases of deformation along the NW flanks of the batholith and include (from early to late), 1), primary flow textures, 2) primary fracture features (e.g. pegmatite-aplite dyke systems), and 3) later mechanical features (e.g. jointing, cataclasis etc). This final stage represents the cataclastic structures described here. Brindley (1954) described these features as post-consolidation effects in the form of marginal zones of shearing. On the northwestern flank of the batholith, the cataclastic effects are coincident with the primary foliation and hence deformation, i.e. the fabrics have been reactivated and sheared. The structures include both ruptural fracture system effects and ductile deformation textures. On steeply, inclined foliation surfaces, Brindley (1954) observed intergranular deformation associated with the development of secondary muscovite along the surfaces. These micas have been smeared out to produce local shear bands of high deformation (section 3.5).

Similarly, Brindley (1957) described a breccia, near Blackrock DART station (BR at locality 1 on figure 3.2) as a "gas" breccia (plate 3.2). Fresh tourmaline in the breccia

ground-mass, sericitisation of plagioclase, chloritisation of biotite and iron pyritic staining occur and are cited as evidence for this mechanism of formation (section 3.5.1).

3.3. Structural Observation and Interpretation

The northern margin of the batholith preserves complex interference structures, which record a time span of up to 400My. All these structures can be classified on shape, form, and kinematics. At key localities, it became apparent that groups of structures were associated with individual shear zones. These shear zones are discussed in detail in section 3.4. The shear zones form convenient reference frames for mapping mesoscopic structures in the field and are briefly outlined below in terms of relative age (section 3.4), from oldest to youngest:

A. Semi-Ductile Sinistral Normal NW-SE Shear Zones
B. Semi-Brittle Reverse Dextral WNW-ESE Shear Zones
C. Brittle-Ductile Normal Sinistral N-S Shear Zones
D. Brittle to Semi-Ductile Normal Dextral NW-SE Shear Zones

3.3.1 Sigmoidal Foliation

Sigmoidal foliation is most dominantly associated with the WNW-ESE shear zones. The mean azimuth from 286 measurements of all planar elements at locality 1 is ~093°. The finite plane trends at ~113° (as measured from field observation). Hence, the mean azimuth mainly reflects the orientations of sigmoidal foliation (figure 3.3a), which ranges in orientation from ~075° to ~113°. If the foliation originally formed by simple shear with no transpression, then this would initially be at 045° to the shear zone. Progressive deformation would then subsequently rotate the foliation planes towards parallelism with the finite shear plane as new planes form at ~068° azimuth. This would not be the case, if the structures formed by dextral transpression, i.e. reactivation of previous weaknesses such as joints, primary foliation etc. Plate 3.3 illustrates an example, ~50m east of the Blackrock breccia, where the foliation planes curve towards the finite shear plane, producing an S-shape sigmoidal pattern consistent with a dextral horizontal sense of shear.

3.3.2 S-C Fabrics

S-C fabrics consist of foliation (S-surfaces) and shear bands (C-surfaces). These fabrics are exclusively associated with the brittle-ductile N-S shear zone (plate 3.4). At locality 3 (Killiney Bay), the N-S shear bands show well-developed S-C fabrics. Relatively large muscovite grains form at an angle of ~35° with trails of muscovite smeared along the C-surfaces (figure 3.3b). For example, at locality 2 (Sandycove), the foliation becomes discontinuous and consistently shows an anticlockwise swing of the fabric into the undeformed shear walls consistent with a sinistral sense of shear.

3.3.3 Tectonic Fish

Tectonic 'fish' form when part of a shear zone becomes structurally isolated between discrete shear bands, fractures, or some other form of structural discontinuity. They are indicative of semi-brittle to brittle-ductile shear zones. Tectonic 'fish' were observed at all localities, except locality 4 and proved to be valuable kinematic indicators.

The majority of tectonic fish occurring within the semi-brittle WNW shear zones, trend between 080° to 090°. Most 'fish' are only exposed on near-horizontal surfaces and have length-to-width ratios of ~3:1. They exhibit sigmoidal S-shaped geometry that is in harmony with a dextral sense of shear. In certain cases, 'fish' are exposed on inclined planes and can be used to as a tool for deducing the vertical sense of shear. For example, at Blackrock park (figure 3.4) the orientation of one 'fish' is such that the long axis is plunging at ~060° to the south, and the extensional axis plunges at ~030° towards ~080° (plate 3.5). The orientation of the fish and the fact that the surrounding fabric swings clockwise in towards the contact of the 'fish' indicates a dextral (top to the north) reverse sense of shear.

Approximately 500m east along the coast, two gullies traverse the shear zone and produce an 'apparent' vertical profile. Abundant tectonic fish exhibit a sigmoidal Z-shape geometry (plate 3.6), and coupled with S-shape geometry on the horizontal surface indicate a dextral reverse sense of shear.

Tectonic fish at the other localities were exclusively exposed on near-horizontal surfaces and hence proved useful for deducing the horizontal sense of shear. At locality 2 (Bullock Harbour), rows of tectonic fish, trending at ~130°, are sub-parallel within the shear bands and have length-to-width ratios of ~5:1. They form S-shaped sigmoidal geometry, consistent with dextral kinematics (plate 3.7), but with less curvature than those that occur at locality 1 (hence, have a lower vorticity).

At the same locality, tectonic fish within N-S shear zones are sub-parallel to the shear zone and have an overall Z-shaped sigmoidal geometry, consistent with a sinistral sense of shear. For example, at locality 2 (Sandycove), foliation planes within the shear bands are parallel to the line of transport and appear non-coaxial i.e. the foliation and shear planes are nearly sub-parallel. However, S-C fabrics and tectonic fish (plate 3.8) show that there is also a component of sinistral shear.

3.3.4 Fault Rocks

Fault breccias and cataclastic rocks occur at locality 1, and fault gouge occurs at locality 3. The largest of the fault breccias occurs at locality one, near the DART station at Blackrock (plate 3.2). A second mixed cataclastic-breccia (plate 3.9) occurs ~750m east, near Seapoint. The two fault breccias that occur at locality 1 (at Blackrock and Seapoint), form lensoidal bands with clasts crudely oriented WNW. The fault breccia, near the DART station is ~45m in length and has a maximum width of ~18m. The clasts vary from pebble size to blocks over a metre in length and width, and are of Granite Type II composition (Brindley, 1957). The matrix is very fine-grained and dark grey in colour. A weak porphyroclast stretch lineation was observed trending ~WNW and plunging in the same direction by ~15°. Assuming a dextral sense of shear, then this would be in harmony with reverse kinematics.

The fault breccia-cataclasite at Seapoint is only just over 75cm in width by ~2m length (plate 3.9). The breccia grades into a lozenge shaped-band of cataclasite, trending WNW-ESE. The cataclasite is exposed in the back of two gulleys (the same gulleys that expose the profiles of the tectonic fish) and is ~6m in length with a maximum exposed width of 2m. However, this thickness is a conservative estimate because the cataclasite was only partially exposed. Relict granitic clasts within a cataclastic-crushed

matrix show crude sigmoidal S-shaped clockwise rotation on sub-horizontal surfaces, consistent with a component of dextral shear. The clasts are generally <10cm with a comminuted ground mass of the same composition. Porphyroclast rotation in both cases indicates dextral movement, although this is equivocal with some clasts giving conflicting sense of shear.

The fault gouge at locality 3 occurs just north of Sorrento Park and is small and discontinuous. The gouge is greyish white in colour and occurs adjacent to a dextrally sheared pegmatite vein. The dextral fault trends ~140° and shows normal throw to the NE (figure 3.9).

3.3.5 Slickensides, Slip-Fibre Lineations and Chatter Marks

Slickensides develop on fault surfaces and are apparently the result of the fine abrasive action of differential fault movement. They are made up of families of slickenlines, which are generally straight, fine scaled and skin deep on fault surfaces, which record the final direction of fault movement. Slip-fibre lineations are produced by the preferred directional growth of minerals during faulting and in the direction of movement. Chatter marks commonly form on fault surfaces and produce a local 'step or topographic relief' of ~5mm. The direction of movement can be deduced from the asymmetrical geometry of chatter marks, where one face of the step is protected from mechanical grinding by the opposite block.

Slickensides and slip-fibre lineations and chatter marks occur at localities 2, 3 and 4. At locality 2, slickensides, slip-fibre lineations and chatter marks have developed on NW-SE shear bands (e.g. plate 3.10). Slip-fibre lineations and pressure seams are associated with pegmatite sills that are concordant with SW dipping planes, which are now exposed to the free surface (plate 3.11). Where pegmatites are absent, the fault planes have taken a polish and are extensively slickensided. Slickenlines are primarily composed of quartz and tourmaline and plunge between 020-028° to the SSW. These kinematics indicators are in harmony with a normal sinistral sense of shear.

There are also numerous slickensides on the brittle-ductile N-S shear bands at locality three. For example, at Killiney bay slickenlines occur on steeply dipping N-S shear

planes and indicate a normal sinistral sense of shear (east-side down). Slickensides and chatter marks have also developed at locality 4 (Dalkey quarry) and occur on brittle NW-SE shear bands (Appendix 2). These kinematic indicators proved more equivocal at this locality, due to sense of shear inconsistencies. In general, the vertical motion primarily appears to be normal (down to the east), and the most consistent horizontal sense of shear indicator on faults at ~120-140° is dextral.

3.3.6 Offset Markers and Sigmoidal Veins

Pegmatitic veins and dykes occur around the entire northern margin of the batholith. They are coarse-grained, composed mainly of quartz and feldspar and range in width from >1cm to ~20cm. At locality 2 (particularly just east of Sandycove harbour), many of the pegmatites have an apparent offset to the left by N-S shear planes. The displacement is centimetres and consistent with a sinistral sense of strike slip. Likewise at locality 3, a similar pattern (albeit to a lesser extent) is observed from Sorrento Point to Killiney Bay. At Sorrento Point, a pegmatite vein crosses a semi-ductile NW-SE shear band and exhibits S-shaped sigmoidal geometry, indicating a dextral sense of shear.

3.3.7 Sigmoidal Drag Fold

Drag folding can be used to determine the sense of shear. These structures represent distortion of bedding and/or foliation due to the shearing of rock bodies past one another. A small sigmoidal drag fold is located just east of the Blackrock bathing pool (figure 3.4 & plate 3.12) which is ~3m in length and ~1.5m in width. It is associated with the semi-brittle WNW-ESE shear zone. The fold can best be described as S-shaped when viewed down plunge, i.e. the product of dextral shearing.

3.3.8 Magmatic Lineation

A primary magmatic lineation was observed at all localities, although, very difficult to discern at locality four. The lineation varies in trend from 0° to 025° and gently plunges towards the N (figure 3.5), although foliation dips steeply to the SE. The lineation appears to be constrictional and the feldspars show Z-shape sigmoidal geometry

consistent with sinistral sense of shear. The lineations are best developed at locality 3 (Sorrento Point).

3.4 Macroscopic Scale - Shear Zones

As mentioned above, structural mapping along the northern margin of the Leinster batholith reveals four systems of planar to curvi-planar coaxial shear zones of differing kinematics ranging in deformational style from brittle to semi-ductile.

3.4.1 Semi-Ductile Sinistral Normal NW-SE Shear Zones

Semi-ductile coaxial shear zones trend NW-SE and dip at ~030° to the SW (figure 3.7). These shear zones can be observed at coastal exposures (e.g. locality 2, i.e. plates 3.13, 3.14), with an area of extent stretching from locality 2 (Scotsman's Bay) to locality 3 (Killiney Bay). The shear zones are best developed along the Sandycove coastal section (plate 3.15). The shear zones have a regular wavelength of ~20m (figure 3.7). Locally, these planes have acted as dilation zones for the emplacement of pegmatitic sills. The sense of shear is normal sinistral and the main kinematic indicators include slickensides and chatter marks, pressure seams, and magmatic lineations.

3.4.2 Semi-Brittle Reverse Dextral WNW-ESE Shear Zones

The southern boundary fault extends to the Blackrock coast. The remnants of a sea-stack are located ~60m NE of Blackrock bathing pool (figure 3.4) at low-water, and measures ~1m by 1m. The lithology is argillaceous limestone, dark-grey in colour and possesses a pervasive ~N-S cleavage. This suggests that the main fault separating the Northern pluton from the Carboniferous limestones swings clockwise from an ENE-WSW to ESE-WNW and deforms the granite along the coast.

The strike-swing in the fault has produced WNW-ESE semi-brittle cataclastic shear zones along the northern margin of the batholith. The line of transport is approximately 113° (plate 3.16), and the sense of shear can be deduced from ENE-WSW sigmoidal foliation (section 3.3.1). The shear zone is ~12km in length, where it can be traced to outcrop at Sandycove. The width of the shear zone varies from ~1m to over 20m. The

shear zone is exposed along the coastline but the shear zone walls are normally poorly exposed (plate 3.17). The zones form an anastomosing network of interference structures, enclosing lenticular lozenges of less-deformed granite. Where the shear zone walls are not exposed, the orientations of sigmoidal foliation provide a convenient frame of reference.

The dip of the shear zones vary depending on the level of strain, (i.e. the strain gradient being a function of distance from the shear zone walls and the finite plane). Where the shear strain is most intensive, dips tend to be very steep to near vertical. As figure 3.8 shows, dips are mostly shallow (~030°) to moderate (~060°) to the south. In some cases, however, dips can be steep to very steep, with shear planes locally dipping steeply to the north (figure 3.8). This occurs on foliation planes, which have themselves been affected by progressive simple shear or transpression. The sense of shear is 'reverse dextral' and the main kinematic indicators include tectonic fish, sigmoidal foliation, drag folds and stretch lineations (section 3.3).

3.4.3 Brittle-Ductile Normal Sinistral N-S Shear Zones

Brittle-ductile coaxial shear zones trend N-S and is vertical to steeply dipping to the east (plate 3.15). The shear zones occur at all localities around the coastal margin of the Northern pluton, but are best developed at localities 2 (figure 3.7) and 3 (figure 3.9), between Bullock and Sandycove Harbour (plates 3.14 & 3.15), and at Killiney Bay respectively. These shear zones are more regular and ductile in nature in comparison with the WNW-ESE shear zones. The structures are ~1-5m in width and cut the granite with a regular wavelength of ~30m (figure 3.7). This has produced thin sub-parallel near-vertical shear bands of coaxial deformation (although with a low vorticity) which separates domains of older granitic structures and pristine well-jointed blocks of equigranular Type II granite (see Appendix 3). These shear zones offset semi-ductile NW-SE shear zones, intersect, and in places, offset the semi-brittle WNW-ESE shear zone (plate 3.7). The sense of shear is 'normal sinistral' and kinematic indicators include tectonic fish, sigmoidal foliation, S-C fabrics, and offset pegmatitic veins (section 3.3).

3.4.4 Brittle to Semi-Ductile Normal Dextral NW-SE Shear Zones

Brittle coaxial shear zones occur at locality 3 (Sorrento Point) and possibly locality 2 (Bullock Harbour). The shear zones trend ~NW-SE and are near vertical to steeply dipping toward the SE. These structures are more brittle in nature and form discontinuous shear zones (figure 3.9 & plate 3.18). The shear zone offsets the brittle-ductile N-S shear zones. The sense of shear is 'dextral normal' and the main kinematic indicators include sigmoidal veins, deflection of joint planes and an extensional lineation (section 3.3).

3.5 Microscopic Scale - Deformation Mechanisms

Over fifteen orientated thin sections were collected and analysed in order to identify deformational mechanisms. Figure 3.6 shows the locations of the samples and the main conclusions are summarised below, illustrated with four thin-sections.

3.5.1Blackrock Breccia

Plate 3.21 shows two thin-sections of the Blackrock breccia. Turner (1950) believed that it represented a sedimentary basal breccia, i.e. based on the proximity of the faulted granite:limestone (Carboniferous) contact. Brindley (1957) suggested that it was a gas breccia.

As plate 3.2 shows, the breccia is notably fresh in character with pieces of adjacent granite (Type II) set in a comminuted micro-breccia ground-mass of the same composition (Brindley, 1957). Plate 3.19a shows a fine-grained matrix, surrounded by strained quartz and feldspar grains. Plate 3.19b shows fragmentary islands of this quartz mosaic. The quartz, feldspar and muscovite grains have mechanically broken down into smaller, disoriented angular fragments. Fluids have permeated the shattered material e.g. sericitisation of feldspars. The matrix is partially opaque and is apparently iron pyrite (Brindley, 1957). Brindley (1957) also reported fresh Tourmaline prisms within the ground-mass and the chloritisation of biotite grains.

The fluids are post-brecciation and Brindley (1957) postulated that they might be due to a final phase of granite consolidation. In this model, he predicted that gaseous fluids were explosive in nature and brecciated cooled marginal granite, whilst continuing pulses (away from the border) were contemporaneously being emplaced and producing volatile expulsion on the margins. The lack of other exotic minerals suggests that an alternative model may be desired. Brindley (1957) reported the presence of a calcite vein within one of the micro-fissures. Therefore, this suggests that the source may have been the adjacent Carboniferous limestones, precluding any possibility that the feature is a gas breccia. It is more likely that these structures are fault breccias. The undulose extinction of quartz and the lack of significant polygonisation are incompatible with the breccia being Caledonian or even Hercynian in age (see section 3.5.5).

3.5.2 Seapoint Breccia-Cataclasite

Due to the difficulty of obtaining a cohesive rock sample of the Seapoint breccia, only the cataclastic part was sectioned (plate 3.20). Plate 3.20a shows a smeared band of muscovite between two feldspar grains. The muscovites do not show fresh, euhedral forms, and hence, these are secondary micas. The crude alignment of the micas shows an S-C fabric. The C-plane crosses the thin-section from left to right and those aligned obliquely form the S-planes. The sigmoidal geometry of the micas and the relationship between the S-C texture indicates dextral sense of shear (in this case, the C-plane was taken from an oriented sample at ~ 120°). In plate 3.20b, there is a number of interlocking quartz grains that appear to have experienced minor polygonisation. This is because the grains do not show undulose extinction, whereas, the larger grains (e.g. the dark grain near the right of the photograph) do. In similar fashion with the Blackrock breccia, the feldspars have secondary alteration (sericitisation of plagioclase).

3.5.3 Shear Zone – Locality 3 (Killiney Bay)

Plate 3.21 is a ~N-S oriented thin-section of a mesoscopic shear zone. The main features are that the large quartz grains display undulose extinction. There is little evidence of polygonised quartz grains, although the largest grains appear to be defined by smaller interstitial units. A number of the microcline feldspars have pronounced cleavages in the form of a series of fissure arrays and uneven cracks. The microcline

grains have also been slightly deformed. In similar fashion to the Seapoint cataclasite, there is secondary formation of muscovites in the feldspars with myrmekitic growths. The micas are in a chaotic orientation and the deformed grains appears to be locally controlled by crystal structure in an overall directed compression. Plate 3.21b shows these secondary micas forming beautiful 'petal' structures (vertical plane).

3.5.4 Non-sheared Granite – Locality 2 (Sandycove)

Plate 3.22 is a thin-section taken from the Sandycove storm-drain (plate 3.15). This rock represents the pristine, non-sheared domains which is sandwiched between ~N-S shear-bands. This particular sample is atypically quartz rich compared with normal microcline-oligoclase-quartz. Quartz is the most stress sensitive mineral and is therefore illustrated here to note the lack of undulose extinction and polygonisation in the non-sheared granites.

3.5.5 Implications

Most deformation processes are thermally activated and hence temperature plays an important role in determining the nature of the dominant flow mechanism (Ashby, 1972). The strain rate also plays a crucial role in determining the deformational style. In general, low temperature and high strain rates favour brittle deformation and higher temperatures and lower strain promotes ductile deformation. But, the crystallographic properties of individual phases means that under a given set of conditions, some minerals may undergo plastic deformation while others deform in a brittle manner. For example, feldspars deform in a brittle manner at low to moderate temperatures and ductile processes operate at high temperatures (Davies & Reynolds, 1996). However, as figure 3.10 shows, the deformation of quartz by crystal-plastic processes occurs over a much broader range of conditions (Kerrich *et al.,* 1977).

Quartz normally deforms by basal slip producing undulose extinction (generally elongated sub-parallel to [0001] plane; Carter *et al.,* 1964) and is a feature that arises due to distortion or bending of the crystal lattice, creating a high concentration of dislocations and other defects. Polygonisation of quartz minimises the energy of the

system by stress-induced grain-boundary migration. This amalgamates smaller grains into larger ones, thus reducing the surface energy of the system.

Cataclasis is the process of brittle fragmentation and rotation of mineral grains. Grain-boundary sliding and diffusive mass transfer mechanisms (Lloyd & Knipe, 1992) normally accompany this. Cataclastic flow is analogous to granular flow and involves the frictional sliding and rolling of particles. This deformational style is characterised by pervasive cracks and sharp, angular grains and fragments (Goshong, 1988). The 'brittle-ductile' transition of quartz occurs at ~300°C for quartz rich rocks (Kerrich *et al.*, 1977; Barker, 1998).

The WNW-ESE shear zones along the northern margin of the batholith are notable for their brittle cataclastic textures. In general, large quartz grains display undulose extinction with partial polygonisation. Secondary growth of muscovite has facilitated cataclastic flow, as the micas have been smeared out along the planes of the original magmatic foliation. There is a general absence of polygonisation of quartz grains in the N-S shear zones with strain being accommodated in the crystal lattice, which is evident from undulose extinction. Strain is accommodated by semi-ductile deformation of muscovite, again preferentially reactivating original magmatic foliations.

Vitrinite reflectance data (Clayton *et al.*, 1989)) indicate that, during Hercynian deformation, limestones in the Dublin region reached peak palaeotemperatures of ~250°C in a geothermal gradient of ~50°C km^{-1} (chapter 4). The known thickness of limestone in the Dublin basin is >2km; ignoring any exhumation of the Leinster granite itself, this implies that the granite outcrops currently exposed along the northern margin of the batholith had a minimum Hercynian palaeotemperature of >350°C. These structures must therefore be post-Hercynian in age, otherwise, strained quartz grains would have been totally annealed and reduced to sub-grains by re-crystallisation. The reconstituted quartz grains and slippage along planes of smeared muscovite, suggests that the strain rate was also relatively low.

3.6 Relative Chronology of Field Structures

The structures exposed at the northern end of the Leinster batholith are characterised by the presence of four shear zone systems. Based on overprinting relationships the oldest shear zone is semi-ductile in deformational style, trends NW-SE, with shallow to moderate dips to the SW, exhibits sinistral normal kinematics, and is associated with pegmatites and extensively slickensided surfaces. Therefore, these structures represent late stages of granite emplacement , i.e. Devonian in age.

These are offset by brittle-ductile shear bands that trend ~N-S, with steep dips to the east, which exhibit normal sinistral kinematics. The main structures associated with these shear zones are S-C fabrics, foliation, and tectonic fish. The relationships between the N-S brittle-ductile shear zones and the WNW-ESE semi-brittle shear zones are equivocal. In places, the WNW-ESE shear zones are deflected and offset sinistrally by the N-S shear bands (e.g. figure 3.3). But, in places the N-S shear bands are themselves locally deflected by the WNW-ESE shear zones, e.g. at locality 2. The WNW-ESE shear zones are semi-brittle in style and are associated with tectonic fish, sigmoidal foliation and breccias.

The youngest shear zones are brittle in style and trend ~NW-SE with steep dips to the NE. This system unequivocally offsets the N-S shear bands at locality 3 and probably at locality 2, e.g. Sorrento Point and Bullock harbours respectively. Structures associated with the shear zone include sigmoidal veins and deflection of joints, fault gouge, and stretch lineations. The shear zone is compatible with dextral normal movement and is the youngest of the four systems.

3.7 Model

The oldest of the four shear zones is consistent with a horizontal maximum compression (σ_1) oriented E-W to WNW-ESE. These structures appear to be syn-granite emplacement, based on the ductile deformational style, contractional kinematics, and their association with pegmatites and aplites. These features are normally related to the final stages of granitic cooling, with fluids and residual silica forming hydrous minerals,

pegmatites and aplites. It is therefore likely that the age of this deformational event is Late Caledonian, i.e. syn-tectonic granite structures.

The brittle-ductile normal sinistral N-S shear zones and the semi-brittle reverse dextral WNW-ESE shear zones are compatible with a NW-SE horizontal (σ_1) and a NE-SW horizontal extension (σ_3). The main strain was probably taken up on the WNW-ESE shear zone, as represented by the preferential development of tectonic fish and fault breccias. The N-S shear zones acted as antithetic Riedel shears [R'] (Woodcock & Schubert, 1994) to the WNW-ESE structures, and are probably more ductile in deformational style due to a lower strain rate (Tchalenko, 1970) and appear to have exploited or reactivated suitably oriented magmatic fabrics (figure 3.11). The brittle normal dextral NW-SE shear zones are compatible with σ_1 oriented SSE-NNW and σ_3 oriented ENE-WSW. (The age of these post-Hercynian structures is discussed in chapter 4.)

3.8 Howth Peninsula

The Howth peninsula comprises the northernmost exposure of the 'Bray Group' in eastern Ireland (e.g. Van Lunsan & Max, 1975). The rocks range in age from Lower to Middle Cambrian and have experienced polyphase deformation. The Bray Group is in fault contact to the west and north with Courceyan aged argillaceous bioclastic limestones (Basal Carboniferous Transgressive facies) and Waulsortian mud knolls (figure 3.12).

3.8.1 Balscadden Fault

The Balscadden fault traverses the Howth peninsula from NE to SW (figure 3.12). The fault forms a NW facing scarp (plate 3.23) and separates the hard-resistant quartzites to the east from the Carboniferous limestones to the west. The physiography and positive and rugged relied (>100m in elevation) east of the fault, forms the northern headland of Dublin bay. To the west, the Carboniferous aged limestones form flat-to-gently undulating landscapes (0-25m elevation). The only exposure of the fault is at Balscadden Bay, on the north side of the peninsula. The fault was once exposed on the

south side of the peninsula, near Sutton, where a thick sticky fault gouge was present (Holland, pers. comm. 1998), but this has since been buried by urban development.

The Drumleck and Elsinore Formations, form the Balscadden fault footwall strata on the north-west of the peninsula and exhibits a variable chaotic mélange that is olistostromic in character. Blocks of quartzite range from a few millimetres to a few metres in size and float in a chaotic sericitic mudstone matrix (Van Lunsen & Max, 1975), variable grey-green in colour. At the contact between the Carboniferous Malahide and Cambrian Elsinore Formations, the fault dips steeply (>70°) to the NW and a fault breccia of ~10m width occurs (plate 3.24). The zone consists of angular clasts ranging from >1mm to <0.5m within a subordinate fine-grained matrix and the breccia is reddened by hematite (plate 3.25). The clasts are predominantly quartzites with no limestone fragments evident. The hematite separates fragments of quartzite (plate 3.25) with no evidence for polygonisation of the clast matrix. In large clasts, the reddening shows an inward propagating diffusion gradient. The quartz grains around the margins show undulose extinction.

Lateritic and reddened weathering surfaces (plate 3.27), including the reddening on the Balscadden fault breccia and the peninsula, suggest that parts of the Cambrian rocks were exposed during Tertiary times and suffered sub-aerial chemical weathering. It is unlikely that the weathering is a Mesozoic (Triassic) product. This is based on orders of magnitude arguments in that it is highly improbable that a lateritic weathered surface would have survived more than 10-20Myr, and particularly not 200-300Myr (for Mesozoic weathering). However, it is possible that the surface is of great antiquity and represents an exhumed ancient surface. AFT modelling (chapters 7 & 8) for such a scenario would imply that the weathering surface is of Early Tertiary age (in similar fashion to the palaeosols of NE Ireland, (e.g. Wilson, 1972; McAllister & Smith, 1997) and has been uplifted in the Late Tertiary (chapter 5). The reddened surface on Howth occurs on the south of the peninsula and has been downfaulted to the SW.

3.9 Structure at Balscadden Bay

The dextral transform hypothesis predicts dextral transpression on the Balscadden fault with a termination horse-tail structure NW of Dublin. Therefore, as a test, the

Carboniferous limestones at Balscadden Bay (adjacent the main fault) were mapped for potential evidence of post-Hercynian deformation.

Structures measured were mapped on to an unpublished base map at 1:1,136 scale (Coupez, 1984). The locality is only exposed at low-water and is ~170m in length with a maximum width of ~100m (figure 3.13). This involved a re-examination of structures (see Coupez, 1984) in the limestones and establishing the orientation of their causal stress systems.

3.9.1 Stratigraphy

The section adjacent to the fault at Balscadden Bay is known as the Malahide Formation (Van Lunsen & Max, 1975). Approximately 15m of stratigraphical section are exposed at this locality. The formation is fossiliferous bioclastic nodular limestone with interbedded shaley partings. The rocks are fine-grained dark-grey coloured biomicrites to wackestones. Individual beds vary in width from around 10cm to 75cm with shale partitions only a few centimetres thick. Fossils present are crinoids, brachiopod (*Productids*), bivalves, corals (*Lithostrotion*) and bryozoan (*Fenestella*). They occur in lenses/pods in a disarticulated manner parallel to bedding. Siliceous nodules occur locally and may indicate the former presence of sponge spicules.

3.9.2 Cleavage and Stylolites

The rocks at Balscadden Bay possess a non-pervasive spaced cleavage. The cleavage is gradational in style, from smooth pressure seams to stylolites. Cleavage refracts and intensifies within shaley partings and produces a slatey cleavage. However, cleavage is most intensive within fold hinges and is non-axial planar. For example, the axis of an anticline, marked as 'A' on figure 3.13, trends at ~65° and plunges 3° to the SW. This fold axis is transected by cleavage striking 30-50°, and hence, cleavage trends anticlockwise to the fold, indicating dextral shear. In the south of the area, a black shaley residue, a few millimetres thick, occurs between stylolitic cleavage planes (plate 3.28).

3.9.3 Intersection Lineation

A bedding/cleavage intersection lineation, (the linear equivalent of the transected foliation) was observed plunging in opposite directions, as the foliation transects the fold axes. The main plunge was between 7° and 18° to the SW (figure 3.13). However, in the NE of the area, the lineation plunge is much less and varies between 2° and 5° on SE facing anticline/syncline limbs. The intersection lineation transects the folds at an angle of approximately 008° anticlockwise to the strike of bedding. This angle progressively decreases from north to south towards the Balscadden fault.

An extensional lineation runs parallel to the fold axis and is particularly pronounced when silicic nodules are present. In profile view, the stretch lineation provides evidence of 'strain softening'. For example, in the south part of Balscadden Bay, rounded porphyroclasts of limestone form a boudin lineation with a shaley matrix that has deformed in a ductile fashion (plate 3.29), and is cut by a red-pink coloured vein.

3.9.4 Slickensides and Minor Fault

Slickensides occur on a 5-8cm wide NE-trending calcite vein (figure 3.13). The sigmoidal geometry of the vein suggests dextral shear. On the opposite wall, there is a 6cm wide, discontinuous fault breccia. The matrix of the breccia is a soft, muddy orange colour and has embedded clasts of the surrounding limestone wallrock. The clasts are generally <1cm in size.

The minor fault is vertical and displaces a 12cm wide calcite vein (trending 150°). About 2m of the surrounding wallrock, on each side of the vein, has been reddened. A thick calcite vein with the same trend and associated reddened wallrock re-appears about 60m to the south.

3.9.5 Veins

Widespread tectonic veining occurs primarily toward the south of Balscadden Bay. This is likely to be due to mass transfer by intercrystalline diffusion. The veins are mostly composed of calcium carbonate (plates 3.29 & 3.30). Two main orientations

were observed. In terms of abundance, these are ranked as NNW and WNW. Stylolites are also plotted on the same rose diagram (figure 3.13). The NNW class are mostly extensional veins with widths varying from 1 to 5cm. There are also thinner joint veins, which also occur within this class. The WNW class ranges in width from ~0.1mm to 30mm. In places, they are cut by the NNW to NNE class, although, the contrary was also observed. Both classes are cut by stylolites/pressure seams, which are cut by red-pink coloured veins.

Within the WNW-ESE class there appear to be two generations of veins, based on morphology and mineralogy. The most abundant type are relatively regular, creamy white in colour. In contrast, the other vein type is orangy-red in colour, irregular along strike, and offset stylolites (plate 3.29).

The NNW class shows apparent dextral offset (plate 3.28). However, the offsets occur at stylolitic surfaces and are probably due to removal of material by pressure solution. An apparent sinistral shear offset was observed with a vein trending 090° (E-W class) which is incompatible with the above. Therefore, it has formed by either a shear offset or pressure solution from a different stress system.

An en-echelon vein array trending NNW-SSE (160°) and dipping to the SW was observed on a semi-vertical cliff face (plate 3.30). Sense of shear on the horizontal plane was consistent with right-handed separation, and reverse sense on the cliff face. The vein array is cut by stylolites. A similar dextral en-echelon array trending 140° is located ~50m north of this cliff face, in the vicinity of the minor fault described in section 3.9.3.

3.9.6 Folds

Two major folds at Balscadden Bay trend NE-SW with a wavelength of ~100m. Two minor folds occur between the two major folds and have a wavelength of ~20m (figure 3.13). The 2 minor folds do not appear to be associated with faulting and display basin and dome geometry. In the north, 3 minor folds trend ENE-WSW and have a wavelength of ~18m. Profiles of two of the major folds toward the north of the area are transected by spaced-cleavage. Both folds are symmetrical and have box-fold

geometry. The presence of a penetrative cleavage in fold hinges, and the apparent offset of the ENE-WSW folds suggests that deformation was achieved by the 'passive' mechanism, i.e. pressure solution permits shortening without rotation and leads to pressure induced removal of material and may account for the abundance of veining in the south of the exposure.

3.9.7 Progressive Dextral Shear

The NE-SW trending Balscadden fault separates the predominantly Cambrian quartzites of the Bray Group from the Carboniferous Malahide Formation. The Balscadden Bay section is characterised by the presence of NE-SW folds and ESE-WNW dextral shear zones, which are semi-ductile in nature. Nearly all macroscopic and mesoscopic structures are structurally compatible with a NW-SE horizontal compression (σ_1) and a NE-SW horizontal extension (σ_3). The NNE-SSW folds and the transection foliation are indicative of a progressive dextral shearing event, and this accounts for the clockwise change in fold axes from north to south. The apparent displacement of the smaller folds in the north is the result of material evacuation by pressure solution. This palaeostress model is compatible with the conjugate structures that cut the northern margin of the Leinster granite.

The age of the deformation is difficult to date; however the folds and the stylolitic cleavage that transects them are typical features of Hercynian deformation in the Dublin Basin. The dextral en-echelon vein system is cut by stylolites, therefore, suggesting that the dextral shear be of the same age. However, about 500m west at Claremont Strand, Carboniferous rocks show no evidence of tectonic deformation (Coupez, 1984). Therefore, deformation at Balscadden appears to be related to a Hercynian dextral shear zone following the Balscadden fault. The evidence for high level cold cataclasis in the breccia zone of the fault and the truncation of a possible palaeovalley (plate 3.23) by the fault suggests that it may have been reactivated during Tertiary times.

3.10 NNW Strand of Southern Boundary Fault (SBF)

Figure 3.1 shows the location of a temporary road section (summer 1998) which exposed a strand of the Southern Boundary Fault (SBF). situated ~16km SW of the city of Dublin and ~2km north-west of the Wicklow mountains. The section exposed bedrock over a distance of ~45m and was orientated ~E-W. The entire section was photographed and structural elements were measured and recorded. Fold profiles were measured as a function of distance from the main fault and fold axes were calculated stereographically. The main structural elements are shown on figure 3.14.

3.10.1 Major Growth Fault

The SBF brings together Silurian phyllites and greywackes of the Kilcullen Group, with Carboniferous Clondalkin Formation (Brigantian-Holkerian) aged basinal dark laminated limestones (Sevastopulo, 1981), forming the southern margin of the Dublin Basin rocks (figure 2.3). Published geological maps show the SBF trending ~E-W in this locality. However, the fault plane that was exposed had an azimuth of 144° and dipped at 066° to the north-east (plate 3.31). A thin band of black coloured, sticky fault gouge (~10cm in width) occurred on the fault plane. Abundant clasts of greywacke and phyllite were embedded in the fault gouge within a muddy calcitic matrix.

3.10.2 Minor Faults

Many minor faults occur along the section and are extensively slickensided. Six minor faults were measured and trend between 068° and 142°. About 5m east of the main basin fault, a sub-parallel fault dipping steeply to the NE showed evidence of syn-depositional movement. A small foot-wall anticline with limestone beds thickening in to the fault plane indicate that it is a growth structure. Most of the other faults trend ~E-W with moderate dips to the north, with the exception of one fault striking 084° and dipping steeply to the south. The slickensided surfaces on the faults provided good kinematic indicators and showed a prevalent, normal sense of movement with a small sinistral component. The fault dipping steeply to the south, however, had a reverse dextral sense of shear.

3.10.3 Slump Features and Porphyroclasts

The SBF formed the basin-bounding fault to the Dublin basin during the Carboniferous. There is substantial evidence for syn-sedimentary slumping on this fault during this time. Carboniferous beds were observed draping over rafts of Silurian quartzite which ranged in size from a few metres (plate 3.32a) to centimetres in dimension (plate 3.32b). The size of the clasts significantly decreases with distance from the basin-bounding fault (plate 3.32b). Many geologists have inferred that Lower Carboniferous syn-sedimentary tectonism occurred (Jukes & Du Noyer, 1861; Hudson & Turner, 1933; Lamont, 1938; Browne, 1965) and corresponds with the Mid Asbian turbidites (chapter 2) and debris flows described in detail by Nolan (1986).

3.10.4 Veins

In addition to extensive calcitic slickensides, there was also a great abundance of calcite veins, cutting the Carboniferous strata. Vein populations show greatest density adjacent to (and permeating) fault planes.

3.10.5 Folds

Four fold profiles in the Carboniferous strata were exposed. The wavelength of the folds was ~10m at the exposure level (plate 3.33). The folds have open profiles and rounded hinges. Fold limbs and, where possible fold hinges, were directly measured. Hinges that were ambiguous to measure were computed stereographically. In general, the fold hinges plunge gently at ~020° to the south. Figure 3.14 shows that the fold hinges progressively rotate anticlockwise towards the main fault. This implies that a component of sinistral strike-slip occurred on the fault, which was probably coeval with folding.

3.10.6 Kinematic Indicator

Plate 3.34 is an oriented thin section taken from the footwall rock (Silurian Kilcullen Group). This micro-fold also shows sinistral ductile kinematic indicators. Northerly trending zones of folding which rotate anticlockwise towards N-S faults, indicating

sinistral zones of shear are typical of the Hercynian structures of the Dublin Basin (Rothery, 1988)

3.11 Implications for Dextral Transform Hypothesis

While geometric reconstructions of palaeostress directions are non-unique, the kinematics of the late post-Hercynian structures cutting the northern margin of the Leinster batholith are compatible with NW horizontal compression and SW horizontal extension. It is probable that most strain was taken up on the ESE-WNW zones as represented by the preferential development of tectonic fish and fault breccias. The structures at Balscadden Bay are also in harmony with this stress system. In general, the structures are the product of dextral transpression, with the N-S shear zones acting as antithetic Riedel shears and are probably more ductile in deformational style due to a lower strain rate. These structures are compatible with a NW-SE σ_1 and a NE-SW σ_3. This is the same as known Hercynian palaeostress systems. Therefore, the distinction of post-Hercynian structures (the granite shear zones) from Hercynian structures (Balscadden Bay structures) rests on the abundance of strained quartz grains and the notable lack of polygonisation.

The youngest NW-SE dextral shears may simply relate to NNW-SSE and ENE-WSW extension. These structures are consistent with dextral transtensional deformation, with σ_1 oriented NNW-SSE and σ_3 oriented WSW-ENE.

The southern boundary fault near Rathcoole has experienced a complex history. The abundance of Lower Palaeozoic blocks adjacent to the fault suggest that during Carboniferous times, the fault was seismically active and had formed a major fault scarp. The fault has been subsequently reactivated with normal sinistral sense of shear. The rocks appear to have experienced a second phase of reactivation, which has produced brittle deformation of the rocks and dextral reverse strike-slip on ~ENE-WSW fault strands.

Based on the dextral hypothesis, the SBF displays transpression in an ENE-WSW trend and the sudden change in strike to ~NNW-SSE has resulted in the fault side-stepping to

a new strand, oriented ~WNW-ESE (near the town of Newcastle, Co. Dublin). The original strand has terminated in horse-tail fashion, and produced a small extensional bridge on the transform.

3.12 Limitations

The majority of structures at Balscadden Bay are probably of Hercynian age, with the exception of the pink-red class of veins which cuts everything. These veins are probably related to the most recent movements on the Balscadden fault. It is also likely that the oldest age for this tectonic activity would be Early Tertiary and younger, based on the present–day geomorphology, i.e. the offset of a palaeovalley, and faulting of a lateritic weathered surface.

Whilst the NW-SE compression appears to correspond with those predicted by the dextral transform hypothesis, it is clear that age constraints are required to further test the model. In particular, the younger NNW-SSE horizontal compression is addressed in the next chapter, with structural onshore-offshore correlation with post-Liassic erosion of the Kish basin, coupled with AFT studies of the Irish Sea region and Tertiary structures in the Lough Neagh-Larne basins of NE Ireland.

CHAPTER 4 – STRUCTURAL ANALYSES OF KISH BANK BASIN AND REGIONAL CORRELATION

4.1 Introduction and Summary

The Kish Bank basin is located on the western Irish Sea margin, ~20km east of the city of Dublin (figure 4.1). The basin lies in relatively shallow water (with an average depth of 60m) and is ~1,500km^2 in extent. The basin forms a sedimentary trough bounded on the western margin by major faults, and pinches out onto basement to the east. The main sedimentary fill ranges in age from Late Carboniferous to Early Jurassic and is separated from the Central Irish Sea basin to the SE by a basement ridge of outcropping Carboniferous and older strata (Naylor *et al.* 1993).

The analyses of well-data, seismic reflection lines, gravity, bathymetry and a high resolution aeromagnetic map has facilitated the construction of a post-Liassic structural model, which complements the models deduced from palaeo-stress reconstruction around the northern margin of Leinster, and on the Howth peninsula. The published geology map of the Kish basin is revised at the end of this chapter based on the above analyses (figure 4.45). This model is correlated and tested with Neogene models for onshore Ireland. Further constraint is derived from testing the model with onshore geomorphology. This is because the topography of a region reflects the time-integrated effects of both tectonic and climatic activity. This may facilitate further constraint on the timing of events (chapters 5, 6 & 7).

Active rifting and deposition (syn-rift) occurred during the Triassic and possibly the Early Jurassic. This gave way to episodic post-Liassic reactivation along Caledonian and Hercynian lines of weakness. Transpressional tectonism resulted in oblique uplift and vertical block faulting, which was occasionally associated with a component of 'domino' rotation. This is supported by thermochronologic and apatite fission track (AFT) data, which indicates significant periods of both exhumation and uplift. Preliminary AFT modelling, published vitrinite reflectance (VR) results (section 4.7.4) integrated with other structural and geomorphological data, indicates that the main

denudational events occurred during the Late Carboniferous-Early Permian (Corcoran & Clayton, 1999) and post-Liassic times.

The Kingscourt outlier has been lithostratigraphically correlated with the Kish Bank basin (Naylor *et al.*, 1993; figure 4.14). In addition, the Permo-Triassic rocks have been regionally correlated across the Irish Sea region (e.g. Green *et al.,* 1997). Apatite fission track analysis, sonic velocity logs, vitrinite reflectance, and a truncated Mesozoic stratigraphy shows that the entire region has experienced major denudation in post-Jurassic times. It is therefore likely that the Kish basin is the remnant of a once much larger Mesozoic basin that may have covered an area from western Britain to the onshore central Irish midlands.

4.1.1 Aims and Objectives

The northern margin of the Devonian aged Leinster batholith, where brittle onshore structures were mapped (chapter 3) displayed post-emplacement brittle deformation, with strained quartz grains and a general absence of polygonisation. Vitrinite data and known thicknesses of Carboniferous limestones for Hercynian times are inconsistent with the deformational style that affected the rocks. Therefore post-Hercynian tectonic models, which probably account for these observed structures are poorly constrained. The proximity of the Kish Bank basin, however, facilitates the extension of onshore structural models, to the offshore domain. Geophysical analyses of the Kish Bank basin provide an opportunity of developing Mesozoic and Tertiary tectonic models. These models can then be subsequently correlated with areas in NE Ireland where known Mesozoic and Tertiary rocks and structures occur (chapters 1 & 5), and facilitiates relative dating of the brittle structures that cut the northern margin of the Leinster batholith.

4.1.2 Methods

The main methods deployed for constructing tectonic models of the Kish Bank basin were an initial desk study of the existing literature and unpublished technical reports. This was coupled with an interpretation of high-resolution aeromagnetic images (data released by World Geoscience), and seismic reflection profiles (data released by the

Department of Petroleum Affairs) in conjunction with 3 well logs and a bathymetry image.

Seismic Reflection Lines

Structural elements from 599km of seismic section (mainly from the western margin of the basin) and the details of three published well logs were used for the construction of Post-Liassic models. Amoco shot most of the seismic coverage of the Kish basin in 1976 and 1977. Enterprise Oil shot additional lines in 1996 and re-processed the Amoco lines.

The lines used in this study are shown on figure 4.2, and the lines highlighted in red are presented as figures in this chapter. It was deemed necessary to select a number of seismic reflection lines (NNW-SSE) which crossed the main faults on the west-side of the basin (section 4.5). Lines conjugate to the NNW-SSE set was also utilised for realising the third dimension. The lines that traverse the basin faults presented here are AIR 78-61, AIR 78-62, AIR 78-63, and AIR 78-64. Petty Ray Geophsyical shot these lines in 1976 for the AMOCO Group. Two regional lines are also included namely TRIST 92-14 and TRIST 92-21. These lines were shot in 1992 and processed by Geoteam AS. Line TRIST 92-14 and TRIST 92-21 cover wells 33/21-1 and 33/17-1 respectively.

Common Depth Profiling

In common depth profiling (CDP), it is arranged that a set of traces recorded at different offsets contain reflections from a common depth point on the reflectors (figure 4.3). The shot-points and detectors have a common mid-point below which the common depth point is assumed to lie. The advantages of CDP surveying is that the CDP gather represents the best possible data-set for computing velocity from the normal move-out effect, and with accurate velocity information, the move-out can be removed from each trace of a CDP gather. This produces a set of traces that may be summed algebraically to produce a CDP stack and increases the signal-to-noise ratio. The fold of the stacking refers to the number of traces in the CDP gather.

Migration and Diffraction

On seismic lines, reflections are mapped directly beneath the midpoint of the CDP gather. However, the reflection point is located beneath the midpoint only if the reflector is horizontal. Migration corrects these distortions and artefacts in seismic profiles, and hence, gives the true location and dip of the reflectors (figure 4.4).

The end of discontinuous reflectors acts as a diffraction point (D) and radiates seismic energy in all directions for any angle of incidence. The greater the distance between the receiver and D, the later the diffracted ray arrives (figure 4.4). Therefore, to reconstruct the true location of the end of the discontinuous reflectors, each signal must be migrated along its constant-travel-time arc to the common point at D.

Pre-Processing of Seismic Database

The AMOCO lines have been 'common depth point' (CDP) stacked 30-fold, and the TRIST lines have been CDP stacked 120-fold. However, only line AIR 78-64 and the TRIST lines have been migrated. Therefore, careful and pain-staking interpretation was required when interpreting seismic piks and faults on AIR 78-61, AIR 78-62, and Air 78-63. In certain cases, the apex of diffraction arcs was used for locating and tracing major faults.

Other Lines

A structural interpretation of the line JS-MANX-16 by Corcoran & Clayton (1999) is also included. This line runs approximately N-S from well 33/17-1 in the north to well 33/22-1 in the south (section 4.2). Also, lines AIR 78-66A and AIR 78-53 were used for the mapping of a palaeo-channel on the western margin of the basin.

Western Isles-North Channel (WINCH) traverse

The Western Isles-North Channel (WINCH) traverse was recorded in 1982 for the British Institutions Reflection Profiling Syndicate (BIRPS) by the Geophysical Company of Norway (GECO). An additional 55km of the WINCH-4A line is also included. The coverage clips the eastern margin of the basin (figure 4.2). The purpose of the WINCH line was to study deep crustal structure of the lithosphere and Caledonian deformation. This, in conjunction with the published interpretation of the

WINCH line (Brewer *at al.,* 1983), was utilised in order to form a regional perspective of deep structure in the region.

Well-Data and Geographical Information Systems (GIS)

To-date, 4 wells have been drilled in the Kish Bank basin. In chronological order (oldest to youngest) these include AMOCO 33/22-1, SHELL 33/21-1, FINA 33/17-1 and ENTERPRISE 33/17-2. Data from all wells except 33/17-2 are published. Three completion logs for the published wells were inspected at the Petroleum Affairs Division (PAD). The observations were supplemented with additional stratigraphical data from Naylor *et al.,* (1993) and Jenner (1981). The stratigraphy was summarised and compiled into MacSection (Macintosh desktop software) and lithostratigraphy was used for correlation.

The location of the wells were entered into ARC/INFO GIS and projected to the 'Irish National Grid' co-ordinate system, in accordance with the Ordnance Survey of Ireland. The projection parameters are listed in table 4.1 below.

Table 4.1

Projection	Transverse
Spheroid	Modified Airy
Datum	Ireland 1965
Scale Factor	1.000035
Reference Latitude	53° 30' N
Central Meridian	8° 00' W
False Easting (m)	200,000
False Northing (m)	250,000

This was coupled with the following digitised layers of spatial information. 1) map of the geology and known major faults (after Broughan *et al.,* 1989); 2) bathymetry; 3) seismic base map, and; 4) aeromagnetic data.

Bathymetry

Bathymetry data was acquired by courtesy of Dr Peter Croker of the Irish Petroleum Affairs Division. The data was pre-processed and compiled with ARC/INFO GIS software into a vector geo-dataset, at 10m interval (figure 4.17 & 4.18). Additionally, the bathymetry coverage was also surfaced using the "triangulated irregular network" model and subsequently gridded. The resultant image allows a visual interpretation of sea bed morphology, and the depiction of potential fault-scarps (section 4.4).

Aeromagnetics

A high-resolution aeromagnetic dataset was acquired from the World Geoscience Group (now known as Fugro Airborne Surveys - FAS). The high-resolution coverage of the Kish Bank basin forms part of a much larger dataset that spans across the central Irish Sea. The dataset covers both the Kish and northern part of the central Irish Sea basins (section 4.6), encompassing an area of ~950km^2. The aeromagnetic dataset is an amalgamation of two compatible surveys. The flight and tie lines run 092-272° and 002-182° at 400m and 1,200m spacing respectively and the survey was flown at a height of 60m above sea level.

The data was gridded and levelled by Fugro Airborne Surveys (FAS). I received a series of images of the dataset and a reduced-to-pole (RTP) XYZ ASCII file of the dataset (total magnetic anomaly). The RTP method is a technique that recalculates total magnetic intensity as if the indicating magnetic field had a 90° inclination. This in effect transforms the magnetic anomaly from dipolar to monopolar, i.e. anomalies are centred over the causative body which simplifies interpretation of the data.

The FAS images are produced by assigning a 'look up table' consisting of a maximum of 500 colours to the data values, and the colour scheme used was a rainbow spectrum, i.e. purple depicting low data values through to red/white representing high data values.

A simulated light source was used to illuminate the data set from a selected elevation and azimuth. The data set onto which the 'sun' is illuminating will give maximum reflectance when the normal vector of the surface (data) is parallel to the direction of the illumination. In a greyscale image these areas are shaded white. When the normal vector of the surface is perpendicular to the direction of illumination the reflectance is

at a minimum and these areas are assigned dark shades. The effect of this type of process is analogous to shading topographic relief maps. The sun angle image will highlight subtle features striking perpendicular to the direction of application.

The ASCII data was compiled and surfaced with 'environmental scientific research institute' (ESRI) GIS software and the magnetic values were grouped into 14 equal interval classes, each assigned a unique colour. With the data gridded, it was possible to calculate the first and second horizontal derivative, using available GIS software. Both derivatives were non-directional and were utilised to emphasise discontinuities in the magnetic data by accentuating the shorter wavelength components at the expense of the longer wavelength features. The second horizontal gradient returns the anomalies to a position overlying the source, i.e. the high frequency data is enhanced even further at the expense of lower frequencies thus increasing linear texture but inevitably enhancing noise, and reducing the signal-to-noise ratio. The resultant second derivative image is not included here because the information conveyed was of poor quality, due to the constraints of the available software at my disposal.

Palaeotemperature Indicators

Due to an unconformity between Lias and the Pleistocene, a regional review of palaeotemperature indicators is presented at the end of this chapter to further our understanding of estimated rock thicknesses that this gap represents.

Bray *et al.*, (1992) showed that the integration of AFT and VR data yields direct estimates of both the time at which cooling from maximum palaeotemperatures began, and the palaeogeothermal gradient at that time. Wherever AFT and VR constraints overlap, the AFT data will provide the minimum palaeotemperature whereas the VR will normally be >110°C. The thermal history prior to cooling from maximum palaeotemperatures cannot be constrained from VR or AFT data. This is because of the dominance of temperature over time in the kinetics of the systems. The determinations of maximum palaeotemperatures in a vertical sequence of samples from a well provide a maximum palaeotemperature profile from which a palaeogeothermal gradient at the time of maximum heating can be estimated. Thus, heating may be due to an increase in basal heat flow or deeper burial, or a combination of both. By constraining and making assumptions about palaeogeothermal gradients, the modelled thermal histories of AFT

data may, in principle be converted to depth-time information and hence the reconstruction of a denudational chronology (Bray *et al.,* 1992; Menzies *et al.,* 1997).

Fission Track Method

Fission tracks are linear trails of disrupted atoms and are produced by the spontaneous fission of the isotope ^{238}U. The fission process occurs at a statistically constant rate and all tracks initially form at ~16μm. However, fission tracks shorten irreversibly when the host mineral is at an elevated temperature as a consequence of a thermally activated diffusion process (see chapter 7 for more details).

All the regional AFT studies presented in chapter 8 use the annealing method of Laslett *et al.*, (1987). This annealing model is based on laboratory annealing experiments performed on a mono-compositional Durango apatite with a F/Cl ratio of c. 0.1 (Young *et al.,* 1969). This apatite is moderately retentive compared to a pure fluorapatite. Extrapolation of the Laslett *et al.*, (1987) Durango apatite model to geological time scales (10^6–10^7yr) predicts a partial annealing temperature range from 60±10°C to 110±10°C. Hence, the interpretation of apatite fission track data relies on an empirical calibration of the relationship between track-length, temperature, and the duration of heating (Laslett, *et al.* 1987; Carlson, 1990).

In samples where the central fission track age of apatite is considerably younger than the stratigraphic age, then this implies that the rock has experienced temperatures in excess of 110±10°C since deposition. Thus, apatite fission track data provides direct estimates of the time at which a sedimentary section began cooling from 110±10°C.

Vitrinite Reflectance Method

Vitrinite is one of the 3 maceral groups recognised and is the major constituent of coals. Temperaure is considered to be the principal factor that controls the increase in the reflectance properties of vitrinite. Chemical reactions, which affect vitrinite particles during organic maturation, are irreversible and their reaction rates rise exponentially with a linear rise in temperature. Hence, the increase in the magnitude of vitrinite reflectance also increases exponentially with a linear rise in temperature. VR was first used as a thermal maturity indicator by Ammosov (1962) for defining maturation levels

of hydrocarbon source rocks (i.e. Robert, 1980). Price (1983) observed that a strong correlation exists between VR and maximum burial temperature from various sedimentary basins. There are numerous proposed models for the conversion of VR to palaeotemperature. One of the most commonly used methods is the linear regression equation below (after Barker & Pawlewicz, 1986):

$$Rm\% = \exp\left[\left(0.000096 T_{max}\right) - 1.4\right]$$

T_{max} = degrees celsius

Another method that is widely used for converting VR data to maximum palaeotemperatures is the kinetic model of Burnham & Sweeney (1989) and Sweeney & Burnham (1990). See chapter 7 for an example of this method.

4.1.3 Previous Work

The existence of the Kish Bank basin was first suspected by Bott (1964, 1968) and Bott & Young (1971) from a gravity survey (figure 4.5). The survey revealed a low gravity anomaly, characterised by steep gravity gradients on the northern and western margins. To the southeast, the gravity anomaly exhibits a gentle gradient onto the Mid-Irish Sea High.

Prior to the shooting of seismic reflection lines over the Kish basin, there was a debate in the literature regarding the cause of the gravity anomaly over the Kish bank area. The gravity low could either be related to a sedimentary basin or granite (perhaps an extension of the Leinster batholith). A number of seismic refraction profiles were shot in 1961 as part of a site investigation for the Kish Bank lighthouse. The velocities of the seabed were 1,706m sec^{-1}, which corresponds to unconsolidated drift. Two further refractors were discovered beneath this layer, one with an apparent velocity of 2,743m sec^{-1} and the deeper one with an apparent velocity of 4,267m sec^{-1}. The former was believed to be at a depth of 88m below the seabed and the latter was postulated to be at a depth of 207m. The latter value is typical of well-compacted sediments or basement

rocks. Seismic reflection profiles during the early 70s confirmed the presence of a deep fault-controlled sedimentary basin.

The presence of Mesozoic sediments was first proposed by Etu-Efeotor (1976) who proposed that the basin fill was "Permo-Trias/Tertiary sediments with a proven thin Liassic sequence in between". Workers at the University of Aberstwyth used Sparker profiles to establish and name the major structures of the basin. Mudstone drag samples were recovered from the sea floor, just north of the main basin bounding fault (figure 4.1) and were dated as Liassic in age (Dobson, 1977; Dobson & Whittington, 1979).

The Amoco Group was granted an exploration license for block 33/22 in March 1976, and licenses for blocks 33/16, 33/17 and 33/21 were added in May 1977. The Amoco Group comprised Amoco Ireland Exploration Co. Ltd (operator), Fina Exploration Ireland SA, BP Petroleum Development Ltd, Aran Energy Ltd, Century Power and Light (Ireland) Ltd, Saga (Ireland) Ltd, and Shenandoah (Ireland) Inc. Amoco shot 253km of reflection seismic data in the Kish basin in 1976, a further 436km in 1977, and 487km were acquired in 1978. This was coupled with gravity and magnetic profiles, which led to the drilling of the Amoco well 33/22-1 in late 1977, on the southern margin of the basin (section 4.2).

The Amoco well was testing a large shallow fault-bounded closure. The well penetrated a thin veneer of Tertiary-Quaternary deposits, overlying Upper Carboniferous Westphalian (or Stephanian) strata. Jenner (1981) published details of the well stratigraphy and produced a map of pre-Tertiary geology, based on well 33/22-1 and seismic reflection lines. Under a 'farm-in' option agreement with the Amoco Group, Irish Shell Petroleum Development Company (operator), in a joint venture with Agip Ireland Ltd, drilled the Shell well 33/21-1 in 1979, near the western margin of the basin. This well tested a four-way closure at Lower Triassic levels, sealed by Keuper Marl (figure 4.10). The test was unsuccessful and the Amoco Group subsequently relinquished the exploration licenses.

A third well, Fina 33/17-1, was drilled in the eastern part of the basin in 1986 by a five-company consortium operated by Charterhouse Petroleum. This well unsuccessfully

tested a horst structure. Details of the 33/17-1 and 33/21-1 wells were published by Naylor *et al.,* (1993).

4.1.4 Regional Setting

The evolution of the Irish Sea basins is directly related to rifting and subsequent break-up of the Pangea super-continent. Rifting was mainly accomplished by transtensional reactivation of pre-existing Caledonian/Hercynian basement structures. The main rifting phase occurred during the Permo-Triassic (Shannon, 1991a; Naylor, 1992), preceded by Hercynian compression, uplift and erosion. Deep seismic profiles show that the continental crust has experienced little to moderate stretching during Permo-Triassic times (figure 4.6). For example, relatively low stretching factors for Permo-Triassic extension has been documented, i.e., β values between 1.1 and 1.3 (Brodie & White, 1995). Figure 4.6 is a structural interpretation of the unmigrated WINCH-4A line (Brewer *et al.*, 1983). The Moho is at an approximate depth of 30 km underneath the Kish basin. The seismic character of the Moho is highly variable under the Irish Sea region, but appears to be at a relatively constant depth of 26-30km. Hence, the upper lithosphere has undergone minimal attenuation (Shannon 1991a).

The Kish Bank basin is one of many numerous fault-controlled half-grabens that extend down the length of the Irish Sea. Figure 4.7 is a map showing the location of Mesozoic basins in the Irish Sea region and adjacent onshore areas. These include the Ulster basin in the north, to the North Celtic Sea basins in the south. The basins are predominantly bounded by NE-SW and NW-SE, and to a lesser extent, N-S trending basin bounding faults. Figure 4.8 is a free-air anomaly (offshore) map of the Irish Sea region. The Mesozoic basins are associated with relatively low gravity anomalies. The orientation of the basins is mostly NE-SW and NW-SE. Steep gravity gradients delimit the basin boundary faults. Some of the basins are bisected by major strike-slip faults. For example, the NW-SE trending Codling Fault zone bisects the Kish Bank and Central Irish Sea basins.

Most of the basins have, on average, a Mesozoic (Permian to Lower Jurassic) fill of 3-5km of sediments (e.g. Shannon, 1991a). The Middle Jurassic appears to be absent in

most of the Irish Sea region, with the exception of the Cardigan Bay basin, where drilling encountered about 760m of Middle Jurassic mudstone and subordinate limestone beds, conformable with an almost complete Lower Lias succession (Barr *et al.,* 1981). The only occurrence of Cretaceous rocks in the Irish Sea region are located on the western side of the Bristol Channel basin. Over 1km of Upper Cretaceous rocks unconformably succeed Lower Cretaceous rocks in the basin. However, these rocks progressively thin and disappear towards the east. (Shannon, 1991b; Naylor, 1992).

4.2 Geology and Structure of the Kish Bank Basin

The early geophysical work of Young (1965) and Bott & Young (1971) defined the major structural elements of the basin, based on gravity data (figure 4.5). To the north the basin is bounded by a major basement horst, the Lambay Ridge. On the southern margin there is a further basement high the 'Wicklow Head Shelf-Mid Irish Sea Uplift' ridge (Dobson & Whittington 1979). Both basement highs show a marked NE-SW to ENE-WSW orientation.

Figure 4.1 is a map of the pre-Tertiary geology of the Kish Bank basin. The map is after Jenner (1981) and Broughon *et al.,* (1989). (The Tertiary-Quaternary deposits form a thin blanket of relatively flat-lying sediments across the basin – sections 4.2 & 4.3.) This map forms the template of figure 4.43, which also takes into account my interpretation of bathymetric data, seismic lines and a high-resolution aeromagnetic data (section 4.9).

Seismic interpretations from well data suggest that over 3000m of Permo-Triassic rocks are present in the basin (Jenner, 1981; Broughan *et al.,* 1989; Naylor *et al.,* 1993). The regional strike of the beds is ~N-S and dip towards the W. The basin has been regionally tilted to the NW, and hence, the strata become progressively older towards the SE, i.e. from Liassic to Carboniferous.

As figure 4.1 shows, the vast majority of pre-Tertiary geology, lying beneath the Tertiary-Quaternary unconformity is the Upper Triassic Mercia Mudstone Group. This pinches out to the south onto the Upper Permian-Lower Triassic Sherwood Sandstone Group, which rests unconformably upon Upper Carboniferous Westphalian sequences.

Towards the north and west, Lower Jurassic (Liassic) sequences are believed to occur in the hangingwalls of the Bray, Dalkey, Lambay and Codling faults.

4.3 Stratigraphy

Deposition of sediment during active extension is normally characterised by small rollover anticlines and growth (thickening) of strata towards the fault footwall, i.e. (syn-rift phase of basin development). Pre-rift strata tend to be rotated and displaced by normal faulting. The two main extensional events in NW Europe occurred during the Permo-Triassic and in the Late Jurassic (Ziegler, 1989). Seismic evidence shows that the Permo-Triassic sequences in the Kish Bank basin represent syn-rift deposition, based on the above criteria (also see Jenner, 1981; Naylor *et al.,* 1993; Corcoran & Clayton, 1999), and the postulated Liassic strata may represent post-rift deposition, i.e. the strata do not appear to thicken into fault planes. The Late Jurassic phase, which is probably more important in terms of hydrocarbons, is present in the North Sea, Celtic Sea and the Western Approaches. But, data for this event are 'missing' in the Irish Sea basins or it never occurred there.

To-date, four wells have been drilled in the basin but only the details of three wells (33/22-1, 33/21-1 and 33/17-1) have been published (i.e. Jenner, 1981, Naylor *et al.,* 1993). However, as figure 4.9 shows, none of these wells encountered Liassic rocks. Jenner (1981) published the stratigraphy of well 33/22-1, and the other 2 wells were published by Naylor *et al.,* (1993).

4.3.1 Well 33/22-1 – Pre-Rift and Basement Geology

Well 33/22-1 is located on the SE rim of the basin (53°12'36'N, 5°37'48W), approximately 30km offshore in water depths of 50m. The well was drilled in 1977 to test a large, shallow fault-bounded closure. The well encountered a major unconformity between Upper Carboniferous Westphalian, (720m thick), and a thin veneer of Tertiary-Quaternary (71m) sediment (figure 4.9). The well proved a potential source for hydrocarbons, and seismic evidence suggests that the Westphalian sequences thicken towards the centre of the basin. The Westphalian sequence unconformably overlies the Lower Palaeozoic rocks, which form the basement in the Kish basin.

The Lower Palaeozoic rocks comprise light green (with subordinate amounts of light brownish) chloritic slates. The crushed samples are undated but Jenner (1981) suggested that they might correlate with the near-shore Bray Group (Lower to Middle Cambrian) – figure 4.11. However, it is also possible that the rocks may belong to the Ribband Group (Upper Cambrian to Arenig).

The Lower Palaeozoic rocks are overlain by a basin wide angular unconformity. Although, the unconformity is difficult to map, due to the relative lack of acoustic impedance between basement and overlying Westphalian strata (e.g. Naylor, 1992). The unconformity of Upper Carboniferous on Lower Palaeozoic rocks marks the removal of the Lower-Middle Carboniferous rocks, seen onshore, by uplift and faulting of the area in Late Carboniferous times.

In well 33/22-1, basal sandstone of 10m thickness unconformably overlies basement and is followed by an Upper Carboniferous package consisting of sandstones, siltstones, claystones and coals (figure 4.9). Coal seams are generally less than 1m in thickness but one at ~11m were encountered in well 33/22-1, proving a potential gas source. The age of the Upper Carboniferous section, encountered in well 33/22-1, ranges from Westphalian 'B' to possible Stephanian age. The absence of in situ *Radizonates aligerens* in the Westphalian section (Nalyor *et al.,* 1993) implies that Westphalian 'A' was not encountered. The uppermost part of the section in well 33/22-1 is unfossiliferous and Jenner (1981) tentatively postulated that the rocks might be Stephanian in age. However, Naylor *et al.,* (1993) suggested that the unit may in fact represent a reddened section of Westphalian 'D', comparable to those widely developed in parts of western England and north Wales.

4.3.2 Wells 33/21-1 & 33/17-1 – Syn-Rift Deposits

Well 33/21-1 is located on the western margin of the basin (53°19'12N, 5°55'50W), ~12km offshore in water depths of 20m. The well was drilled in 1979 to test a four-way closure at Lower Triassic levels (figure 4.10). Well 33/17-1 is located just east of the CFZ (53°22'12N, 5°36'36W), ~30km east of Howth Head in water depths of 70m. The well was drilled in 1986 to test a horst structure (figure 4.11). Well 33/21-1 terminated at a total depth of 2338m (at Lower Triassic levels) and well 33/17-1 terminated at a

total depth of 2030m (at the top of the Permian) – figure 4.9. Both wells encountered the Upper Keuper Marl of the Mercia Mudstone Group (Late Triassic), representing >1.5km and >2km of Permo-Triassic section in wells 33/17-1 and 33/21-1 respectively, and seismic evidence suggests as much as 3km of Permo-Triassic section is present in the Kish Bank basin.

4.3.2.1 Permo-Triassic Facies

Active rifting occurred after the Hercynian orogeny and deposition of the Permo-Triassic facies occurred during this event. The reactivation of Caledonian faults and sediment supply from the Hercynian Mountains to the south, sourced the Kish and other Irish Sea basins. This is mainly controlled by intrabasinal faults (i.e. Jenner, 1981), and possible salt escape. Complementary stretching and flexural load of sediment created the main regional facies pattern. However, the thickness of the Permo-Triassic section does vary locally (see below). Fault movements, and minor halokinesis (Jenner, 1981) mainly controlled these local depositional patterns, which are superimposed on the regional pattern.

The Upper Keuper Marl sequence is dominated by red-brown claystones and is substantially thicker in well 33/17-1 than the equivalent package in well 33/21-1, thicknesses of 397m and 156m respectively. However, there is substantially more upper saliferous stratigraphy in well 33/21-1, indicating the presence of more salt west of the Codling Fault zone, i.e. 691m in comparison with only 51m in well 33/17-1. This may indicate salt escape to the west of the CFZ and may explain the fact that the gravity low is most intense west of the CFZ (-5mGal) due to a thicker salt layer (figure 4.8).

The Middle Keuper Marl and Lower Saliferous beds are also marginally thicker in well 33/21-1. However, halite is rare in the Middle Keuper Marl, which is dominantly claystone and siltstone. The main exploration target in the Kish basin, the Sherwood Sandstone Group (SSG) is of relatively equal thickness in both wells 33/21-1 and 33/17-1, at 1,033m and 929m respectively. However, the top of the SSG occurs at a greater depth in well 33/21-1 than well 33/17-1, i.e. 1,355m (below sea level) compared with 1,007m (below sea level) in well 33/17-1. This probably relates to greater erosion, particularly if salt escape has occurred, as this would produce thicker deposition.

4.3.2.2 Onshore Lithological Correlation with the Kingscourt Half-Graben

At Kingscourt, an 18m basal conglomerate of Permian age oversteps Lower Palaeozoic basement and Upper Carboniferous (Westphalian 'A') rocks (figure 4.12). The conglomerate gives way to interbedded red plastic mudstones and gypsum up to 130m thick. Westphalian 'A' is missing in the Kish basin and Westphalian 'C-D' and Stephanian sequences, which are present in well 33/22-1 are absent at Kingscourt. However, the Permian conglomerate and the 130m thick mudstones and gypsum units are equivalent to the Collyhurst Sandstone and Manchester Marl formations respectively (Jenner, 1981; Naylor, 1992; Naylor *et al.,* 1993). Therefore, the Kingscourt graben may represent the remnant of numerous Permo-Triassic depocentre that includes the Kish basin and other basins in the Irish Sea and onshore western England (figure 4.7).

4.3.3 Post/Syn-Rift Liassic Rocks (?)

Figure 4.13 is a geoseismic section (interpreted by Broughan *et al.* 1989) across the south-western margin of the Kish Bank basin (labelled G-G on figure 4.1). The interpretation shows a substantially thick sequence of Liassic sediments beneath relatively flat-lying Tertiary-Quaternary sediments. However, no Liassic rocks were encountered in any of the wells. Therefore, what is the evidence that led Broughan *et al.,* (1989) to postulate that there was over 2km of Lias sequences preserved in the hangingwall of the Bray fault?

There is a great deal of evidence to suggest that there was once a much more extensive Lower Jurassic section present in the Irish Sea region. The Mochras borehole on the Welsh coast encountered 1.3km of Liassic sequences in the Cardigan Bay basin (Woodland, 1971). Seabed coring on the flank of the St George's Channel basins also encountered Liassic shales and limestones (Whittington *et al.,* 1981).

Onshore, lower Liassic rocks are present in the Ulster basin (figure 4.14), and outcrop along the coastline, i.e. Magilligan Point and Portrush (Co Derry) and, Whitepark Bay and Larne (Co. Antrim). Lias sections have also been penetrated in boreholes with almost 250m of Sinemurian to Lower Pliensbachian sediments present in the Port More

borehole (figure 4.14). The rocks comprise "grey calcareous mudstones locally containing thin ribs and interbeds of grey siltstones and grey fossiliferous limestones" (Broughan *et al.*, 1989). Lower Liassic rocks have been sampled from the seabed just over the northern margin of the Kish Bank basin (figure 4.1), and Lamplugh *et al.* (1903) refer to Liassic fossils from onshore clay deposits at Kill o' the Grange (Co. Dublin).

Dobson & Whittington (1979), based on seismic evidence, argued that a remnant Liassic section might conformably rest upon the Mercia Mudstone Group, adjacent to the main basin bounding faults. In addition, Jenner (1981) estimated a maximum of 300m of preserved Lias section.

The identification of the Kueper Sandstone pik on the section is extrapolated from well 33/21-1. Broughan *et al.,* (1989) suggest that the "inferred base-Jurassic level is harmonious with the interval observed elsewhere in the basin". Therefore, based on seismic stratigraphy (Broughan *et al.,* 1989) the reflectors above this pik are interpeted as Liassic sequences. The seismic character of this package has been extraplotated along the hangingwalls of the Dalkey and Lambay Fault zones, with the maximum thickness adjacent the Bray Fault zone.

Individual reflectors within the Lias section, as illustrated in section 4.5, are mostly discontinuous in extent. Although, the spacing between reflectors remains sub-parallel and fairly constant into the fault, suggesting that the Bray Fault zone was largely inactive during this period of deposition (Liassic?). Figure 4.11 shows that Cambrian aged rocks of the Bray Group are exposed <4km onshore at Bray Head. Therefore, if the onshore geology of the Lower Palaeozoic to Middle Carboniferous underlies the Kish stratigraphy (Upper Carboniferous to Lias), then this implies a minimum throw of between 4-6km, even if the rocks interpreted as Lias are actually older, i.e. maybe a combination of a thicker Late Triassic and thinner Early Jurassic (Lias).

In general, the Liassic strata retain parallelism with considerable distance (basinward) from the Bray Fault zone (section 4.2). Hence, the palaeoenvironment would appear to be one primarily of uniform deposition. Based on this interpretation, the Jurassic section that abuts against the Bray Fault zone is of considerable thickness, and Broughan *et al.,*

(1989) believes a figure of 2,700m is a reasonable approximation of thickness. Therefore, the extent of Liassic strata in the Kish Bank has been interpreted from both the seismic character of the postulated Lias section, correlation of discontinuous reflectors, and the occurrence of Lias-aged dredged samples (Dobson, 1977, Dobson & Whittington, 1979) to the north of the basin. However, geophysical evidence (section 4.6) suggests that the Liassic dredged sample just north of the basin, is probably a glacial erratic (exotic) and not sub-crop, which has been transported westwards by the Irish Sea ice sheet during the last glaciation.

4.3.4 Post-Liassic Preservation

In the Kish basin, an angular unconformity exists between the Triassic and relatively flat-lying Tertiary-Quaternary (section 4.5) sediments. The Tertiary-Quaternary section reaches thicknesses of ~0.7ms[twt]. The Tertiary-Quaternary section is thicker in well 33/21-1 (183m) than well 33/22-1 (71m). In well 33/17-1 the section is almost double (381m) that of well 33/21-1. The base of the Tertiary-Quaternary (below sea level) in wells 33/22-1, 33/21-1 and 33/17-1 is 121m, 203m and 451m respectively. This indicates that well 33/22-1 is on a relative high (despite deeper waters than well 33/21-1), and well 33/17-1 has been influenced by extension on the Codling fault. Naylor *et al.*, (1993) tentatively suggest that the Tertiary-Quaternary section in well 33/17-1 is of Pliocene age or older, based on "poor miospore recoveries".

Many of the major faults of the Codling Fault zone cut the Tertiary-Quaternary unconformity (figures 4.15 & 4.16), and part of this package has been slightly rotated and deformed. For example, the Tertiary-Quaternary unconformity forms a small hangingwall anticline near shot-point 400 (figure 4.15). The reflectors maintain equal spacing over the structure. Hence, the fold must be tectonic and not a syn-depositional structure.

The two simplest scenarios for the unconformity is that there was a general lack of deposition in post-Liassic times, and/or, a significant period of post-Liassic uplift and erosion which subsequently removed post-rift deposits. These two scenarios are discussed in section 4.7.

4.4 Structure

The main structural elements within the basin are N-S trending anticlines/synclines (figure 4.10) that plunge to the north. These folds deform the Liassic sequences therefore are post-Liassic, and probably Tertiary in age. Monoclinal flexures, shallow dome structures, and intrabasinal faults also occur (i.e. Jenner, 1981). The western boundary of the basin is fault-bounded by the NW-SE Bray Fault zone, and the NE-SW trending Dalkey Fault zone, forming a half-graben structure (section 4.5). To basin is bound to the north by the Lambay Fault zone. To the south, onlap of the basement high (Wicklow High) is evident from seismic sections. Hence, the overall basin configuration therefore is of two "trap-door" like half grabens, hinged to the south against basement, and separated by the Codling fault to the east.

4.4.1 Codling Fault Zone (CFZ)

As noted earlier, the basin is divided in two by a major NW-SE normal dextral fault zone, the CFZ. The fault zone has produced an apparent net dextral displacement of between 4 km (Dobson & Whittington, 1979) and 6km (Jenner, 1981) based on the offset of the Dalkey and Lambay faults (figure 4.1). The CFZ also has an extensional component of displacement (figures 4.15 & 4.16).

4.4.2 TRIST-92-21

Figure 4.16 is a structural and stratigraphical interpretation of line TRIST-92-21 and shows a small section of the SW-NE trending TRIST-92-21 line, which covers the CFZ and well 33/17-1. The main features are a “negative” flower structure and a horst block. The flower structure has dropped basement from ~1.7ms[twt] to ~2.5ms[twt]. Both the basement and Carboniferous sections are highly faulted with block rotation, and the reflectors do not show any change in spacing towards the fault planes. Hence, the Carboniferous forms the pre-rift package. The Permo-Triassic shows little evidence of growth into major faults, although, growth has occurred locally, i.e., see ‘S’ labelled on figure 4.16. However, the strata drape the pre-rift geology, and hence, form the syn-rift stratigraphy. The horst structure is located between shot-points 6400 and 6200. This structure was tested as a potential play by well 33/17-1, with the Collyhurst sandstone

reservoir being the exploration target. The horst has been faulted after the deposition of the Permo-Triassic rocks.

Between shot-points 6500 and 6350, reflectors are truncated and columns of acoustic turbidity are present. This is probably related to the escape of biogenic gas along fault conduits. These faults must have been active (and/or reactivated) in recent times; otherwise, the gas pockets would now be barren. This is supported by the relatively thick Tertiary-Quaternary sequences that unconformably overlie the Permo-Triassic. These sequences reach a maximum thickness of ~0.7ms[twt], with thick fault wedges evident. The fault zone cuts the Tertiary-Quaternary sediments.

4.4.3 Bathymetrical Expression

As figure 4.17 shows, the bathymetric NW-SE trending lineament coincides with the CFZ. Water depths increase to the east. For example, at line 1 on figure 4.18, water depths increase from ~100m to ~145m over a distance of 3km to the east. In similar fashion, water depths increase from ~75m to 140m over a distance of 2km on line 2. Hence, the CFZ possess a fault scarp dipping to the ENE, on the present-day sea bed. Video stills (figure 4.19) of a strand of the CFZ (figure 4.17 for location) were taken in 1997. The images show considerable relief (figure 4.19). At this locality, the elevation difference is about 20m. Dredged samples of the scarp were recovered and the crushed samples comprised carbonate cemented sandstones (Croker, pers. comm. 1998).

4.4.4 Implications

Figure 4.15 is a structural and seismic stratigraphical interpretation (modified from Corcoran & Clayton, 1999) of the NNE-SSW JS-Manx-16 seismic section. This line shows a similar pattern to the TRIST-92-21 line (figure 4.16). The CFZ forms an asymmetrical 'negative' flower structure, with the key faults forming the southern part of the fault zone. From examination, there is little seismic evidence of thickening of Permo-Triassic sequences into the Codling faults; therefore, it is unlikely that the fault-zone was active during Mesozoic rifting (e.g. see Naylor *et al.*, 1993).

The NW-SE orientation of the fault zone suggests that it probably formed initially during the Caledonian or Hercynian orogenies when faults of this trend are abundant. Dextral shearing is comparable to the Bann-Newry dextral strike-slip fault zone in north-east Ireland (Jenner, 1981), and similar NW-SE dextral faults in south-west England, such as the Sticklepath fault. These faults have been active since Oligocene times. A relatively thin accumulation of Tertiary sediments blankets the Kish basin, and displays subtle thickening against fault strands. As mentioned above, the fault zone cuts the Tertiary-Quaternary unconformity. Therefore, the fault has been reactivated during Tertiary times.

Recent seismic activity was reported along the Codling fault; a M_l4 event occurred in 1982 (Croker, 1995). This recent activity is probably responsible for opening fresh conduits for gas migration. Active gas seeps along the Codling fault have been reported by Croker (pers. comm. 1998) and is evident on Figure 4.16. Corcoran & Clayton (1999) interpret the present-day distribution of shallow gas accumulations as a result of bacterial activity in Namurian-Westphalian coal beds. There is also evidence of the build-up of Carbonate sea mounds along the trace of the Codling fault in the Kish basin, which are composed of carbonate-cemented sandstones (figure 4.19).

4.4.5 Bathymetrical Features – Faults?

The general trend of sea-floor morphology on figures 4.17 & 4.18 is ~N-S and NW-SE. The average depth over the Kish basin is 60m with maximum depths of 130m. The average depth across the whole Irish Sea is 80m with maximum depths of 180m. The N-S feature, which is ~10km east of Dublin Bay and labelled the Kish Bank on the map, represents a major sand wave, and average water depths are around 12m. A N-S elliptically shaped feature occurs to the south, 10km to the east of Kilcoole town (labelled 'K' on figure 4.17). The feature, or hole, is approximately 4.5km by 0.7km in length and width respectively. Average depths adjacent to the hole are in the order of 20-40m. However, maximum depths within the hole reach a maximum of 120m (over a distance of 0.3km). The feature occurs within the Bray Fault zone, and probably reflects glacially scoured fault gouge.

A similar feature occurs approximately 18km NE of Howth Head, the Lambay Deep (labelled 'LD' on figure 4.17). Water depths range from 50m to 130m. Jenner (1981) suggested that the Lambay Deep might be associated with local salt escape along the fault plane. Croker (1997) noted that the Codling fault is suspected of being a route for migrating hydrocarbons and postulated that the feature may indicate persistent venting of shallow gas. The feature is remarkably similar (in geometry, orientation and association with major NW-trending fault zones) to the onshore one east of Kilcoole, i.e. the Kilruddery fault (chapter 5). It is highly unlikely that there has been salt escape and/or hydrocarbon migration at this latter locality. Therefore, it is probable that the Lambay Deep may also be the manifestation of glacially eroded fault gouge as noted by Croker (1997).

Approximately 18km further east, another ~N-S co-linear feature (about 20km in length), separates relatively shallow water of ~40m from deeper water at depths of ~100m (labelled 'SW' on figure 4.18). Whilst the feature is more or less aligned ~N-S, it swings around to the NNW on the northern margin, and towards the SSE on the southern margin. Therefore, the feature may represent a fault (with E-W extension), or it may represent sand wave migration and tidal scour.

Near the eastern margin of the image, a N-S trending feature (labelled 'A' on figure 4.18) separates relatively shallow waters (50m) to the east, from deeper waters (160m) to the west. The change in water depths occurs over a variable distance ranging from <1km to ~5km. The feature extends for the full distance of figure 4.18 and may represent a normal fault, conjugate to the Codling Fault zone, forming a small graben that pinches out to the south. If the feature is a fault scarp, then the steeper gradients (in comparison with the Codling fault) may be explained by fault orientation. This fault/feature trends N-S whereas the Codling fault runs NW-SE. The kinematics of the Codling fault is believed to be dextral normal, based on displacement of the Dalkey and Lambay faults (figure 4.1), in harmony with ENE-WSW extension. Therefore, displacement on this feature would be mostly taken up by extensional movements (i.e. σ_2 ~NNW-SSE, σ_3 ~ENE-WSW, σ_1 vertical). The N-S fault/feature coincides with the 'Mid-Irish Sea Uplift Ridge'. It is therefore highly probable that the feature is a fault,

which has experienced relatively recent movement (in a similar manner to the Codling fault).

4.5 Onshore-Offshore Correlation of Dalkey and Bray Fault Zones

On the published geological map of the Kish Bank basin, the Dalkey and Bray faults are shown intersecting at an obtuse angle (figure 4.20). As shown below, both fault zones exhibit considerable throw. As noted earlier, the faults probably originated during the Caledonian orogeny. Therefore, the faults probably have onshore equivalents. The shallow water, however, makes seismic reflection too hazardous, and a CHIRP (shallow high resolution seismic reflection) survey across the intersection (and indeed Dublin Bay) was unsuccessful at imaging sub-bottom structures due to thick sand banks absorbing the seismic energy.

One of the main reasons for studying the structure of the Kish basin was to attempt a correlation with onshore tectonic models along the northern margin of the Leinster batholith and the Howth peninsula (chapter 3). Shannon (1991a) speculated that a set of NW trending fractures some 5km onshore (from the Bray and Dalkey fault intersection) may be the onshore equivalent of the Bray Fault zone (a flower structure similar to the Codling Fault zone – figure 4.10). Similarly, the youngest structures mapped along the northern margin of the batholith (see previous chapter) trend NW-SE, are brittle in deformational style, and are dextral normal in kinematics. The Bray Fault zone is post-Liassic and is extensional in nature. If the fault zone has been reactivated by the same stress system that affected the Codling fault, then the fault zone will be dextral, and may correlate with onshore structures with displacement during Oligocene-Recent times.

Seismic lines on the western margin of the basin were utilised (figure 4.20). This was necessary to create an offshore tectonic model. In particular, evidence of onshore faults intersecting the main basin bounding faults was an important aim. This is because traditional geological maps show the Balscadden and Blackrock (NE extension of southern boundary fracture) faults linking up, across Dublin bay. However, gravity gradients and outcrop at Blackrock are in disagreement with this. Therefore, this requires a fault to be present off the S and SW of Howth, i.e. Cambrian aged quartzites onshore and Carboniferous limestone offshore. Additionally, the preferred onshore

model from chapter 3 is in harmony with the Blackrock fault curving to an ENE to WNW orientation around the Leinster margin, which is also compatible with a limestone stack on the coast constraining the fault rocks, just north of Blackrock DART station (chapter 3). However, it must be noted that the absence of evidence is not evidence in itself. It merely states that a particular boundary condition is still valid, given the available data and constraints.

4.5.1 Line AIR 78-61

Figure 4.21 shows AIR 78-61 which extends from ~3km south of Howth Head to ~2km east of Bray Head, trending on an azimuth of 355°. The Bray and Dalkey Fault zones lie between shot-points 75-110, and shot-points 300-400 respectively. The line is unmigrated and the faulted contacts have produced a great deal of diffraction. However, apices of the diffraction arcs facilitate the recognition and location of faults. Therefore, due to the poor quality of the seismics, the interpolation of seismic facies is a crude approximation from which only major structures can be identified. The boundaries between the main facies are poorly constrained.

The postulated Liassic package is conformable with the underlying Permo-Triassic package, and forms an apparent hangingwall syncline with the Bray fault, and an apparent hangingwall antiform with the Dalkey fault. The beds strike ~N-S, therefore the axial plane of the folds is ~ perpendicular to the line of the section. A strand of the Bray fault cuts the Tertiary-Quaternary package (near shot-point 75), which conformably overlies the Permo-Triassic facies. The Tertiary-Quaternary reflectors form a small hangingwall syncline with this fault strand. The Tertiary-Quaternary section reaches a maximum thickness of 0.4ms[twt] where flat-lying reflectors onlap the Lias in the hinge of a fold (between shot-points 100-300). This suggests Tertiary displacement on the faults.

4.5.2 Line AIR 78-62

As figure 4.2 shows, this line is parallel to AIR 78-61 and is ~2 km further east. The line cuts the Bray fault and Dalkey fault at shot-points 830-810 and shot-points 280-270 respectively. Figure 4.22 shows that Top Carboniferous has been dropped across the

Dalkey fault system from ~0.3ms[twt] to 3.0ms[twt]. The Lias section is thickest against the Bray fault at 1.8ms[twt], compared with ~1.0ms[twt] against the Dalkey fault. The Lias is at a greater depth in this line (1.7ms[twt]), in comparison with AIR 78-61 (1.1ms[twt]). This may suggest that either the section is faulted out with depth (scissors fashion) and/or basement has deepened. The Lias forms a hangingwall syncline against the Bray fault. Near shot-point 420, the Lias is truncated against Triassic strata. It appears that the Lias is down-faulted between both the Bray and Dalkey faults, but is also affected by an intra-basinal fault.

As in line AIR 78-61, an outer strand of the Bray Fault zone cuts the Tertiary-Quaternary package. Subtle thickening of this package into the inner strand of the Bray fault is also evident. Thickening of this package has also occurred on an intrabasinal fault, near shot-point 580. At this locality a small normal fault dips towards the north and has thickened the package by ~0.1ms[twt]. The Dalkey fault also appears to cut the Tertiary-Quaternary, but the evidence is poorly constrained from the seismics. This is because water depths at the locality are very shallow (12m) and it may be that the apparent offset is actually due to seismic multiples.

4.5.3 Line AIR 78-63

This line (figure 4.23) is parallel to line AIR 78-62 but 2km further to the east. The line begins immediately NE of the Bray fault, within the Kish basin. However, an inner strand of the Bray fault appears at depth, at ~1.0ms[twt]. The line crosses the Dalkey Fault zone at shot-point 300 (figure 4.23). The Liassic section reaches a maximum depth of ~1.7ms[twt], and is truncated by the Bray fault at depth, but forms a hangingwall syncline at shallower depths (i.e. ~1.2ms[twt]). A small positive flower structure occurs between shot-points 480-290. The main Dalkey fault trends NE to NNE, whereas the fault on the southern margin of the flower structure (truncating the Lias) trends NW and is sub-parallel to the Bray fault. Hence, the Dalkey fault offsets the flower structure. A small fault offsets Tertiary-Quaternary, Carboniferous and basement near shot-point 75. The fault is near vertical in comparison with the fault on line AIR 78-62 (between shot-points 150-100), which was relatively shallowly dipping towards the north. Basement and Carboniferous rocks have undergone pre-rift deformation and display tilt block geometry.

4.5.4 Line AIR 78-64

This line is parallel with all the previous 3 lines and is likewise 2km to the east of line AIR 78-63. The line cuts the Bray fault and the Dalkey fault at shot-points 1-100 and shot-point 11,500 respectively (figure 4.24). The antiform at shot-point 600 is part of the same structure which well 33/21-1 was testing. The spacing of reflectors over the structure remains constant therefore the fold is probably tectonic and is post-Liassic but pre-Tertiary in age. The fold has been subsequently thrusted with top toward to the south. The fault does not offset the Tertiary-Quaternary unconformity. The Tertiary-Quaternary section remains relatively uniform at ~ 0.2 to 0.3ms[twt]. The flower structure on line AIR 78-63 is located between shot-points 720-800. The seismic character of the reflectors (underlying the Tertiary-Quaternary) to the north of shot-point 800 look similar to the Liassic south of shot-point 700, but it is likely that the pattern represents Permo-Triassic facies, based on the decreasing depth of the basement towards the Dalkey fault. Further evidence is provided from an aeromagnetic dataset, which is discussed in the next section. The Lias also forms a hangingwall syncline against the Bray fault.

4.5.5 Palaeo-Channel (?)

On all the four AMOCO lines, a particular feature stands out. On AIR 78-61 (figure 4.21), between shot-points 90-320, there is onlap and overstep of the Lias section by flat lying reflectors, which are themselves subsequently overstepped. On line AIR 78-62 (Figure 4.22), the same pattern is repeated between shot-points 290-580, and similarly on line AIR 78-63 between shot-points 740-600 (figure 4.23) and line AIR 78-64 between shot-points 200-320 (figure 4.24). On line AIR 78-66 the feature occurs between shot-points 1610-1710 (figure 4.25), on line AIR 78-53 the palaeo-channel is located between shot-points 1210 and 1290 (figure 4.26). As figure 4.27 shows, the channel varies in width between 1km and 4km, broadening towards the west. In some cases (but not all), the feature is centred over the axial plane of the hangingwall syncline; therefore, the channel has probably exploited weaknesses in the Lias strata, i.e. along the fold hinge.

4.5.6 Discussion of Implications

In all 4 seismic lines, basement in the hanging wall is higher against the Dalkey fault than with the Bray Fault zone. This is probably due to higher rates of displacement on the Bray fault. The thickest syn-rift deposits lie adjacent to the Bray Fault zone. The Permo-Trias syn-rift package thins northwards towards the Dalkey fault, and also thins towards the SE. The Lias strata form a hangingwall syncline against the Bray Fault zone, although locally, small antiforms have formed towards the top of the section.

All of the fold structures appear to be post-Liassic in age. Likewise, many of the faults have block rotated the Lias, and, vertical block movement have also occurred locally, e.g. the flower structure in AIR 78-63 (figure 4.23). Thrusting has also occurred in conjunction with folding, although, the vast majority of faults appear to be transtensional. The fault which occurs north of the Dalkey fault on lines AIR 78-62 (figure 4.22) and AIR 78-63 (figure 4.23) may represent a ~N-S trending fault, which swings clockwise into Dublin bay (the fault is vertical in an N-S orientation and shallowly dips to the north in an ENE orientation). This is supported by the coincidence of a magnetic lineament (section 4.6).

If the interpretation on AIR 78-64 (figure 4.24) is sound, then it is unlikely that there is as much Liassic in the hangingwall of the Dalkey fault as indicated on figure 4.20. The Tertiary-Quaternary section is relatively uniform, and unconformably overlies the Lias and oversteps onto the Carboniferous. However, in places it appears that the Tertiary-Quaternary has been offset by the main basin bounding faults, particularly the Bray fault. There is little evidence of faults intersecting the main basin faults from onshore.

As figure 4.27 shows, there appears to be a meandering palaeo-channel, which migrates westwards, i.e., an increase in width towards the west. This may be related to a topographical high to the east during Palaeogene or Neogene (?) times.

4.6 Aeromagnetic Survey – Structural Implications

The coverage of the aeromagnetic survey for the Kish bank basin is shown on figure 4.28. The data and all subsequent images have been projected to the 'Irish National Grid' co-ordinate system, in accordance with the parameters listed in table 4.1.

Figure 4.28 is a contour map, which spatially summarises a magnetic histogram, i.e. large values are common and low values are maxima and minima. It can be seen that the magnetic anomalies 'T' and 'V' have the lowest frequency but represents the highest and lowest magnetic values on figure 4.29. Therefore, a 'quantile' classification is used, in order to stretch the main population.

4.6.1 Total Magnetic Intensity (Reduced-to-pole [RTP])

Figures 4.29 & 4.30 shows the total magnetic intensity for the Kish basin. Figure 4.29 was generated from an ASCII file (with a cell-size resolution of 100m), whereas figure 4.30 was created by World Geoscience, using in-house software. The magnetic values range from 48,231 nanoTesla (nT) to 48,654nT. The values have been given a look-up table (red graduation colour scheme), assigned to 14 classes, where light to dark red correspond to relatively low and high magnetic values respectively. Figure 4.30 has likewise been assigned a look-up table using a rainbow spectrum colour scheme (i.e. purples and blues to reds and whites representing low and high magnetic values respectively). The mean value is 48,353nT and the standard deviation of the frequency of magnetic values is 34nT. This depicts a distribution of values asymmetrically skewed to the left (lowest being to the left). Additionally, the modal value is 48,341nT, although a second, smaller peak occurs at 48307nT.

The lowest magnetic values occur in the extreme south and west of the area of extent as represented by the light red colours on figure 4.29 and the purples and blues on figure 4.30. Each of these two low magnetic bodies have an area of ~106km^2 and ~279km^2, using 48,330nT as the cut-off value of the upper limit. A smaller magnetic low occurs in grid 500E 300N (labelled 'T' on figure 4.32) and depicts the lowest values in the area of interest. The anomaly is oriented NNW-SSE and is ~3km^2 in area, using 48,240nT value as the cut-off. A circular anomaly with high magnetic values around the southern

circumference and low magnetic values in the centre (labelled 'D' on figure 4.32), occurs in grid 400E 500N, and is ~8km^2 in area.

A large positive anomaly occurs in the lower half of the image (represented by dark reds on figure 4.29, and reds and whites on figure 4.30), and extends east and beyond the extent of the magnetic image. The anomaly is oriented E-W and is ~25km^2 in area, using the 48340nT value as the lower limit cut-off. Smaller positive anomalies occur in the extreme NW of the magnetic extent (labelled 'V' on figure 4.29).

Observation & Interpretation

The 2 aeromagnetic images (figures 4.29 & 4.30), crudely depict the overall configuration of the Kish basin. In general terms, broad areas of distinctive magnetic signature represent relative depth to basement. For example, well 33/22-1 encountered a thin veneer of Tertiary-Quaternary sediments (71m), and 720m of Carboniferous sequences, which unconformably overlay basement. The magnetic values at this locality are dark reds and reds and whites on figure 4.29 and figure 4.30 respectively. These colours form a broad area of ~25km^2 and from seismic evidence, this represents an area of shallow basement, known as the Wicklow High. In contrast, well 33/21-1 encountered 183m of Tertiary-Quaternary and 2km of Permo-Triassic (without penetrating basement, albeit, seismic evidence shows that the well at total depth must have been close to Top Carboniferous (figure 4.10)). The magnetic values at this locality show light reds on figure 4.29 and purples and blues on figure 4.30. These values form a NE elongated zone which encompasses an area of ~279km^2. The area corresponds with a low gravity anomaly that ranges from –5 to 0mGal. The gravity values increase towards well 33/22-1, i.e. rising to 15mGal over a distance of 15km. Surprisingly, the major faults are not clearly imaged.

4.6.2 First Horizontal Derivative of Total Magnetic Intensity (RTP)

ArcGrid GIS software was used to create a non-directional first horizontal derivative map of the total magnetic intensity. This process has the effect of emphasising discontinuities in the magnetic data by accentuating the shorter wave-length components at the expense of the longer wave-length features. Unfortunately, this inevitably increases noise. Nevertheless, important information can be deduced. The

rate of change of the magnetic intensity (gradient) has been given a 'quantile classification (13 classes) – figure 4.31. The areas, which show the highest gradient and the magnetic anomalies, are labelled 'T', 'V' and 'D'. The image also highlights a NW, NE and N linear trend, north of 300 N.

Observation & Interpretation

The first horizontal derivative image highlights linear texture in the image, which shows an overall ENE-WSW Caledonian trend. The Codling and Dalkey faults are now more clearly imaged in comparison with the total magnetic intensity map (compare with figures 4.29 & 4.30). All the wells are located on areas with relatively low change in the magnetic gradient with the exception of well 33/22-1, which is on the edge of a steep gradient. This probably represents deeper basement, from the Wicklow High (shallow) and southwards towards the Central Irish Sea basin (deeper).

4.6.3 High Frequency – Pseudo-Depth Slice One, Two & Three

Figures 4.32, 4.33 & 4.34 show various images derived from the Total Magnetic (RTP) intensity image with the application of high pass separation filter (pseudo-depth slicing). In each case, the images show progressively deeper structure (at the expense of the shallower structure). The northern part of the Central Irish Sea basin (south of ~280 northing) has been omitted from the pseudo depth sliced images to preserve clarity. This 'pseudo depth slice' filter operates in a similar way to a spectral shaping filter (Cowan & Cowan, 1993) by progressively acting on the amplitudes of frequencies outside the chosen range (figure 4.35). The result is to "focus" the frequency content of images by removing the shallow sourced signals and decreasing the strength of the deep sourced signals, i.e. it isolates frequency bands that represent various depths in the crust. Hence, figures 4.35, 4.36 & 4.37 show relatively shallow (high frequency, low amplitude) structure by removing the effects of basement, which has a lower frequency and higher amplitude (figures 4.38 & 4.39).

Observation & Interpretation

The magnetic anomaly 'T' is clearly visible and has high magnetic values around the margins but low values in the centre (figure 4.33). This is similar to anomaly 'D'. However, anomaly 'D' displays these characteristics on the RTP image (figure 4.29),

whereas, anomaly 'T' did not. This is probably due to the size of the anomalies, with the margins of 'T' being completely masked by the overall log negative values. Whereas, the margins of anomaly 'D' are sufficiently large enough to have their own distinctive magnetic signature.

Both these anomalies lie along the trend of the Codling fault. The extreme high and low values must be related to the high magnetite content (which is the primary control on the magnetic response of rocks). The very high frequency of the margins is probably related to the cooling of an igneous intrusion, and during crystallisation the polarity of the magnetic field switched.

In section 4.4.1, it was shown that the Codling fault was probably initiated during the Caledonian orogeny, but was largely inactive during Permo-Triassic rifting, and was then reactivated during the Palaeogene. The anomaly 'T' shows a slight clockwise rotation, and therefore was probably emplaced on a jog on the fault. The opening of the North Atlantic during Early Tertiary times produced vast amounts of igneous rock (British Tertiary Igneous Province), for example, the Mourne Mountains and the Antrim plateau lavas (see chapter 1). In addition, it has been documented that Tertiary dykes in the north of Ireland, and probably in the Irish Sea, show a similar reversal of the magnetic field, from the margins inwards, and also along strike. The magnetic anomalies 'T' and 'D' are therefore likely to be basic igneous intrusions of Early Tertiary age. The dextral sigmoidal geometry of the intrusion implies that it is syn-tectonic, i.e. the intrusion was emplaced during faulting, and may be at the intersection of an ENE-WSW to NE-SW fracture. Thus, the Codling fault was active during the Early Tertiary.

Relatively high magnetic values occur to the south of the Lambay fault. TRIST-92-21 shows uplift of basement west of the Codling Fault zone, whilst the magnetic high lies on the east downthrown block. It is therefore unlikely that the high is due to shallower basement but instead corresponds with an increase in the magnetite content of the basement rocks. This is most likely to be a Caledonian effect, i.e. the Portrane-Lambay Ordovician volcanics. The ridge has been offset dextrally by ~4km by the Codling fault.

On figures 4.33 & 4.34, a linear ridge of relatively high magnetic values (reds and whites) occurs between Howth and the Dalkey fault (labelled 'F' on figures 4.33 & 4.34), i.e. grid 300E 300N. The ridge runs sub-parallel to the Dalkey fault and the gravity contours and begins to swing clockwise around Howth Head, in similar fashion to the gravity contours. This may represent a fault associated with the Dalkey fault system, or it may simply represent Pre-Cambrian folds, e.g. the Caledonian syncline in the Bray Group of Howth (figure 3.12).

Figures 4.32, 4.33 and 4.34 pick out the Codling fault offsetting the Dalkey and Lambay Fault zones. The Lambay Ridge is also clearly illustrated as well as the white circular areas in the top left of the map (anomaly 'V'), surrounding Lambay Island. These high anomalies correspond with the Portrane-Lambay Ordovician volcanics. To the south, the Wicklow High is similarly offset dextrally by the Codling fault, a feature, which was not seen in the RTP image. In addition, there appear to be two relative magnetic highs on the Wicklow High, which may or may not have been offset by faulting. A gravity ridge (+30mgals) also corresponds with these volcanics and the Portane-Kildare high (chapter 2), i.e. it probably represents Pre-Cambrian basement with local Ordovician basic volcanic centres. The offset on the Codling Fault zone could also explain the magnetic ridge discussed above.

4.6.4 Low Frequency – Pseudo-Depth Slice Four

Figure 4.36 shows a processed image derived from the total magnetic intensity (RTP) image. The images correspond to the longer wavelength component of the frequency domain and depict deeper levels of the crust.

Observation & Interpretation

The low-frequency image illustrates the overall basement structural architecture. The Lambay Fault zone stands out particularly well in comparison with the total magnetic RTP image (figure 4.30) and the high frequency pseudo-depth images (figures 4.32, 4.33 & 4.34). The other major basin bounding faults are also clearly visible (with the exception of the Bray fault, which is only partially covered by the aeromagnetic survey) and thus probably reflect the reactivation of Caledonian faults during the Hercynian (e.g. see Corcoran & Clayton, 1999), Permo-Triassic rifting and 'later' deformational

events (chapter5). The extreme high and low areas of magnetic signature are visible (albeit, with very subdued boundaries), indicating that their presence on the higher frequency images (with sharper discontinuities and linear texture) are real features and not merely magnetic noise. The Wicklow High exhibits two relatively high magnetic peaks (which are also imaged on the RTP anomaly map; figures 4.29 & 4.30). The overall orientation of the main magnetic gradients is NE-SW, NW-SE, and E-W.

4.6.5 Azimuth Images – Pseudo-Depth Slice 2 to 4

An azimuth image is derived from the pseudo-depth slice by taking the total horizontal derivative. This technique centres the peak of the derived signal over the maximum gradient of the curve and resolves linear, low amplitude, high frequency anomalies. The resultant azimuth images are illuminated using a colour (Red, Green and Blue) linked to dip azimuth (i.e. NW, N, NE respectively), an image enhancement technique which alleviates the directional bias introduced by false sun illuminations. This, in effect, offers a better identification of geological anomalies. However, the main disadvantage is the decrease in signal-to-noise ratio and the normalising effect on linear anomaly width, which thus removes an important characterisation criterion.

Observation & Interpretation

Azimuth 4 (figure 4.37) conveys the least amount of geological information. The image highlights a deep NW-SE, NE-SW and E-W structural grain. Of particular interest however is the strong ~E-W lineament which well 33/22-1 lies along (labelled 'W' on figure 4.37). Azimuth 4 (figure 4.37) images anomalies 'T', 'D' and 'V' clearly. The Lambay, Codling, and to a lesser extent, the Dalkey faults exhibit a relatively strong magnetic lineament. Similarly, lineament 'F', east of Howth, exhibits a strong gradient lineament. The northern margin of the Wicklow High, labelled 'M' on figure 4.42a, likewise produces a strong lineament.

One particular strong NW trending lineament (labelled BF on figure 4.37 & 4.38) occurs east of well 33/17-1, which has a corresponding low (blue colour) magnetic signature and probably represents a major basement fault. Figure 4.38 show that the lineament crosses the postulated Lias-Triassic boundary. The lineament terminates to the NW against a fault strand, which is itself truncated by the Codling fault. Therefore,

it is likely that the lineament represents a major basement fracture, which was mostly inactive during Tertiary times, i.e. the fault is not seen on the total magnetic intensity image, and the Codling fault truncates a fault that appears to offset the lineament.

In azimuth 3 (figures 4.39 & 4.40) and azimuth 2 (figures 4.41 & 4.42), the signal-to-noise ratio (SNR) has decreased in relation to azimuth 4 (figure 4.37). The azimuth 2 image (figure 4.41) contains the lowest SNR. This can be illustrated by picking a discontinuous lineament and tracing it over geological boundaries (figure 4.42). Notwithstanding, it can be shown on figure 4.42 that the majority of lineaments do terminate near geological boundaries. However, the overall lineament pattern cancels out any inherent noise associated with some of the lineaments. Both figures 4.39 & 4.41 show that magnetic azimuths can be grouped into distinct zones of lineament pattern. For example, on both figures 4.39 & 4.41, the dominant lineament pattern is NE-SW and NW-SE north of 400N. South of 400N but north of 300N, the main lineament pattern is still NE-SW and NW-SE, but another group of ~N-S oriented lineaments are present. To the SE (south of 300N), across the Wicklow High, the main pattern is WNW-ESE, although a strong NW-SE pattern (representing deeper structure filtering through to the higher frequency images) is still evident (i.e. azimuth 3 – figure 4.39). The boundary to the change in lineament pattern corresponds with a major fault, which bounds the southern margin of the Wicklow High. The change in orientation across the fault is not sharp. However, the lineaments exhibit a Z-shaped sigmoidal geometry across the fault. This may suggest a sinistral component of slip on the fault (a topic which is explored in greater detail in chapter 5).

4.6.6 Implications

The high frequency, low amplitude images highlight areas of shallow source with low magnetic susceptibility. This probably reflects faulting within the sedimentary section. With the exception of the small negative anomaly east of the Codling fault, the low amplitude of the residual anomalies within the Kish Bank basin suggests that the shallow section is free of volcanics. The small negative anomaly east of the Codling fault appears to be an igneous body and the polarity has switched from positive to negative during emplacement and cooling. The sigmoidal geometry and orientation in

respect to the Codling fault suggests that the body was emplaced within an overall a dextral transtensional environment.

The deep-seated NE-SW and NW-SE trends are fairly well developed. The combination of NE and NW trends may have controlled the compartmentalisation of magnetic basement and probably had a marked influence on rifting and subsequent uplift and erosion. The change in lineament pattern over the Wicklow High, which corresponds with a broad area of high magnetic values, implies recent movement on the fault bounding the southern margin of the Wicklow High. The sigmoidal swing in the lineament pattern across the fault suggests a sinistral sense of displacement.

4.7 Post-Liassic History – Regional Correlation

Many fault-controlled half-grabens, filled with 3-5km of Permian to Lower Jurassic sediments (Shannon 1991a), extend down the length of the Irish Sea (figure 4.7). The basins are bounded by mainly NE-SW and NW-SE faults, which produce strong gravity lineaments (figure 4.8). Mesozoic stratigraphy occurs in the western and eastern parts of the Irish Sea region with the oldest rocks occupying the central part. A first order inference therefore is that the Irish Sea region is a horst which has been inverted along the central high and suffered extensive post-Liassic erosion before subsiding to form a graben in post Pliocene (?) times.

4.7.1 Kish Bank Basin

As illustrated in section 4.2, thick Triassic to Liassic sequences are preserved in the hangingwalls of the western boundary faults of the Kish basin (figure 4.1). The basin is cut by the NW trending Codling fault, which is a Tertiary aged structure. The basin is hinged towards the SE and E against shallow basement rock of ~Lower Palaeozoic age and Upper Carboniferous potential hydrocarbon source rocks. The ENE-WSW Wicklow High was a positive feature during Triassic rifting, shown by seismic evidence of Triassic sequences onlapping the structure. The southern margin of the Wicklow High (the northern boundary of the Central Irish Sea basin) is faulted, and the block has been back-rotated towards the north, in harmony with regional tilting. It was suggested

in section 4.6 that the Wicklow High fault is a sinistral transpressional structure, but what is the age?

4.7.2 Irish Sea Region - Integrated AFT and VR Data

The amount of denudation based on AFT data is a function of the palaeogeothermal gradient at the time the rocks were at 110±10°C. The determination of the palaeogeothermal gradient can also provide insight into the cause of heating and subsequent cooling (Bray *et al.,* 1992). For example, if heating were due to a higher basal heat flow, then the palaeogeothermal gradient at the time of maximum palaeotemperatures would be higher than the present-day geothermal gradient. On the other hand, if heating were due to deeper burial followed by uplift and erosion with very little change in the basal heat flow, then the palaeogeothermal gradient would be the same as the present gradient. And, if the heating were the result of igneous intrusion and/or the circulation of hot fluids, then the palaeogeothermal gradient would produce a non-linear palaeotemperature profile.

There have been several studies of AFT, VR and integrated VR and AFT in the Irish Sea region and onshore in NW England (Lewis *et al.,* 1992; Green, 1987; Green *et al.,* 1993; Green *et al.,* 1997; Green *et al.,* 1999), which have proven useful for giving insights to the Tertiary history of the region. Lewis *et al.,* (1992) analysed AFT data from several wells in the eastern Irish Sea region, the Isle of Man and onshore outcrop in the Lake District, the Carlisle-Vale of Eden basin, the Lancashire Moors/Pennines and North Wales.

Forward modelling of parameters resulting from likely thermal histories, showed that samples of Permian to Triassic age have been totally annealed and AFT ages have been reset since the rocks were initially deposited (Green *et al.,* 1997). The samples had retained mean track lengths (MTL) of ~14μm, and hence must have cooled rapidly after having been reset, i.e. to prevent further annealing and reduction of MTL. Modelled thermal histories show that AFT samples had attained maximum palaeotemperatures of 110±10°C at c.65 ± 5Ma (Lewis *et al.,* 1993; Green *et al.,* 1993; Green *et al.,* 1997).

Lewis *et al.,* (1992) assumed a palaeogeothermal gradient of 30°C km^{-1} based on earlier studies by Green (1989) and published VR data from the East Irish Sea basin and assumed a surface temperature of 10°C. Based on these parameters, Lewis *et al.,* (1992) concluded that between 2.7km and 3.3km of erosion was required to satisfy the observed data, i.e. that the maximum palaeotemperatures were the product of deeper burial and not higher basal heat flow because the palaeogeothermal gradient is similar to the present-day (Bray *et al.,* 1992).

Green *et al.,* (1997) analysed AFT and VR data from a number of wells in the Irish Sea region and stated that the palaeogeothermal gradients were indistinguishable from present-day values, and hence, maximum palaeotemperatures recorded by AFT and VR data were mostly due to burial and subsequent denudation through the Tertiary. Green (1999) states that most of the wells from the UK North Atlantic Margin and around the British Tertiary Igneous Province show no direct evidence to suggest elevated basal heat flow during Early Tertiary times.

The Larne-2 well in NE Ireland (figure 4.7) was drilled in close proximity to Tertiary basaltic lavas and AFT data from Permo-Triassic rocks reveals Early Tertiary palaeotemperatures from which cooling began some time between 70Ma and 50Ma. However, there is very little variation in palaeotemperatures over a depth of 3km suggesting that this event is characterised by a low palaeogeothermal gradient (i.e. <35°C km^{-1}). Hence, the heating event is due to burial followed by subsequent uplift and erosion of between 1km and 2km with the rocks cooling from 110±10°C at the beginning of the Early Tertiary. This is consistent with an episode of major regression that commenced in the latest Cretaceous and continued until earliest Tertiary times. This led to differential erosion and the establishment of karst topography at the top of the Ulster White limestone (plate 1.1), which was subsequently covered by Palaeocene lava flows.

Therefore, the AFT data appear to imply that there was widespread Early Tertiary uplift and denudation, with the largest denudation values in the East Irish sea. This same event has been correlated onshore in Northern England (Green, *et al.,* 1997) and has led to the concept of an Irish Sea dome (Cope, 1994; 1998). However, a different pattern also occurs over the Irish landmass (see chapters 7 & 8).

4.7.3 Other Lines of Evidence

This cooling event may correlate with a major unconformity at the K-T boundary in the North Celtic Sea basin (chapters 1 & 8) and an unconformity between the Jurassic and Palaeogene deposits in the Cardigan Bay basin (Naylor, 1992). In the Western Approaches, chalk porosity data suggest that Tertiary uplift and erosion affected both troughs and depocentres (Hillis, 1991), despite the general absence of any recognisable inversion structures. In addition, Roberts (1989) analysed VR data from a number of wells in the Irish Sea, which he interpreted as indicative of elevated palaeotemperatures prior to cooling, commences in the Early Tertiary with 2km of eroded section. This implies a first-order of uplift and erosion of the entire region.

Sonic velocity data supports this denudational event, although, the magnitudes are much less (Turner & Phillip, 1998). However, this is because a reference well is chosen as representing normal compaction, which is highly unlikely if the whole region has experienced denudation. Thus, estimates from sonic velocity studies of ~1km should be viewed as minimum values only.

4.7.4 VR Studies in the Kish Bank Basin and Adjacent Areas

In the Kish basin, recorded Rm% for Westphalian B-D in well 33/22-1 range from 0.83% to 1.35%. In well 33/21-1, VR determinations of Rm 1.23% to 1.67% were recorded from the Trias interval (Haughey, 1987). However, the confidence levels of these values are low due to the relative paucity of vitrinite and the possible occurrences of re-working.

By using a composite approach (i.e. analysing a number of wells – figure 4.43) in interpreting VR data, Corcoran & Clayton (1999) showed that peak palaeotemperatures from Westphalian/Stephanian sequences in wells 33/22-1, 42/12-1 and 42/16-1 are in the range of 110-245°C, whereas, peak palaeotemperatures from Jurassic sequences in wells 42/17-1 and 42/21-1 are in the range of 50-100°C. This implies palaeogeothermal gradients of 74-78°C km^{-1} for wells 33/22-1, 42/12-1 and 42/16-1. Similar palaeotemperatures and palaeo-gradients were calculated from the onshore Carboniferous aged Dublin basin (e.g. Fernandes, 2000).

Corcoran & Clayton (1999) assumed that the measured present-day geothermal gradient of 26°C km^{-1} in well 42/12-1 is representative of other wells in the region. Hence, the relatively high palaeogeothermal gradients must be due to an increase in basal heat flow (after Bray *et al.*, 1992) suggesting an earlier (i.e. pre-Tertiary) heating and subsequent cooling event. Green *et al.*, (1997), using a combination of AFT data from the Permian-Triassic level, and VR data from Carboniferous samples provides supportive evidence for an earlier (pre-Tertiary) thermal event.

In contrast, the elevated palaeotemperatures from the Jurassic samples in wells 42/17-1 and 42/21-1 recorded an estimated palaeogeothermal gradient of ~ 26°C km^{-1}. The similarity of this palaeogeothermal gradient to the present-day geotherm suggests that the heating of this section was due to deeper burial and subsequent exhumation. Therefore, the two differing geothermal gradients must be the result of different heat flows at the time. Corcoran & Clayton (1999) attribute the earlier, hotter gradient to a Hercynian thermal event and subsequent establishment, post-Stephanian-Early Permian inversion, led to a heat-flow from Jurassic times and onwards, similar to the present-day values.

Jenner (1981) estimated that ~3km of erosion was required to explain the high maturity levels in well 33/22-1. Corcoran & Clayton (1999) calculated ~1.5km of erosion from well 33/22-1. This large discrepancy is due to the palaeogeothermal gradient utilised to calculate denudation. Jenner (1981) used the present-day geothermal gradient whereas Corcoran & Clayton (1999) calculated denudation based on the palaeogeothermal gradient at the time the VR was at maximum palaeotemperatures. However, this estimation of exhumation must be a minimum because net exhumation was calculated from well 33/22-1 relative to the present-day seabed, and the amount of material removed during Hercynian inversion is unknown. Thus, the 1.5km (Corcoran & Clayton, 1999) and 3km (Jenner, 1981) of erosion for well 33/22-1 must be viewed as the minimum and maximum limits respectively. AFT analysis of this well would be a valuable tool for estimating post-Permian cooling (i.e. Early Tertiary).

4.8 Discussion and Regional Correlation

Based on regional correlation, there were at least two cooling events in the Kish basin, 1) Stephanian-Early Permian, and, 2) Early Tertiary. The latter cooling event is primarily responsible for the exhumation and regional tilt of the Kish basin, which has truncated the stratigraphy. As a result, only remnants of Lias sequences are preserved, primarily restricted to the hangingwalls of the major faults (in particular the Bray fault). A relatively thin veneer of Tertiary-Quaternary sediment subsequently oversteps these sequences. The existence of ?Pliocene or older aged lignites in well 33/17-1 (Naylor *et al.*, 1993) indicates that the area was sub-aerial at this time, and has subsequently experienced subsidence.

4.8.1 Age of NW-SE Compression and NE-SW Extension Palaeostress System

It was shown in chapter 3 that palaeotemperatures of granite outcrop along the northern margin of the Leinster batholith was >300°C, in Hercynian times. These temperatures would mean that quartz grains would deform in a ductile fashion. The WNW-ESE reverse dextral shears that cut the granite outcrops are notable for their brittle, cataclastic deformation style, and the textures show that quartz grains are highly strained (undulose extinction) with little polygonisation. Therefore, these structures are post-Hercynian in age.

Geoffroy *et al.*, (1996) undertook brittle deformation studies of Tertiary basaltic lava flows outcropping in NE Ireland, and reconstructed palaeostress tensors using the inversion methods of Angelier (1989, 1991). They document NW-SE compression and NE-SW extension during the Palaecoene. This relates to syn-magmatic extension, i.e. dyke emplacement. However, they were unable to establish whether or not dyke emplacement occurred under a pure extension (σ_1 vertical), an extensional strike-slip regime (σ_2 vertical), or a combination of both. It is possible that this stress system also prevailed during the Early Tertiary in the Leinster region. In this case, the maximum compression (σ_1) is horizontal. AFT studies show that an Early Tertiary cooling/denudational event affected the whole region, including the Leinster batholith (chapter 7). Therefore, it is possible that the WNW-ESE reverse dextral and N-S

normal sinistral conjugate structures accommodated this denudation (uplift) event as inversion structures.

4.8.2 Age of NNW-SSE Compression and ENE-WSW Extension Palaeostress System

The NW trending Codling Fault zone transects the Kish basin. Pprevious workers have speculated that the Codling Fault zone is aligned with the dextral normal Newry Fault zone, which is known to have been active both during and after the Oligocene (Charlesworth, 1953; George, 1967; Jenner, 1981; Kerr, 1987; Parnell *et al.,* 1988; Readman *et al.,* 1997; Geoffroy *et al.,* 1996). These correlations are based on the evidence that both fault zones are Tertiary structures and have similar geometry and kinematics (section 4.4.1)

As shown in chapter 1, the Lough Neagh-Larne basin has a fill that ranges in age from Permian to Late Tertiary (George, 1967; Reid, 1971; Wilson, 1972; Fletcher, 1977; Thompson 1979; Wilkinson *et al.* 1980; Penn, 1981; Illing & Griffith, 1986; Smith 1986; McCann, 1988; Parnell *et al.,* 1989; McCann, 1990; McCaffrey & McCann, 1992). Boreholes in the Lough Neagh basin have confirmed the presence of a 300+m thick succession of interbedded lithomarge, pyroclastics and lacustrine deposits, which are interpreted as Oligocene in age (Parnell *et al.,* 1986). In addition, Oligocene aged rocks occur in the Ballymoney area.

These deposits are the result of transtensional reactivation of basement faults, which created accommodation space for the establishment of freshwater lacustrine environments (George 1967; Parnell *et al.* 1986) that produced thick accumulations of siliciclastic and lignite deposits. The area was subsequently subjected to compressive stresses, NNW-SSE horizontal compression and ENE-WSW horizontal extension; (e.g. Kerr, 1987; Millar, 1990; Geoffroy *et al.,* 1996). This produced gentle warping and erosion of the Lough Neagh Group. The contemporary section is preserved in the footwall of major northeast-striking faults downthrown to the south (figure 4.44).

4.9 Implications

Structural control and regional correlation suggests that the dextral transform model is potentially of Early Tertiary age, and is probably coeval with up to ~3km of denudation in the Irish Sea region. The NW-SE brittle normal dextral structures are due to a later stress system, of probable Oligocene age and younger, which is probably related to fault-controlled subsidence of the Irish Sea region which may have been as young as Pliocene in age. The dextral transform model cannot readily explain this. Therefore, the aims of the thesis are broadened to account for this.

For example, the projected traces of the Wicklow High structures intersect the Irish coast just north of Wicklow Town and have reactivated the Callowhill and Southeastern Boundary fault, and the East Carlow Deformation zone (figure 4.45), producing geomorphic features in the present-day landscape (chapter 5). This implies that the Wicklow High fault is conjugate with the Codling fault. The intersection angle is greater than 60°, and therefore would result in sinistral transpressional deformation on the bounding fault. This is in harmony with the sinistral sigmoidal pattern of magnetic lineaments (section 4.6). In order to test this new, younger model, analyses of topography and satellite lineaments are undertaken in chapters 5 & 6.

CHAPTER 5 - TOPOGRAPHIC ANALYSES OF SE IRELAND

5.1 Introduction

The topography and relief of a region is a reflection of the time-integrated effects of both tectonic and climatic activity. Landform development is closely related to the underlying structure and the processes that act upon the exposed surface, i.e. weathering, fluvial, mass wasting, volcanic, glacial, aeolian, and tectonic. Therefore, investigation of the geomorphological record provides a tool for evaluating the role of active tectonics in the development of landforms.

The main aim of this chapter is to attempt to correlate the post-Liassic model of chapter 4, with the analysis of Tertiary aged fault movements in SE Ireland. In particular, the onshore projection of the Wicklow High fault correlates with the Callowhill fault and East Carlow Deformation zone (figure 4.45). These onshore structures also correspond with topographic ridges and depressions. Therefore, the cause of this feature needs to be established. On a more general level, one of the main problems of this is to discriminate and partition the role between endogenic and exogenic processes. Exogenic processes act upon the exposed surface and include the action of water, ice, wind and biota, which result in denudation and a net reduction in the elevation of a region. Endngenic processes however are constructional in nature and include crustal uplift (orogenic and epeirogenic) and igneous activity.

In general, it is shown in this chapter that endogenic processes have, until very recent times, been the dominant mechanism, which has shaped the present-day landscape of SE Ireland. The main exogenic processes include glacial erosion and deposition during the Quaternary and fluvatile erosion and deposition during the Holocene. Much of this erosional activity is concentrated along pre-existing structural discontinuities. Fluvial processes are the most important indicators that recent tectonic activity (endogenic) has occurred. Much of this is due to reactivation of faults during Neogene times (chapter 7) and the time lag is shown by the occurrence of river knick-points and wind-gaps as fluvial incision attempts to achieve a state of 'dynamic' equilibrium. Based on our knowledge of the likely timescale adjustments of rivers (Summerfield, 1991), it is

shown that this tectonic and erosional activity reflects the time lag between tectonic uplift and positive isostatic feedback. In essence, the rivers are responding to epeirogenic fault block movements due to isostatic re-adjustments along discrete blocks of shallow crustal rock, bound by major fractures.

5.1.1 Methods and Materials

The main methods used in this chapter are spatial analyses of various datasets using ESRI GIS software. The main materials include:-

- High resolution (50m) digital elevation data from the Ordnance Survey
- Bedrock geology from GSI maps
- Additional information on bedrock structure
- Statistical analysis of the relationships

An outline of these methods and materials is given below.

Digital Elevation Models (DEMs)

DEMs represent elevation at the Earth's surface (chapter 2) at given points. Terrain analysis relates to the determination of geomorphological and geological features that are distinct functions of elevations or which can be inferred from knowledge of elevations (Collins, 1975).

Spatial evaluation and study of the topography of SE Ireland and associated geomorphological landforms was carried out using Ordnance Survey digital elevation data with ESRI GIS software (i.e. ARC/INFO, ArcGrid and ArcView). The data originated as 20 x 20km tiles of contour data (Cad format). The tiles were initially converted to ARC/INFO line coverages (including contour elevation attributes). The TOPOGRID interpolation method was then applied to each tile at a 10m cell-size.

After running the TOPOGRID model on each tile (Hutchinson, 1988, 1989) for specific detail and algorithms for this model), it was necessary to hillshade the DEM to visually inspect for errors such as a wrongly coded contours. Once all tiles were converted, they were then stitched together using the MERGE (ArcGrid) command and the grid

resampled from 10m to a 50m spaced lattice (using the bi-cubic interpolation method); a practical and adequate resolution to work with in terms of file-size and accuracy of the results.

The DEMs can be displayed as contoured surfaces to identify the main geomorphic features. These representations can be used to identify key geomorphic features, surfaces and boundaries, in a similar fashion as with a traditional topographic map. The advantage of the DEM is that it allows a broad range of map scale and elevation resolutions when evaluating features of significant interest.

Hillshading of DEMs produces a shaded relief grid by the projection of an artificial light source onto the surface and determining reflectance values, i.e. it produces a shadowing effect. This preferentially highlights linear features perpendicular to the light source azimuth. Hillshading gives an overall impression of the terrain, which is biased in the direction of illumination.

The reflectance value at each cell is generated from the cosine of the local illumination angle. For sun position (S, A), the shade is defined as:

$$I = 255(\cos(S)\sin(\mathbf{s})\cos(\mathbf{a}-A) + \sin(S)\cos(s))$$

where **s** and **a** are local slope and azimuth angles at a cell. The constant 255 is used to scale the shade for display.

All hillshades in this chapter are illuminated from the NW.

Topography statistics

The Geological Survey of Ireland kindly provided the 1:100,000 maps (sheet 16, Kildare-Wicklow; and sheet 19, Carlow-Wexford) in digital format. The data were in Cad format, and needed to be converted to both ARC/INFO coverage and ArcGrid raster. The data required some further pre-processing, i.e. assigning a geological look-up table to polygons and grids. This data was used to statistically describe and measure the relationship between geology and various topographic variables (i.e. elevation, slope and relief).

Slope

The SLOPE command in ArcGrid was used to produce a slope grid (rate of change in degrees). The algorithm identifies the maximum rate of change in elevation, from each cell to its neighbours. The slope function fits a plane to the topographic (z) values of a 3x3 cell neighbourhood around the processing or centre cell. The direction the plane faces is the aspect for the processing cell. The slope for the cell is calculated from the 3x3 neighbourhood using the average maximum technique (Burrough, 1986). At the edge of the grid, cells will be assigned the centre cell's value. Hence, the slope calculates the rate of change in elevation. The formula is given by:

$$\frac{opp}{adj} = \sqrt{\left(\frac{\delta z}{\delta x}\right)^2 + \left(\frac{\delta z}{\delta y}\right)^2}$$

$$b = aTAN\left(\frac{opp}{adj}\right) \times 57.29578$$

This value represents the centre value (one dimensional) of a 2500m^2 pixel. Therefore very steep to vertical slopes will be averaged out over the pixel area. Reducing the pixel resolution to 100m^2 will resolve slightly steeper slopes. But, the extra detail would not significantly enhance the results and conclusions, and the higher resolution will detrimentally affect computational performance and consume computer disk space.

Relief

The relief grid was computed from the DEM by using the FOCALRANGE command in ArcGrid. For each cell location on the DEM, the algorithm finds the range of values within a specified neighbourhood and sends it to the corresponding cell location on the output grid. By trial and error, the neighbourhood shape was a 10x10 square to capture hill-slope length (i.e. crest to base). The shape and size of the square gave the best results for highlighting the magnitude of relief for specific areas of interest.

Ohmori (1983) showed that denudation is positively correlated with relief. The relief grids for the Vartry (section 5.4.12), Bunclody (section 5.5.13) and Glen of Imail areas (section 5.6.14) represent the difference between the maximum and minimum elevation for a 500 x 500m box. Slope has a strong positive correlation with relief (Summerfield,

1991). In general, areas of relatively high elevation normally have high relief and steep slopes. However, this is not always the case, e.g. areas of high elevation such as the Tibetean plateau have internal drainage systems with local base-level ~4,000m above sea level (asl). Thus, this particular area shows relatively low relief and slope.

Correlation Matrix

The correlation matrix was used to derive the relationship between slope, relief and elevation. This covariance statistic computes the average of the products of deviations for each data point pair. The covariance between two variables depends on the magnitude of the data values. Dividing the covariance by the standard deviations of the 2 variables guarantees that the correlation coefficient will always be between –1 and +1 and provides an index that is independent of the magnitude of the data values.

Descriptive Statistics

Descriptive statistics summarise the elevation distribution per rock type and slope category (i.e. the angle of slope for a given area was categorised into 5° bins and assigned elevation values based on their spatial location, with higher slope angles lumped together to yield significant statistical results). The distribution of lithology with slope and relief is also summarised. The standard deviation measures the spread of the values and the skewness measures the width of the distribution. Skewness measures the extent to which the bulk of the values in a distribution are concentrated to one side or the other of the mean, e.g., positive skewness indicates a distribution with an asymmetric tail extending toward more positive values and vice versa. The formula is given by:

$$\frac{n}{(n-1)(n-2)}\sum\left(\frac{x_j-\bar{x}}{s}\right)^3$$

5.1.2 Concepts

The four concepts which underpin this study are that: 1) landscapes evolve through time and changes in the assemblages of landforms are predictable; 2) abrupt changes may occur due to thresholds being exceeded; 3) the interaction of landscape evolution with

change in thresholds, results in complex processes, and; 4) a change in form implies a change in process. Mitchell (1985) highlighted the following variables which need to be considered when assessing the development of the Irish landscape: 1) lithology of rocks; 2) rock structures; 3) climate, and; 4) weathering regimes and duration.

5.1.3 Regional Setting and Previous Work

The Wicklow and Blackstairs Massifs (the Leinster Mountain chain) dominate the topography of SE Ireland (figure 5.1). The Wicklow Massif forms a broad, gently rolling upland and trend approximately NE-SW and are ~50km in length by ~30km in width. The highest elevation is the Lugnaquillia Mountain (921m), which is located towards the southern margin of the Massif. South of Lugnaquillia Mountain, the Blackstairs Mountains and the Tinahely hills (termed here the Blackstairs Massif) form the southern continuation of the uplands. The chain forms a series of NE-SW to NNE-SSW trending ridges of low mountains and hills, with widths varying between 2 and 5km. The highest mountain in the Blackstairs Massif is Mount Leinster (795m). A number of low-lying valleys cross the range (section 5.5).

To the south and west of the Leinster Mountain chain, around Hacketstown and Tullow, and extending SW to the River Barrow below Goresbridge is a broad plain, known as the Tullow Lowland, which is at elevations of 100m to 130m (figure 5.1). To the north of the Wicklow Mountains, a broad dissected plain extends from the mountain front of Three Rock Mountain (~550m) to the town of Dun Laoghaire, situated on the southern side of Dublin Bay (figure 5.2). To the west, the elevation falls to form a gentle undulating landscape dominated by glacial depositional features, such as drumlins and eskers (Warren, 1985). On the east, the elevation decreases more suddenly, producing steeper topography (figure 5.2).

Drainage

On the eastern margin of the Wicklow Mountains, the rivers drain from the NW and NNW, have a relatively small watershed and are only a few kilometres in length. However, on the western margin, the rivers flow west then north (the Liffey) or south (Slaney) – figure 5.1. These rivers have much larger catchments, and are an order of magnitude greater in length than the eastern rivers (i.e. the Slaney is ~80km in length).

The Derry River flows southwest parallel to the Blackstairs Massif to join with the Slaney, and the Derry Water flows NE to join with the Aughrim River.

Geology

The Leinster Mountain chain and the Tullow Lowland (figure 5.3) occur on the Leinster Massif, which is formed of both igneous and sedimentary rocks ranging in age from Lower-Middle Cambrian to Lower Devonian sediments and flanked by Carboniferous rocks. The main igneous rocks are the Leinster batholith, which covers an area of over 1500km^2. O'Connor and Brück (1978) obtained a Rb-Sr whole rock isochron age of 404±24Ma from the northern margin of the batholith. Geochemically, the batholith is a 2-mica peraluminous S-Type. The batholith intrudes Ordovician aged metasediments of the Ribband Group (Appendix 3) and has produced a structural and thermal metamorphic aureole.

On the NW flank of the batholith, the aureole is ~0.5km in width, whereas in the SE, the aureole is ~6km wide. The variation in width is because the batholith is asymmetrical along a NNW-SSE trending axis. The granite has a moderately dipping SE contact on the SE flanks, but steep contacts on the NW flanks and in places the contact is vertical or steeply dipping inwards (Brindley, 1957). The northern boundary of the batholith forms the southern coastline of Dublin bay, and is in fault contact with the Carboniferous aged limestones of the Dublin basin (figure 5.5).

The batholith consists of 5 dome-like units arranged en-echelon along a NNE axis (figure 5.3). As figure 5.5 shows, the 5 units (from north to south), are the:

- Northern Pluton;
- Upper Liffey Valley Pluton (satellite to above);
- Lugnaquillia Pluton;
- Tullow Pluton, and;
- Blackstairs Pluton.

Each pluton, with the exception of Lugnaquillia, shows concentric internal zonation. The Lugnaquillia pluton is more irregular both in shape and internal zonation

(Appendix 3). The nomenclature of the granite types is after Brindley (1953) and Brück & Reeves (1976), and is described in Appendix 3.

Uplift of Leinster Mountain Chain

There have been much debate in the literature about the age of uplift and subsequent development of the topography of the Leinster Mountain chain. The lack of post-Carboniferous rocks in the region has meant that geologists have mostly ignored the question of Mesozoic-Tertiary tectonics that is obviously responsible for the formation of the present-day landscape. Much of the debate has therefore been tackled by geomorphologists (e.g. Mitchell, 1985, and, Davies, 1970).

The presence of granitic pebbles, derived from the batholith, occur in the Upper Devonian Old Red Sandstone (ORS) of Counties Kilkenny and Waterford (Jukes, 1862; Capewell, 1956). In Co. Kilkenny, the Upper Devonian ORS onlaps the schist to rest on the batholith. Therefore, the southern part of the batholith was at least partially unroofed at this time. Similarly, in the Courceyan Dublin basin to the north, granitic fragments occur in Viséan limestones up to a distance of 5km from the margins of the batholith (Montgomery, 1864-67; Ball, 1888). Hence, parts of the batholith were exposed during Carboniferous times.

One argument is that the Leinster Mountain chain has formed a topographic high since Mid-Palaeozoic times, and has undergone continuous denudation ever since (Stamp, 1949; Wills, 1951; Freeman, 1950). However, roof pendants are still present on parts of the batholith, for example, the schist cover that crosses the peak of Lugnaquillia Mountain. In view of parts of the batholith already being exposed in Late Devonian-Early Carboniferous times, it is unlikely that roof pendants could have survived since then. Others have suggested that the batholith was probably protected by a younger sedimentary cover, which has recently been eroded, to expose the granite and the more resistant schist septum and roof pendants (i.e. Jukes, 1862; Cole, 1922; Cole & Hallissy, 1924; Charlesworth, 1953). These workers noted that the present-day river systems of SE Ireland are discordant with respect to structure. The main rivers were inferred to have once flowed over a younger sedimentary cover, which exhibited different topography and relief to the present-day landscape. Thus, as erosion stripped away the younger sedimentary cover, the rivers were superimposed on a much older underlying

structure, and hence may have inherited a palaeotopography of probable Carboniferous or Permian age. The Late Cretaceous was a time of maximum global sea-level rise and therefore the cover rocks are most likely to be chalky limestone. This is supported by the widespread occurrences of pieces of flint in glacial deposits (Davies, 1970; W.E.A. Phillips pers. comm., 1999).

Davies (1959, 1970) noted that the granitic summits of the Wicklow Massif are probably very close to the original roof of the batholith. He suggested that the northern portion of the mountain chain had only recently lost its protective schist and younger cover, to expose the granite beneath. Whereas, in the Tullow Lowland the granite had been exposed for a greater period of time and hence has been more deeply eroded.

Towards the SE of the Tullow Lowland, a long, narrow ridge of hills stretches from the River Slaney, at Bunclody, and trends NE for ~17km (figure 5.2). These hills are underlain by schist and marginal granite, and were termed the "Tinahely Hills" by Davies and Stephens (1978), and as the "Myshall/Ow Block" by Mitchell (1980, 1981, 1985). Interestingly, the hills rise to 280m above the Tullow Lowland, but they do not form a watershed. Five rivers cross the ridge of hills, and an additional 3 dry valleys or "wind gaps" occur (section 5.5). Hence, it has been suggested that the Tullow Lowland must have stood higher than the ridge if the rivers initially flowed across it (i.e., Farrington, 1927; Davies, 1959; Davies & Stephens, 1978).

However, the Tullow Lowland area is associated with the lowest negative Bouguer anomaly of –35mGal in the country (figure 5.4). The gravity anomaly in Ireland tends to produce a negative Bouguer anomaly, where granites of sufficient mass are present at the surface or sub-surface (chapter 1). Therefore, the regional Bouguer gravity suggests that the granite is thickest in this area. In addition, Brück & O'Connor (1980) have provided field evidence that the Tullow Pluton has not been deeply eroded; as features associated with roofing still exist. Other immediate problems are the occurrence of roof pendants on parts of Lugnaquillia pluton. Hence, the lack of denudation suggests that the mountain chain has not been high since Carboniferous times. Thus, the hypothesis of the trans-ridge valleys with consequent streams is difficult to sustain (Mitchell, 1985).

5.1.4 Scope of chapter

The areas labelled on figure 5.2 have been identified by previous workers as areas of geomorphic interest, which may be tectonic in origin (Farrington, 1927 1929; Davies, 1959, 1970; Mitchell, 1980; Mitchell, 1985). The main areas are the:

- Vartry Plateau/Basin (section 5.4);
- Glen of Imail basin (section 5.6);
- Myshall Ow block (section 5.5);
- Aughrim/Kildaven Interblock depression (section 5.5);
- Annagh Avoca block.

All areas listed above, with the exception of the Annagh Avoca block, are re-evaluated in this chapter with the aid of GIS spatial analysis. The Annagh Avoca block forms part of ongoing research by another postgraduate student and will therefore not be discussed here.

5.2 Topography – Mechanisms & Processes

The denudation of a landscape is dependent on the erodibility of the rock. The erodibility is controlled by the interaction of many internal and external variables. The internal variables or classes of rock properties are 1) hardness, 2) water absorption and transmittance ability, and 3) rock strength. External variables can be encapsulated into physical and chemical weathering. In general, igneous and metamorphic rocks are generally more resistant than sedimentary rocks to chemical weathering. The susceptibility of minerals mimics the Bowen crystallisation sequence, i.e. olivine and calcium plagioclase (high temperature) are the most sensitive and alkali feldspar, and especially quartz (low temperature) are the least sensitive or inert. In sedimentary formations, resistance to chemical weathering increases with grain size, and quartz content. In addition, those sandstones that are calcium carbonate cemented (i.e. drusy calcite spar cements) are more susceptible to weathering than quartz cements. However, physical weathering is normally the dominant process. For example, on a global scale, the ratio of physical to chemical weathering (or denudation) is 6 to 1 (Summerifeld, 1991).

Erodibility also depends on the amount of regolith covering a slope. For example, Young's (1972) model of slope evolution consists of two main modes (weathering limited and transport limited). Weathering limited processes will dominate on slopes with thin regolith because removal of material exceeds weathering rates. On the other hand, transport limited processes will be dominant on slopes with thick regolith where rates of weathering exceed transportation rates.

Schumm & Chorley (1966) studied scarp evolution in the near horizontal strata of the Grand Canyon. They concluded that cementation, porosity, orientation and spacing of joints and bedding planes, controlled the development of scarp form. Hence, thick beds with high porosity, widely spaced joints, and quartz cements, would be the most resistant to weathering.

5.2.1 Bedrock Structures

In the Leinster Mountain chain all the rocks have been deformed and are foliated, faulted and heavily jointed. These structures were produced by the Caledonian orogeny. Structural inheritance during the Hercynian event reactivated many of the Caledonian structures, which were in favourable orientation to σ_1, i.e. the parallelism of Hercynian and Caledonian structures in east Central Ireland (chapter 2). The Leinster batholith probably acted as a rigid indenter during Hercynian tectonism, propagating northwards and causing the E-W trending folds of the Carboniferous rocks of the Dublin basin (e.g. Keeley, 1995). During Mesozoic times, those structures which were in favourable orientation to the extension direction, would have reactivated as transtensional faults (figure 5.3), as indicated by the reactivation of the near offshore Bray fault where thick wedges of Triassic sequences are present in the hangingwall (chapter 4). The faults in the Leinster Mountain chain have also been recently reactivated during both Palaeogene and Neogene times (chapter 7). Based on the post-Liassic model, faults oriented ~N-S could have reactivated as extensional structures. Faults that trend ~E-W may show reverse movements, depending on the magnitude of the horizontal compression, and those which are ~NW-SE and NE-SW would produce dextral and sinistral strike-slip respectively.

5.2.2 Climatic Fluctuations

Climatic changes will also have a marked influence on both weathering and transport rates. Chemical weathering rates will be greater under tropical, wet conditions, in comparison with cold, tundra climates. On the other hand, cold climates are more susceptible to physical weathering, in terms of periglacial processes, i.e. freeze/thaw cycles, solifluction and mass wasting etc. And, the action of glaciers produces wide-scale erosion and deposition, which is evident in SE Ireland (Farrington, 1934; Warren, 1985). Deposition of glacial material can subsequently impede weathering rates, i.e. rates of weathering being greater than transportation and thus resulting in deep regolith cover.

It is beyond this study to discuss the field of Tertiary climatic variation other than to concur with Mitchell (1985) that the elevations and landforms of SE Ireland are mostly pre-Pleistocene in age, and have been merely enhanced by the action of glaciers scouring out corries and valleys. The widespread distribution of core stones, inselbergs (tors) and areas of deep chemical weathering preserved in ice floor shadow zones support this view (Mitchell, 1981). Glacial erosion produced an overall reduction in the elevation of the mountain chain, but a relative increase in the heights of the tallest peaks due to the isostatic response of unloading (chapter 7).

In general, resistant rocks will generally be associated with high elevations, steep slopes and relief. According to Gerrard (1988), these areas will experience relatively slow denudation rates. The relationship between geology and 1) elevation, 2) slope and 3) relief for all three areas of study (i.e. the Vartry, Bunclody and Glen of Imail localities) are investigated.

5.2.3 Elevation Histograms

Ringrose & Migon (1997) illustrated the usefulness of elevation histograms, and their conceptual model is used here. Figure 5.10 shows theoretical slope profiles and their corresponding elevation histograms. These models show that an elevated surface has experienced some degree of denudation towards a base-level. Three hypothetical slopes and their corresponding histograms are considered and include (1), base-level dominant,

(2) plateau dominant, and (3) transitional. If an area is experiencing base-level dominant processes, then this implies a mature landscape with only small remnants of an upland terrain. The second case would represent an upland terrain with relative underdevelopment of incision to a new base-level. The third case would be a mixture between these two end members, i.e. preserved upland with erosion to base-level fairly well developed. The main point is that dissected upland terrains should be categorised by bimodal distributions and base-level terrains would be unimodal and skewed towards low elevations (i.e. tending towards sea-level or other local base-level).

Of course, real upland elevations will have greater complexity and should be considered when interpreting histograms. For example: 1) tilted surfaces will broaden the corresponding mode of the histogram; 2) elevated palaeosurfaces will have local inherent relief and will broaden the mode of the histogram, and; 3) landscapes are polycyclic, i.e. they represent periods of tectonic uplift, denudation, and subsequent rejuvenation.

5.2.3.1 Leinster Mountain Chain & Tullow Lowland

Figure 5.11a is an elevation histogram of the Leinster Mountain chain including the Tullow Lowland. The distribution is unimodal with a peak in the 90 to 140m elevation range. This is considerably less than the mean and median, which have the same elevation value of 460m. The standard deviation is 266m and the distribution is asymmetrically skewed towards base-level elevations. Figure 5.11b is an elevation histogram of the Wicklow Mountains. The distribution is arguably bimodal (unimodal if frequency binned into large enough classes) with two peaks at 130m and 190-210m. The mean and median values are 460m. The distribution is similar to figure 5.11a, in that it is asymmetrically skewed towards base-level elevations. Overall, there is a greater frequency of intermediate elevations of 300-540m elevations.

5.2.4 Preliminary Interpretation

The long tail of infrequent high elevations on the upper parts of all the elevation histograms probably reflect the removal of material by glacial erosion, in a similar

fashion to the Kintail area in Scotland (see Ringrose & Migon, 1997). Both regional figures show that SE Ireland is transitional between plateau and base-level dominant processes. Hence, the topography is at an advanced stage of transition (i.e., the modal elevation is 100-150m, but would be at sea-level for a base-level dominant landscape. This pattern may be because: 1) the landscape is approaching the idealistic mode of sea-level; 2) or, the landscape was base-level dominant but a recent sea-level fall has occurred; 3) or, it may be due to recent tectonic uplift. As shown in the remainder of this chapter, the most likely cause is recent tectonic uplift. Post-glacial isostatic rebound may also account for a few 10s of metres of uplift in recent times.

5.3 Areas of Study

Any tectonic change in the topography of a region (all other variables remaining equal) will result in a landscape with rejuvenated drainage, as rivers incise to attain a new state of equilibrium. Therefore, landforms may not fit the post-Liassic model predictions; if the tectonic event occurred at a time greater than the duration it takes for exogenic processes to remove the evidence by denudation. Therefore, the timing of fault reactivation of bedrock structures is crucial. This clearly requires further work to establish the time lag between uplift and fluvial incision rate, which accounts for climate and a quantifiable erodibility index for the various lithologies within the Leinster Mountain chain.

In order to test the model from chapter 4, three specific areas of study have been selected. This is based on model predictions of reactivated major structures such as the East Carlow Deformation zone (ECDZ) and observations by previous workers (section 5.1.4) that have highlighted geomorphological landforms of potential tectonic origin. The three study areas are illustrated on figure 5.5 and the geology of each area of interest is described in Appendix 3.

5.4 Vartry Area

The Vartry area is located on the eastern margin of the Wicklow Massif and covers an area of ~25km by 15km. The area stretches from Killiney Bay in the north to the town of Glenealy in the south (figure 5.12).

5.4.1 Elevation

The topography of the area is illustrated on figure 5.12. The elevation histogram has three populations, which have been categorised in this study as the 1) Coastal surface, 2) Vartry surface and, 3) the Djouce surface. The modal elevation occurs at ~15m, representing the Coastal surface. The second largest peak occurs at ~230m and is associated with the Vartry surface. This surface was termed the Vartry plateau by Farrington (1929) and as the Vartry peneplain by Freeman (1960). The third population has an elevation peak ranging from 515m to 535m. This population has a wide spread of values and corresponds with the Djouce surface. This relatively high elevated surface has much greater inherited relief, than the previous 2 surfaces, as indicated by the spread in the population (section 5.4.12).

Based solely on the elevation histograms, this indicates that the topography does not equate to a mature, base-level dominant landscape, but one that exhibits a polycyclic pattern. The 2 largest populations suggest that the two corresponding surfaces appear to be dominated by similar processes, transitional to 'local' base-level dominant. Whereas, the upper surface is mostly plateau to transitional in nature. However, this population has been greatly modified by glaciation and pre-glacial valleys (e.g. the Lough Tay-Lough Dan wind-gap).

5.4.2 Elevation Profiles

Figure 5.12 also shows two elevation profiles that cross all three surfaces. Profile A begins in the west at a maximum elevation of 600m (Djouce Mountain). Elevation quickly decreases from 600m to 300m over a distance of 2km. At the foot of the Djouce escarpment elevation begins to gently rise across the Vartry surface. At the transition from the Vartry to Coastal surfaces, elevation rises slightly and then decreases at a fairly rapid rate. Profile B shows a similar pattern. The profile is at a maximum elevation in the west (370m) on the lower slopes of Scarr Mountain. The elevation then flattens out over the Vartry surface, with a slight increase in height to the east. Elevation then slightly rises over Ballymaghroe and decreases rapidly, a drop of ~220m elevation, on to the Coastal surface (40m). Both profiles show a sudden decrease in elevation between the Djouce and Vartry surfaces, and the Vartry and Coastal surfaces.

These are termed here the Djouce and Vartry escarpments. One of the main aims is to assess the likelihood that these escarpments may be tectonic in origin?

5.4.3 Bedrock Structures

In the north of the area, a slice of the Bray Group (Carrickgollogan klippe) overlies the Maulin Formation of the Ribband Group (figure 5.16). Four sub-parallel WNW-ESE dextral fractures, the Glencullen, Glenasmole-Glencree, Sally Gap and Lough Dan fractures (from N to S respectively) cut the granite in the Vartry area. A major thrust bounds the Bray Group on both the west and north margins, bringing Lower-Middle Cambrian aged rocks over Upper Cambrian to Lower Ordovician rocks of the Ribband Group. The Bray Group is bound to the south by a NE-SW trending reverse fault, the Southeastern Boundary fault. Part of the fault complex bounds a ~NE-SW elongate band of the Bray Head Formation (Carrick Mountain), which contains thin slithers of quartzite. Further south, a complex set of ENE, NNE and NNW faults juxtapose the Wicklow Head and Glencullen Formations against the Maulin Formation.

A major NE-SW fault, the Callowhill fault, extends from the coast, and passes just north of Kilcoole town. The fault cuts through the Bray Group, which offsets the Bray Head and Devil's Glen Formations with an apparent right lateral sense of separation. The fault continues into the Maulin Formation where it juxtaposes the Maulin and Devil's Glen Formations for ~2.5km. The fault then appears to terminate, probably due to lack of exposure to the west. Between this fault and the south-eastern boundary fault to the south, the Devil's Glen and Bray Head Formations are in fault contact to the NE, and exhibit a complex faulted pattern to the SW with the Maulin Formation.

The NNW-SSE trending Kilruddery fault occurs about 2km west of Bray Head. This fault is not exposed and has been inferred on lithological and topographic grounds (Shannon, 1991a). There is also a change in the strike of bedding from ~E-W on the eastern side of the fault and NNW-SSE on the western side.

There are numerous folds in the Bray Group which trend ENE-WSW to NNE-SSW. Many of the axial planes of these folds, parallel the Bray Thrust on the NW and N margin. An anticlinal fold axis, south of the Vartry reservoir, is slightly anti-clockwise

to the Callowhill fault and the fold axis appears to be sinistrally offset by the fault. There is also a major NE-SW fault in the western part of the area, which downthrows the thrust mass of the Bray Group against the Ribband Group

A mineral foliation occurs close to the margins of the Northern pluton (figure 5.16). The foliation is defined by the alignment of biotites, and to a lesser extent by feldspar, quartz and muscovite. The magmatic foliation is concordant with schistosity and bedding in the aureole rocks. Near the coast, bedding is ~E-W to ENE-WSW. Westwards, this changes to a NE-SW direction.

5.4.4 Bouguer Gravity Anomaly

Figure 5.13 shows the Bouguer anomaly (based on the DIAS maps) draped over the topography at the Vartry area. A large variation in the regional gravity field is evident, ranging from a minimum of –5mgal to a maximum of 35mgal. The minimum and maximum gravity values underlie the granite and Bray Group respectively. The gravity trend is mainly NNE-SSW, parallel to the batholith margins. This changes to an ENE-WSW trend, just south of the Callowhill fault. The gravity high in the Wicklow town area corresponds with a horst of Ribband Group rocks and probably relates to uplift of the underlying Pre-Cambrian basement. This change in trend is related to the gravity high, which may be picking out shallow Moho, and/or, a large, dense mafic body at depth. The contours also show a sinistral bend across the East Carlow Deformation zone.

5.4.5 Metamorphic Aureole

In the Vartry area, and much of the eastern margin of the Leinster Mountain chain, the Ribband Group is structurally overlain by the Lower-Middle Cambrian aged Bray Group (figure 5.16). The Bray Group is situated between the towns of Bray and Wicklow, and covers an area of ~200km^2. The rocks have been translated from the E and SE, and now overlie the Ribband Group (Maulin Formation). The thrusting post-dates the emplacement of the batholith, and in the NE the fault oversteps the outer aureole.

The aureole is divided in two, and consists of an inner aureole of schists (composed of staurolite and andalusite) and an outer aureole of phyllites. The contact between the inner and outer aureole is gradational in style, with a decrease in schistosity and subsequently phyllitic texture, with distance from the granite country rock contact. Brück (1968) summarised this general pattern into 3 stages: 1) Stage 1:- high grade contact metamorphism; 2) Stage 2:- pneumatolytic retrogression; and, 3) Stage 3:- further retrogression to regional conditions.

The aureole at the Vartry area has a variable width of ~2-4km, generally, increasing in width towards the SW. The inner aureole of schist tends to remain fairly constant in width at ~500m. The aureole is developed within the Maulin Formation.

5.4.6 Elevation - Ribband Group & Aureole

Rocks of the Ribband Group span the entire elevation range, from sea-level to a maximum height of 695m (figure 5.15a). However, the metamorphosed aureole rocks tend to be concentrated on higher ground. The mean, median and modal elevations are 230m, 218m and 214m respectively. The standard deviation is the second largest within the Vartry area (figure 5.15b), reflecting the spread of elevation values about the mean. The skewness is the largest (figure 5.15c) because most of the rocks are low-lying, with the aureole rock forming the moderate to high elevations. Only a small portion of the Ribband Group rock occurs on the Coastal surface, i.e. the Ballylane and Wicklow Head Formations in the SE of the area of study. A small part of the Maulin Formation occupies the Coastal surface, and a larger fraction occurs on the western margin of the Vartry surface. But, a large portion also occupies the Djouce surface (figure 5.13).

The contact aureole trends NNE-SSW (figure 5.14), and is slightly oblique to the margin between the Vartry and Djouce surfaces. The inner aureole is composed of andalusite, staurolite hornfelsed schists derived from the Maulin formation and the outer aureole is composed of mica schist-phyllite. Differential erosion should preferentially denude the phyllites to a greater extent than the schists. The hornfels schists should be the most resistant to erosion (with the exception of the Bray Group quartzites) and should therefore be expected to produce the highest elevations, form the steepest slopes,

and produce the greatest amount of relief. The summits of Maulin, Knockree, and Djouce Mountain (725m) cut across from the inner aureole (Knockree) to the outer aureole (Djouce Mountain).

The outer aureole ranges in elevation from sea-level (Killiney Bay) to ~660m, with mean and median values of ~300m and 320m respectively (figure 5.14). Similarly, the inner aureole ranges from 45m (although these rocks attain sea-level just north of the Vartry area of study) to ~720m, with mean and median values of 340m and 320m respectively. Thus the inner aureole reaches a maximum elevation that is 40m greater than the outer aureole. However, the averages are similar. The modal elevations, on the other hand, are much lower than the averages, i.e. the inner and outer aureoles have values of 200m and 120m respectively.

The aureole rocks have the largest standard deviation and asymmetry (figure 5.14b) of all the rock types, which reflects the extreme range, i.e. from sea-level to the highest elevation of 720m (figure 5.15a). The average elevations of ~300m correspond with the third elevation population, i.e. the Djouce surface (figure 5.11). However, the lower modal values mean that much of the aureole rock is at low to intermediate elevations, i.e. the aureole overlaps with the Vartry surface (figure 5.14). This is reflected by the relatively large degree of skewness at 0.3 of the elevation histogram (figure 5.15c). Although, some of the variability is due to fault controlled NW-SE to WNW-ESE valleys that cut into the surface, e.g. Glencullen, Glencree, Sally Gap, and Lough Dan fractures).

5.4.7 Elevation of Bray Group – Quartzites & Greywackes

The Bray Group forms the lowest elevations (figures 5.16 & 5.17), and accounts for the first and second populations (surfaces) of the elevation histogram, i.e., underlies the Coastal and Vartry surfaces (figures 5.16 & 5.17). The maximum elevation of the group is 480m and this is attributed to quartzite, i.e. the summit of Great Sugar Loaf Mountain. The average elevations for quartzites (mean 194m and median of 182m respectively) are much higher than the Bray Group as a whole (mean 154m and median of 137m respectively). Therefore, despite the fact that quartzites represent a mere 4%

of the Bray Group, these values will marginally push up the elevation of the Bray Group.

The Vartry escarpment occurs entirely within the Bray Group (figures 5.16 & 5.17), with elevations between 100m and 200m. As figure 5.16 shows, most of the escarpment is underlain by greywacke of the Bray Head Formation. Although, the southern part of the escarpment is underlain by thicker bedded greywackes of the Devil's Glen Formation.

5.4.8 Elevation - Northern Pluton

Rocks of the Northern pluton underlie much of the Djouce surface. The maximum elevation of the Northern pluton is 690m, slightly less than the Ribband Group. The highest elevations underlain by plutonic and Ribband Group rocks are War Hill (690m) and Djouce Mountain (725m) respectively. Although, west of Lough Bray Upper (just outside area of study) the Kippure Mountain reaches an elevation of 757m on granite. The Northern pluton has higher average elevations than the aureole i.e. the mean (390m), median (413m) and mode (519m). This is comparatively higher than the Ribband Group, i.e. the mean (230m), median (218m), and mode (214m) and both the inner and outer aureole rocks (mean and median are 294m and the mode is 119m). The Northern pluton is the only rock type to have a modal value greater than mean and median. The high modal value for the Northern pluton, in comparison with the mean and median are reflected in the smallest skewness of –0.3 for all rock types (figure 5.15c). The mode for the Northern pluton is 200m higher than the inner aureole rocks (~200m). The Northern pluton reaches sea-level, north of the area of study. Thus, the minimum elevation within the Vartry area for the Northern pluton is 80m. Therefore, part of the higher average is due to spatial distribution, but the overall magnitude is much greater than the next highest rock type (Ribband Group).

5.4.9 Elevation - Other Igneous Rocks

Other igneous rocks make up <3% of the solid geology. The mean, median and modal elevations are 302m, 230m and 219m respectively. These rocks have the second largest skewness in the Vartry area due to their sporadic distribution over a large range of

elevations. Most of the igneous bodies are biased towards lower elevations, i.e. skewed more towards the minimum elevation of 108m, as opposed to the maximum of 521m. Therefore, they have no relevance to the major topographic surfaces.

5.4.10 Slope

In a mature and stable geological terrain, the steepest slopes of an area would predictively occur on lithologies that are most resistant to erosion by ice, water, exfoliation and spalling, landsliding etc. These rock types would be expected to produce the highest elevations and highest slopes. One exception would be where a vertical-sided prism of very hard resistant rock caps much softer erodible lithologies (albeit, the boundaries would still be resolved as steep slopes averaged over the pixel area). Based on a crude estimation of rock type resistance to erosion within the Vartry area, those rocks of most to least resistance would probably be quartzite, the inner aureole schists, granite, sandstones, greywacke (non-aureole Ribband and Bray Groups) and the outer aureole phyllites. Hence, the quartzites and inner aureole schists should be associated with the steepest slopes.

Slope types of the Vartry area can be crudely classified into those associated with glacial deepening of earlier fault-controlled valleys, those solely due to lithology, and those that relate to faults and those that are fluvial in origin. The steepest slopes (figure 5.18) occur on the Djouce surface, where the areas have been modified by glacial erosion along pre-existing (Tertiary) valleys following fault zones, e.g. the steep ~ N-S slopes surrounding Lough Tay and the E-W to NNW-SSE slopes that bound Lough Dan (glacial type). Other areas of relatively moderate to high slope include the Devil's Glen (fault type), Glen of the Downs (fault type), Bray Head (lithology type) and the mountain slopes of Great and Little Sugar Loafs (lithology type), Djouce Mountain (fault type), Maulin and Tonduff North (combinations of lithology, fault and glacial types). Areas of moderate slope include Carrick Mountain (lithology and glacial type), the Vartry and Djouce escarpments (fault type), the incised channels of the rivers Dargle (fluvial type), Glencullen and Glencree (fault type). The Vartry and Coastal surfaces are generally areas of very low slope.

5.4.10.1 Slope & Elevation

Table 5.1 below shows the statistical relationship between elevation, slope and relief for the Vartry area. The relationship between elevation and slope is moderately positive, with a correlation of 0.55. However, the relationship between maximum elevations and slope steepness displays a weak negative correlation (figure 5.19a). The mean and median elevations show a fairly indifferent relationship between slopes of 1 to 20°, where the elevation is ~330m. This subsequently shows a slight negative correlation between slopes 21 to 30°, where the elevation value is ~300m. At this point, the mean and median diverge with a slight increase in elevation between slopes of 36 to 40°. The mean elevation of these steep slopes is ~330m and the median is ~260m. Both the mean and median fall in elevation with increasing slopes, with the median and mean dropping to ~60m and ~80m respectively on slopes of 41 to 45° (figure 5.19a).

Table 5.1

Vartry Area	Minimum	Maximum	Mean	Standard Deviation
Slope	0	50	5	5
Relief	1	298	46	45
Elevation	0	721	159	160

CORRELATION MATRIX	Slope	Relief	Elevation
Slope	1	0.90	0.55
Relief	0.90	1	0.63

The largest standard deviation (SD) of ~195m occurs on the lower slopes of 1 to 10°. The SD then drops to ~140m on slopes of 21 to 35° (figure 5.19b). The maximum and minimum elevations of these slopes of 1 to 10° are between sea level and 720m.

Therefore, these relatively gentle slopes occur on all elevations in the Vartry area. A slight increase in the SD to 160m then occurs on relatively steep slopes of 41° to 45°. This is significant because it implies that steeper slopes are not restricted to the higher elevations and in fact, the maximum elevation of this slope category is only 453m and also occurs at a minimum elevation of 22m (i.e. Bray Head).

The skewness is fairly flat at ~0° on slopes of 1° to 30°, indicating that the modal peaks are very close with the mean and median values. Hence, the frequencies are close to a gaussian or normal, symmetrical distribution. A slight dip in the curve to – 0.5 occurs on slopes ranging from 31° to 35°, indicating an asymmetrical distribution with skewness towards higher elevations. The skewness then increases exponentially to 72 on the slopes of 40° to 50°. This is interesting because it means that the steepest slopes mainly occur on relatively low elevations and the highest ground generally produces low slope angle. If exogenic processes have been dominant, then the highest elevations should show the highest slope because the most resistant lithologies to weathering would produce bold relief. This is not the case and therefore implies that endogenic processes are also important, i.e. faulting, uplift etc.

5.4.11 Slope & Geology

The Vartry area is dominated by relatively low to moderate slopes (figures 5.18, 5.19 & 5.20). The steps in the curve (figure 5.20) re-emphasise the fact that the landscape is not mature and the kinks represent the escarpments that separate the elevation surfaces. These also include glacial modification of Tertiary fault controlled valleys.

5.4.11.1 Bray Group (Greywacke and Quartzite)

The modal slope value of the Bray Group (greywacke and quartzite) is 4° (figure 5.19a) and the mean and median are 7° and 6° respectively. The Bray Group slope distribution is highly asymmetrical. Figure 5.19c shows that the Bray Group has the highest skewness and hence the highest proportion of very low slope. Figure 5.21b shows that over 90% of slope is achieved on gradients of 10°, and very few slopes of greater steepness occur. The Bray Group rocks display the maximum slope of any rock type within the Vartry area, i.e. the maximum slope is 50° (figure 5.23a). But, they display

the lowest mean, median and modal slopes. And figure 5.23b shows that 12% of Bray Group rock occupies areas of zero slope (or flat ground), representing the largest of all rock types.

By solely considering the quartzites, the curve shows a very different slope distribution (figures 5.23). The slope histogram for quartzite is more evenly spread and the rocks have the lowest skewness of all lithologies. This is because the mean, median and modal slope values of 13°, 12° and 11° respectively (figure 5.22a), closely resemble a normal distribution (figure 5.23a). The quartzites in general occupy the largest average slopes with ~40% of slope being >10°. However, these rocks also display lowest maximum slope value of 29° (figure 5.22 & 5.23). This is the converse to the Bray Group as a whole because the greywackes have the steepest slopes in the area of study. Therefore, this clearly illustrates that the steep slopes in the Bray Group rocks are not lithologically controlled. These steep slopes occur along the eastern and northern margins of the Vartry surface and must be fault controlled to explain the observations.

5.4.11.2 Ribband Group

The modal slope value for the Ribband Group (aureole and non-aureole rocks) is 6° (figures 5.23 & 5.25) and the mean and median are 9° and 8° respectively. The Ribband Group slope distribution is highly asymmetrical, skewed towards relatively moderate to low slope values. The average slopes are higher and slightly more evenly spread than those of the Bray Group (figure 5.23a). However, over 8% of the Ribband Group underlies flat ground (figure 5.23b). Slopes of 1° to 13° accounts for over 80% of the Ribband Group rock (figure 5.25b). In comparison to the Bray Group, these rocks tend to form slightly steeper slopes.

The average slope of the inner and outer aureole rocks are higher than the Ribband Group as a whole (figure 5.26), with a mean, median and mode of 11°, 10° and 6° respectively (figure 5.23a). The modal slopes are much lower than the mean and median, implying that relatively high slopes are not a common occurrence, i.e. the long tail of high slopes of low frequency (figure 5.26a). The highest elevations of the Ribband Group are on aureole schists of the Maulin Formation at 38°. Hence, the steepest slopes are on the most resistant lithologies. Approximately 2 % of aureole

rocks underlie flat ground (figure 5.23b), and these probably occur on the Djouce surface.

5.4.11.3 Northern Pluton

The average slopes of the Northern plutonic rocks is notably higher than the Bray Group and are marginally higher than the Ribband Group, but less than the aureole rocks. The modal slope of the granite rocks is 6° (figure 5.27a), although, the mean and median are 10° and 9° respectively (figures 5.23 & 5.27). The maximum slope values are relatively high at 48°. Slopes up to 13° occupy over 80% of the Northern pluton (figure 5.27b). Less than 2% of the rocks underlie flat ground (figure 5.23b). Hence, the pluton underlies the highest ground, which is most deeply dissected by glacially modified Tertiary fault-controlled valleys

5.4.11.4 Hypsometry - Differences & Similarities of Slope Distributions

As shown on figure 5.16, there is a wide variation in rock type in the Vartry area. Therefore, normalising slope and frequency (hypsometry) can provide a clearer picture of what rock type is associated with slope type (figure 5.28).

As figure 5.28 shows, the largest proportion of the Bray Group slope distribution is very low, i.e. these rocks peak at a low normalised slope of 0.1. The Bray Group curve shows a sharp increase of ~6 to ~11% frequency over this 0.1 increment. The peak of the distribution is fairly sharp and then decreases to 6% again at 0.2. The curve decreases further and has a long tail of low percentage values but high normalised slope, i.e. <1% at 0.4, which means that much of the highest slopes on Bray Group rocks are more atypical than for any of the other lithologies. The quartzite envelope is very irregular with many shorter curves superimposed on a longer wavelength. The envelope reaches a peak at 0.2 (7.5%). The curve then decreases at 0.3 and drops to <1% at 0.6. The tail is shorter than the Bray Group as a whole. This shows that the Bray Group rocks have a large distribution of relatively low slopes, with the higher slopes mostly associated with the quartzites.

The Ribband Group has a smooth envelope with a broad rounded peak between 0.1 and 0.3 with a maximum of ~8.5%. The curve then decreases to less than 1% by 0.5 normalised slope. The aureole peaks at 0.3 normalised slope at a frequency of ~7%. The aureole rocks have the biggest percentage of low to moderate slope, surpassing the quartzite envelope. These rocks also have the shortest tail. This shows that these rocks have a larger distribution of relatively high slopes.

Some of the steepest slopes within the Vartry area are underlain by rocks belonging to the Northern pluton. The Northern pluton has a steeper increase than the Ribband Group (but not as much as the Bray Group) at low values of normalised slope. The percentage of slope reaches a maximum of 7% at 0.2 normalised slope. This then decreases <1% at 0.5 normalised slope. Hence, these rocks have the longest tail of relatively very low frequency at high normalised slope. This shows that the steepest slopes are associated with the Northern pluton than any other rock type within the Vartry area. This probably relates to the NW-SE fault controlled valleys, which have been over deepened by valley glaciers. It also shows that areas of most resistant rock type do not produce the highest slopes. This in part may be due to the nature of the regolith because areas of blanket drift and peak bog (such as the granite) may be more resistant to exogenic processes than the schists (these are more prone to freeze/thaw cycles).

5.4.12 Relief

Within the Vartry area, there is a strong positive correlation of 0.9 (table 5.1) between slope and relief (i.e. relief being the difference between the maximum and minimum elevation over 500m length scale). The correlation between relief and elevation also shows a reasonable positive correlation of 0.63. Figures 5.29a and 5.29b are both relief maps. Fig5.29b is draped over a topographic hillshade (illuminated from NW). The Coastal and Vartry surface have little relief, with ranges between 1m and 25m. However, on parts of the surfaces, relief of small extent does occur and varies between 75m and 190m at Bray Head, and a maximum of 293m at the Great Sugar Loaf.

The Vartry escarpment forms a thin, arcuate ridge of relatively moderate to high relief, i.e. ~100m to ~160m. The highest on the escarpment occurs just to the south of the Great Sugar Loaf and reaches maximas of between 120m and 180m on Downs Hill

(figure 5.29b). The Vartry escarpment shows a ~NNE-SSW trend, and an E-W ridge that connects an apparent offset with Dunran Hill (relief of 150m). South of Dunran hill, the apparent offset escarpment follows a similar NNE-SSW trend, which is cut by the Devil's Glen (relief of 100m). The escarpment abruptly terminates just south of the glen against the NE-SW Carrick Mountain, which has relief of 85m to 130m.

The Djouce surface shows greater variability of relief, in terms of frequency and magnitude, e.g. the summits of Djouce Mt, Luggala, Maulin and Tonduff North, all of which have relief between 200m and 300m. This reflects greater dissection of this surface by Tertiary valleys, which have been glacially deepened.

The relief histogram is unimodal, and highly skewed towards low relief values. The modal relief is ~28m and the mean and median are much higher at ~135m. The modal values represent a large proportion of both the coastal and Vartry surface, but also include, albeit to a lesser extent, the Djouce surface. As relief increases, the frequency of occurrence decreases exponentially (figure 5.29c). Hence, the lowest relief occurs on the lowest elevation. But, the highest relief also occurs on the lowest elevation, which probably relates to faulting along the Vartry and Djouce escarpments, and possibly, the Devil's Glen.

5.4.12.1 Bray Group & Quartzite

The Bray Group (quartzites and greywacke) and just the quartzites have the highest maximum relief of all the rock types (figure 5.30a). However, the mean and median for the Bray Group is also the lowest of all rock types, i.e. 136m and 135m respectively. The relief histogram is unimodal (figure 5.31a) with a modal value of about ~30m. The quartzite on the other hand has a mean and median of 144m and 142m respectively. The relief histogram is also unimodal (figure 5.31b), but the distribution is much more spiky and irregular in comparison with the Bray Group. The modal relief is ~75m.

The quartzite of the Bray Group produces some of the highest relief within the Vartry area and the greywackes form much of the low ground. Although, one must bear in mind that the Bray Group occupies 42% of the total outcrop area, whereas quartzite comprises only 4% of the Bray Group, and 1.6% of the total geology within the Vartry

area. In general, the Vartry escarpment is the dominant relief feature of the area and is underlain by greywacke, which overall, forms the lowest average relief.

5.4.12.2 Ribband Group & Aureole

Rocks of the Ribband Group and the Northern pluton show the lowest maximum relief of ~279m and ~280m respectively (figure 5.30a). However, the mean and median of the Ribband Group are similar to the quartzites, i.e. 139m, albeit, the aureole is marginally higher (mean and median of 140m). The maximum relief of the aureole is the same as the Ribband Group (279m) and hence, the schists and phyllites are mostly responsible for the highest relief.

The relief histograms of both the Ribband Group (figure 5.31c) and aureole (figure 5.31d) show a very similar pattern of distribution. Both distributions are unimodal and have a similar modal value of ~80m. The aureole makes up about one third of the total outcrop of the Ribband Group. Therefore, for the Ribband Group to have the same values as the aureole suggests that the unmetamorphosed rocks also produce similar types of relief.

5.4.13.3 Northern Pluton

The Northern pluton has marginally higher average and maximum relief values than the aureole (figure 5.30a). The mean and median relief of the Northern plutonic rocks are 142m, only 3m greater than the Ribband Group. Therefore, like slope, there is very little difference between the Ribband Group and the Northern pluton. The relief histogram of the Northern pluton resembles the Ribband Group distribution. The distribution is unimodal with a modal relief of ~60m. This reflects the importance of fault-controlled valleys, which are probably Early Tertiary in age and coeval with the WNW-ESE dextral structures that occur on the northern margin of the granite (chapter 3).

5.4.13.4 Standard Deviation and Skewness

The standard deviation for all rock types is similar and only varies from 76m to 80m. This indicates that most of the lithologies produce low to moderate relief, and only locally does relatively high to very high relief occur. The standard deviation for the Bray Group (including quartzites) is high due to the general differences between low relief greywacke and high relief quartzite. The quartzites and the Northern pluton have the lowest standard deviation because these rocks consistently produce relatively moderate to high relief. Both quartzite and the Bray Group have the largest skewness. The Bray Group is particularly skewed towards low relief. The distribution of the Northern pluton is also skewed towards the lower relief, but not to the same extent as the Bray Group (figure 5.30c). These skewed distributions reflect areas of fault control, which produce high relief, in comparison with the more general low relief that typifies the Vartry area.

5.4.14 Fluvial Geomorphology

The Vartry area is bounded in part by low-relief blocks, the Vartry and Coastal, and to a lesser extent, the Djouce surface. The Vartry surface is bounded by the Great Sugar Loaf Mountain (quartzite) on the north, a ridge of hills to the east (Vartry escarpment), and mica-schist hills (Djouce escarpment) to the west. The Vartry surface lies between 180m and 300m and slopes toward the west (figure 5.32) at 1-2° (figure 5.18) and is separated from the coastal surface by the Vartry escarpment that is 100m to 400m asl.

5.4.14.1 Vartry Surface

The Vartry surface is covered with young glacial deposits (Farrington, 1934; Warren, 1985), but also appears to be composed of fresh rock (Davies, 1966). The surface is drained by a series of small rivers that flow to the east, across the escarpment (figure 5.33). Each of these streams has incised a steep-walled, bedrock gorge across the eastern escarpment; the depth of the gorge depends on catchment drainage area. The Vartry River flows south along the axis of the surface before turning abruptly east (figure 5.33), and escapes through the Devil's Glen.

5.4.14.2 Vartry Escarpment and Knickpoints

Longitudinal stream profiles through gorges reveal bedrock knickpoints, 25m to 120m high, along the Vartry escarpment, consistent with a fall in base-level relative to the headwaters of each catchment (figure 5.34). Four of these rivers are highlighted on figure 5.33. The Dargle River crosses the escarpment at the most northerly end. Each of the rivers produces a knickpoint (figure 5.34), where it crosses the escarpment. All the rivers show steep gradients as they cross the ridge (i.e. the grey rectangle on figure 5.34 represents the location of the Vartry escarpment).

The largest gorge that cuts the Vartry escarpment is the Devil's Glen. The glen forms a deep ~E-W cut in the Vartry escarpment, with steep slopes averaging at between 35° to 45 and relief of ~100m (figure 5.29a, b). If the Vartry escarpment had not been breached by the Devil's Glen, the Vartry surface would now hold a natural lake. Farrington (1934) suggested that the glen was a glacial melt-water channel. However, this does not explain the coincidence of the gorge with the Vartry escarpment. Hence, it is likely that the Devil's Glen and the other gorges may be due to incision across a fault plane escarpment (Mitchell, 1985), and that hill-slope gradients are being actively maintained by fluvial incision in response to base-level fall.

5.4.14.3 Discussion

The rocks of greatest resistance to erosion, quartzite and schists, occur at moderate to high elevations. The quartzites form the highest ground underlain by the Bray Group and produce rugged peaks, i.e. the Little and Great Sugar Loaf Mountains. The quartzite hills or knolls have clearly been recently sculpted by ice and frost shattering to form the current morphology. Likewise the inner aureole schists of the Maulin Formation form the highest elevations of the Ribband Group. However, the granodiorite to adamelites of the Northern pluton form mostly moderate to high elevations. Thus, the granite is dominated by plateau processes, i.e. the Djouce surface. Whereas, the greywackes, shales and slates of the Bray Group and the Ballylane and Wicklow Head Formations (Ribband Group) tend to form relatively low-lying ground dominated by base-level processes, i.e. the Vartry and Coastal surfaces.

The relative elevation of various rock type does appear, in part, to be controlled by lithological characteristics like hardness, size and composition of grains, and metamorphic grade. For example, the quartzites of the Bray Group rise spectacularly as hills and mountains of rugged relief, in comparison with the surrounding low-lying greywackes. The inner aureole schists are associated with high elevations, but the less resistant granite produces even higher average elevations, which increases further east (Mullacleevaun Mountain). Therefore, differential erosion does not appear to be the dominant process. As figure 5.36a shows, the Djouce surface mostly occurs on granite and forms a relatively high elevated block. However, the phyllites of the Maulin Formation underlie the summit of Djouce Mountain, which attains the maximum height of 725m within the Vartry area.

The relationship between slope steepness and magnitude of relief with rock type is less clear. The greywackes of the Bray Group and those that have not been metamorphosed by the granite, particularly the Ballylane and Wicklow Head Formations, form the lowest slope and relief. However, the aureole and quartzites form much of the moderate to high slopes and both rock types display similar histograms and normalised slope profiles. However, the quartzites display less difference in slope distribution with the Northern pluton than the more resistant aureole rocks. This is similar with the Ribband Group, in comparison with solely the aureole rocks. The Bray Group shows the largest difference in distribution with the other lithologies because most of this rock type forms very low slopes.

The elevation histograms depicted three distinct surfaces. These are, from low to relatively high elevation, the Coastal, Vartry, and Djouce surfaces. The Vartry and Coastal surfaces are predominantly underlain by greywackes of the Bray Group and, to a lesser extent, the Ballylane and Wicklow Head Formations of the Ribband Group. Elevation, slope and relief increase on the Vartry escarpment, which separates the Coastal and Vartry surfaces (figure 5.36a, b, c). This is not a lithological contact and it cuts across the strike of the Bray Group rocks. The escarpment is crossed by numerous streams and rivers, draining the eastern Wicklow Mountains. Where the rivers cross the escarpment, incision has occurred producing a series of knickpoints. However, the knickpoints are clearly not the result of contrasts in bedrock erodibility. It is also

unlikely that the escarpment is due to preferential erosion by glacial processes. The escarpment may be due to coastal erosion and the surface now represents a raised beach. But, it is highly unlikely that the escarpment is a palaeo sea-cliff because bedrock elevation at the base of the escarpment varies from 90m to 140m along strike.

In addition, erosion of the coastal surface does not explain the westward tilt of the Vartry surface, nor does it explain the sharp southern termination of the block just south of the Vartry River. Davies (1966) argued that the Vartry surface was a series of sub-aerial pediments cut into bedrock, but this explanation fails to explain the limited spatial extent of the surface, its westward tilt, the abrupt escarpment on the eastern margin, and the Djouce escarpment on the west. The escarpment is also offset; for example, Dunran Hill has an apparent sinistral displacement of 80m at the 100m contour. Hence, the Vartry escarpment does not correspond with any mapped geologic boundary, and is mostly underlain by greywackes of the Bray Head and Formation.

The Djouce surface shows a more equivocal relationship between elevation, slope, relief and rock type. The Djouce escarpment is partly underlain by outer aureole schists but strikes obliquely to the foliation of these rocks. Thus, the simplest explanation is lithological control. But, again this does not explain the general westerly tilt of the Djouce surface. The change in slope and relief between similar lithologies of the Bray Head and Devil's Glen Formation (greywackes) may be lithologically controlled but it also coincides with an easterly dipping thrust fault (figure 5.36a, b, c). As figure 5.36a shows, the westerly tilt of the Vartry surface changes to the east at the location of this thrust. The easterly dip then increases over the second thrust that separates the Bray Group greywackes from the Ribband Group. Slope increases further (foot of Djouce escarpment) over a normal fault, entirely within the phyllites of the Maulin Formation. Therefore, the contact between the phyllites and the schist does not produce a change in slope or relief, and may be due to relatively recent tectonic movements on the ancient fractures (figure 5.36b). It is possible, however, that the fault rock has been preferentially denuded and hill-slope gradients are pinned on these lines of weaknesses.

The most resistant rocks tend to create areas of high relief, such as the quartzites of the Great Sugar Loaf and the schists of Djouce Mountain. But, high slope and relief with or without low elevation also occur on relatively soft greywacke, and possibly, highly

jointed granite. Thus, areas of high slope and relief that are underlain by relatively hard, resistant lithology are probably the exception.

5.4.14.4 Conclusions

The geomorphic landforms of the Vartry area appear to record recent tectonic activity. The Vartry escarpment is the topographic expression of a previously unmapped dip-slip fault (figure 5.37). In this model, the Vartry surface is the uplifted and back-tilted footwall, and is in turn bounded on its western side by another dip-slip fault that separates it from the relatively high elevated Djouce surface and Wicklow Mountains to the west. Tilting of the footwall away from the fault is well documented in geologic and geodetic studies of active dip-slip faults (e.g., King & Ellis 1990). The magnitude of tilting is difficult to constrain without discrete geologic or geomorphic markers. However, if the present-day land surface was largely established before significant displacement occurred on the escarpment then the magnitude and wavelength of tilting on this surface are then consistent with ~200m of displacement on the eastern escarpment (figure 5.37). However, this is a rough approximation and is a highly speculative and non-unique result.

Dextral motion on the WNW-ESE to NW-SE fault controlled valleys that mostly cut the Djouce surface (e.g. the Lough Dan-Glencree fault; D.Jordan pers. comm., 2000) are probably reactivated under similar stress conditions as the WNW-ESE reverse dextral shears that cut the northern margin of the batholith (chapter 3). Therefore, based on regional correlation outlined in chapter 4, the movement is likely to be Early Tertiary in age. This is supported by AFT data, which also implies that later faulting occurred during the Late Tertiary (chapter 7).

The two steeply southeast-dipping fault strands that bound the offshore Wicklow High (i.e. the Callowhill and Southeastern Boundary faults) offset the Vartry escarpment. These faults show sinistral topographic offsets of the Vartry escarpment (chapter 4). The northern strand, the Callowhill fault, offsets the 200m contour by ~1.7km, and the maximum topographic elevation is 80m higher on the south side of the fault. The southern strand, the southeastern boundary fault (northern extension of East Carlow Deformation zone), is offset by ~2.7km, and the maximum elevation is 120m higher on

the south side (figure 5.37). If the projected, onshore fault strands share the same southeast dip as the offshore counterparts, this implies almost identical sinistral-reverse kinematics on both structures, with a strike-slip to dip-slip ratio of ~22.5:1. Similarly, the incised channel of the Dargle may be fault controlled, corresponding with the onshore extension of the Dalkey fault (figure 5.37). The escarpment does not cross the major fault structures and terminates against the Avoca block.

To the north, the termination of the Vartry escarpment coincides with a branch of the dextral Glencree fault, which shows a restraining bend in the Great Sugar Loaf area. This would explain the high standing block from Bray Head (greywacke) to the Little and Great Sugar Loaf Mountains (quartzite). These must also be bounded on the north side by a further strand of the Glencree fault. Therefore, these hills probably represent 'pop-up' structures on transpressional bends.

To conclude, (1) dip-slip motion has occurred along the eastern margin of the Vartry surface, and (2) during or after this deformation, sinistral-reverse displacement occurred along the Wicklow High fault strands. The kinematics of slip on the Wicklow High fault strands, as derived from geomorphic offsets are similar to the kinematics inferred above from offset magnetic lineations and seismic reflection data; such slip could have occurred under the same stress system that drove displacement on the Codling Fault zone. Hence, the palaeostress system that drove endogenic processes appears to be in harmony with post-Liassic tectonic models of the Kish Bank basin (chapter 4).

5.5 Bunclody Area

The Bunclody area covers part of the Tullow Lowland and the Blackstairs Massif. The area is ~20km by 25km. The town of Tullow (Co. Carlow) lies to the north of the area and the towns of Ballon and Myshall (Co. Carlow), Shillelagh (Co. Wicklow) and Bunclody (Co. Wexford) all lie in the area of study (figure 5.38).

5.5.1 Elevation

Figure 5.38 is a digital elevation model and elevation histogram for the Bunclody area. The histogram has one population and is unimodal. This is a much simpler distribution

in comparison with the Vartry area. The modal peak is ~95m. The histogram indicates that transitional to base-level processes are dominant. The mean elevation is 138m and the standard deviation is 99m. The distribution is highly skewed towards low elevations. This is because much of the area to the north forms the Tullow Lowland, an area of relatively flattish ground with mostly small glacial depositional topography. On the other hand, an area of relatively high elevation but of small extent occurs in the SW. Hence, the large skew in the distribution reflects relatively few high elevations (i.e. Mount Leinster reaches a maximum elevation of 795m) and large low elevations.

5.5.2 Preliminary Interpretation

The Bunclody area appears to be approaching a mature landscape, i.e. base-level dominant. This is due to the flatness of the Tullow Lowland. Therefore, the intriguing observation from this is that the mode is higher than the local base-level. Is this due to relict uplands or recent tectonic activity? It is unlikely to be a relict upland because the aureole schists tend to be more resistant to weathering than granite, yet the highest ground is underlain by granite (figure 5.40). Also, the Tinahely Hills and the major topographic low to the SE, occupied by the Derry River, are aligned along the East Carlow Deformation Zone (ECDZ). The ECDZ can be traced north to the southern boundary of the Vartry escarpment and into the Kish Bank basin where Tertiary sinistral transpression displacements have been inferred (chapter 4).

5.5.3 Elevation Profiles

Line A is a NE-SW trending profile that traverses from the summit of Mount Leinster, to the Slaney and Derry River valleys. Elevation drops rapidly from 795m to <200m, at the bottom of a small corrie. Elevation increases to ~350m on top of John's Hill and then decreases to <50m over the Slaney River valley. This rises over a small ridge (~180m) before falling again into the Derry River valley. Line B is a NNW-SSE trending profile that traverses from the Tinahely hills (in the north) to the N facing flanks of Gibbett Hill. Elevation is initially between 280-300m on the Tinahely hills. This decreases towards the SSE, over the Derry Valley. Elevation subsequently increases again to ~300m on the top of Gibbet Hill. Both profiles highlight the relative low elevation and geometry of the river valleys.

5.5.4 Bedrock Structures

The major structure at the Bunclody area is a NE-SW trending shear zone (figure 5.40), which mostly dips to the SE, namely the East Carlow Deformation Zone (ECDZ; McArdle & Kennedy, 1985). The shear zone is approximately 2.5km in width and crosses the entire Bunclody area. The ECDZ is ~100km in total length (including the Southeastern Boundary fault in the north-east), and extends from the Arrigle Massif near Inistioge (Co. Kilkenny) to the towns of Kilcoole and Rathnew (Co. Wicklow) in the NE. McArdle *et al.,* (1987) suggested a possible extension of the shear zone to the NE, to incorporate the Southeastern Boundary fault. This is an interpretation supported here.

The shear zone runs between the Tullow and Blackstairs plutons where most of the shearing has occurred in the country rock, i.e. pelites semi-pelites, andesitic lavas, tuffs, and pelites of the Maulin Formation (and members). Parts of the Tullow pluton margins are also sheared, and the shear zone cuts through the Blackstairs pluton on its western border. However, the sheared rock has been affected by contact metamorphism. Hence, the development of the shear zone occurred during and immediately after granite emplacement. The shear zone is normal dip-slip with a component of sinistral shearing. Kinematic indicators are based on a consistent sinistral vergence of the F_2 folds and of the steep S_2 schistosity. The shear zone is cut by numerous, mainly ~ NNW trending faults. The Slaney River runs parallel to the largest of these fractures.

A number of small NE-SW Caledonian folds occur in the SE of the area and are offset by NNW-SSE faults. The general trend of foliation is NE-SW. The strike of foliation swings from a NE-SW trend, adjacent the folds to a NNE-SSW trend towards the Slaney River. To the west of the Slaney River, and south of the shear zone, there is a similar strike swing in foliation toward the north, with the strike changing from NE-SW to NNE-SSW towards the west. The foliation in the country rock is generally concordant with the magmatic foliation of the Blackstairs pluton. The foliation of the sheared country rock, within the ECDZ, generally strikes NE-SW, dipping SE, although in places, this changes to the NW (in the northern part of the shear zone) suggesting a flat and ramp type of geometry for the structure.

5.5.5 Bouguer Gravity Anomaly

Figure 5.41 shows the Bouguer anomaly draped over the topography at the Bunclody area. The variation in regional Bouguer gravity is greater in this area than in the Vartry area, i.e. the total variation is 54mgal in comparison with 40mgal. The minimum and maximum values are –26mgal and 29mgal and underlie the Tullow pluton and the Ribband Group respectively. The main trend is NE-SW. However, this trend exhibits a small s-shaped jog, west of the town of Bunclody, reflecting the outcrop of the Blackstairs pluton.

5.5.6 Metamorphic Aureole

At the Bunclody area, the aureole is much greater in width at ~6km. This aureole bifurcates between the Tullow and Blackstairs plutons in the SW. The inner aureole various between ~750 and 1,500m in width. The aureole is developed on the rocks of the Maulin Formation and associated members (plate 5.2 & figure 5.38).

5.5.7 Ribband Group & Aureole

The Ribband Group rocks (including aureole) rocks occupy ~53% of the geology (Appendix 3), and mostly occupy the southern portion (figure 5.40) of the study area. The highest parts occur along the contact with the Tullow pluton (inner aureole), due to the relative resistance of the schists and phyllites. The Oaklands and Ballylane Formations occupy the SE part and produce relatively low-lying ground (figure 5.40). This is because these rocks have only experienced low-grade regional metamorphism and have a higher erodibilty than the hornfels rocks.

The Ribband Group attains a maximum elevation of 676m and a mean and median of 151m and 122m respectively (figure 5.42a). The modal value is fairly low at 95m, although this is slightly higher than the outer aureole. The inner aureole is mostly responsible for pulling up the average for the Ribband Group rocks as a whole. With the exception of aureole rock, the Ribband Group predominantly occupies the relatively low elevations in the SE of the area of study. This has produced a highly skewed distribution (skewness of 1.3) towards lower elevations (figure 5.42c). The standard

deviation is large because of the elevation range of the inner aureole rocks and those that have only experienced regional low-grade metamorphism (figure 5.42b).

At Bunclody the outer aureole covers an area, spanning the entire Derry Valley, the "Aughrim-Kildaven interblock depression" of Mitchell (1985). The aureole extends over part of the SE margin of the Blackstairs Massif (figure 5.39). The summit of Mount Leinster is on granite, but aureole rocks form part of the northern and eastern flanks, and climb to a maximum elevation of ~680m. The inner aureole and ECDZ corresponds with the relatively low-lying Tinahely Hills. This association however diverges in the SW where the inner aureole widens and bifurcates around the NE margin of the Blackstairs pluton. Both the outer aureole and ECDZ reach maximum elevations of ~445m. The minimum elevation of the inner and outer aureole are ~40m and ~9m respectively, and for the ECDZ is ~20m. Although, part of the aureole rocks fall with the shear zone.

The inner aureole schists reach substantially higher elevations than the outer aureole phyllites (e.g. the summit of Slievebawn is 520m on inner aureole rock, and Kilbramish hill reaches a height of 404m on outer aureole rock; figure 5.42a). The schists have a mean and median of 240m and 220m respectively. Whereas, the outer aureole has a mean and median of 130m and 120m.

The ECDZ has a mean and median of 180m and 170m (figure 5.39). The mode for the inner and outer aureoles are 165m and 69m respectively, whereas the ECDZ has a modal elevation of ~145m. The relatively low modal values for the ECDZ and the outer aureole are due to the fact that much of the area occurs on the low ground of the Tullow pluton and Ribband Group. Additionally, relatively high denudation due to differential erosion of fault rock within the ECDZ may have also been a contributing factor. Also, the Tullow pluton produces low elevations but on the margins of the ECDZ, the height is much higher than anywhere else. This suggests that the ECDZ has produced uplift with or without preferentially weathering of the Derry River valley.

Hence, elevation differences in the inner and outer aureole rocks can be accounted for by differential erosion. But, the higher elevations of the ECDZ and the fact that it is partly underlain by aureole rocks and the Tullow pluton (which generally forms the

lowest elevations), suggests that the structure has probably been actively uplifting the SE part of the Blackstairs Massif.

5.5.8 Tullow Pluton

The Tullow pluton forms relatively low elevations (the Tullow Lowland) in the northern part of the area of study. The maximum elevation that occurs on the Tullow plutonic rock is ~360m (figure 5.42a) although the mean elevation is only ~120m and the modal is ~80m. Hence, the elevation distribution has the largest skewness (figure 5.42c) at this area, with a bias towards low elevations. In contrast, the rocks have the lowest standard deviation (70m), which reflect the limited range of elevations underlain by this lithology. In addition, the Tullow Lowland extends westwards and cuts across Lower Carboniferous limestones which show evidence of Tertiary weathering features such as hum and doline topography (Mitchell, 1981), de-dolomites and the Miocene-Lower Pliocene deposits of Hollymount and Ballyelin (Watts, 1985; Mitchell, 1981; Naylor, 1992). The lowland also shows relict granite hills (tors) and abundant granite core-stones (Phillips, pers. comm. 2000). These features suggest that the Tullow Lowland represents a mature base-level etch plain of Tertiary age.

5.5.9 Blackstairs Pluton

The highest elevation of ~795m occurs on the Blackstairs pluton (Mt Leinster). These rocks are located in the SW of the area of study (figure 5.38). The mean and median are 385m and 364m respectively (figure 5.42a), and the modal elevation is 288m. (figure 5.42a) These rocks show the largest standard deviation and the smallest skewness (figures 5.42b & 5.42c). This is due to the large range of elevation (i.e. 690m) and spread of values around the mean. The skewness is low because most of the elevations occur in the SW, associated with the highest topography (figure 5.42c). Hence, the granitic rocks form the highest elevation and not the inner aureole schists. This rules out differential weathering as the dominant force.

5.5.10 Other Igneous Rocks

There are very few other igneous rocks within the Bunclody area (<2% - Appendix 3). Most of these are in the form of felsic intrusive rocks, and are highly sheared within the ECDZ (figure 5.40). The rocks occur over a range of elevations from ~ 20m to ~ 580m, with averages of between ~80m and 210m (figure 5.42a).

5.5.11 Slope

The steepest slopes (>30°) within the Bunclody area mostly occur in the SW, on the flanks of Mt Leinster, Black Rock Mountain and Slievebawn (figure 5.43). The striking feature is the orthogonal relationship between these high uplands. Long, narrow arête ridges trend ~E-W and ~N-S, and merge below the summit of Mount Leinster. Moderate slopes occur along the Tinahely hills to the NE, i.e. the north facing slopes of Gibbet Hill, Aghawle Upper, Seskin, and Cronelea. Similarly, steep slopes occupy the incised channel of the Slaney River, over the southern part of the Tullow Lowland.

A vast area of low slope occupies much of the Tullow Lowland, and the area to the SE (floodplain of the Slaney River). In addition, thin ribbons of low-slope trend sub-parallel to the Slaney channel and cross the hill front (i.e. there are about 7 of these NNW-SSE valleys).

Many geomorphic landforms have a NE-SW and NW-SE trend. And, as mentioned above, a subordinate ~ E-W and N-S trend also occurs in the SW of the area of study (figure 5.43). The flanks of the NE-SW hill-crests and those, which surround Mt Leinster, are of moderate to high slope. This illustrates the importance that pre-existing structural (Caledonian) trends have played in controlling the subsequent development of the landscape.

5.5.11.1 Slope and Elevation

The relationship between slope and elevation is positively correlated at 0.72 (table 5.2). The maximum elevation shows a weak negative correlation, decreasing from a high of ~800m on gentle to moderate slopes. The minimum elevation shows a very weak

positive correlation on slopes of 1° to 25° (figure 5.44a). However, this becomes strongly positive on slopes ranging from 26° to 35°, corresponding with an increase in elevation from 25m to ~475m. Likewise the mean and median show similar values on slopes of 1° to 35°, with an increase in elevation from ~275m to ~620m. The largest standard deviation occurs on slopes of 11° to 15° due to a wide spread of elevations and an anomalous modal value of ~340m (figure 5.44b). The standard deviation then falls with increasing steepness of slope indicating a tighter elevation distribution about the mean. Additionally, the highest skewness occurs on the gentler slopes indicating a greater asymmetry, with an elevation distribution skewed towards lower elevations, and a long tail of low frequency for moderately higher values, i.e. >200m. The steepest slopes have a negative skewness, with values biased towards higher elevations (figure 5.44c).

Table 5.2

Bunclody Area	Minimum	Maximum	Mean	Standard Deviation
Slope	0	34	4	4
Relief	1	271	45	38
Elevation	4	790	138	100

CORRELATION MATRIX	Slope	Relief	Elevation
Slope	1	0.92	0.72
Relief	0.92	1	0.79
Elevation	0.72	0.79	1

In comparison with the Vartry area, there is a stronger relationship between elevation and slope (and relief) in the Bunclody area.

5.5.12 Slope and Geology

The Bunclody area is an area dominated by relatively low slopes (figure 5.45). Histograms of slope and lithology are therefore mostly skewed towards low values, with the notable exception of the Blackstairs pluton.

5.5.12.1 Tullow Pluton

The smallest average slopes within the Bunclody area are underlain by the Tullow pluton. The smallest maximum slope values occur on these rocks, at 20°, which occur on the southern margin in contact with the ECDZ. The mean and median slopes are 5° and 3° respectively and the mode is 2° (figure 5.46a). The skewness is also fairly large on the Tullow pluton (~1.3). Slopes of 1° to 8° occupy over 80% of the cumulative frequency (figure 5.46b). Over 28%, of the Tullow plutonic rocks (5 times greater in magnitude than any other rock type) produce areas of relatively flat ground. Most of the low to moderate slopes are granite inselbergs (tors).

5.5.12.2 Blackstairs Pluton

The Blackstairs pluton shows a completely different relationship to slope (figure 5.44a). The slope distribution is unimodal with a modal range of 10° to 13° (figure 5.48a). The steepest slopes on the pluton reach a maximum of 33°, with mean and median slopes of 13° and 12° respectively (figure 5.48a). Slopes of 1° to 17° represent 80% of the cumulative frequency, the highest, by an order of magnitude, of all rock types (figure 5.48b). The cumulative frequency curve also displays an S shaped geometry. The skewness for the Blackstairs pluton is one of the lowest in the area of study (0.4) indicating moderate slopes are a normal occurrence and the rocks form almost zero (0.06% or 0.01km^2) flat ground (figure 5.47). This is partly due to the relatively small area of Blackstairs outcrop in the area of study. It also illustrates that differential weathering is not dominant because the erodibility is more for granite than inner aureole rocks. But, the granite forms the highest ground.

5.5.12.3 Ribband Group & Aureole

The maximum slope of the aureole and Ribband Group rocks is 27° and the mean and median are 8° and 7° respectively (figure 5.44a). The slope distribution is highly skewed toward low values, with a mode of 4° (figure 5.51a). Slopes of 1° to 10° accounts for over 80% of cumulative frequency (figure 5.51b). About 3% of the aureole rocks underlie areas of flat ground (figure 5.47b). The near coincidence of mean and median slopes is reflected in a relatively small skewness of 1. About 5% of the Ribband Group underlie areas of flat ground, which is mostly in the SE of the Bunclody area (figure 5.47b).

Non-Aureole Rocks of Ribband Group

The Oaklands & Ballylane Formations of the Ribband Group have only experienced regional low-grade metamorphism. These rocks occur in the SE of the Bunclody area of study (figure 5.40). The rocks form a maximum slope of 22° and a mean and median of 5° and 4° respectively. The modal slope is even lower at 2° (figure 5.52a). Over 80% of the cumulative slope frequency of these rocks befalls on slopes of 1° to 6° (figure 5.52b). These values are all much lower than the combined values of these rocks and the aureole (Ribband Group). Therefore, it appears that the thermal aureole that affects the Maulin Formation has had a fundamental influence on the elevation and slope characteristics, and hence, the aureole rocks are more resistant to erosion than the protolith equivalent.

5.5.12.4 East Carlow Deformation Zone (ECDZ)

The ECDZ partially coincides with aureole rocks. Therefore, these rocks have not been separated. This structure shows a broad histogram distribution (figure 5.53) that is slightly asymmetrical. The structure occupies maximum slopes of 21°, and the mean, median and mode have the same value of 7° (figure 5.44a). The modal slope is slightly less at 6°. The average slopes are higher than most of the other lithologies with the exception of the inner aureole schists and the Blackstairs pluton (figure 5.44a). Less than 1% of the shear zone area underlies flat ground (figure 5.44b), surprisingly less than the aureole rocks, i.e., denudation would be expected to erode away to base-level much of the fault rock (line of weakness). The slight asymmetry and the subtle

difference between the average slope values are reflected in a very low skewness of 0.5 (figure 5.44c). Over 80% of cumulative frequency takes up slopes of 1° to 10°. The cumulative frequency curve increases at a lesser rate than all the other curves, except the aureole (figure 5.53b). This may indicate recent tectonic activity otherwise the shear zone would be denuded to a flat plain, i.e. like the Tullow Lowland.

5.5.12.5 Hypsometry - Differences & Similarities of Slope Distributions

The hypsometries of almost all rock types begin at fairly low percentages of low normalised slope (figure 5.54), and then increase steeply (straight to convex) before tailing of in a much gentler fashion (concave slope). The Tullow pluton on the other hand begins at a peak (18%) and then smoothly decreases with a concave curvature, with a gradient slightly less to that of the Ribband Group curve. The curve drops below 1% frequency where normalised slope is 0.8, producing a comparatively flat tail.

The emplacement of the Tullow and Blackstairs plutons (figure 5.40) has effected most of the Maulin Formation, and associated members. The thermal aureole comprises of schist and phyllite. Do the steepest slopes of the Ribband Group occur on aureole rock? The slope distribution of the Ribband Group is more skewed towards low slopes than the aureole (figures 5.40& 5.51) but not to the extent of the non-contact metamorphic rocks of the Ribband Group (figure 5.52). The maximum slope of the aureole rocks are 27° (figure 5.44a), whereas, those rocks of the Ribband Group that have not been thermally effected by the igneous intrusions have a maximum of 22°. The mean and modal slopes on the aureole schists and phyllites are 9° and 6°, and 8° and 4° respectively. However, on those rocks that have only experienced low-grade regional metamorphism (i.e. mainly but not exclusively the Ballylane and Oaklands Formations) the mean slopes are only 5° with a mode of 2°, the same as the Tullow pluton. Hence, the degree of metamorphism has had a profound effect on slopes within the Ribband Group, with a decrease in metamorphic grade corresponding with lower slopes.

This is highlighted on figure 5.54a & b. The Ribband Group shows an initial sharp increase in percentage on low normalised slopes. The curve peaks at 11% frequency and then displays a smooth concave curve for higher values of normalised slope. The Ribband Group drops below 1% frequency at 0.6 and hence has a long tail for high-

normalised slope. By breaking the Ribband Group into two components (based on whether or not the rocks have experienced contact metamorphism) highlights the effects in terms of rock hardness. The high percentage of very low normalised slope for non-aureole rocks s even greater, attaining a high of 15% frequency. The curve then falls to 1% frequency at 0.5, and the tail then flattens out dramatically. Whereas, the aureole slope curve increases at a slower rate for low normalised slopes and reaches a peak just <10% frequency. Both curves intersect at ~0.2 normalised slope (8%) and the aureole envelope then decreases more smoothly, dropping below 1% frquency on values of 0.7. In summary, steeper slopes are more abundant in the aureole rather than in the non-aureole lithologies of the Ribband Group.

The Blackstairs pluton curve shows an increase in percentage from <1% to ~6.5% on 0.3 normalised slopes. The envelope then decreases at a much steeper rate than the Ribband Group. Superimposed on this there are also smaller events, producing an irregular, jagged curve. The curve drops below 1% at 0.8, and hence, has a very short tail of high-normalised slope. This indicates that these rocks form a much higher proportion of relatively moderate to high slopes than any other lithology and that exogenic processes are not dominant. Since these rocks mostly occur under Mount Leinster, this may imply that the mountain has only recently been unroofed. However, due to the small occurrence of these rocks in the Bunclody area, they may not be producing the most statistically significant results.

The Tullow pluton curve is dramatically different from the all other curves (figure 5.54a). The curve begins at relatively very high percentages (~18% frequency) for extremely low normalised slope (0.1 to 0.2). This then displays concavity as it smoothly decreases with increasing normalised slope. The curve falls below the 1% frequency on normalised slopes of 0.7, producing a moderately short tail of high slope values. This illustrates the fact that the Tullow pluton lithology forms relatively gentle slopes.

As noted above, the ECDZ has relatively high slope values that compare in magnitude with the aureole rocks. Only the inner aureole schists and the Blackstairs pluton producing slightly higher average slopes. The hypsometry curve shows a relatively large percentage of low to moderate normalised slopes. The curve shows that the shear

zone has the highest percentage of moderate to high-normalised slope, falling below the 1% frequency on normalised slope values of 0.8. The fact that much of the ECDZ occurs on the Tullow pluton, suggests that the topography of the shear zone is primarily controlled by tectonic rather than differential weathering processes.

5.5.13 Relief

The relationship between relief and slope displays a very strong positive correlation (table 5.2) of 0.92. Relief and elevation likewise displays a strong positive correlation of 0.72. Figures 5.55a & b are relief maps, with the latter draped over a digital elevation model and illuminated from the NW. The relief map of Bunclody shows that areas to the NW and SE are of very low relief. These valleys are mostly v-shaped and are probably fluvial in origin, although, there are no through-going streams at present.

Dry river valleys or 'wind gaps', trending ~NNW-SSE, cross the Blackstairs Massif (Tinahely Hills) and produce thin wisps of low relief (40m to 60m), between areas of moderate to high relief, i.e. the hills Barnacashel, Seskin and Cronelea.

5.5.13.1 Ribband Group & Aureole

The low relief area in the SE is underlain by the Oaklands and Ballylane Formations of the Ribband Group. The average relief of these formations in this particular area is ~35m (figure 5.55). Although, in general, the average relief for the Ribband Group is 116m, and attains a maximum of 238m (figure 5.56a). Most of this relief occurs on the aureole rocks. The slope statistics for the maximum and averages of the metamorphic rocks are the same for the Ribband Group. The relief histograms are almost identical other than the aureole rocks have a slightly larger modal peak of ~40m (figure 5.57b) in comparison with a peak of ~32m for the Ribband Group (figure 5.57a). However, the standard deviation is larger for the Ribband Group (figure 5.56b), and the skewness is also marginally higher (figure 5.56c), which is a reflection of the relative low relief in the SE of the area of study.

5.5.13.2 Tullow Pluton

The Tullow Lowland is underlain by rocks of the Tullow pluton and corresponds with the modal peak of ~ 12m on the relief histogram (figure 5.55a, b). The maximum relief that occurs on the Tullow pluton is 169m and the average is 84m (figure 5.56a). Although, the average relief over the Tullow Lowland is <15m (not including sheared granite within the ECDZ) and the modal relief is ~18m (figure 5.57c). The Tullow pluton has the lowest standard deviation (figure 5.56b) and skewness of all rock types (figure 5.56c). This is because most relief values are generally very low, and that moderate relief is atypical. Hence, the Tullow plutonic rocks generally form an area of low relief, except within the ECDZ where relatively recent tectonic uplift has probably occurred.

5.5.13.3 Blackstairs Pluton

To the SW of the town of Bunclody, the highest relief in the area of study occurs. In this area (the northern part of the Blackstairs Mountains), the highest relief of 170m to 270m corresponds with Mt Leinster, Black Rock Mountain, and Slievebawn. The area is mostly underlain by rocks of the Blackstairs pluton and, to a lesser extent, inner aureole schists. The Blackstairs pluton is associated with the areas of highest relief with a maximum of 270m (figure 5.56a) and an average of ~145m. This is in striking contrast with the Tullow pluton, which has a maximum relief of only 170m and an average of 85m. The plutonic rocks exhibit the largest standard deviation of all rock type (figure 5.56b). This reflects the wide range of relief about the mean, i.e. these rocks have the largest range of relief (i.e. 248m). The skewness is relatively small (figure 5.56c) indicating that most of the moderate to high relief is the norm. The relief histogram for the pluton is quite spiky and irregular, but essentially displays a bimodal distribution, with a mode at ~100m, and a second peak at ~200m (figure 5.57d).

This may be due to a branch of the ECDZ bifurcating around the outer margin of the pluton. The fault will then be in a NE to NNE trend and with NW-SE maximum compression, this will result in tectonic uplift, producing Mount Leister, analogous to that proposed for the quartzite summits in the Vartry area. This implies an Early Tertiary uplift because subsequent NNW-SSE compression and ENE-WSW extension

will result in Tran tension, possibly resulting in further footwall uplift as a consequence of higher denudation and isostatic compensation.

5.5.13.4 Influence of Structure - East Carlow Deformation Zone (ECDZ)

The overall NE-SW structural grain (figure 5.40) is reflected in the relief of the area. Three NE-SW sub-parallel hills of moderate relief, ~2.5km in width, occur to the east of the town of Bunclody, labelled 1 to 3 on figure 5.54b. These areas include the hills of Cronelea and Gibbet Hill, which are underlain by the Ribband Group and form inner and outer aureole rock of schists and phyllites respectively. Therefore, relief appears to be strongly influenced by pre-existing geological structure. For example, the East Carlow deformation zone (ECDZ) is associated with a NE-SW zone of moderate relief (figure 5.55b) and has an average of 91m, and a maximum of 193m (figure 5.55a). The relief histogram for the shear zone is unimodal with a peak of ~72m (figure 5.57e). The distribution is relatively symmetrical apart from a small tail of moderate to high relief (low frequency). The symmetry is reinforced by a relatively small standard deviation (figure 5.56b), and the long tail of moderate to high relief produces the second largest skewness (figure 5.56c). Therefore, this appears to suggest that the shear zone is tectonic and has produced higher relief, irrespective of lithology.

5.5.14 Fluvial Geomorphology

The NE-trending ridge of hills in the area of study, i.e. the Tinahely Hills of Davies & Stephens (1978), produces a narrow ridge of low hills which continues into the relatively high ground in the SW (figure 5.58). The height of the Tinahely Hills above the Tullow Lowland is variable along strike, but ranges from several 10s of metres to over 400m. Much of this variability is due to the presence of a number of NW-SE-trending valleys that divide the ridge into discrete hills (Farrington, 1927). Along the entire length of the Blackstairs Massif (i.e. the Tinahely hills and Blackstairs Mountains) within the confinces of the study area, there are only three valleys that contain present-day catchments: from northwest to southeast, these are the headwaters of the Derry River, the River Slaney, and the River Barrow. Within the Bunclody area, there are 7 valleys, and only two contain rivers: the Slaney and Derry River. The Derry River flows concordant to the NE Caledonian structure, but the Slaney River cuts

topography and structure. The 5 other valleys or passes lack thoroughgoing streams, and now forms wind gaps (figure 5.59a). The significance of these winds gaps is discussed in section 5.5.15.

The escarpment that forms the northwestern margin of the Blackstairs Massif is roughly coincident with the contact between the Tullow pluton and rocks of the Maulin Formation (section 5.4.0). The contact between the two rock types has been sheared by the NE-SW trending Caledonian ECDZ (figure 5.59b). Towards the southern end, the ECDZ diverges from the topographic escarpment, which is then developed entirely within the Blackstairs pluton.

The River Slaney undergoes striking changes as it flows over this escarpment. Across the southern part of the Tullow Lowland, the river is incised <10m and has a moderate sinuosity of 1.36 (figure 5.58). Upstream of the escarpment, the course of the Slaney abruptly becomes almost perfectly straight for 7km, with a sinuosity of 1.02. Along this reach, the river also begins to incise; incision increases from <10m to 50m as the river crosses the escarpment. Downstream of the escarpment, sinuosity abruptly increases to 1.37 for 10.5km through the Blackstairs Mountains. On the southeast side of the range, sinuosity decreases to 1.17 as the river approaches base-level. These changes in sinuosity and incision are consistent with the response of an alluvial river to tectonic uplift (Ouchi, 1985; Schumm, 1986). With energy slope held approximately constant, the river decreases its sinuosity (and increases slope) upstream of the uplift axis and increases in sinuosity downstream. This produces an incised meander (labelled *M* on figure 5.55b) as it crosses from the Tullow Lowland and flows through the northern end of the Blackstairs Massif. The meander produces moderate relief of 30m to 130m on rocks of the metamorphosed Kilcarry Member of the Maulin Formation (Ribband Group). However, the Slaney has incised along a ~15km reach north of the escarpment (figure 5.58), which implies that the river is responding to rock uplift over a relatively broad region.

5.5.15 Discussion

The granitic rocks of the Blackstairs pluton produce the highest elevations in the area of study. Conversely, the granitic rocks of the Tullow pluton occupy the lowest

elevations. The granite types of both plutons are similar in terms of texture and composition, and jointing is similar within both plutons. Therefore, differential erosion is unlikely to be the prime mechanism forming the topography. However, it is possible that the Blackstairs pluton has been until very recently, protected by a capping of schist (i.e. the inner aureole rocks extend up the northern and western flanks of Mount Leinster) whereas the Tullow pluton has been exposed for a greater duration to exogenic processes with little or no protective schist roof rock. However, a very large negative Bouguer anomaly occurs over the Tullow Lowland (figure 5.41), and therefore, the granite appears to be thickest here, making the idea of greater denudation unlikely.

The western margin of the Tullow pluton forms an unconformity with Lower Carboniferous sediments, predominantly carbonates. As there is no evidence of faulting, the sub-Carboniferous unconformity can be projected over the Tullow Lowland reaching an estimated height of no more than 100m above it (figure 5.60). Therefore, this is the maximum amount of post-Carboniferous elevation and erosion attained by the pluton. Evidence was presented in section 5.1.4 that the present-day surface, which cuts across the Tullow Lowland and the Lower Carboniferous rocks to the west, is of Tertiary age with a thin veneer of Quaternary till. It is evident then that the steep slopes, notable relief and relatively unweathered bedrock of the Blackstairs Massif must be the product of tectonic uplift during the Tertiary (figure 5.59).

The highest elevation is underlain by granite on Mount Leinster, but schists rise up the northern flanks to a height of 285m. The aureole rocks tend to form higher elevations than the non-metamorphic rocks of the Oaklands and Ballylane Formations. Figure 5.61 shows that most of the change in hill slope and relief is not lithologically controlled. The one exception being between rocks of the Tullow pluton and the inner aureole schists of the Monaughrim Member of the Maulin Formation (Ribband Group). But, the differences are not great, and the metamorphic lithological control has had less of an effect on topography than in the Vartry area.

The antecedence of the Slaney River and the presence of wind gaps across the escarpment, bounding the NW margin of the Blackstairs Massif show that the drainage system of the Bunclody area developed on a landscape that was very different from the present topography. The Rivers Nore and Barrow also cross the escarpment further

southwest (figure 5.62). Davies (1970) considered that the rivers might have originally established a southeast-flowing system on a widespread, low-relief depositional surface, which he believed to be composed of Cretaceous chalk (section 5.1.4). Later workers (e.g., Evans & Clayton 1998) have argued that between 0.7km and 1.5km of covering rocks have been removed from chalk outcrops at Ballydeenlea, Co Kerry (see chapter1), lending credence to the idea that a significant thickness of Cretaceous and Cenozoic sediments may have covered large areas of southern Ireland. Evidence for an original cover of Cretaceous chalk in County Wicklow is provided by the presence of flint pebbles in locally derived fluvio-glacial gravels in the upper Slaney valley (Phillips W.E.A, 2000). The idea of an original cover is supported by apatite fission track models (chapter 7).

In this scenario, the rivers are gradually let down across the landscape as the Cretaceous and Cenozoic sediments are removed. But, it is highly improbable that the present topography of the Blackstairs Massif was buried and then re-exhumed from beneath a chalk cover. This scenario also fails to explain the widespread occurrence of wind gaps in the Blackstairs Massif, and does not account for the abrupt changes in sinuosity along the Slaney River (figure 5.59). This scenario also requires differential erodibility between the Tullow Lowland and the Blackstairs Massif to explain the present topography. As already noted, it is unlikely that the Tullow pluton was ever elevated to the same extent as other parts of the batholith. The continuity of the Blackstairs pluton across the topographic escarpment also rules this out.

In addition, a parallel valley (Aughrim/Lildaven corridor of Davies & Stephens, 1978; and the Aughrim/Kildaven Interblock depression of Mitchell, 1985) runs between the NW and SE escarpments of the Blackstairs Mountains and Tinahely hills, (including the Annagh/Avoca block of Mitchell, 1985). This valley extends 32km from the NE slopes of Mount Leinster to the NE of the town of Aughrim. Water drains into the valley and forms the Derry River and Derry Waters and flows SW and NE to join with the Slaney River and Aughrim River at Kildavin respectively. In the middle of the valley, the floor is choked with outwash gravels and glacial material (Mitchell, 1985). Only small amounts of water flow into the valley and it is therefore unlikely that the present form can be fluvial or glacial in origin. Mitchell (1985) suggests that the valley or depression may be fault controlled.

The topography of the area of study may be due to reactivation of the ECDZ, with the southeastern side upthrown (figure 5.63). If the ECDZ dips southeast, as inferred by McArdle & Kennedy (1985), and if the Bunclody area has experienced similar tectonic stresses to the Vartry area, then this implies a reverse component of dip-slip motion. Displacement along the zone would behead the smaller catchments crossing the escarpment whose stream power was insufficient to keep pace with rock uplift (e.g., Burbank *et al.* 1996). Only the largest rivers such as the Slaney, Barrow and Nore would possess sufficient power to maintain their existing courses.

5.5.16 Conclusions

The changes in sinuosity and incision along the Slaney are consistent with the response of an alluvial river to rock uplift; energy slope is held approximately constant as the river decreases its sinuosity (and increases its slope) upstream of the uplift axis and increases its sinuosity downstream of the uplift axis (Ouchi, 1985; Schumm, 1986). The transition from straight to meandering occurs approximately at the contact between the Monaughrim and Kilcarry members (semi-pelitic and volcanic) of the Maulin Formation. Incision along the Slaney is not limited to the region southeast of the topographic escarpment, which indicates that the river is responding to rock uplift over a relatively broad (~15km: figure 5.63) region. If the escarpment were due to differential erosion, i.e. contrasts in erodibility between the Tullow Lowland and the Blackstairs Mountains, then incision would only occur within the high-standing Blackstairs pluton rocks. These rocks would control the rate of river incision, and there would be no need for the river to incise into the Tullow Lowland. This shows that there is broad zone of Tertiary uplift across the Blackstairs Massif.

To sum up, it is probable that endogenic processes of Tertiary (probable Neogene) age have resulted in uplift of the Blackstairs Massif relative to the Tullow Lowland. Apatite fission track data also supports this conclusion (chapter 7). The presence of the major Caledonian East Carlow Deformation zone probably acted as a line of crustal weakness that has been reactivated during the Tertiary. If the structure has experienced relatively recent strike-slip movements then transpressional uplift and transtensional subsidence would occur at fault bends. The structure also correlates with the onshore-offshore

faults strands in the Vartry area (figure 5.37) and the southern margin of the Kish Bank basin

5.6 Glen of Imail Area

The Glen of Imail area is located on the SW margin of the Wicklow Massif, just north of the Tullow Lowland. The study area lies between the Kings River to the north and just south of the town of Baltinglass to the south. The area is 25km by 15km and includes the highest peak in the Leinster Mountain chain, the Lugnaquillia Mountain. This area was selected because the Glen of Imail appears to be a potential fault basin, and there are numerous wind-gaps along the Baltinglass escarpment to the south (figure 5.64).

5.6.1 Elevation Histogram

Figure 5.64 is a digital elevation model and histogram for the Glen of Imail area. The elevation histogram exhibits a weak bimodal distribution. The modal peak is ~115m and a second large peak occurs at elevations of ~155m. A third more equivocal small peak occurs at much higher elevations at ~620m (labelled 1, 2 and 3 respectively). The modal peak mostly represents the floor of the Glen of Imail (referred to as the Glen of Imail basin by Mitchell, 1985), the Tullow Lowland and the large area to the west (labelled on figure 5.64 as the Kilcullen surface). The second peak mostly represents the foothills of the Leinster Mountain chain. The third peak represents a high level surface and spans from Lough Forrib in the north to Slieveman and Corriegasleggaun in the south (figure 5.64). Transitional-base-level processes mostly dominate the first two peaks, whereas the third peak corresponds with plateau processes. The distribution is highly skewed towards relatively low elevations showing that the base-level processes are dominant.

5.6.2 Preliminary Interpretation

The Glen of Imail area has experienced plateau and transitional-base-level processes. The Kilcullen surface and the Tullow Lowland are dominated by near base-level processes. Both areas are separated by an ~E-W trending escarpment of relatively low-

lying hills, i.e. from Corballis hill in the west to Slieveboy mountain in the east (figures 5.64 & 5.65). The Slaney is the only river that crosses the escarpment. If base-level processes have been at work for a large period of time (e.g. 30Myr), then one would expect the Slaney River to flow ~10km further west and around the escarpment. This suggests that the escarpment may be a recent tectonic feature. The other area of low elevation is the Glen of Imail (figure 5.64 & 5.65). The headwaters of the Slaney River occur here on the western flanks of Ben Leagh. The floor of the Glen of Imail basin is of low elevation but surrounded by much higher hills and mountains. The scoop shape of the basin is quite unlike the narrow, linear valleys typical of those that occur in Leinster Mountain chain.

5.6.3 Elevation Profiles

Figure 5.64 shows two elevation profiles. Line A is an ~E-W profile that traverses the crests of hills that form, what is termed here, the Baltinglass escarpment. Elevation is at a maximum of ~600m on Corrig Mountain in the east. To the west, the crests and valleys of the three low-lying hills show an overall reduction in elevation. Line B is a WNW-ESE profile that traverses from the highest to some of the lowest elevations over a distance of 13km. The profile starts at ~900m near the peak of Lugnaquillia Mountain in the east. This falls quite rapidly over a distance of 3km to an elevation of 400m. The elevation then increases slightly for ~1km over Camarahill. The elevation then decreases again at a gradient of ~0.5 for a distance of 500m. At ~220m, the elevation then decreases very slowly, and represents the floor of the Glen of Imail, referred to here forth as the "Glen of Imail basin".

Line A depicts the numerous wind-gaps that lie along the escarpment and shows an overall reduction in elevation to the west. It is likely that this is an analogous situation to that of the ECDZ, with only the largest river, the Slaney, being able to maintain incision due to tectonic uplift. This is supported by apatite fission track data (chapter 7). The Glen of Imail basin is shown on maps to represent a lithological control (figure 5.66). However, there is no outcrop on the basin floor and the underlying Glen of Imail quartz-diorite is inferred from erratics (Brück & Reeves, 1983). Therefore, it is possible that the basin may be of tectonic origin and/or represent mass wasting of the Lugnaquillia surface by landslides.

5.6.4 Bedrock Structures

A major WNW-ESE fault (figure 5.66) extends across the area from ~2km south of Brewell Hill (near the N9) and runs through the Glen of Imail basin, supporting the postulate that the geomorphic feature is tectonic in origin. Brück & O'Connor (1980) and Brück & Reeves (1983) continue the fault over the slopes of Lugnaquillia Mountain, passing just south of the summit and linking up with the Ow River fracture. The fault appears to dextrally offset the ECDZ, which would be consistent with similar kinematics of other NW-SE to WNW-ESE fractures (i.e. the Lough Dan fracture – see chapter 7).

The Slaney River follows the line of the main fault through the Glen of Imail basin. To the north, the Glenmalure fracture cuts both the Lugnaquillia pluton and the Butter Mountain Formation. To the west, two NE-SW trending faults are offset by the Glen of Imail fault. These are the Athgarret fault and the Hollywood shear zone. The Athgarret fault shows an apparent dextral offset of ~1.5km. The Hollywood shear zone shows a much smaller offset. On published GSI geology maps, this shear zone terminates suddenly against the Tullow pluton.

A number of NE-trending fold axes, with wavelengths of ~500m, parallel the Athgarret fault between 1km and 4km to the west. The eastern limbs of the folds have been overturned and the folds are upward facing to the NW, bringing the relatively older Tipperkevin Formation to the surface. The strata youngs to the NW due to recumbent folding. In general, bedding, magmatic foliation and schistosity in the aureole rocks strike NE-SW and are sub-parallel to the granite margins.

5.6.5 Bouguer Gravity Anomaly

Figure 5.67 is a Bouguer anomaly map draped over topography of the Glen of Imail area. The Bouguer anomaly at this area has a range of 20mgal, with a minimum and maximum of –23mgal and –3mgal respectively. The relatively low values are due to the Tullow and Lugnaquillia plutons. The Kilcullen Group is associated with the highest Bouguer values.

In the NE, the gravity trend is ~N-S to NNE-SSW, and crosses the margin of the Tullow pluton to the south. This coincides with the highest Bouguer anomaly values, which show that the Tullow pluton is a more deep-seated feature than the Lugnaquillia pluton. The gravity changes to an ~E-W trend in the western half of the map, which reflects the northern boundary of the Tullow pluton. The –7 to –5 gravity contour is dextrally offset by ~4km and coincides with the Glen of Imail fault.

5.6.6 Metamorphic Aureole

The contact aureole varies in width from 10m to 3.8km. The aureole is widest where it is in contact with the inferred Glen of Imail quartz-diorite boundary down the NW side of the Lugnaquillia pluton (figure 5.68). The minimum widths are associated with the schist septum which separates the Northern and Lugnaquillia plutons, and lenses of septum that partially separates the Glen of Imail quartz-diorite from Percy's Table granodiorite (figure 5.66).

A relatively thin aureole of phyllite (~70m in width) trends east-west along the contact with the Tullow pluton. This trend continues eastwards between a tongue of the Carrawaystick aplite, and the Glen of Imail granodiorite. The aureole then swings towards the NE and passes over the summit of Lugnaquillia. Branches of this roof pendant also occur as a discontinuous band running NW from the Lugnaquillia summit.

5.6.7 Ribband Group & Aureole

The aureole is dominantly of pelitic schist and phyllite. The maximum elevation of the aureole is 921m over Lugnaquillia Mountain (figure 5.68). The mean and median elevations are 350m and 300m respectively. A small fraction of the Butter Mountain Formation has also experienced contact metamorphism. Likewise, the Glen Ding Formation of the Kilcullen Group forms aureole rock along the contact with the Tullow pluton, forming the most western part of the Baltinglass escarpment (figure 5.68). The aureole rocks have a lower modal elevation than the average, i.e. ~180m (figure 5.69a). These metamorphic rocks also share the largest standard deviation (with rocks of the Lugnaquillia pluton) and represent the fact that aureole rocks occur on the maximum and near minimum elevations in the area of study, with a large deviation about the mean

(figure 5.69b). The elevation distribution of the aureole rocks is skewed towards lower values (figure 5.69c). Hence, the mean and median elevations are not typical of the overall distribution. Differential erosion is therefore unlikely to be the dominant process controlling elevation of the aureole rocks.

5.6.8 Tullow Pluton & Kilcullen Group

Most of the low ground is underlain by the Tullow pluton and the Kilcullen Group (figure 5.66). The maximum elevations of the Tullow pluton and Kilcullen Group are ~ 413m and ~310m respectively. The mean and median elevations of the Tullow pluton are 162m and 150m, which compares with a mean and median of 167m and 162m for rocks of the Kilcullen Group (figure 5.69a). The modal elevations for both rock categories are slightly lower than their respective means and medians. A modal elevation of 150m is associated with the Kilcullen Group, which are 20m higher than that of the Tullow pluton. Hence, in terms of elevation, the Tullow pluton ranks as the lowest. The Tullow pluton has a slightly larger standard deviation (figure 5.69b) than the Kilcullen Group, indicating a much greater variability of elevations. The skewness is likewise larger as the Tullow pluton rocks occur at higher elevations but have much lower averages than the rocks of the Kilcullen Group (figure 5.69c).

5.6.9 Lugnaquillia Pluton

The Lugnaquillia pluton reaches a maximum elevation of ~900m, and has the highest mean and median elevation of ~400m of all rock types. The modal elevation is almost half the mean and median, at ~200m (figure 5.69a). This distribution, and hence, the elevation range has a large standard deviation about the mean. These rocks also have the lowest magnitude of skewness at just 0.3, due to the mean and median sharing the same value. The high elevations mostly relate to the Glendalough Adamellite, whereas, the lowest are associated with the Glen of Imail quartz-diorites. One argument is that these high elevations are due to shielding from the schist caps. But, this is unlikely to be the case for reasons outlined below.

5.6.10 Northern Pluton

The Northern pluton attains a maximum elevation of 624m with a mean and median of 355m and 350m respectively (figure 5.69a). However, just as in the Vartry area, these rocks have a modal elevation slightly higher than the mean and median. The standard deviation is moderate at 80m (figure 5.69b) but the skewness is small at 0.4 (figure 5.69c). The rocks of the Northern pluton have the second highest average elevation within the Glen of Imail area. Hence, the shielding of the Lugnaquillia pluton from erosion by schist septum does not appear to have played a significant role, otherwise, the Northern pluton would be more comparable with the Tullow pluton.

5.6.11 Other Igneous Rocks

Other igneous rocks make up a very small proportion of the total geology (Appendix 3). Taken together, these rocks attain a maximum elevation of 684m, with mean, median and modal values ranging from 198m to 158m. The minimum elevation is 120m (figure 5.69a), and forms the largest skewness of all rock types (figure 5.69c). Hence, in the grand scheme of things, these rocks have little influence on the geomorphology of the area.

5.6.12 Slope

The steepest slopes (>40°) within the Glen of Imail area occur in the east, over the high elevation surface (figure 5.63). Most of the high slopes are the result of glacial erosion and occur on mainly ~E-W and ~NW-SE trending valley sides, i.e. the Ow River and Glenmalure valleys which have been eroded along fault zones. The highest slopes occur on the southern side of Lugnaquillia Mountain and the Ben Leagh ridge (figure 5.70). Moderate slopes occur on most of the upland areas and also along the Baltinglass escarpment. The Tullow Lowland, Kilcullen surface and the Glen of Imail basin also occurs on low to very low slope (figure 5.69). In general, low slopes occur over the Glen of Imail basin, Tullow Lowland and the Kilcullen surface, ranging from flat to 5°. The steepest slopes occur over the mountain chain in the east, i.e. areas of steep slope form NW-SE to WNW-ESE flanks.

5.6.12.1 Slope and Elevation

The relationship between slope and elevation in the Glen of Imail area has a moderately positive correlation of 0.67 (table 5.3). The maximum elevation shows an indifferent relationship for slopes of 1° to 35°, and holds an elevation of ~900m. On slopes >35°, maximum elevation has a negative correlation (figure 5.71a). A weak positive correlation exists between slopes of 1° to 35° and elevation, ranging from ~460m to ~650m. On slopes >35°, the relationship with elevation is negatively correlated, and the mean and median diverge slightly, with the mean slightly higher. Slope steepness has a weak to moderate positive correlation with elevation (figure 5.71a). The standard deviation of elevation decreases from gentle slope to steep (figure 5.71b) whereas skewness is relatively low with the exception of slopes of 40° to 45° (figure 5.71c). This indicates that there is a general spread of slope steepness over the Glen of Imail area, with the steepest values associated with the lower slopes of the Wicklow Massif.

Table 5.3

	Minimum	Maximum	Mean	Standard Deviation
Slope	0	49	6	5
Relief	1	363	56	48
Elevation	88	921	258	156

CORRELATION MATRIX	Slope	Relief	Elevation
Slope	1	0.92	0.67
Relief	0.92	1	0.74
Elevation	0.67	0.74	1

5.6.13 Slope and Geology

The western and most southern parts within the Glen of Imail area are dominated by large areas of low slope, underlain by turbidity sequences of the Kilcullen Group and granite of the Tullow pluton variety. The eastern part consists mostly of moderate to high slope (figure 5.70) and is underlain by granite of the Northern and Lugnaquillia plutons, and aureole schists of the Ribband Group. Low slopes occur on the floor of the Glen of Imail basin and on the high elevation surface that surrounds the peak of Lugnaquillia which are underlain by Glen of Imail quartz-diorite and Percy's Table granodiorite respectively. In general, the plutonic rock produces the steepest slopes with the exception of the Tullow pluton. This illustrates that differential weathering is not a dominant process and fault reactivation is probably the most important mechanisms maintaining hill slopes.

5.6.13.1 Ribband Group & Aureole

The Ribband Group forms maximum slopes of 41°. The mean and median slopes have values of 9° and 8° respectively (figure 5.72a). The modal slope value is slightly lower at 5° (figure 5.72a). Most of the Ribband Group is aureole rock and hence the slope statistics are very similar. The aureole slope histogram has slightly more moderate and less low slopes than the Ribband Group as a whole (figure 5.72c), with a higher mean and median of 10° and 9° respectively (figure 5.73a). Overall, the Ribband Group slope histogram is slightly more skewed towards lower slopes than the aureole, indicating that the schists and phyllites produce higher slopes than their protolith equivalent. About 80% of the cumulative frequency of the Ribband Group and the aureole schists occur on slopes of 1° to 13° (figure 5.72c). A greater proportion of the Ribband Group underlies areas of flat ground, about 7%, in comparison with 5% for aureole rocks (figure 5.72b). Much of the flat areas that underlie the aureole rocks occur on the outer western periphery of the Glen of Imail basin.

5.6.13.2 Tullow Pluton

The maximum slopes on the Tullow pluton are 19°(figure 5.73a). The Tullow rocks have the lowest mean and median slopes with values of 4° and 3° respectively (figure

5.73a). The histogram distribution is highly skewed towards very low slopes, and has a modal peak of 2° (figure 5.75a). Over 80% of the cumulative frequency occurs on slopes of 1° to 4°. In similar fashion to the Tullow rocks at Bunclody, over 25% of the Tullow plutonic rocks underlie areas of flat ground (figure.5.73b). The rocks of the Tullow pluton have the highest skewness of slope distribution (figure 5.74), reflecting very low slopes and the low occurrence of moderate gradients. Hence, these rocks are associated with low slope and elevation.

5.6.13.3 Kilcullen Group

The maximum slope of the Kilcullen Group rocks is the same as those of the Tullow pluton, i.e. 19° (figure 5.73a). The mean and median are slightly higher at 4° and 3° respectively. The slope histogram shows a similar pattern to the Tullow pluton with a modal value of 4° (figure 5.76a). The cumulative frequency is also similar to the Tullow pluton with just over 80% occupying slopes of 1° to 4° (figure 5.76b). About 17% of the rocks underlie areas of flat ground (figure 5.73b). These rocks form the relatively flat and mundane ground to the west of the Wicklow Massif.

5.6.13.4 Lugnaquillia Pluton

The Lugnaquillia pluton has the highest maximum slopes within the Glen of Imail area, with a value of 49° (figure 5.73a) occurring about 0.5km south of the peak of Lugnaquillia Mountain. The mean and median also occupy the highest slopes of 11° and 10° respectively (figure 5.73a). The slope histogram distribution is skewed towards low elevations, with a modal peak at 11° (figure 5.77a). The cumulative frequency shows that much of the granite occupies moderate slopes, i.e. over 80% occurs on slopes of 1° to 15° (figure 5.77b). Only ~3% of the pluton underlies areas of flat ground (figure 5.73b), with most of this occurring on the upper elevations. Hence, these rocks form the highest slopes and elevations.

5.6.13.5 Northern Pluton

The Northern pluton produces maximum slopes of ~28°, with a mean and median of 9° (figure 5.73a). The slope histogram distribution resembles that of the Lugnaquillia

pluton, except that the former has a much shorter tail of high slopes (figure 5.78a). The mode occurs at 7°. About 80% of the cumulative frequency occurs on slopes of 1° to 12° (figure 5.73b). Less than 2% of the rocks underlie flat ground, the minimum for all rock types (figure 5.73b). Hence, these rocks also form relatively high slope and elevation, despite having no protective aureole schist roof pendants. This suggests that this batholith was unroofed earlier than the Lugnaquillia pluton.

5.6.13.6 Hypsometry - Differences & Similarities of Slope Distributions

The Tullow pluton curve has the highest proportion of low normalised slope, at ~15% frequency and increases to 21% frequency on normalised slope values of 0.1 (figure 5.79a). From 0.2 to 0.6, the slope decreases at a non-linear rate, and falls below 1% frequency by 0.5. The decrease from 0.6 to 1 is gradual and produces a long flat tail of high normalised slope. The curve is similar to the Kilcullen Group, with the latter showing less amount of low normalised slope and slightly higher low to moderate values. The Northern pluton curve is much flatter but has a higher proportion of moderate normalised slope than any other rock type. Between 0.2 and 0.3 normalised slope, the frequency percentage increases from 2% to a peak of ~8% frequency. And from 0.4 to 0.7, the slope decreases to less than 1% frequency and has a relatively short tail of high values. The Lugnaquillia pluton envelope increase from ~2% to ~ 6.5% frequency by 0.2. This then decreases to less than 1% by 0.5. Hence the envelope has a fairly long tail. The Ribband Group and aureole are near identical, except that the Ribband Group has relatively lower normalised slope and less moderate values (figure 5.79b).

The fact that the Northern and Lugnaquillia plutons have similar average slopes, and are dominated by a larger percentage of moderate to high normalised slopes implies that the schist septum and roof pendants have not shielded the Lugnaquillia pluton to any great extent, other than to create more rugged slopes of very local extent. If this was not the case, then the Northern pluton should have much gentler hill-slope gradients. The aureole rocks do not appear to control the development of slope within the Glen of Imail area. The greatest slope magnitudes occur on the Lugnaquillia and Northern plutons. The Tullow pluton on the other hand forms very low slopes. The granite varieties of the Tullow and Northern plutons are similar in composition and texture,

therefore, the relative rock resistance to weathering does not appear to be the dominant process at work.

5.6.14 Relief

The relationship between relief and slope displays a very strong positive correlation (table 5.3) of 0.92. The relationship between elevations also displays a strong positive correlation of 0.74. Figures 5.80a and 5.80b are relief maps, with the latter draped over a digital elevation model and illuminated from the NW. The relief map of The Glen of Imail area shows that the eastern part (western Wicklow Massif) is an area of moderate to high relief. The Baltinglass escarpment also shows as an area of moderate relief, with the Tullow lowlands to the south showing very low relief. The Kilcullen surface is also an area of low relief, but slightly more moderate than the Tullow lowlands. The relief histogram shows that the area is mostly of low relief, with a modal relief of ~35m, in comparison with an average (mean) of 173m.

The Slaney River produces two gorges, where relief is moderate on either side. The first, labelled 'G' on figure 5.80b is at the lip of the Glen of Imail basin and has incised into aureole schists of the Butter Mountain Formation. The second gorge, labelled 'B' on figure 5.80b, cuts the Baltinglass escarpment where the river then flows south across the Tullow lowlands. A number of NNE and NNW wind gaps cross the escarpment (figures 5.65 & 5.80).

5.6.14.1 Ribband Group & Aureole

The Ribband Group and aureole display very similar relief characteristics (figure 5.81a). The maximum relief of these rocks is 317m with a mean of 148m (figure 5.81a). The relief histogram is unimodal with modal relief of ~50m, although most values range from ~30m to ~80m (figure 5.82a). The aureole has a similar relief histogram with similar average values (figure 5.81a). The mode on the other hand is much higher at ~80m, with most values ranging from ~50m to 85m. There is also less occurrence of low relief, which makes the Ribband Group distribution base heavy (figure 5.81b). The Ribband Group rocks have the second largest standard deviation of 86m (figure 5.81b), a reflection of the wide range of relief, and the relative low average values produce a

small skewness of 0.07, which nevertheless is the largest of all rock types (figure 5.81c). Hence, there is little difference in relief between the aureole and Ribband Group (aureole and non-aureole rocks).

5.6.14.2 Tullow Pluton

The rocks of the Tullow pluton underlie the Tullow lowlands, south of the Baltinglass escarpment (figure 5.60). The maximum relief that these rocks produce is 170m and an average of 83m (figure 5.83). The relief histogram distribution is highly skewed towards very low values of relief, with a mode of ~20m (figure 5.83). The distribution is highly spiky with the second lowest standard deviation of 48m (figure 5.81b). This is similar to the Tullow pluton in the Bunclody area. The relief is even lower in this area because the rocks haven't been partially uplifted.

5.6.14.3 Kilcullen Group

The Tullow pluton produces the lowest slope however the rocks of the Kilcullen Group form the lowest maximum and average relief, i.e. 125m and 62m respectively (figure 5.80a). But, the slope histogram distribution shows a higher modal relief of 30m and a larger, more frequently occurring tail of moderate relief, i.e. from ~60m to ~115m (figure 5.83). This is reflected in the lowest standard deviation of 36m (figure 5.81b). Hence, in general, the Kilcullen Group does underlie areas of low to moderate relief, whereas the Tullow pluton mainly underlies areas of low relief.

5.6.14.4 Lugnaquillia Pluton

The maximum relief in the Glen of Imail area of study occurs on rocks of the Lugnaquillia pluton, i.e. a maximum of 363m (figure 5.85). The average relief is also highest of all rock type at 175m (figure 5.81a). The relief histogram distribution is unimodal with an anomously high peak at ~75m although the range is from ~50m to ~125m. The standard deviation is the highest of all rock types indicating a large range of elevations about the mean (figure 5.81b). The skewness is less than the aureole rocks however indicating a more evenly spread distribution of relief values (figure 5.81c). It

is unlikely that schist roof pendants are shielding the pluton, otherwise, the aureole rocks would have the highest relief.

5.6.14.5 Northern Pluton

The Northern pluton is characterised by maximum relief values of 194m and an average of 97m (figure 5.81a). The relief histogram distribution is unimodal and has a high modal value of ~85m, although, the highest occurrences range from ~45m to ~100m (figure 5.85). The standard deviation is 55m showing that there is a large range of relief values spread relatively evenly about the mean (figure 5.86). The distribution is almost symmetrical and hence has a skewness of about 0.006 (figure 5.81c). This supports the general conclusion above that schist roof pendants are not the main reason for the high relief of the Lugnaquillia pluton.

5.6.15 Geomorphology

The Glen of Imail basin is located in the west of the study area (west Co. Wicklow) and has a centripetal drainage, choked by Midlandian glacial deposits (Mitchell, 1985) and underlain by the Glen of Imail quartz-diorite. The basin is surrounded by areas of high slope, elevation and relief (figures 5.87b & 5.88) of schists (the Butter Mountain Formation) and is transected by a major WNW-ESE trending fault, the Glen of Imail fault (figure 5.87a), which links up with the Ow River fracture (figure 5.87a). The River Slaney's headwaters are located on the eastern margin of the basin. The river flows initially west, along the trace of the Glen of Imail fault and forms a gorge, labelled 'G' on figure 5.87a. The river then swings around Spinians hill towards the south, and forms a steep gorge, labelled 'B' where it crosses the Baltinglass escarpment (figure 5.87).

Despite the strong contrast in elevation and relief of the Baltinglass escarpment, only one large river (the Slaney) flows across the escarpment (figure 5.87). The longitudinal profile of the Slaney shows no change in gradient across the escarpment. East of the Slaney, a number of small catchments drain the Glen of Imail basin. These catchments are typically incised 10 to 20 m into bedrock as they cross the escarpment; these deeply incised valleys are set into much larger valleys or gaps between hills. The drainage

divide between north- and south-flowing catchments lies only ~1km north of the topographic escarpment (figure 5.87). At the base of the escarpment are a number of coarse, lobate, bouldery deposits. While poorly exposed, these appear to be mass wasting or debris flow deposits derived from the escarpment to the north.

5.6.15.1 Glen of Imail Basin

The rocks of the Tullow pluton and Kilcullen Group underlie the areas of lowest elevation, slope and relief. The highest occur on rocks of the Lugnaquillia pluton, with the exception of the Glen of Imail basin. The Northern pluton produces more varied elevations, slope and relief. However, the relative high comparative values with those of the Lugnaquillia pluton suggest that the aureole schists are not primarily the cause of the steep topography.

The relationship between the topographic variables and geology is not straightforward. For example, figure 5.88a is a NNE-SSW geological cross-section that shows that the Glen of Imail basin is at relatively low elevations and is underlain by rocks of the Lugnaquillia pluton. The basin is flanked to the north and south, mostly by aureole schists of the Butter Mountain Formation. The Carrwaystick aplite of the Lugnaquillia pluton also forms fairly high elevations, which drops fairly rapidly on to the rocks of the Tullow pluton. The Northern pluton in the north forms moderate elevations. Figure 5.88b & c show relatively high slope and relief at the contact between the Tullow and Lugnaquillia plutons, although relatively high slopes also occur over the Tullow pluton with no apparent lithological or tectonic control. Some of the largest areas of steep slope and relief are not associated with the aureole schists but are on the Glen of Imail quartz diorites that underlie the basin, ruling out lithological control. The Northern pluton forms the lowest slopes and relief along section. Hence, lithology appears to have played a minor role in shaping the topography. The aureole schists do produce high elevation but the hill-slope gradients and relief are not lithologically controlled.

5.6.15.2 Baltinglass Escarpment

The Baltinglass escarpment forms a linear, but discontinuous WNW-trending ridge of hills and valleys that separates the western Wicklow Massif from the Tullow Lowland

to the south (figure 5.87a, b). The escarpment is expressed as a linear range with heights that are variable along strike, but nowhere less than ~50m. At its westernmost end, the escarpment is roughly coincident with a complex contact between the Tullow pluton of the Leinster granite to the south and Ordovician phyllites of the Glen Ding Formation. The eastern 10km of the escarpment lies entirely within the Lugnaquillia pluton (McConnell & Philcox, 1994). As figure 5.88 shows, the escarpment marks a strong contrast in elevation, slope and relief. North of the escarpment, relief between valley bottoms and adjacent ridge crests is commonly in excess of 300m, whereas the greatest valley-to-ridge relief in the Tullow Lowland is less than 50m.

The escarpment is only partly coincident with mapped lithologic boundaries, mostly at the western margin where the topography is more subdued and outcrop is poor. Thus, the main contrast in erodibility, between granitic rocks and Ordovician phyllites (Farrington, 1927), lies to the north of the escarpment. Hence, a lithologic origin of the escarpment seems unlikely. Another possibility is that the escarpment is a palaeo-seacliff. The base of the escarpment lies at an elevation of ~130m asl along most of its length, and Mitchell (1980) mentioned an outcrop of Pliocene (?) shallow marine shells from the edge of the Tullow Lowland in Co. Carlow, at a present elevation of 150m. However, the escarpment is strikingly linear, and the close proximity of the drainage divide to the escarpment is unexplained by this model.

Mitchell & Ryan (1997) suggested that the escarpment might be tectonic in origin based on its linearity, with a vertical displacement of at least 800m. The linear nature of the escarpment is consistent with range fronts associated with active dip-slip faults (e.g., Wallace, 1978). Based on the Tertiary dextral transform palaeostress (NW-SE compression and NE-SW extension), movement on this structure was probably dextral reverse. However, more recent dip-slip motion (chapter 7) would cause northward tilting of the region north of the escarpment create and maintain a drainage divide very close to the fault (Ellis *et al.*, 1999). Short, southward draining streams are incised into the upthrown block, consistent with base-level fall along the escarpment.

5.6.17 Conclusions

The geomorphic landforms of the Glen of Imail area tend to point to recent tectonic activity (endogenic processes) as the main mechanism to have shaped the present-day topography of the western part of the Wicklow Massif. Exogenic processes now appear to prevail and are lowering the elevation of the region, and producing small landforms controlled by differential erosion superimposed on a greater tectonic imprint. It is these smaller topographic features that have led many previous workers (section 5.1.4) to propose that the whole area has been high since Carboniferous times, pointing to the small effects of differential weathering as evidence for this hypothesis.

Figure 5.89 show a possible tectonic model based on the stress systems derived from the Kish, Vartry and Bunclody areas. In this model, the Glen of Imail basin is faulted on the eastern margin, and the Glen of Imail fault has produce dextral transpression. In a similar manner, a WNW fault bounds the Baltinglass escarpment producing dextral transpression, in a similar fashion to the WNW trending Blackrock fault (chapter 3), and possibly followed with subsequent dip-slip.

5.7 Discussion of Conclusions

The landscape of SE Ireland is consistent with the model proposed in chapter 4. All three areas can be explained by Early Tertiary and Late Tertiary stress models. During the Palaeogene, NW-SE compression with NE-SW extension would initially produce transpression on WNW-ESE structures and transtension on ~N-S to NE-SW fractures. Hence, the Baltinglass escarpment and the Glen of Imail fractures would have reactivated with dextral transpression. The East Carlow Deformation zone would mostly produce reverse motion and the Vartry and Djouce faults will produce dextral transtension. Palaeostress then rotated clockwise to a NNW-SSE compression with ENE-WSW extension. This would have resulted in further extension on the N-S oriented fractures, compression on the Baltinglass escarpment and sinistral transpression along the East Carlow Deformation zone.

The analyses of topography appear to support this premise. For example, the Bray Group rocks have low mean elevation, slope and relief, but show that the steepest slopes

and relief. The Tullow Lowland is also an area of low elevation, slope and relief, but show relatively high values along the margin where it is in contact with the ECDZ. The Northern pluton has similar topographic characteristics to the Lugnaquillia pluton, indicating that schist roof pendants have had little influence on the development of the geomorphology.

In general, the Leinster Mountain chain is an area of moderate to low slope, elevation and relief. The area is now dominated by transitional processes, denuding the topography towards a mature landscape. However, plateau processes (Djouce surface) and base-level processes dominate particular surfaces, i.e. the Djouce surface and Tullow Lowland respectively. For example, dip-slip motion is likely to have occurred during Late Tertiary times on the Vartry and Djouce faults. In chapter 7, apatite fission track analysis indicates that the Leinster Mountain chain has experienced a late phase of faulting.

CHAPTER 6 – LANDSAT™ LINEAMENT ANALYSIS

6.1 Introduction

The main aim of this chapter is to use LandSat lineament analysis to test the conclusions of the previous chapter, i.e. the 3 structural interpretations for the 3 study areas in the Leinster Mountain chain and Tullow Lowland. An additional aim is to provide a regional lineament model for SE Ireland. Outcrop exposure over the Leinster Mountain chain is relatively poor, thus, lineaments are potentially useful for tracing potential faults. This is because faults may leave subtle topographic features that are visible as a lineament shadow on aerial and/or satellite images. Also, fault planes may offer preferred avenues of movement for moisture for plants and hence the trace may be revealed by vegetation patterns. In addition, fault activity is likely to disrupt the rock on either side, and differential weathering of fault rock may produce a topographic depression. Active or recent faulting may also produce a topographic scarp detectable by LandSat imagery. It will be shown that the lineament analysis in this chapter did not contribute any new knowledge about Mesozoic-Tertiary structural history of the region but can be a valuable structural tool in low lying areas with a scarcity of outcrop.

6.1.1 Methods and Materials

The main sections of this chapter are concerned with analysis of:-

- LandSat™ Imagery,
- Digital Elevation Models,
- Known NW-SE to WNW-ESE faults,
- Lineament pattern.

LANDSAT System

NASA launched the LandSat system in 1972. LandSat 1, 2 and 3 carried the multi-spectral scanner, which has a spatial resolution of 79x56m. The first 2 satellites carried 3 spectral bands (0.5-0.6μm [green], 0.6-0.7μm [red] and 0.7-0.8μm [near infrared]). LandSat 3 carried an additional band (0.8-1.1μm [near infrared]).

The primary source of remote sensing is the electromagnetic spectrum from the sun. Solar radiation that hits the Earth is reflected, absorbed or transmitted. The spectral response between various objects depends on:

- radiometric resolution of sensor
- atmospheric scatter (i.e. visible blue)
- surface roughness
- spatial variability within the scene

Thematic mapper was introduced to LandSat 4 and 5, as an upgrade and improvement to the MSS sensor. These satellites give higher spatial and spectral resolution. The spatial resolution is 30m, with the exception of Band 6, which is 120m. The thematic mapper sensor has seven spectral bands, which can detect the following parts of the electromagnetic spectrum:

Bands1-4: 0.45-0.9μm (visible blue to near infrared)
Band 5: 1.55-1.75μm (mid infrared)
Band 6: 10.4-12.5μm (far infrared)
Band 7: 2.08-2.35μm (mid infrared)

Normally, band 7 (mid-infrared) is used for geological applications, for the discrimination of rock types, hydrothermal alteration zones etc. However, in this study, the following bands were used:

Band 3:-	0.63-0.69μm	Visible red
Band 4:-	0.76-0.9 μm	Near infrared
Band 5:-	1.55-1.75μm	Mid infrared

Band 3 is useful for plant-type discrimination (due to chlorophyll absorption), band 4 detection is critically linked with moisture (complete absorption by water and hence facilitates delineation of shorelines), and band 5 is indicative of moisture content (soil, vegetation, discrimination of snow from clouds etc). These bands were used, instead of Band 7, and proved useful for detecting geomorphic features such as ridges, depressions and steep slope (i.e. thin regolith and hence little moisture).

6.1.2 Previous Study

The image of SE Ireland was derived from an EC study, the CORINE (Co-ordination of information on the environment) land-cover project (Briggs, 1991). This involved the compilation of complete LandSat™ coverage for Ireland, which was acquired between 1989 and 1990. The LandSat coverage of SE Ireland used in this study is a subset of the CORINE database (figure 6.1). The original LandSat image was processed and filtered to produce an integrated regional lineament map. The techniques utilised included HIS (hue, saturation, intensity), principal components analysis (PCA), 3x3 kernel directional filters (for enhancing lineaments in a particular direction) and image histogram stretch. These techniques are discussed in more detail later. Lineaments were digitised from each image and re-integrated to form a regional linear map. The digitising of lineaments is the most subjective part of this kind of analysis and it is important to maintain objectivity.

In order to convey information about the spatial pattern of lineaments, it is useful to produce statistical summary maps. Thus the lineaments were generated into an ASCII file and inputted through various statistical filters (see below). The statistical results are summarised as a series of maps that are divided into 25km^2 cells, which have values ranging from 1 to 255. A ramped rainbow spectrum (natural break classification) is then applied to the maps.

6.2 Regional LANDSAT Coverage of SE Ireland

The regional coverage of SE Ireland encompasses the Leinster Mountain chain and the Tullow Lowland. Figure 6.1 is the satellite image with rivers and lakes/reservoirs draped over a digital elevation model (two times vertical exaggeration). In general, the Slaney and Liffey Rivers can be seen flowing south and north respectively. Large areas of red and pink colour represent the Wicklow Massif, whereas the relatively flat areas of low elevation are mostly green coloured, i.e. the Tullow Lowland.

6.2.1 WNW-ESE to NW-SE Lineaments

Brück & O'Connor (1980, 1982) interpreted a series of lineaments or photo-linears (after Hoppin, 1974) using LandSat1 and LandSat2 imagery and 1:30,000 aerial photographs. Most of these lineaments are superimposed on the LandSat5 image of this study (figure 6.2).

Most of the lineaments are associated with valleys and faults in the Leinster Mountain chain. Faults can be observed cutting the Lower Palaeozoic rock, but, the establishment of fault control in the valleys from field evidence is weak due to poor exposure and offsets of the granite:schist boundary are the most important control. Table 6.1 below lists the lineaments, which are displayed on figure 6.2, and whether or not they correspond with known faults.

Table 6.1

LINEAMENT/TREND	FAULTS	APPARENT OFFSET
A-A: Glencullen - WNW	yes	dextral
B-B: Glenasmole-Glencree - WNW	yes	dextral
C-C: Sally Gap - WNW	yes	dextral
D-D: Lough Dan – WNW to NW	yes	dextral
E-E: Glendasan - WNW	yes	dextral
F-F: Glenmalure - NNW	yes	sinistral

Table 6.1 (continued)

G-G: Ow River (Glen of Imail) - WNW	yes	dextral
H-H: Moyne - WNW to NW	yes	?
I-I: Tinahely - WNW	yes	?
J-J: Shillelagh – WNW	yes	?
K-K: Slaney River - WNW	yes	?
L-L: Clody River - NW	no	?

Most of the lineaments are ~20km in length. The linears are most prominent in the Northern, Lugnaquillia and Blackstairs plutons. Brück & O'Connor (1980, 1982) have shown that these lineaments appear to be spatially correlated with hydrothermal alteration zones, base mineralisation, and explosion breccias. This apparent genetic relationship led Brück & O'Connor (1980, 1982) to conclude that the transverse lineaments are faults that developed primarily in response to a Caledonian stress field.

While this may be true (i.e. that the lines of weakness are syn-tectonic) it is likely that these have been reactivated during Tertiary uplift of the Massif, and hence, why they are detectable on LandSat imagery. In chapter 3, it was suggested that the Caledonian-aged 'explosion breccia' of Brindley (1952) on the Blackrock coast was actually a Tertiary fluidised fault breccia. This may also be the case with the other known fault breccias. Based on overprinting relationships along the northern margin of the batholith, it is possible that these lineaments have experienced at least two possible reactivation phases (chapter 3). The lineaments would have initially been reactivated by NW-SE horizontal compression to produce dextral transpression. The second phase would produce dextral transtension as a result of a maximum or intermediate NNW-SSE horizontal compression and ENE-WSE extension. In chapter 7, apatite fission track modelling indicates that these lineaments/faults have been reactivated during both Palaeogene and Neogene times, particularly, the Lough Dan and Moyne (Baltinglass) faults.

6.2.2 Hue Intensity Saturation (HIS)

The original CORINE image was converted from RGB to HIS (figure 6.3). The HIS parameters are perceived independently by the human eye, and therefore each one of them can be manipulated without causing any interfering effects to any of the other two components. HSI transformation provides a highly flexible and simple means of producing an excellent result based upon the original bands. Given light of a particular colour, the hue corresponds to the dominant frequency of the light, the saturation corresponds to the purity of the light (how much white light is mixed with the coloured light) and the intensity corresponds to the magnitude of the energy of the light. For example pink and red have the same hue, however red has a much higher saturation. The hue and saturation when combined are known as the chromaticity of a colour. Thus the chromaticity and intensity of a colour can be considered independently, which could be useful to remove to some extent the influence of lighting effects and shadows (sun illumination).

However, note that Hue is undefined if R=G=B. Additionally, colours with very low intensities, which are indistinguishable from black to the human eye, can have large variations in their hue and saturation values. The formula is given by:

$$a = \min(R, G, B)$$

$$I = \frac{R+G+B}{3}$$

$$S = 1 - \frac{3}{R+G+B} \times a$$

$$H = \cos^{-1}\left(\frac{(0.5 \times (R-G) + (R-B))}{\sqrt{\left((R-G)^2 + (R-B)(G-B)\right)}} \right)$$

Lineaments from the HIS image were integrated into the regional lineament map but this technique was not particularly useful. This is because all the lineaments captured from the

HIS image were also detected and digitised from the directional filtered images. Therefore, the HIS model was not used for the local lineament study.

6.2.3 Principal Components Analysis

Principal components analysis (PCA) is a type of 'feature selection', which allows data to be compacted into fewer bands, a form of data compression. PCA identifies the optimum linear combination of the original channels that can account for variations of pixel values in an image. The optimum values for coefficients are calculated by a procedure that ensures that values account for maximum variation within the entire image. Thus, the set of coefficients provides the maximum amount of information that can be conveyed by any single channel formed by a linear combination of all original channels, and hence reduces the size of the data set by eliminating replication of information. A PCA image was derived from the original CORINE image in producing the regional lineaments. This technique was also used for the three study localities (i.e. the Vartry, Bunclody and Glen of Imail areas).

6.2.4 Direction Filtered Images

Edge enhancement and directional filtering emphasise linear texture by sharpening the image in a given direction. This involves the amplification of the deviation of each pixel intensity form the local average, which is computed from the 4 adjacent pixels. As discussed in chapter 1, the main structural grain in SE Ireland is NE-SW and NW-SE. Therefore, NW-SE and NE-SW directional filters, using 3 by 3 kernels were applied to the original image to produce regional lineament maps. This technique proved useful in detecting the dominant lineaments and is used for the three areas of study. A prominent ~N-S topographic feature is evident for the Vartry area (chapter 5), therefore, the N-S filter was also applied to each area of study, for the potential identification of similar features, hitherto, undetected in the Leinster Mountain chain. The matrices for the box filter kernels are shown on the next page.

$$\text{NE-SW}\begin{pmatrix}-1 & -1 & 2\\ -1 & 2 & -1\\ 2 & -1 & -1\end{pmatrix} \qquad \text{NW-SE}\begin{pmatrix}2 & -1 & -1\\ -1 & 2 & -1\\ -1 & -1 & 2\end{pmatrix} \qquad \text{N-S}\begin{pmatrix}-1 & 2 & -1\\ -1 & 2 & -1\\ -1 & 2 & -1\end{pmatrix}$$

6.3 Statistical Analysis of Lineaments

Lineaments are narrow zones of subtle tonal change. Geological lineaments arise from subtle alignments of discontinuities and gradients in pixel values. Lineament maps also contain non-structural 'noise', which needs to be extracted. Lineaments are real features but their geological significance is uncertain and thus require interpretation in conjunction with other data sources such as zones previously known from structural work and other studies including topographic analyses.

Figure 6.4 is the regional lineament map derived from all the processed and filtered images mentioned above. Note the prominent lineament that follows the strike of the East Carlow deformation zone (ECDZ).

6.3.1 Rose Diagram

The regional lineament map is summarised by using rose diagrams (relative frequency circular histogram graphs). Two types of rose diagram were produced, both being length weighted. Figure 6.5 is a rose diagram that shows all lineaments for the entire area. The second type divides the area into 25km^2 pixels (figure 6.6) and hence breaks down the main lineament orientations to a smaller scale.

Figure 6.5 succinctly summarises the regional orientation of LandSat lineaments for SE Ireland. The dominant trend is NW-SE, and then NE-SW. Of course, the directional filtering of the imagery will naturally enhance particular orientations and suppress others, with the other directions being detected from the PCA image. Figure 6.6 summarises the regional lineaments on a sub-cell basis. The relationship of faults, obtained from the GSI maps, and to the major inferred faults from chapter 5 are also shown. Many of the sub-cell

rose diagrams shows tjat these NW-SE peaks corresponding with the major faults, which have been eroded by Quaternary glaciers. Most of the rose diagrams that occur along the trace of the ECDZ show a dominant NE-SW peak. Towards the NE end of the structure, the rose diagrams also show a relatively large NW-SE peak. To the south of the ECDZ, there are a number of N-S peaks corresponding with the numerous N-S trending faults. Hence, over the main part of the Wicklow Massif, the rose diagrams show NW-SE peaks corresponding with the lineaments of Brück & O'Connor (1980, 1982).

6.3.2 Entropy

Entropy is used to measure the degree of randomness of lineaments and is derived as follows:

$$RE\% = \left(\frac{-100 \sum_{i=1}^{k} \left[n_i - \log(n_i) \right]}{\log(K)} \right)$$

where:

n_i = frequency of samples in each class

K = number of classes = 180°/class interval

If RE=100, then lineaments exhibit a perfectly uniform distribution of data in all class intervals. Hence, as RE tends towards 100, this implies a greater random distribution. Changes in RE may be related to development of fracture patterns associated with uplift and faulting.

Figure 6.7 shows the entropy (or randomness) of the regional lineament dataset. The highest entropy values correspond with an area to the west of Wicklow Head and the southern extremity of the Vartry surface. The area is associated with a large density of small but closely spaced faults on GSI maps. The area is also coincident with the Southeastern Boundary fault, or the NE extension of the ECDZ (McArdle & Kennedy,

rose diagrams shows tjat these NW-SE peaks corresponding with the major faults, which have been eroded by Quaternary glaciers. Most of the rose diagrams that occur along the trace of the ECDZ show a dominant NE-SW peak. Towards the NE end of the structure, the rose diagrams also show a relatively large NW-SE peak. To the south of the ECDZ, there are a number of N-S peaks corresponding with the numerous N-S trending faults. Hence, over the main part of the Wicklow Massif, the rose diagrams show NW-SE peaks corresponding with the lineaments of Brück & O'Connor (1980, 1982).

6.3.2 Entropy

Entropy is used to measure the degree of randomness of lineaments and is derived as follows:

$$RE\% = \left(\frac{-100 \sum_{i=1}^{k} [n_i - \log(n_i)]}{\log(K)} \right)$$

where:

n_i = frequency of samples in each class

K = number of classes = 180°/class interval

If RE=100, then lineaments exhibit a perfectly uniform distribution of data in all class intervals. Hence, as RE tends towards 100, this implies a greater random distribution. Changes in RE may be related to development of fracture patterns associated with uplift and faulting.

Figure 6.7 shows the entropy (or randomness) of the regional lineament dataset. The highest entropy values correspond with an area to the west of Wicklow Head and the southern extremity of the Vartry surface. The area is associated with a large density of small but closely spaced faults on GSI maps. The area is also coincident with the Southeastern Boundary fault, or the NE extension of the ECDZ (McArdle & Kennedy,

1987). Along most of the ECDZ within the regional area of study, entropy displays relatively high values ranging from 165 to 255.

A small area of high entropy occurs in the northern part of the Glen of Imail basin and extends northwards to the headwaters of the King's River. This is probably due to greater relief and outcrop. Another ~N-S trending zone occurs just west of the ~N-S Slade Valley fault (figure 6.7) and continues for ~15km north, extending to the Carboniferous aged Dublin basin. Another ~N-S trending zone occurs just south of the Carrickgollogan klippe zone of intersection between the Djouce fault (chapter 5) and the Glencree Fault zone. The SE part of the regional area of study (NW of Mizen Head) is occupied with moderate entropy, whereas, much of the central part of the Leinster batholith has low to moderate entropy. These areas with moderate to high entropy seem to be associated with some of the major fault zones. Areas of high entropy also appear to be associated with better outcrop and relief (~100-200m; figure 5.80), and therefore, this technique is not ideally suited for testing models such as those of chapter 5, when high quality DEMs are available (figure 6.7).

6.3.3 Intersection Density

Intersection density is derived by calculating the sum of lineament intersections divided by the area of the cell. Figure 6.8 is a map of the intersection density of lineaments. The ECDZ again corresponds with a zone of relatively high values, although, these are only moderate in place within the Bunclody area, which is reflecting the quality of outcrop and relief in the area (chapter 5). To the south of Wicklow Head, there is a ~N-S trending zone of relatively high values that corresponds to an area of high-density faulting. This area is known as the Avoca Block and outcrop over the area is relatively good. To the south of Bray Head, a ~N-S trending zone of 20km by 5km (10km wide just west of Bray Head) of high to very high values occurs, and corresponds with the Vartry escarpment and the intersection of the Djouce and Glencree fracture systems. Most of the values are low to moderate within the Vartry and Djouce surfaces. Further west, the Leinster batholith, and

the low ground of the Kilcullen and Ribband Groups are also dominated with low lineament intersection densities.

6.3.4 Length Density

Length Density is derived by dividing the length of the lineament by the area of the cell. Figure 6.9 shows the length density of LandSat lineaments. As in the previous two figures, the largest area of high to very high values occurs just west of Wicklow Head. However, the length density shows a much larger area, extending from the southern extremity of the Vartry surface, extending south and over the Avoca block. The ECDZ is an area of moderate to high values, and also the northern part of the Hollywood shear zone, and Slade Valley fault, with values ranging from ~100 to 245 and reflects the intersection of NW-SE and N-S fractures. The area extending from the northern margin of the Glen of Imail basin to the King's River Valley also displays high values. Again this is probably a function of better outcrop and relief (section 6.3.2; figure 5.80). This area forms the NW margin of a much larger block of moderate to high value that extends SE and incorporates the Avoca block. The overall pattern is similar to the entropy and intersection densities, in that, areas of better outcrop and higher relief show the largest values.

6.3.5 Lineament Spacing

The lineament spacing image is calculated and dividing the average spacing between lineaments with the area of the cell. Figure 6.10 shows the degree of lineament spacing. The areas that had high values of entropy, intersection and length densities now show low lineament spacing. This is expected because a high entropy means a high degree of randomness of lineament orientation and this is normally associated with a high density of intersection, although, not necessarily long lineaments. Hence, these patterns would probably mean that the lineaments are closely spaced and will exhibit relatively low spacing values.

6.3.6 Interpretation

All the statistical lineament images tend to show a common thread that areas with high values of entropy, intersection density, length density and low spacing tend to be positively correlated with dense areas of faulting. Areas, which show dense faulting, reflect relatively good exposure and hence this is illustrated by the LandSat™ lineament analysis. As noted in the previous chapter, these areas are also associated with geomorphic landforms, i.e. the Vartry, Avoca and Myshall blocks, the Aughrim-Kildaven interblock depression, and the Glen of Imail basin (figure 5.2). Thus, the analysis of lineaments is a useful tool for detecting topographic features that may or may not be structurally controlled. The statistical significance of the lineaments clearly demonstrates that these are detecting structural features, i.e. the association of high values and known occurrences of faults. This may be due to differential erosion along the fault planes, which will experience a greater degree of chemical and physical weathering. The weathered rock material would then be scoured by glaciers, producing U-shaped valleys, arête ridges etc.

Entropy, intersection density and length density all show moderate to high values for the Vartry area and moderate to low values for the Bunclody area. The Glen of Imail area is also mostly low but moderate to high values occurs from the Glen of Imail basin to the Kings River valley. Relatively high values also occur just east of the Slaney River on the Baltinglass escarpment, with the exception of relatively low length density. The spacing of lineaments all show the opposite values, i.e. low where entropy, intersection and length densities are high. This merely highlights areas of reasonable outcrop and relief, and therefore, structural control has already been established from field mapping. Thus, the regional lineament analysis only gives the interpreter a first, general impression of a regional scene.

6.4 Vartry Area

Figure 6.11a is the CORINE image of the Vartry area and figures 6.11b,c are the same LandSat™ scene draped over digital elevation models. Figure 6.11b (vertical exaggeration

x4) is facing NE and picks out the line of quartzite hills of Great and Little Sugar Loaf Mountains and the greywackes of Bray Head, and the Djouce and Vartry faults. Figure 6.11c (vertical exaggeration x2) is facing west and shows the relatively high Djouce surface to the west and the NW-SE Tertiary fault controlled valleys.

6.4.1 Lineament Capture and Interpretation

Figures 6.12a, b, c and d are the processed images (PCA and directional filtering) that were used for capturing (or digitising) the additional lineaments (figure 6.13a). The lineaments were captured from each individual image and then re-integrated to form one image. As figure 6.13a shows, the highest density of lineaments occur in the west and north-west, i.e. the Djouce surface where regolith is thinnest and slope and relief is relatively high at >30° and >200m respectively. These areas are deeply dissected along fault zones, which have been deepened by Quaternary glaciers. The Vartry and Coastal surfaces, on the other hand, have much fewer lineaments due to thicker regolith and lower slopes of ~<5° and relief of ~<10-50m. Lineaments tend to increase in occurrence along a wide zone around the Vartry and Djouce escarpments.

Figure 6.13b is a sub-cell rose diagram of the lineaments and the spatial occurrence of faults is also shown. This is to highlight the relationship between faults and lineament. For example, the rose-diagrams have strong parallel histogram peaks with the Callowhill and Southeastern Boundary faults, the two strands that correlate with the offshore Wicklow High (chapter 4). In addition, in the NE of the area of study, a similar rose diagram pattern is repeated although no faults have been recognised in this area. Hence, the rose diagrams may be picking out a hitherto unrecognised fault, which is probably an extension of the Glencullen and Glencree fault systems (figure 5.37). The most obvious feature of the rose diagram peaks is the swing into parallelism with major faults, i.e. peaks swing anticlockwise into parallelism with the Callowhill fault indicating a sinistral sense of shear. There are also 2 peaks along the Djouce fault which probably corresponds to the trend of the fault (~N-S) and the strike of the Ribband Group rocks (~NNE-SSW).

Figure 6.14 is a grid of average lineament direction (0° to 179° azimuth) with a pixel size of 1km, and faults and geological boundaries are also overlain to show the spatial relationship. This is an effective representation because it removes the clutter of faults and rose diagrams of the previous figure. The grid shows approximately the same picture as figure 6.13b. However, there are some notable differences. Due to the decrease of cell size ($1km^2$ in comparison with $6.25km^2$ for the sub-cell rose diagrams), smaller, local effects have a greater influence. For example, the Vartry escarpment is not clearly shown, with grid codes trending ~ E-W and not ~ N-S as would be expected. This is because the grid is picking out the gorges incised by the rivers that cross the escarpment (e.g. the Devil's Glen). In order to pick out larger features, it would simply be a case of increasing the cell size.

6.4.2 Conclusions

The lineament analysis shows that the highest density occurs over the Djouce surface and along faults, which were deduced from the previous chapter. The peaks on the rose diagrams show the main fault trends but also pick out the Caledonian strike and the relationship to the fracture. The rose diagram peaks also give the sense of shear as lineaments swing into the main fault zones. The lineament direction grid is not as clear although different trends can be identified, depending on the required scale. Nevertheless, the image does not give the sense of shear of major faults. It does however give a first-order impression of the overall trends within a given area.

6.5 Bunclody Area

Figure 6.15a is the CORINE image of the Bunclody area and figures 6.15b,c are the same LandSat™ scene draped over digital elevation models (vertical exaggeration x2). Figure 6.15b is facing NE and gives a bird's eye view along the strike of the ECDZ. The shear zone partially bounds the Blackstairs Massif to the SE, and the Tullow Lowland to the NW. A series of NNW-SSE valleys or wind gaps cross the mountain chain, east of the Slaney River. Figure 6.15c is facing north and shows the high elevation of Mount Leinster in the

SW and the Derry River valley partly coincide with the trace of the ECDZ. The River Slaney has incised into the Tullow Lowland and shows a sudden change in sinuosity as it crosses the ECDZ. This is likely to be due to tectonic uplift (section 5.5.15).

6.5.1 Lineament Capture and Interpretation

Figures 6.16a, b, c, d is all filtered images that were used for the enhancement and capture of LandSat lineament (figure 6.17a). As figure 6.17a shows, there are relatively very few lineaments over the Tullow Lowland, particularly to the west of the Slaney River. The most prominent or set of lineaments over the Tullow Lowland are those associated with the Slaney River channel.

Figure 6.17b are sub-cell rose diagrams and faults. The wind gaps to the NE cross the Blackstairs chain and produce prominent NW-SE peaks. The ECDZ forms a narrow zone of NE-SW peaks. Over the Mount Leinster area in the SW, the rose diagrams form a cross of N-S and E-W peaks.

Figure 6.18 is a grid of average lineament direction and the association with faults and geological boundaries. The Slaney River is clearly imaged with lineament directions of ~141° to 167°. The ECDZ on the other hand is typified with a variety of lineament directions ranging from ~50° to 179°. This appears to be picking out transverse structures such as the wind-gaps labelled 'W' on figure 6.18, e.g. the wind-gaps consistently show lineament directions of ~140° to ~170°. Similarly, the Slaney River lineament shows directions of ~140° to the north and south of the ECDZ. However, this is already rather obvious from the original CORINE image.

6.5.2 Conclusions

The lineament analysis of the Bunclody area is more equivocal than the Vartry area. This probably reflects poor exposure and relatively low slope and relief over much of the area. The study has failed to supplement the topographic analysis. But, it does show the major

faults (i.e. the NE-SW peaks of the rose diagram along the strike of the ECDZ and the NNW-SSE peaks for the wind-gaps). The lineament direction image on the other hand is not very constructive other than giving a first-order impression of trends at a small-scale. This would change for larger cell resolution but at the expense of detail.

6.6 Glen of Imail Area

Figure 6.19a is the CORINE image of the Glen of Imail area and figures 6.19b,c are the same LandSaT™ scene draped over digital elevation models (vertical exaggeration x2). Figure 6.19b is facing NNE and shows the Baltinglass escarpment which separates the Tullow Lowland to the south from the Wicklow Massif and Glen of Imail basin to the north. Figure 6.19c is facing north and shows that the head of the River Slaney begins in the Glen of Imail basin, where the Little Slaney joins the main river. The river then flows west and then turns south, incising a gorge as it crosses the Baltinglass escarpment. Note that there are no other rivers crossing the escarpment (section 5.6.15).

6.6.1 Lineament Capture and Interpretation

Figures 6.20a, b, c, d is the filtered images that were used for lineament capture (figure 6.21a). As figure 6.21a shows, most of the lineaments occur over the higher elevations of the Wicklow Massif. The Tullow Lowland is an area of relatively low lineament occurrence due to low relief (<30m) and poor exposure. Likewise, relatively few lineaments occur over the Kilcullen surface for similar reasons (section 5.6).

Figure 6.21b shows a dominant ~E-W orientation of rose diagram peaks along the foot of the Baltinglass escarpment. The fault controlled Ow River and Glenmalure valleys also show strong NW-SE to NNW-SSE peaks on the rose diagrams. The area to the NW, the Kilcullen surface, shows that the peaks are parallel with the Hollywood shear zone and the Athgarrett fault. The rose diagrams that depict the Baltinglass escarpment appear to be offset, west of the Slaney River, by about 2 km to the NW. A relatively random pattern of

lineament occurs towards the NE of the area and may relate to a termination zone of the Glenmalure fault.

Figure 6.22 shows a similar pattern to the rose diagrams, with the escarpment having azimuths of ~77° to ~116°. A NW-SE zone of azimuths of ~128° to ~154°, offset the escarpment in the vicinity of the Slaney River. This offset also coincides with the termination of the Hollywood shear zone, which may imply that the fault continues further south than shown on the published GSI geology bedrock maps. However, there is no apparent offset in the Tullow pluton and Kilcullen Group contact ruling out an apparent dextral offset of ~2km. However, exposure in this area is poor and it is possible that the contacts are incorrectly mapped.

6.6.2 Conclusions

The lineament analysis depicts the major structure that was identified in chapter 5, i.e. the Baltinglass escarpment. The Hollywood shear zone and Athgarrett faults are also depicted. The Glen of Imail-Ow River and Glenmalure faults can only be seen in the major valleys of the Wicklow Massif. For example, the Glen of Imail-Ow River fault no longer shows as a lineament where it enters the Glen of Imail basin.

6.7 Discussion of Conclusions

LandSat™ and lineament analysis of the Leinster Mountain chain shows the major structures that cut the area. The areas, which are most strongly identified, occur where slopes are steepest and relief is highest. The statistical images are clearly picking out the ECDZ and areas of fault intersection. The peaks on the rose diagrams of Vartry area show the sense of shear, i.e. the peaks swing anticlockwise towards parallelism with the northern strands of the ECDZ. The peaks also show the main trend of the ECDZ in the Bunclody area and lineament direction picks out smaller features such as the NNW-SSE wind-gaps. This is similar in the Glen of Imail area where the Baltinglass escarpment is clearly shown

but this is because of the contrast in relief of the Tullow Lowland and the Wicklow Massif to the north and north-north-east.

The original aim of this chapter was to test the structural models of chapter 5 and to identify previously unrecognised structures. Whilst the lineament analysis gives a first-order impression of major structural elements, it unfortunately fails to test or supplement the detail of the structural models obtained from high-resolution digital elevation data. Therefore, in the absence of good quality topographic data, LandSaT^{TM} is useful for identifying the major structures. However, the quality of lineament is limited to areas of moderate to high relief and reasonably good exposure, i.e. reflection of electro-magnetic waves is a function of surface roughness. Areas of thicker overburden hold more moisture and hence absorbs energy. This wouldn't be as much of a hindrance in areas of arid climate or when bedrock structures such as faults act as zones of active ground-water flow.

CHAPTER 7 - AFT STUDY OF THE LEINSTER MOUNTAIN CHAIN

7.1 Introduction and Summary

Apatite Fission track (AFT) analysis is a tool that can be used for unravelling the thermo-tectonic history of a region. In this chapter, the thermal, denudational and tectonic uplift history of the Leinster Mountain chain and the Tullow Lowland (SE Ireland) is evaluated. Apatite fission track-length distributions, apatite dating and modelled thermal histories for a selection of key samples from the Leinster batholith, are used to re-construct the thermo-tectonic history of the Wicklow Massif. A geological cross-section that closely follows the Wicklow Massif drainage divide shows potential evidence for faulting. Forward modelling of AFT samples from SE Ireland provides evidence for 4 cooling events that occurred during the Triassic-Mid Jurassic, the Early Cretaceous, the Early Palaeogene and the Neogene. The samples along the Wicklow Massif profile display a fossilised partial annealing zone, offset by major NW-SE fractures implying that the most recent phase of faulting along these structures is Neogene and younger in age.

7.1.1 Aims

Structural mapping of brittle structures along the northern margin of the Leinster batholith (chapter 3) has been correlated with structures in the offshore Kish Bank basin (chapter 4). This tectonic model has been subsequently correlated with onshore geomorphic landforms based on topographic (chapter 5) and LandSat (chapter 6) lineament analysis. These models provide evidence of Mesozoic-Tertiary tectonics. Thus, the main aim of the AFT analysis is to identify exhumation (and burial) events particularly during Tertiary times. Evidence for fracture systems that controlled exhumation events is also considered and evaluated. A final aim is to quantify denudation and 'tectonic uplift' rates during Tertiary times.

7.1.2 Apatite Fission Track Method

Professor Philip Allen initiated the Tertiary Uplift of Ireland Project (TULIP) in 1998 as a co-operative programme between Trinity College Dublin, Imperial College, and University College London. The main aim of the research project, funded by ARCO plc, was to provide a quantitative picture of the post-Hercynian thermal and denudational history of Ireland based on an apatite fission track study. Members of this Department (Philip Allen, Alex Densmore, Joe Galewski, Adrian Phillips, and various others including myself) collected outcrop samples and two additional borehole samples were obtained from George Sevastopulo. The AFT samples were analysed by Andrew Carter (University College London Fission Track Laboratory) and modelled by Kerry Gallagher (Imperial College London) to obtain most likely time temperature trajectories and their uncertainties. Previous raw data in the public domain was also remodelled in order to provide a fully consistent set of results.

During the period February-October 2000 I have worked as a Research Assistant with Professor Philip Allen on the TULIP project. Therefore, I have been able to assimilate and interpret the most pertinent information derived from the AFT project into my thesis (chapters 7 & 8). In chapter 4, the AFT method was introduced and the procedures and caveats to the interpretation of the results are outlined below.

AFT Dates

When an atom of ^{238}U decays by spontaneous fission, it splits into 2 highly charged fission fragments, which are approximately equal in mass and are propelled in opposite directions. The passage of these highly charged masses produces linear trails of disrupted atoms. The fission process occurs at a statistically constant rate and all tracks initially form at ~16μm (Gleadow *et al.* 1986). However, fission tracks shorten irreversibly when the host mineral is at an elevated temperature. This is a consequence of thermally activated diffusion processes.

Fission track ages require an estimate of the relative abundance of the parent and daughter product, i.e. the number of ^{238}U atoms and the number of spontaneous fission tracks per unit volume. Spontaneous tracks can be counted. To determine the ^{238}U abundance, the sample is irradiated with low-energy thermal neutrons to induce fission in ^{235}U. The number of induced tracks is indicative of the abundance of ^{235}U, and hence ^{238}U because the ratio $^{235}U/^{238}U$ is constant in nature.

The external detector zeta (ζ) calibration is the most commonly used analytical method for age determination (the International Union of Geological Sciences Working Group's recommended approach – Hurford, 1990a, b) and was applied to the TULIP samples. This method relies on the etching of spontaneous tracks. An external mica detector is then attached to the etched surface and thermal neutron irradiation induces fission tracks, which register in the detector. The induced tracks on the mica detector are then etched for optical revelation. Observation and measurement of fission track density and length is then conducted under transmitted light using a high-resolution microscope.

For the TULIP samples, spontaneous fission tracks were revealed by etching polished apatite grain mounts with 5N HNO_3 at 20±1°C for 20 seconds. Mounts were irradiated in the thermal facility at the Riso Reactor at the National Research Centre, Roskilde, Denmark (cadmium ratio (thermal/epithermal + fast neutrons) >200), using the external detector method. Fluence was monitored using Corning uranium standard glass dosimeter CN-5. Muscovite mica external detectors were etched after irradiation using 48% HF acid at 20±1°C for 55 minutes. Observation and measurement of the fission track density and confined track lengths was conducted under transmitted light using a Zeiss™ axioplan microscope with a total dry magnification of x1250. Reflected light was used as a tool for discriminating individual tracks. Horizontal confined fission track lengths were measured using a digitising tablet calibrated before each analysis against a stage micrometer. Ages were determined using the zeta calibration method (43 determinations for analyst Carter give $\zeta_{CN5} = 339\pm5$).

The age for the zeta calibration method is calculated as follows:-

$$t = \frac{1}{\lambda_d} Ln\left(\lambda_d \frac{P_s}{P_i} P_d \zeta g + 1 \right)$$

t = age

P_s = spontaneous track densities

P_i = induced track densities

λ_d = the σ decay constant of ^{238}U

P_d = track density in a dosimeter to monitor neutron flux in reactor

g = geometry factor (see Gallagher 1998)

ζ = constant of proportionality made up of other parameters (see Gallagher 1998)

The uncertainty or age error is calculated as follows:

$$\sqrt{\frac{1}{N_s} + \frac{1}{N_i} + \frac{1}{Nd} + \left(\frac{Se\zeta^2}{\zeta} \right)}$$

N_s = no. of tracks in determining P_s

N_i = no. of tracks in determining P_i

N_d = no. of tracks in determining P_d

$Se(\zeta)$ = standard error on estimate of ζ

The fission track ages are an average estimate of the individual single grain ages. The 'central' age is mostly quoted and represents the weighted mean of the log normal distribution of single grain ages (Galbraith & Laslett, 1993). The central age is the preferred sample age estimate because it is more robust to outliers and non-Poissonian variations (Gallagher, 1998). The TULIP samples are reported as the central age together with the percentage age dispersion or relative error (R.E.%) about the central age (Galbraith & Laslett, 1993).

Track Measurements

Fission tracks form randomly in 3D and measurements of track-density for age determinations are based on a 2D sample with tracks intersecting an internal polished and etched surface. Hence, the probability of a long track intersecting a surface is greater than that for a short track. Therefore, since the age is determined by counting the number of tracks, then the apparent age will get older for a sample with larger tracks. As fission tracks are shortened with increasing temperatures then fewer will be counted and hence the age estimate becomes younger. Confined tracks are those that occur below the internal surface. The etchant reaches these tracks through cleavage and cracks. Hence, there is an implicit bias against sampling shorter tracks (e.g. Green, 1988). The advantage of counting confined horizontal tracks therefore is that the full etchable length can be observed and hence the distribution yields the most optimum representation (Gleadow *et al.,* 1986; Green *et al.,* 1989).

As each track forms at a different time, then they all experience a different proportion of the total thermal history of the host rock. Hence, the track length data provides important information about the temperature variations experienced by a given rock, while the fission track age provides information about timing and duration of these variations (e.g. Menzies *et al.* 1997). The interpretation of fission track data currently relies on an empirical calibration of the relationship between track length, temperature and heating duration (Laslett *et al.*, 1987; Carlson, 1990). Hence, the fission track data can be used to model the thermal histories quantitatively (e.g. Lutz & Omar, 1991; Corrigan, 1991; Gallagher, 1995). Thus, the most important parameters in fission track analysis are the track lengths.

Apatite Annealing Models

Predictive annealing models for apatite allows the quantitative reconstruction of the thermal history for the upper several kilometres of the crust. The thermal histories are generated by forward modelling (Duddy *et al.,* 1988; Green *et al.*, 1989a, b; Willet, 1992; Crowley, 1993) or by some optimisation procedure using the observed data as constraints (Corrigan, 1991; Lutz & Omar, 1991; Gallagher, 1995). The thermal history of the TULIP samples was modelled using a stochastic (optimisation) search procedure outlined in Gallagher

(1995) incorporating the annealing method of Laslett *et al.*, (1987). This annealing model is based on laboratory annealing experiments performed on a mono-compositional Durango apatite with a F/Cl ratio of c.0.1 (Young *et al.*, 1969). This apatite is moderately retentive compared to a pure fluorapatite. Extrapolation of the Laslett *et al.*, (1987) Durango apatite model to geological time scales (10^6 – 10^7 y) predicts a partial annealing temperature range from ~60°C to ~110°C with an uncertainty of about 10°C.

One of the major limitations of the Laslett *et al.*, (1987) model is that it does not predict sufficient annealing at temperatures less than ~60°C. This is because for volcanics or volcanogenic sediments, that have generally considered to have undergone no significant post-eruption heating, the observed mean track lengths are around 14 to 14.5μm while the Durango standard predicts them to be about 16μm (e.g. Vrojlik *et al.*, 1992). Consequently, thermal history simulations can be biased towards inferring rapid, recent cooling from ~60°C to surface temperatures with consequent overestimates of denudation, i.e. Neogene to present. However, Galbraith & Laslett (1993) developed a model that is more sensitive to temperatures <60°C. But, the model formulation was not applied to the Durango apatite data. Gallagher (in prep) has adopted the Galbraith & Laslett (1993) model and has applied it to the Durango apatite data given by Green *et al.*, (1986). The TULIP samples were subsequently re-modelled using this modified annealing model.

The key difference between the two annealing models is the assumption of the error distribution on the data. The Laslett *et al.*, (1987) model transforms the data before fitting them, and assumes the variance is constant in the transformed data. However, the revised model does not make this assumption and fits the observed data directly. Relative to the Laslett *et al.*, (1987) model, this revised model leads to more annealing, particularly at lower temperatures.

7.2 Interpreting AFT Data

Fission tracks continually form in the host crystal at a statistically constant rate by radioactive decay. Therefore, each track experiences a different portion of the total thermal

history for a given sample and hence the track-length distribution and the apparent fission track age represent an integrated record of the total thermal history as the sample passes through the partial annealing zone (PAZ). The AFT age will only coincide with the time the sample was at a maximum palaeotemperature of 110±10°C if the rock has rapidly passed through the PAZ and has cooled quickly to a temperature at which the rate of thermal annealing is negligible (<60±10°C), and there has been no subsequent re-heating events (figure 7.1).

If the samples have younger AFT ages than the host rock then they have been completely reset, i.e. temperatures >110±10°C, and track retention will begin only after cooling below this point (marked with an asterisk on figure 7.2). Thus, rapid cooling to temperatures <50°C will produce relatively long tracks (>14μm), forming a unimodal track length distribution and hence the AFT age approximates the time of cooling. However, if the rock cools at a slow constant rate from 110±10°C to surface temperatures, then the resulting track length distribution is negatively skewed. This reflects the wider range of temperatures experienced by the retained track lengths and will be biased towards longer tracks (figure 7.1).

If the host rock initially resided within the PAZ, then the track length distributions have a component of relatively short and long tracks formed during pre- and post-cooling respectively (figure 7.2). The track-length distributions in this case will be bimodal with a short MTL of ~10 to 12μm and the AFT age will be somewhere between the young cooling age and the older undisturbed (stratigraphic) age. In other words, the bimodality of the track-length distribution and the value of the AFT age is dependant on the portion of pre- and post-cooling tracks (e.g. Green, 1986; Brown *et al.*, 1994; Menzies *et al.*, 1997). In essence, tracks that are longer than the MTL represent relatively recent cooling (i.e. new tracks formed at palaeotemperatures <60±10°C). Whereas, tracks less than the MTL typically represent pre-cooling or partially annealed tracks. If the samples are not significantly affected by a thermal event, or any other event over a timescale similar to the measured AFT age then the undisturbed sample would initially reside at temperatures

<50°C, and the majority of the fission tracks would be ~13 to 14 μm, reflecting the contribution of pre-cooling and post-cooling tracks.

In the following sections, it will be shown that the AFT central age of the TULIP samples is significantly younger than the host rock. This implies that the apatite grains derived from sedimentary rock have been totally reset post-deposition. Apatite derived from granite will indicate the time at which the rock cooled below 110±10°C. The MTL of the samples are ~12 to 13μm indicative of significant thermal annealing, and the track-length distributions show relatively few track lengths that are >14μm (Appendix 4). This implies that the samples attained temperatures <60±10°C during relatively recent times otherwise there would be significantly more long tracks.

7.3 AFT Samples - TULIP Database for Leinster Mountain Chain

Figure 7.3 shows the location of published/unpublished (Keeley *et al.*, 1993; Gleadow, unpublished; McCulloch, unpublished; McCulloch, 1993, 1994) and TULIP AFT samples in the Leinster area, and the raw data are listed in table 7.1 below.

Table 7.1

Sample	Easting	Northing	Central Age (Ma)	Age Error	Height (m)	MTL (μm)	MTL Error
LG5	326450	226040	142	±5	90	12.85	±0.12
LG7	325990	225550	127	±4	150	12.85	±0.15
LG8	327135	226371	131	±4	2	12.60	±0.15
LG10	324100	225459	151	±6	40	12.53	±0.27
LG11	318739	223458	166	±4	240	12.55	±0.12
LG13	317600	223400	181	±5	450	12.28	±0.13
LG14	315090	218000	177	±5	420	12.78	±0.12
LG15	314290	215140	178	±5	470	12.72	±0.12
LG16	312940	212200	173	±4	500	12.50	±0.14
LG17	309280	205200	170	±5	570	12.22	±0.17
LG18	309794	205293	152	±4	520	12.71	±0.11
LG21	307600	199200	156	±5	400	12.28	±0.10
LG23	288770	185165	169	±5	110	12.38	±0.13

Table 7.1 (continued)

LG26	293700	188250	167	±7	260	12.47	±0.15
LG36	303180	191200	174	±7	825	12.57	±0.12
LG2	321580	228571	165	±4	25	12.43	±0.15
LG3	325700	228000	138	±4	2	12.91	±0.16
LG6	326247	226304	133	±5	115	12.42	±0.15
LG12	317890	224230	169	±4	440	12.24	±0.12
LG19	311500	203000	147	±4	370	12.93	±0.15
LG20	311310	203994	149	±4	250	12.66	±0.11
LG22	310090	198140	177	±4	250	12.45	±0.12
LG28	282743	152564	205	±6	795	12.60	±0.13
LG30	278140	153114	169	±7	200	12.56	±0.14
LG32	86582	173267	136	?	110	12.74	?
Gleadow16	301002	207552	201	±5	205	12.54	±0.17
Keeley2	271240	139464	130	±7	115	12.39	±0.19
O160086	316003	208559	137	±13	380	12.27	±0.17
O178232	317799	223188	162	±33	440	11.73	±0.21
O192193	319198	219326	127	±6	220	12.27	±0.16
S708434	270804	143352	149	±6	20	12.35	±0.13
T131797	313103	179657	182	±8	65	11.81	±0.45
T183855	318298	185459	184	±12	130	12.03	±0.21
T251889	325102	188859	217	±10	55	13.02	±0.16

7.3.1 Wicklow Massif - Geological Profile and AFT Samples

Figure 7.5 is a NE illuminated digital elevation model, which shows the location of the geological profile and TULIP samples that fall along this line. The profile trends ~NNE-SSW, from Dublin Bay to the Tullow Lowland. The bedrock geology is predominantly granite (figure 7.6) and the profile crosses the Northern, Lugnaquillia and Tullow plutons (the geology of which is described in Appendix 3). Also included are the location of the NW trending satellite lineaments and major faults (chapter 6). NE Illumination clearly highlights the NW linears/fractures which bound blocks of ~5km to 7km width.

Spatially, the youngest AFT central ages occur in the NE (near sea-level) and generally increase towards the SSW, i.e. from LG8 to LG14 the age increases from a minimum of 127±4 Ma to a maximum of 177±5Ma.

7.3.2 Fossilised PAZ Profiles

As figure 7.2 shows, if there is an increase in the rate of denudation after a period of prolonged stability, then the base of the existing PAZ profile will move upwards towards the new mean surface producing an exhumed PAZ (Brown *et al.*, 1994; Fitzgerald *et al.*, 1995). The break of slope in the new profile indicates where the apatite ages were reduced to zero prior to exhumation (i.e. the AFT age will coincide with the time the rock cooled below 110±10°C). However, one complication of interpreting such low-temperature thermochronological data is that the subsurface isotherms may be differentially compressed due to the topography with geotherms highest under valleys (Gallagher, 1998). This can be significant for low-temperature stability systems and age-elevation gradients may give overestimates of the true rate of denudation (e.g. Mancktelow & Grasemann, 1997).

The TULIP samples occur over a maximum relief of ~850m. This would require an extremely high geothermal gradient to exhume the PAZ. For example, consider a palaeogeothermal gradient of 30°C km^{-1}. This would require a minimum of ~1.7km of relief to exhume the PAZ. Therefore caution is required when interpreting the TULIP samples.

7.3.2.1 Regional

As figure 7.2 illustrates, the relationship between elevation and central age is mostly linear (positive) within the PAZ. Plots of central age against elevation for all the Leinster samples are shown on figure 7.4a and display a weak correlation of 0.35 (figure 7.4a). The linear relationship represents a weak fossilised PAZ. Complication to the ideal linear relationship between AFT central age and elevation (fossilised PAZ) may arise from the reactivation of faults that post-dates cooling (<60±10°C). Such faulting would need to be relatively young

(Neogene to Quaternary) due to the small number of long fission tracks (>14μm) suggesting that cooling towards surface temperatures (above the PAZ) is a recent event.

7.3.2.2 Geological Profile – Elevation/Central Age

Figure 7.7a is a plot of elevation against central age for the AFT samples that lie along the ~NNE-SSW geological profile. The elevation ranges from sea level at Sorrento Point to a maximum elevation of ~835m on the high flanks of Lugnaquillia Mountain, and the central ages range from 127Ma to 181Ma. In general, the age increases with elevation (correlation of 0.67) and the data appears to show two sub-parallel concave-up profiles. This relationship is similar to AFT age-elevation profiles from the European Alps (Wagner *et al.*, 1977), which have an elevation range in the order of 3km. Therefore, inferring that the TULIP results are analogous with these European studies is somewhat misleading. But, if the final cooling was of sufficient magnitude to produce the present-day topography (i.e. a young rejuvenated landscape), then the comparisons might not be as outlandish as initially envisaged.

Interpretation

Figure 7.7a shows two possible fossilised PAZ profiles. Profiles 1 & 2 display two sub-parallel 'best-fit' linear cooling paths. Profile 1 corresponds with samples LG8, LG5, LG10, LG11, LG14, LG15, LG13 and probably LG16. Profile 2 represents samples LG21, LG17, LG18(?) and LG36. Profile 1 and 2 occur to the north and south of the Lough Dan fault respectively. Hence, it is possible that the Lough Dan fault has been reactivated and the area to the north of the structure has been downthrown. This is compatible with the change in topography (south side being higher) across the fault. This may account for the change in AFT profiles and the older ages at lower elevations to the north. Additionally, to the south of the Lough Dan fault, there is a relatively large difference between samples LG36 (174±7Ma), LG26 (167±7Ma) and LG23 (174±7Ma). Sample LG26 does not fit with profile 2. Also, the increase in age between samples LG26 and LG23 is the opposite of what would be expected, i.e. central age increases instead of decreasing between the two samples. This may indicate that they lie adjacent to a dip-slip fault.

7.3.3 Boomerang Plots – Leinster Mountain Chain

Green (1986) showed that if an area experiences a discrete phase of exhumation, then the AFT age and MTL define a diagnostic pattern (as long as each sample has experienced different amounts of cooling or denudation). In this case, the MTL will initially decrease with age and at intermediate ages the MTL will be at a minimum. As the age continues to decrease the MTL will then progressively increase again. This concave-up pattern is known as a 'boomerang' plot and the mechanics of interpretation have been described elsewhere in detail (Green, 1986; Brown *et al.*, 1994).

The range of AFT central ages reflects variations in the proportions of two track-length populations that formed before and after a cooling episode. If the plots do not show the distinctive boomerang pattern, then this implies a more complex thermal history indicating a coeval cooling from a range of pre-denudational palaeotemperatures (Green, 1986, 1988; Gallagher, 1998). The boomerang plot can be used to estimate the timing of the last major cooling episode. The timing is indicated by the youngest AFT ages if the MTL are ~14 to 15μm. This is typical of samples that have cooled from 110±10°C and hence only preserve tracks that formed after the initiation of the last phase of cooling. The intermediate ages have shortened MTLs, which reflect a mixture of pre- and post-cooling. The oldest ages, on the other hand, are associated with a larger proportion of older tracks with a long MTL reflecting pre-cooling temperatures.

7.3.3.1 Regional

Figure 7.4b is a plot of central age against MTL and approximates a boomerang plot. As mentioned above, the boomerang plot can be used to estimate the timing of the last major cooling episode. The timing is indicated by the youngest AFT ages for intermediate MTL, typically ~14 to 15μm. However, the MTL for the TULIP samples are ~12 to 13μm, less than the typical 14 to 15μm for estimating a major cooling episode. Nevertheless, figure 7.4b shows that a major cooling episode occurred between ~170Ma to 180Ma (Mid

Jurassic) and is supported by thermal models (section 7.3) and hence cooling appears to have occurred at this time.

7.3.3.2 Geological Profile – Age/MTL

Figure 7.7b is a boomerang plot of MTL against central age for the AFT samples that occur along the profile. Samples LG5 and LG8 have relatively high MTL, whereas, sample LG7 is lower than would be expected for a simple cooling history profile. These samples have the youngest central ages. However, the oldest AFT ages show a sudden increase in MTL, with the exception of sample LG13, and hence, broadly resemble a boomerang plot. But, there are many outliers and the MTL are relatively short at ~12 to 13μm suggesting a complicated and protracted cooling history (as shown on figure 7.7b). This indicates that the cooling history is more complicated than the simple scenario outlined earlier and implies that all the samples have resided in the PAZ for a considerable length of time (in equilibrium with elevated temperatures that are >60±10°C <110±10°C).

The boomerang plots are most meaningful for inferring the most recent major cooling episode if track lengths are >13 to 14 μm. The plot points to a major cooling episode during Mid Jurassic times, which conforms with the regional pattern for SE Ireland (figure 7.4b) and represents the first major cooling event (see section 7.3.2).

7.3.4 AFT Profiles – Evidence for Faulting

In the north (figures 7.6 & 7.7), the difference in AFT central ages between samples LG8 (coast) and LG7 (Killiney Hill) are 131±4 Ma and 127±4 Ma at 2m and 250m above sea level (asl) respectively. The central ages of these samples are within error which make the proposal of a fault to the north for explaining these differences rather speculative. However, structural observations in Dalkey Quarry (chapter 3) and at Sorrento Point show NW trending dextral normal faults downthrowing to the NE and there is a topographic hollow (wind-gap) to the N of Killiney Hill. Therefore, the differences in central age may be

compatible with fault movements. The faulting probably post-dated the final cooling episode and has offset the fossilised PAZ.

The AFT central age for LG10 (151±6Ma), ~2km to the S of Killiney Hill is located within a topographic low. The elevation drops (concave slope) from 250m to 110m over a distance of 2km between samples LG7 and LG10. This topographic feature extends at least 8km WNW. The difference between the central ages cannot be accounted for by error alone. Thus, the evidence suggests potential faulting, with downthrow to the south implying that Killiney Hill is a small horst.

The AFT age from samples LG15 to LG16 (figure 7.7) decreases slightly from 177±5Ma to 173±4Ma with a corresponding but subtle increase in elevation from 470m to 500m respectively. This latter sample is in close proximity to the Sally Gap fault and may be in the footwall and not on the hangingwall as shown on figure 7.6 (the location of the faults have a precision error of ~100–500m). However, whilst this fault may have been reactivated to produce the decrease in central age with a subtle increase in elevation, the evidence for recent offsets is ambiguous due to the small elevation range and the central ages are all within error.

Notwithstanding, the decreasing trend continues from samples LG16 to LG17, with a fall in age from 173±4Ma to 170±5Ma respectively over a 70m increase in elevation. Again, the sample ages are within error although the age for LG17 would be predicted to increase with elevation. Sample LG18 is significantly different with an age of 152±4Ma over a small horizontal distance of 200m to the north from sample LG17, and is 50m lower than this latter sample (i.e. sample LG17 and LG18 are located at the top and middle of Carrigshouk mountain respectively). The Carrigshouk Mountain is probably situated on a NE trending fault scarp between the Djouce surface (chapter 5) and the uppermost Mullacleevaun surface (W.E.A. Phillips, pers. comm., 2000), and hence, the change in age may be due to movement on this structure.

However, an alternative explanation may be due to significant variations in apatite chemistry between the two samples. O'Sullivan & Parrish (1995) showed that significant changes in apatite fission track ages for small plutonic rocks in the Coast Ranges of British Columbia were due to compositional variations, i.e. such that chlorine-rich apatites retained older ages than fluorine-rich grains. This could be the case to explain the differences in central age for samples LG17 and LG18. Although, the relatively small distance between the two samples in apparently homogenous granite points to further faulting (i.e. between the Djouce and Mullacleevaun surfaces). If faulting has produced the observed differences, then this implies that fault movements occurred <20Ma (section 7.3).

The AFT central age decreases from sample LG17 to LG21 (156±5Ma) with a fall in elevation from 570m asl to 400m asl. The central age then increases from sample LG21 to LG36 (174±7Ma) with an elevation increase of 375m. All these samples fit the exhumed PAZ profile 2 as shown by figure 7.7a.

As noted earlier (section 7.2.2), the central age from sample LG36 (174± 7Ma) to LG26 (167± 7Ma) shows a decrease in age with elevation but not by the magnitude predicted from the relationship between central age and elevation (figure 7.7a), i.e. sample LG26 does not fit with profile 2. Sample LG23 displays a subsequent increase in age to 174±7Ma (Tullow Lowland) with a further decrease in elevation of 110m, the converse to what would be expected i.e. central age should decrease with elevation (figure 7.7a.). Hence, sample LG21 has the same apparent AFT age as sample LG36 with 725m of relief between both samples (i.e. a fall of 725m elevation over a horizontal distance of <15km). This suggests that the Tullow Lowland has been lowered in elevation by fault movements, a conclusion reached in chapter 5. Therefore, the Moyne linear (Baltinglass escarpment) is in fact a major fault and the Tullow Lowland forms the downthrown block.

7.3.4.1 Track-Length Distributions

The fission track length distributions are mostly bimodal (Appendix 4), with modal peaks of ~12 to 13μm. A second very small population occurs between ~3 to 6μm. (But, track

counting tends to be biased towards longer track lengths.) The main populations tend to be negatively skewed towards shorter track lengths with samples in the northern part of the region showing the highest skewness towards short track lengths. This is indicative of long residence times in the PAZ (i.e., samples have equilibrated and have partially annealed). All samples have relatively few long track lengths, indicating recent cooling below 60±10°C.

7.4 Thermal Modelling

Due to the complicated cooling history of the Leinster samples (as indicated by the track-length distributions in Appendix 4), and the limited range of elevation, it is difficult to extract likely thermal histories solely based on the central age and track-length distributions. Thermal modelling of the samples is necessary to extract the maximum information about exhumation events.

The form of an individual thermal history is based on inserting cooling events where required to fit the fission track-length clusters. This ensures that random variations producing unresolved heating events are minimised. However, if the modelled palaeotemperature remains more or less constant over a given time interval, this does not mean that progressive heating of the sample to that temperature has not occurred over that time interval. Instead, the modelled thermal history reflects the lack of resolution when heating from a low temperature to a higher temperature. Consequently, a static thermal history may be inferred during a period of burial, with the maximum temperature occurring at the time of maximum burial and little resolution on the earlier, lower temperature part of the thermal history. This has the effect of damping burial (heating) events in a thermal history. Flat portions of the time-temperature trajectories (Appendix 5) should therefore be viewed with some caution, but do indicate an upper limit to the palaeotemperature during this interval. In section 7.3.2, this is assumed to represent further heating in the thermal history, although the strict interpretation is no cooling.

7.4.1 Hercynian Thermal Event

Vitrinite Reflectance data from Carboniferous and Devonian aged rocks (Clayton *et al.*, 1989) shows Rm values of ~3% to 4% (figure 7.8a). The observed VR data is converted to palaeotemperatures using the kinetic models of Burnham & Sweeney (1989) and Sweeney & Burnham (1990) and shows palaeotemperatures (figure 7.8b) >250° over SE Ireland.

This early heating event may have been due to high heat flow, deeper burial or a combination of both. The high palaeogeothermal gradients measured in well 33/22-1 (Corcoran & Clayton, 1999) and from rocks in the Dublin basin (Fernandes, 2000) implies that the geotherm was much hotter during the Carboniferous (i.e. ~70-74°C km^{-1}). Therefore, assuming a palaeogeothermal gradient of ~70°C km^{-1} and palaeotemperatures of ~250°C, the TUILP samples must have been at depths of ~5km during Late Carboniferous times. Clayton *et al.*, (1989) attributed these high palaeotemperatures to a Hercynian thermal event (chapter 4).

7.4.2 Time of Cooling from Maximum AFT Palaeotemperatures

As figure 7.9 shows, all the Leinster samples cooled below 110±10°C between 252Ma and 158Ma (Upper Triassic to Middle Jurassic) with a mean age of 220Ma (Upper Triassic). All samples have older cooling ages than apparent AFT central ages. For example, the AFT central ages range from 127Ma to 181Ma (Mid Jurassic to Lower Cretaceous) with a mean central age of 161Ma (Mid Jurassic). These results, coupled with the nature of the track-length distributions (Appendix 4), strongly suggests that the samples initially resided within the PAZ for a significant period of time, and hence, the track-length distributions display pre- (~3 to 6μm) and post- cooling (~14 to 15μm) track length populations. The samples, therefore, began to cool from palaeotemperatures of 110±10°C during Late Triassic to Mid Jurassic times (as indicated by the boomerang plots, figures 7.4b & 7.7b).

These results are in harmony with earlier apatite fission track studies from southern Ireland (Keeley *et al.*, 1993), where the stratigraphic ages lie in the range of 360Ma to 365Ma, and

the AFT 'pooled' ages range from 154Ma to 226Ma (figure 7.10). The MTL are also very similar with the TULIP samples, i.e. mean track lengths range from 11.98±0.64μm to 12.68±0.14μm.

All the samples along the geological profile (and indeed in SE Ireland) have been totally annealed and initially began cooling (<110±10°C) in the Late Triassic to Mid Jurassic (Mid Cimmerian tectonism). Sample LG13 has the oldest AFT central age (181±5Ma) along the profile and the oldest cooling age of 252Ma (figure 7.9). Hence, this sample places a minimum age on the thermal annealing event. If no further annealing of sample LG13 had occurred since this time (and likewise for the other samples at their respective track retention cooling times) then the MTL would be ~14μm. The average AFT central age for the TULIP samples is much younger at 161Ma and the MTL are <13μm in length. This indicates either another cycle(s) of heating/cooling or an extremely protracted cooling history from maximum palaeotemperatures to surface temperatures.

The Mid Jurassic reddened clay deposit at Cloyne (Higgs & Beese 1986) and Upper Jurassic to Lower Cretaceous marginal marine-terrestrial clays near Carrick-on-Suir, Co. Kilkenny (Higgs & Jones, 2000), indicate that parts of southern Ireland were exposed at this time (Naylor, 1992). In addition, Lower Jurassic (Sinemurian) sediments in the Celtic Sea and Fastnet basins are thought to have been derived in part from exposed Old Red Sandstone in SW Ireland and from the Leinster Massif (Petrie *et al.*, 1989) indicating uplift and erosion of these areas. Where Mid Jurassic sediments are present (chapter 1), a Leinster Massif source is invoked to explain upper Bathonain-lower Callovian red-beds prograding into the Celtic Sea area. Therefore, this rules out the protracted cooling scenario and implies a composite cooling history with cycles of cooling and heating. Subsequent heating events will lie entirely within the PAZ otherwise the central age would be much younger and the MTL would be >13μm to 14μm, i.e. if >110°C then the central age would be reset and thus have a younger closure age.

The time-temperature trajectories of the Leinster profile samples (Appendix 5) display a complicated path. In general, three post-Jurassic cooling events and two heating events

occur. Two exhumation events, spanning from the Early Cretaceous to the Palaeogene, affect almost all the Leinster samples with cooling of ~20°C to 40°C. Samples LG17, LG21, LG5, LG14 and LG15 show cooling between ~125Ma to 90Ma (Early Cretaceous [Aptian-Albian-Cenomanian]). The second cooling event affects samples LG16, LG18, LG8, LG10, LG7, LG11, and LG13 between ~100Ma to 58Ma (Late Cretaceous to Palaeogene [Palaeocene]). The Aptian-Albian-Cenomanian event may correspond with known unconformities in basins on the western Atlantic seaboard (chapter 8) and the Ulster Basin (chapter 1), e.g. minor rifting in the Porcupine basin occurred at this time (Tate 1993), which may have led to transient thermal uplift of the onshore areas including the Leinster Massif. The second event corresponds with uplift and erosion of the postulated chalk cover over SE Ireland (chapter5) and most of the Irish landmass (chapter 1). This correlates with the unconformity between the Campanian-Maastrichtian aged limestones of the Ulster basin and the overlying Palaeocene basalts of the Tertiary Igneous province (chapter 1). Palaeotemperatures at the beginning of the Tertiary range from 60°C to 90°C over much of SE Ireland.

Most samples then experienced further heating of ~10°C (Mid-Late Palaeogene), placing the rocks back in the upper part of the PAZ. All the samples experience a final cooling during the Neogene to present-day temperatures. However, part of this relative cooling is an artefact of the model parameters (i.e. an assumption of present-day surface temperature of 20°C), which is why the error estimate for the time-trajectories is relatively large. Notwithstanding this final kick (Neogene times) in the time-temperature trajectory, the overall net effect can be used to model denudation; and the relative lack of track lengths >14μm (Appendix 4) indicates a final, but relatively recent cooling event.

7.5 Denudation Estimates

By making assumptions about the palaeogeothermal gradient or palaeo-heat flow, the thermal history, in principle, can be converted to depth-time information to reconstruct a

denudational chronology (e.g. Bray *et al.*, 1992) for outcrop samples as follows:-

$$\Delta D = \frac{P(t_1) - P(t_0)}{g}$$

ΔD = denudation;
P = palaeotemperature;
t_0 = initial age;
t_1 = older age;
g = palaeogeothermal gradient.

7.5.1 Estimate of Tertiary Palaeogeothermal Gradients for SE Ireland

A number of estimated palaeogeothermal gradients are available from profiles of vitrinite reflectance in boreholes (chapter 4). This technique relies on the extrapolation of best-fit VR profiles upwards to the appropriate surface temperature. There may be problems in the use of a linear extrapolation where thermal conductivity contrasts characterise the upper part of the basin fill (Holliday, 1993), in the parameterisation of the temperature-reflectance relation (Rowley & White, 1998) and in the recognition and removal of the effects of fluid flow on reflectance values (Green *et al.*, 1997). Nevertheless, VR profiles (Corcoran & Clayton, 1999), augmented where possible with apatite fission track data are widely used to estimate palaeogeothermal gradients.

Palaeogeothermal gradients estimated from VR and AFT profiles vary considerably (Bray *et al.*, 1982; Lewis *et al.*, 1992; Murdoch *et al.*, 1995; Scotchman & Thomas, 1995; Green, 1986; Green *et al.*, 1997; Duncan *et al.*, 1998; Green, 1989; Corcoran & Clayton, 1999, and others) even within relatively small sub-basins. For example, palaeogeothermal gradients of between 10°C km^{-1} and 50°C km^{-1} have been estimated in the East Irish Sea and Solway basins (Green *et al.* 1997). Therefore, there is some merit in estimating palaeogeothermal gradients for the Irish landmass through a thermal model derived from subsidence history. A large number of boreholes show a period of Permo-Triassic to Early Jurassic stretching followed by thermal relaxation (Rowley & White, 1998), with stretch factors of less than

1.4. For example, the subsidence history and VR profile of 42/21-1 can be satisfactorily explained using two periods of stretching (in Sherwood Sandstone and Penarth Group times) with β values of between 1.2 and 1.3 and a radiogenic heat contribution from the upper crust. The palaeogeothermal gradients in this model range from approximately 40°C km^{-1} in the Triassic to 22°C km^{-1} in the Late Tertiary (P.A. Allen, pers. comm. 2000). Similar geotherms are implied (but not directly given) in the much more extensive study of Rowley & White (1998). Hence, a palaeogeothermal gradient of 22°C km^{-1} was used for calculating Tertiary rates of denudation for AFT samples located along the Leinster geological profile (figure 7.6).

7.6 Estimates of Tectonic Uplift

The effects of erosion in elevated areas induce isostatic rebound that compensates for the mass of removed material. Therefore, denudation estimates are not solely due to tectonic uplift but also to isostatic rebound. However, increasing rates of denudation may also be due to non-tectonic processes. External variables such as climatic change or base-level fluctuations can affect the rate of denudation and hence produce isostatic imbalance. To complicate matters, tectonic changes may also have a knock-on effect. For example, in chapter 5, it was suggested that the River Slaney crosses the East Carlow Deformation zone because there was enough stream power (incision rate) to keep pace with uplift. Whereas, wind-gaps further along the structure were now abandoned. Therefore, a tectonic change in one part of the system is balanced somewhere else until the landscape is back in 'dynamic' equilibrium. Hence, to convert denudation to tectonic uplift, independent geological constraints are also desirable. Thus, by selecting the AFT profile along the drainage divide, it is hoped that this will minimise non-tectonic variables, e.g. fluctuating fluvial incision rates, river avulsion etc. Of course, it is impossible to rule out of hand that the drainage divide hasn't deviated from it's present location during the Tertiary. For example, Late Cretaceous-Early Tertiary landscapes are envisaged to have been sculpted from a flat-lying Late Cretaceous chalk cover, and the present-day rivers have stripped this blanket cover to superimpose on essentially, a pre-Cretaceous basement (chapter 5).

With this in mind, estimates of tectonic uplift can be calculated using the equation of Chadwick (1985):

$$\Delta U = \Delta E \frac{(\rho_m - \rho_c)}{\rho_m} - \Delta H$$

ΔU = tectonic uplift;
ΔE = denudation;
ΔH = sea - level at time of uplift minus present day;
ρ_m = density of mantle rock $(3.3g\ cm^{-3})$;
ρ_c = density of eroded strata $(2.8g\ cm^{-3})$.

Brown (1991) has shown that it is possible to isolate the tectonic uplift component from the amount indicated by erosion in regions where independent evidence constrains the elevation of the palaeosurface and where the change in sea level can be calculated. As chapter 8 illustrates, Ireland has experienced kilometre-scale erosion during the Tertiary and therefore this evidence is not preserved. Whilst it is clear that the Irish landmass became emergent during the Tertiary, eustatic changes have occurred during Tertiary times (Haq *et al.*, 1987) and the influence of sea-level changes are addressed in chapter 8. Hence, tectonic uplift values quoted below (table 7.2) do not account for eustatic changes.

Table 7.2

Old Model			*New Model*		
Sample	Denudation (m)	Tectonic Uplift (m)	Sample	Denudation (m)	Tectonic Uplift (m)
LG5	1973	314 - ΔH	LG5	1067	170 - ΔH
LG7	1973	314 - ΔH	LG7	1067	170 - ΔH
LG8	1973	314 - ΔH	LG8	1067	170 - ΔH
LG10	2698	429 - ΔH	LG10	1667	265 - ΔH
LG11	2245	357 - ΔH	LG11	1765	281 - ΔH
LG13	2405	383 - ΔH	LG13	1590	253 - ΔH
LG14	2146	341 - ΔH	LG14	1168	186 - ΔH
LG15	2145	341 - ΔH	LG15	1193	190 - ΔH

Table 7.2 (continued)

LG16	2188	348 - ΔH	LG16	1248	199 - ΔH
LG17	1878	299 - ΔH	LG17	932	148 - ΔH
LG18	1878	299 - ΔH	LG18	932	148 - ΔH
LG21	2225	354 - ΔH	LG21	1299	207 - ΔH
LG23	2005	319 - ΔH	LG23	1052	167 - ΔH
LG26	2116	337 - ΔH	LG26	1173	187 - ΔH
LG36	2443	389 - ΔH	LG36	1520	242 - ΔH

7.6.1 Interpretation

As table 7.2 shows, the values for denudation and tectonic uplift based on the new annealing model (Gallagher, in prep) are significantly less than the older annealing model of Laslett *et al.,* (1987) for the Tertiary. Whilst the old annealing model tends to overestimate denudation for recent cooling, the new annealing model tends to be too conservative (Gallagher, pers. comm. 2000) and this should be kept in mind when quantifying denudation and hence tectonic uplift results.

Samples LG5, LG7 and LG8 all display identical amounts of denudation and tectonic uplift for both old and new annealing models respectively (table 7.2). This indicates that these samples have all shared the same thermal and tectonic history post-Triassic times. This suggests that the fault movements inferred in section 7.3 are relatively small. However, figure 7.11 show that the denudation and tectonic uplift changes significantly over a relatively small horizontal distance (high gradients). For example, the central age (151Ma) and elevation (40m) of sample LG10 in comparison with adjacent samples LG5, LG7 and LG8 (central ages range from 131 to 142Ma at elevations of 2m to 150m) may be due to differential erosion of the Type1 granodiorite (LG10) relative to Type2 microcline porphyritic granite (LG5, LG7, LG8). Alternatively, the lack of evidence for regional differential erosion reflected in the regional geomorphology (chapter 5), the presence of wind-gaps, and the fact that much of the ground is actually underlain by Type2 granite implies that the differences are probably due to recent faulting with or without differential weathering. The age of the faulting must be at least Miocene, which post-dates cooling of

the samples below 50-60°C (Appendix 5). This may explain the apparent present-day 'horst topography' of the Killiney Hill area.

Table 7.3

Samples	Tectonic Uplift (m) - ΔH *Old Annealing Model*	Tectonic Uplift (m) - ΔH *New Annealing Model*
Profile 1 (section 7.2.2.2)		
LG8	394	170
LG5	314	170
LG10	429	265
LG11	357	281
LG13	383	253
LG14	341	186
LG15	341	190
Profile 2 (section 7.2.2.2)		
LG21	354	207
LG26	337	187
LG17	299	148
LG36	389	242

In section 7.3.2.2, profiles 1 and 2 displayed sub-parallel exhumed PAZ paths (figure 7.7a) with the likelihood that profile 1 had been downthrown to the north (by about 200m) by the Lough Dan fault. As table 7.3 shows, both profiles display similar modelled estimates of denudation and tectonic uplift, suggesting that potential faulting must be young in age. Similarly, the Tullow Lowland sample LG23 has tectonic uplift values of 319–ΔH (old) and 167–ΔH (new) compared with 337–ΔH (old) and 187–ΔH (new) for sample LG26. This argues for movement on the Moyne/Baltinglass fault to be Neogene in age (i.e. palaeotemperatures <50-60°C). This is an interpretation that also honours the exhumed PAZ profiles (section 7.2.2.2).

Figure 7.11 reinforces the notion of relatively recent faulting. To the south of the Lough Dan fault, denudation (and tectonic uplift) is higher over the mountain peaks (e.g. sample LG36, Lugnaquillia Mountain) and lowest in the valleys (e.g. sample LG21, Lough Nahanagan). The greatest relief occurs to the south of the Lough Dan fault and denudation tends to exhibit a strong positive correlation with relief (e.g. Ohmori, 1983). However, this correlation becomes weaker, north of the Lough Dan fault. For example, sample LG10 (Church View Road, Co. Dublin) shows greater denudation and tectonic uplift than the adjacent samples of LG5 to LG8 (Killiney Hill to Sorrento Point). Hence, the denudation is higher over areas of lower relief and elevation. This may be due to faulting and/or differential erosion. This appears to support the earlier postulation that there is a fault situated to the S of Killiney Hill.

7.7 Summary of Conclusions

As Appendix 5 shows, most of the AFT samples have resided in the PAZ throughout most of the Tertiary. This factor, coupled with the limited range of elevation over the Wicklow Massif, hampers the evaluation of Tertiary tectonics and the identification of potential structures that have played a key role in the recent tectonic and geomorphic development of SE Ireland. Notwithstanding, the AFT data does show that the region has experienced cooling (exhumation) events at the beginning of both the Palaeogene and Neogene, with the former event showing the greatest degrees of cooling, and hence denudation and potentially tectonic uplift. This corresponds with the regional pattern over much of the Irish landmass (chapter 8) and the Irish Sea region (chapter 4) where block faulting and epeirogenic tectonics appear to have dictated the pattern of inversion (Irish Sea dome) and the form of the present-day topography (chapter 5 & 8).

The major cooling events that have affected the Wicklow Massif (and indeed SE Ireland) are; (1) Stephanian/Early Permian (VR data); (2) Triassic to Mid Jurassic; (3) Early Cretaceous; (4) Late Cretaceous; (5) Palaeogene; and, (6) Neogene. These cooling events are also punctuated by heating events (~10-40°C). As the time-temperature trajectories show (Appendix 5), not all samples experienced all the cooling and heating events and a

few display relatively simple cooling paths. This is not simply restricted to samples that occur along the Leinster geological profile but are representative of SE Ireland (e.g. sample LG28 [Mount Leinster]). Therefore, whilst some areas were cooling (exhumed) other parts were experiencing subtle heating (deposition). Additionally, the magnitude of heating and cooling cycles differs between samples, implying differential erosion and deposition. For example, major Caledonian/Hercynian fractures would probably accommodate the greatest amounts of vertical motions. This includes the East Carlow Deformation zone and the NW-SE faults that traverse the Leinster Mountain chain.

However, the limited range of elevation across the Wicklow Massif hinders a more rigorous quantitative and qualitative account of the Tertiary history than what has been presented here. Hence, it is beyond the limits /resolution of the AFT data to correlate and quantify offsets of faults over small distances. However, it has been shown that the AFT data does provide some information on faulting over large horizontal distances, e.g. Lough Dan and other faults. Furthermore, the AFT central age and track-length distributions, and thermal modelling provide both a general qualitative and quantitative picture regarding cooling paths and amounts of denudation.

CHAPTER 8 - REGIONAL IMPLICATIONS OF MODELS FOR SE IRELAND

8.1 Introduction and Summary

In SE Ireland, there is a general absence of post-Carboniferous aged rocks. The notable exception being the Wexford Outlier, which contains Permo-Triassic sequences. However, despite the lack of stratigraphic resolution, AFT models and independent structural and geophysical models point to episodic tectonics throughout the Mesozoic-Tertiary.

8.1.1 Aims & Objectives

In order to provide a thorough evaluation of the regional implications of these models derived for SE Ireland, it is necessary to look at the entire Irish landmass and the continental shelf to the west. The aim of this chapter is therefore to assess the regional implications of tectonic models proposed for SE Ireland to the entire landmass using the AFT method. An evaluation is extended to the continental shelf west of Ireland using well and seismic data, with particular emphasis on the Porcupine basin. Sediment budget analysis is undertaken to correlate sediment source and sink, i.e. matching the denudation events onshore with offshore unconformities and major periods of clastic input. Finally an attempt is made to reconstruct palaeotopography.

8.1.2 Methods and Materials

The main methods and materials of this chapter are listed below:-

- AFT Analysis (section 8.3);
- Analysis of aeromagnetic data (section 8.4);
- Analysis of seismic reflection data (section 8.4);
- Analysis of logged wells (section 8.4).

8.2 Tertiary Stress Models of SE Ireland

It was shown in chapter 3 that structural mapping of brittle fabrics that cut the northern margin of the Leinster batholith, coupled with faulting, displacement of a lateritic weathering surface on the Howth peninsula, and brittle structures at a road section near Rathcoole, are compatible with two post-Hercynian stress systems. These are:

1) horizontal σ_1 oriented NW-SE and σ_3 oriented NE-SW, prior to;
2) horizontal σ_1 oriented NNW-SSE and σ_3 oriented ENE-WSW.

In general, two stress systems have been identified from structural mapping of onshore brittle structures along the northern margin of the Leinster batholith (chapter 3). The structures are in harmony with a horizontal σ_1 oriented NW-SE and σ_3 oriented NE-SW post-dated by a younger stress system with horizontal σ_1 oriented NNW-SSE and σ_3 oriented ENE-WSW. A microscopic analysis of deformational mechanisms of onshore outcrops (chapter 3) and structural correlation with the offshore Kish Bank basin (chapter 4) suggests a post-Liassic age for both stress systems. Regional correlation with NE Ireland, where suitably aged rocks exist (chapter 4), and correlation with onshore studies of geomorphology and LANDSAT lineaments of SE Ireland implies an Early Palaeogene age for the early stress system and a Neogene age for the later one (chapters 5 & 6).

Apatite fission track (AFT) studies show that a minimum of 4 post-Hercynian cooling events affected the region of SE Ireland. The Leinster batholith appears to have been unroofed during Late Triassic to Mid Jurassic times. Differential uplift also played a role in the development of the region during the Early Cretaceous and Early Tertiary (chapter 7). A final cooling event occurred in the Neogene and appears to have been primarily responsible for the formation of the present-day landscape (chapters 5 & 7). The onshore structures that are compatible with the NW-SE compression and NE-SW extension may have acted as key structures that accommodated Early Tertiary uplift. The NNW-SSE compression and ENE-WSW extension is probably Neogene in age and has

accommodated recent differential uplift (tectonic and isostatic) and subsidence of SE Ireland and the Irish Sea.

These stress systems may explain the occurrences of warm springs (chapter 2) and anomalously thick deposits of sand and gravel at the end of fault terminations. This is because onshore continuation of offshore fault structures and the potential reactivation of major Caledonian and Hercynian fractures as transform fault zones would be strongly controlled by the strike of the Caledonian and Hercynian folds. For example, near the E coast, the strike is ~E-W and swings to the NE-SW a few kilometres inland. Thus, the stress systems above (particularly the youngest) would preferentially reactivate ancient fractures and propagate new faults in an E-W direction. However, the swing in structural grain to NE-SW would prevent reactivation resulting in a zone of fault terminations. These zones would result in horsetail termination structures with both dilational and compressional features (figure 8.2).

8.2.1 Regional Implications

In chapters 3 & 4, correlation of stress systems deduced from the northern margin of the Leinster batholith and the Kish basin were compared and regionally correlated with stress models from NE Ireland. An Early Tertiary (postulated Irish Sea dome; Cope, 1994, 1997) event, based on AFT studies of the Irish Sea region (Lewis *et al.* 1992; Green *et al.* 1993, 1997, 1999), VR analysis (Jenner 1981; Corcoran & Clayton, 1999) and sonic velocity studies (Turner & Phillip, 1998) was correlated with the Kish Bank basin (chapter 4). The correlation showed that the WNW-ESE brittle structures (i.e. due to NW-SE compression and NE-SW extension) that cut the Leinster Granite are probably due to reactivation of magmatic fabrics and (chapters 2 & 3) is likely to be of Early Tertiary age. And this is probably coeval with the general uplift of the Irish Sea region. Further correlation with NW-SE dextral structures that cut the NE margin of the granite and produced displacement on the Codling fault is correlated with the Lough Neagh Larne basin (chapter 4) and is at least Oligocene in age. This is correlated onshore with geomorphic landforms of the Leinster Mountain chain (chapters 5 & 6), and backed up

with an AFT study (chapter 7) which shows that this stress regime (NNW-SSE compression and ENE-WSW extension) is probably Pliocene and younger in age.

Despite the lack of stratigraphic resolution for Mesozoic-Tertiary tectonics in SE Ireland, these methods have led to a working model, which replaces the original dextral transform hypothesis (chapter 1). The AFT modelling of surface exposures facilitates progress in assessing the thermal and denudational history of the region. In order to test the model, it is necessary to utilise AFT data for the whole of the landmass to evaluate similarities and differences with the thermal, denudational and tectonic history of SE Ireland. Analysis of the stratigraphic and structural evolution of the Porcupine basin provides another important test (see section 8.4) in terms of unconformities and periods of clast input.

8.3 AFT Analysis – A Test

The TULIP AFT database consists of 145 samples with 88 of these obtained from previously published and unpublished sources. Figure 8.1 shows the locations of the AFT samples. Appendix 6 lists the grid co-ordinates, lithology, stratigraphic interval, Central Age and MTL for all samples.

The TULIP samples were obtained from a wide range of lithologies across Ireland (except the Munster basin in southern Ireland). The best apatite yields were derived from basement granites. Some lithologies such as the Hibernian Greensand from the Ulster basin did not yield sufficient quantities of apatite. In general, thermal aureoles were avoided, with the exception of sample DQ1 (Doonan Quarry, Co. Fermanagh) which was obtained from the Devonian aged sandstone directly adjacent to a Tertiary dyke. Also, sample G222329 (McCulloch, 1993) was obtained from a Carboniferous aged sandstone that forms the thermal aureole of a Tertiary aged gabbroic sill.

8.3.1 Methodology

The AFT method is described in detail in chapter 7. All thermal histories are modelled using the conventional Laslett *et al.* (1987) annealing model. The outcome of the modelling process is a thermal history represented as a series of discrete time-temperature points for each sample (with linear interpolation between points adjacent in time). Palaeotemperature maps for a certain time in geological history can then be constructed for a particular time ranging from 1Ma to 300Ma. A palaeotemperature map for the Early Tertiary (65Ma) is constructed using the Laslett *et al.* (1987) annealing model (figure 8.7). The spatial variation of total denudation (66Ma to 10Ma), which is used for palaeotopographic reconstructions (figures 8.21 & 8.22) is also based on the Laslett *et al.* (1989) model (figure 8.18). The 10-0 Ma thermal history is not included due to the large uncertainties in the annealing model at such low temperatures.

Surface Interpolation of Maps

Maps are contoured using ESRI GIS (Arc View) software. The Inverse Distance Weighted (IDW) interpolator was used to produce a surface resolution of $1km^2$. This method determines output cell values using a linearly weighted combination of a set of sample points. The weight is a function of inverse distance. The input of sample points was limited to 12 using the nearest neighbour method. The power parameter in the IDW interpolation controls the significance of the surrounding points upon the interpolated value, a higher power resulting in a smaller influence from distant points. The power used in the interpolation of the contours was 2. The output value for a cell using IDW is limited to the range of values used to interpolate, that is, the maximum and minimum values constrained by the original palaeotemperature range. Since the IDW is a weighted distance average, the average cannot be greater than the highest or less than the lowest input (Watson & Philip, 1985). The resulting surface is the best estimate of what quantity is on the actual surface for each location. However, this method will tend to smooth out potential discontinuities in the original data.

The contour values are ramped to a 'Natural Breaks' classification scheme. This method identifies breakpoints between classes using the Jenk's optimisation statistical formula. This method minimises the sum of the variance within each of the classes and finds groupings and patterns inherent in the data.

Construction of Denudation Maps

The denudation map of 66 to 10Ma uses a constant palaeogeothermal gradient of 22°C km^{-1} and avoids the uncertainties in thermal conductivity of the missing section by implicitly assuming it is constant (Allen *et al., in prep*). In the absence of information to the contrary, it is common to assume that the palaeogeothermal gradients are constant over time (e.g. Bray *et al.* 1992). Palaeogeothermal gradients will probably be spatially variable and will be a function of variable amounts of stretching and the distribution of variegated radiogenic crust (Allen & Allen 1990). There is no evidence of Tertiary differential stretching on the Irish landmass. Also, Green *et al.* (1999) found no evidence for elevated basal heat flow during the Early Tertiary along the Atlantic margin, despite widespread igneous activity at this time. Therefore, it is assumed that the modelled thermal history reflects depth of burial.

The precision of the denudation estimate varies in space and time. Factors that contribute to the uncertainty are the annealing model, the geothermal gradient, and the inferred timing of cooling episodes. Allen *et al.* (*in prep*) considers an uncertainty of 10°C on the temperature difference between two times for a given sample. This is coupled with a 20% uncertainty on a geothermal gradient of 30°C. This implies a combined uncertainty of ~400m to 500m on the denudation estimate. Fortunately, uncertainties in timing of cooling are not too severe for relatively long time intervals as adopted here.

8.3.2 Results

AFT analysis of SE Ireland shows that the region has experienced multiple cooling and subtle heating cycles in post-Hercynian times. Keeping in mind the caveats discussed in chapter 7, these are interpreted as representing periods of denudation (cooling) and

deposition (heating). In total, the AFT modelled thermal histories show that there are primarily 4 cooling events spanning from the Late Triassic through to the Late Tertiary. The main cooling events are:-

1. Late Triassic to Middle Jurassic
2. Early Cretaceous
3. Early Tertiary (Palaeogene)
4. Late Tertiary (Neogene)

8.3.3 Central Age - Observation & Interpretation

Samples for AFT analysis were obtained from rocks that have stratigraphic ages ranging from Pre-Cambrian to Triassic. The majority of the samples were obtained from Devonian granites and sandstones. The AFT central ages range from 394Ma to 28Ma, with an average of 163Ma (figure 8.3a).

The oldest ages are from the NE corner of Ireland. Sample RB1 (Red Bay, Co. Antrim) has a central age of 369Ma and was obtained from Triassic rocks (figures 8.1 & 8.3a). Sample D243261 is just north of RB1. This sample has the oldest central age of 394±48 Ma and was obtained from Devonian sandstone. The apatite grains from sample D243261 therefore must have attained total annealing immediately after deposition and have never been buried more than ~2km since the Triassic because the AFT and stratigraphic age are similar. The AFT age for sample RB1 is much older than the stratigraphic age indicating that this sample has not experienced total annealing, and therefore has similar provenance characteristics as sample D243261 to the north. The provenance for the Triassic deposit (RB1) therefore has a northerly derivation. D243261 was sampled from the Highland Border Ridge (HBR). This implies that the Triassic sandstones in NE Ireland were probably derived from the upstanding HBR during early Mesozoic times. Furthermore, based on the thermal history of sample D243261, this suggests that the HBR has not attained maximum palaeotemperatures of 110±10°C in

post-Devonian times, and that sample RB1 has not attained these temperatures in post-Triassic times.

The youngest AFT central ages are from samples MG1 and MG2 (the Mourne plutons, Co. Down). The samples are from the Eocene granites (chapter 1) and MG1 and MG2 have central ages of 36Ma and 28Ma respectively (figures 8.1 & 8.3a). U/Pb SHRIMP age determinations in zircons give crystallisation ages of 55.5±1Ma (Meighan *et al.*, 1999). It is unlikely that these granites were emplaced at depths of less than 3km (I.Meighan pers. comm. 1998). Therefore, within 20Myr, the granites have been unroofed, requiring a time-averaged denudation rate of ~60m Myr^{-1}.

A NNE trend of relatively old AFT central ages (170 to 250Ma) occupies the central spine of the island (figure 8.3a). Most of the samples are derived from inliers surrounded by Carboniferous limestones, e.g. Slieve Bloom in Counties Laois and Offaly. The general implication is that the samples from Central Ireland have been <110±10°C >60±10°C for at least 170Myr.

In southern Ireland, most samples are derived from Devonian sandstones or granites and have much younger central ages indicating total annealing since deposition of the host rocks. As mentioned in section 7.3.2, the earliest heating was in excess of 200°C based on VR, probably due to Hercynian thermal effects (Clayton *et al.* 1989). The fact that the AFT central ages post-date this event supports this conclusion. As shown in section 7.3.2, thermal modelling shows that a minimum of 4 cooling events has occurred since the Hercynian orogeny.

Samples from Connemara show a wide range in central ages. Near sea level the Galway granite yields central ages of ~120Ma. Whereas to the north and west, at elevations up to ~300m, the ages increase to a maximum of ~230Ma, i.e. sample GL (figures 8.1 & 8.3). Preliminary analysis shows that this region has also experienced a similar uplift history to the Leinster Mountain chain. However, as figure 8.4 shows, the exhumed profiles are much steeper, indicating that Tertiary uplift is more intense in this region.

Two samples, G222329 (Killala Bay) and DQ1 (Doonan Quarry), in NW Ireland (figure 8.1) have relatively young central ages of 56±5Ma and 73Ma and were obtained from Carboniferous and Devonian sandstones respectively. The Killala Bay (Co. Mayo) sample G222329 is in the thermal aureole of a Tertiary gabbroic intrusion which gave a ^{40}Ar-^{39}Ar cooling age of 58±1 Ma (Thompson, 1985). Sample DQ1 is also in the thermal aureole of a Tertiary dyke (Appendix 6).

The area between Dublin to the Longford Down Massif displays relatively young central ages <90Ma along the coastline. Samples inland are slightly older and range in age from 90Ma to 160Ma, although sample N955793 is much older than sample N-1442, where the ages are 212±32Myr and 85Ma respectively (figures 8.1 & 8.3a). The relatively young age of sample N-1442 (Co. Meath) is because the apatite grains are from a depth of 205m in a borehole. In general, there is a NNE-SSW axis of old central ages dividing the landmass into 2 ~equal halves. This represents an area of relatively low relief and hence low denudation that also corresponds with a relatively low Bouguer gravity anomaly indicating that crust is relatively thick under the Central Midlands. Hence, the area is less susceptible to thermal uplift events and differential uplift/subsidence.

8.3.4 MTL – Observations & Interpretation

The MTLs range from 10.87 to 14.54µm with a mean of 12.57µm (figure 8.3b). As figure 8.3b shows, the majority or modal MTL values are ~12.30 to 12.66µm. The longest MTL is associated with sample DQ1 (Doonan Quarry) at 14.54µm, which shows that the sample has cooled rapidly from maximum AFT palaeotemperatures. The Mourne samples also have MTL of 14µm (MG1) and 14.36µm (MG2).

Sample GA (Killary Harbour) has a relatively high MTL of 12.85µm (i.e. mean is 12.57µm) but an old central age of 227±23Ma (i.e. mean is 163 Ma). This indicates that this sample has experienced rapid cooling in the Triassic and has resided below the temperature of the PAZ (i.e. <60±10°C) for a significant period of time since then.

A number of samples have relatively short MTL but do no show spatial variability (figure 8.3b). This implies that significant partial annealing has occurred due to complicated cooling paths (Late Jurassic to Early Cretaceous). Samples V316967 and Q690321 from SW Ireland (Co. Kerry) also display short MTL of 11.78±0.24μm and 11.57±0.24μm implying that these samples have experienced significant partial annealing.

Sample F4 (Kingscourt) has a central age of 166Ma and has a MTL of 11.93μm (figure 8.4). This indicates that the sample experienced a great deal of partial annealing and probably resided in the PAZ until fairly recently. In NW Ireland (Co. Donegal), central ages range from ~165Ma to 200Ma, with MTL of ~12.15μm to 12.44μm and indicate that a cooling event occurred during Late Triassic-Mid Jurassic times. In a similar pattern to the 'central age', there is a corresponding NNE-SSW trend of relatively short MTL (<12.5μm) traversing the centre of the landmass.

8.3.5 Partial Annealing Zone

Figure 8.5a is a map showing the time at which the surface samples cooled below 110±10°C. The area around Dundalk Bay has cooled the most recently from maximum palaeotemperatures. Most of the samples have entered the PAZ in the last 100Myr, and have an average cooling time of 50Myr with a strong peak at Oligocene-Miocene times. However, the average time of cooling to 110±10°C for all samples is 219Ma, with a modal peak at 240Ma.

Most of the samples that form the NNE-SSW axis across Ireland, cooled below maximum palaeotemperatures >270Ma. Samples T103114 and Keeley1 (figure 8.1), near the Wexford outlier, and the other samples from the Triassic level, i.e. F4 (Kingscourt) and RB1 (Red Bay) all cooled through maximum palaeotemperatures at 270Ma to >300Ma. With the exception of RB1, all Triassic samples have younger AFT ages than the stratigraphy, but cooling paths are much older. This suggests that the apatites are detrital and have inherited the thermal histories of their provenance, i.e. similar to adjacent samples from basement rocks. The grains have not attained

temperatures >110±10°C in post-Triassic times. However, the samples have been partially annealed to explain the younger central ages. In the case of RB1, the sample has experienced very little annealing because the central age is much older than the Triassic.

The Killala Bay (G222329) and Doonan Quarry (DQ1) samples have central ages that are similar to the time that both cooled below 110±10°C, indicating relatively quick cooling. The Doonan Quarry sample was removed from the palaeotemperature map in order to pick-out the strong spatial NNE-SSW trend of old cooling ages that occupies the central spine of the country.

The most interesting conclusion is that the Triassic samples have been derived from local sources and supports the notion of local derivation, restricted to half-grabenal structures, i.e. sediment derived from fault scarps. Also, those samples that are Tertiary in age (MG1 & MG2) and which have been re-set by Tertiary intrusion (DQ1 & G222329) display relatively rapid cooling to temperatures <60±10°C. For example, figure 8.5b shows that the Killala sample cooled below <60±10°C by ~50Ma, i.e. 5Myr to travel through the PAZ. Given a palaeogeothermal gradient of 22°C km^{-1}, this implies a denudation rate of between 130 to 200m Myr^{-1}. A decrease in denudation then must have occurred, otherwise the samples would have been totally exhumed between 40Ma to 30Ma.

Parts of Connemara cooled below <60±10°C over 100Ma (figure 8.5b). Whereas samples from the Galway granite attained this temperature at about 50Ma, and sample M117426 is very recent at ~20Ma. The Slieve Bloom outlier appears to have cooled below 60±10°C at 100Ma, whereas to the NW (the Sligo Bay area) and NE (the area around Belfast to Strangford Lough), palaeotemperatures did not cool below <60±10°C until Neogene times.

The difference between maximum and minimum palaeotemperatures defines the duration that samples resided within the PAZ (figure 8.6a). This shows that the average samples have a residence time in the PAZ of ~169Myr (figure 8.6b). Samples surrounding the

Dundalk Bay and the Mourne Mountains in the NE (Co. Down) have spent the least amount of time in the PAZ.

The two samples from Red Bay (Co. Antrim) in the north-east and sample C380251 (Inishowen peninsula, Co. Donegal) show relatively moderate durations of <120Myr, indicating that these samples have had an early thermal history and have been shallower than the PAZ (1 to 2km depth in the upper crust) for a significant period of time, i.e. sample C380251 cooled <60±10°C at ~180Ma. This may also be attributed to very low palaeogeothermal gradients and/or poor thermal conductivities of the host Dalradian rocks. This could in effect place the samples at much deeper levels, i.e. a palaeogeothermal gradient of 10°C km^{-1} would push the top of the PAZ to a depth of 5 to 6km. Green *et al.* (1999) showed that the palaeogeothermal gradients in this area are indeed very low, despite widespread igneous activity during the Early Tertiary.

Parts of Connemara also show relatively low to moderate residence times within the PAZ (figure 8.6). The longest residence times occur along the NNE-SSW axis across the centre of the island and in parts of the extreme SE of Ireland (i.e. Rosslare complex, Hook Head and the Wexford outlier). Also, samples around the Cork harbour area (i.e. Keeley 3 & Keeley 5) have experienced residence times >200Myr. It is probable that these areas have experienced cooling and heating cycles in and out of the upper part of the PAZ, i.e. the thermal modelling is unable to resolve re-heating cycles (section 7.1.3). For example, the Cloyne deposit (adjacent sample Keeley 3) indicates that this area was partly exposed during Jurassic times and figure 8.5b shows that these samples most recently cooled below 60±10°C at ~40 to 48Ma. Therefore, the samples must have been re-buried post-Jurassic times. And the depth has to be sufficient to place the host rock at temperatures >60±10°C. However, the temperature could not have been much greater than this, otherwise the central age would be younger than the current ages of 185 to 200Ma, i.e. samples Keeley 3 and Keeley 5 have central ages of 187±16Ma and 212±12Ma respectively. This is supported by relatively short MTLs of 11.96±0.64µm and 12.12±0.29µm and standard deviations >2µm, i.e. showing that the track-length

distributions have a large spread about the mean indicative of bimodality of pre- and post-cooling tracks.

8.3.6 Palaeotemperatures Early Tertiary

As discussed in chapter 4, the AFT analysis of borehole samples from the Irish Sea region (particularly the southern part), and the adjacent onshore areas of N England (i.e. Lake District and Pennines; Green 1989; Green *et al.* 1993, 1997) indicate that these areas were at palaeotemperatures of >110±10°C until the beginning of the Palaeogene. Green *et al.* (1997, 1999) found no evidence for elevated palaeogeothermal gradients at this time and thus attributed the palaeotemperatures and subsequent cooling to exhumation of section. However, the situation onshore Ireland is slightly different with samples having generally attained maximum palaeotemperatures during Late Triassic times (i.e. 219 Ma; figure 8.7). As figure 8.7 shows, these surface samples that were at maximum palaeotemperatures during the Early Palaeogene are exclusively associated with Tertiary igneous activity, i.e. the Mourne granites and thermal aureoles of dykes (e.g. DQ1). However, samples O115935 and O171846 (south side of Dundalk Bay, Co. Louth) are the exception and also show maximum palaeotemperatures at this time. This may in part reflect locally enhanced heat flow as a precursor to the Mourne intrusions immediately to the north.

Over much of the country, the vast majority of samples during the Early Tertiary were at temperatures of ~60 to 80±10°C (figure 8.7). There are only a few exceptions to this and include sample GE (Killary fjord, Co. Galway), samples F1 and BS1 (Barnesmore Gap) ENE of Donegal Bay, sample N955793 on the Balbriggan block, and samples RB1 and D243261 around Red Bay in Co. Anritm, and sample C380251 at Inishowen. The palaeotemperatures of all these samples were <50°C at the beginning of the Early Tertiary. As a consequence, the annealing model of Laslett *et al* (1987) is poor at resolving the Tertiary thermal histories for these samples.

8.3.7 Major Periods of Cooling

As mentioned in section 8.2, SE Ireland experienced 4 cooling events during Mesozoic-Tertiary times. But, the time-temperature paths of these samples showed that great variability existed. In other words, whilst most samples experienced cooling with variable magnitudes, other samples display deposition (no cooling).

The first post-Hercynian cooling event in SE Ireland occurred during Triassic to Mid Jurassic times. As figures 8.8a & 8.8b show, denudation calculated for the upper Early Jurassic time slice is relatively low. Deposition occurs in the NE and E, consistent with known Liassic deposits in the Ulster basin and the Kish Bank basin. But, the general pattern over Ireland is of weak denudation.

The second cooling event occurred in the Early Cretaceous (figure 8.9). Denudation over most of Ireland during this time is weak, with deposition in central-south the extreme SE and N of Ireland. However, in similar fashion with most of SE Ireland (Leinster Massif), Connemara was also experiencing cooling (denudation) at this time. The implication of deposition in the N and NE of the country is that these sediments have subsequently been eroded prior to the end of the Cretaceous or during the Tertiary. Likewise, the area of deposition in southern Ireland is consistent with thick Lower Cretaceous deposits in the Celtic Sea region.

The third cooling event to effect SE Ireland occurred at the beginning of the Palaeogene (figure 8.10). For the entire island, there are generally areas of localised strong denudation adjacent to areas of weak denudation or subsidence. The centre of Ireland was an area of deposition at this time, possibly from the massifs around the margins, and possibly from the Irish Sea region, i.e. from the putative Irish Sea dome (see Cope, 1994; 1998). This cooling event is consistent with strong denudation of the Irish Sea region (chapter 4) and erosion of the Cretaceous chalks in the Ulster basin. This unconformity can also be traced to most of the basins offshore, i.e. Bristol Channel & Celtic Sea, North Channel & Malin, North Porcupine and Slyne-Erris-Donegal basins (section 1.3).

The final cooling event in SE Ireland began in Late Palaeogene-Neogene times and is reflected in the present-day topography of the region, i.e. the Leinster Mountain chain (see chapter 5). Denudation across the country is very patchy with a predominance of denudation over subsidence during this time period. This is consistent with the widespread occurrence of continental non-marine deposits (Naylor, 1992; Jones & Drew, 2000). However, east-central Ireland experienced weak denudation (figure 8.11) at this time. This may explain the occurrences of Mid to Late Tertiary sediments in the Irish Sea basins, i.e. in the Kish Bank basin there is 381m and 183m of Tertiary-Quaternary sediments preserved in wells 33/17-1 and 33/21-1 respectively (chapter 4).

8.4 Porcupine Basin

The Porcupine basin is the largest of the Irish offshore basins and lies ~150km to 250km west of the Irish mainland. The basin forms a N-S grabenal feature bounded to the north by the Slyne Ridge, to the east by the Irish mainland shelf, and to the west by the Porcupine Ridge (figure 8.12). The basin merges into the Goban Spur basin to the south (chapter 1). The basin mirrors the Porcupine Seabight bathymetric feature with water depths ranging from ~300m in the north to >2000m in the south.

An E-W basement ridge marks the southern boundary of the North Porcupine basin (NPB) and has acted as a transform fault during Tertiary times (Tate, 1993). The NPB is an extension to the Slyne, Erris and Donegal basins, which have evolved as a wrench modified rift system (Tate & Dobson, 1989b). A small NE-SW graben connects the NPB to the Main Porcupine basin (MPB). The basement ridge demarcates the northern limit of significant basin extension in the Porcupine basin, which conform to the general McKenzie (1978) stretching model, showing a typical steers head profile (Croker & Shannon, 1987) from Mid-Jurassic levels.

8.4.1 Methods and Materials

Wells

Six composite well logs were obtained from Total Oil Marine plc and have been logged. These were supplemented with additional published wells and are listed in table 8.1 below. Well logs are summarised in Appendix 7 and are shown on figure 8.13.

Table 8.1

Operator	Well	Year	Latitude	Longitude	RT Elev. (m)	TD (m)	Water Depth (m)
Composite well logs courtesy of Total Oil Marine plc							
BP	26/28-1	1979	53.0414	-12.5586	28	3315	374
Phillips	35/8-1	1978	52.7169	-12.4183	26	4420	430
Shell/Agip	35/13-1	1977	52.5975	-12.4197	24	4405	482
Phillips	35/15-1	1980	52.5825	-12.1120	30	3688	308
Amoco	35/18-1	1988	52.4850	-12.5314	22	3901	566
StatOil	35/19-1	1985	52.4378	-12.2794	26	5552	479
Published Sources							
BP	26/22-1A	1978	53.2269	-12.7078	26	2573	344
Deminex	34/15-1	1977	52.5753	-13.1228	23	4446	482
Elf	35/2-1	1978	52.9756	-12.6131	13	3995	391
Deminex	35/6-1	1978	52.7044	-12.9603	24	3959	486
Phillips	35/8-2	1981	52.7747	-12.4650	86	4633	422
Shell/Agip	35/29-1	1978	52.1139	-12.3078	24	2900	804
Chevron	36/16-1	1979	52.4769	-11.9383	30	2747	250

Seismic Reflection Profiles

Key seismic reflection profiles of the Porcupine basin were obtained from Total Oil Marine's regional database (figure 8.13) using Landmark Seisworks software on a mainframe workstation and are shown in Appendix 8. These lines are still confidential and therefore their designation and precise location are omitted (figure 8.2). However, the lines still serve to highlight the important unconformities, and illustrate the extent of siliciclastic input that probably relate to denudation pulses form onshore areas.

The lines were shot in 1981 and 1993 by Geco-Prakla (UK) Ltd – Schlumberger and HGS – Western Geophysical respectively. The reflection lines have all been migrated

60-fold. The acoustic impedance coefficient on the seismic lines (i.e. measured perpendicular pressure at the hydrophone) is measured in γ (gamma) units, i.e. strong and weak reflectors produce dark blues and reds respectively.

Olivier Wattez (Total Oil Marine geologist) interpreted the stratigraphic horizons shown on the seismic lines and his interpretation for the entire database was used to produce two-way time maps (Appendix 9). The stratigraphic horizons (or piks) selected from the seismic lines to produce the maps are as follows:

Eocene-Oligocene unconformity;
Top Chalk (unconformity);
Mid-Aptian unconformity, and;
Base Cretaceous unconformity.

Certain areas on the Mid-Aptian and base Cretaceous unconformity maps (i.e. in the vicinity of wells 35/8-1 and 35/8-2) had not been interpreted on the individual lines at the time of compilation and are therefore not shown. However, this does not imply that there is no evidence for these unconformities, e.g. well 35/8-2 shows that the Lower Cretaceous is unconformable with the Late Jurassic sequences. Depths on these maps are in two-way time, for example, 800ms to top Chalk represents two-way travel time.

8.4.2 Structure & Stratigraphy

The Porcupine basin has experienced 2 periods of major stretching and 1 final minor rifting episode with phases of subsequent thermal relaxation. Stretching factors in the NPB have values of $\sim\beta = 1.5$ with ~3km of Mesozoic-Tertiary section preserved. In the MPB however, stretching factors are an order of magnitude higher, reaching maximum values of $\beta = 6$ (White *et al.*, 1992; Tate, 1993). There is over 10km of Mesozoic-Tertiary rocks preserved in the MPB. Hence, the tectono-stratigraphy of the Porcupine basin can be sub-divided into pre-rift, syn-rift and post-rift thermal subsidence phases. The three major syn-rift episodes defined by (Sinclair *et al.*, 1994) are (1) the Triassic to

Early Jurassic; (2) Late Jurassic (Tithonian) to Early Cretaceous (Mid-Valanginian); and, (3) the Aptian-Albian.

8.4.2.1 Pre-Rift Rocks

Pre-rift rocks are mostly pre-Hercynian in age (Croker & Shannon, 1987). Devonian to Early Carboniferous rocks were encountered in well 35/15-1 and Upper Carboniferous rocks were cored in wells 26/28-1, 34/15-1, 36/16-1 (Appendix 7). Relatively thin Autunian rocks conformably overlie Stephanian sequences in well 34/15-1, the only occurrence of Permian strata (although see well 35/19-1, Appendix 7) in these wells. The wells are drilled in to footwalls of major ~N-S basin bounding faults. For example, well 35/15-1 encountered Dinantian rocks of the Sinell Horst (footwall) and Mesozoic-Tertiary rocks of St Gobnet's Graben, and well 26/28-1 encountered an ~ E-W fault with the footwall block downthrown to the south.

In well 35/19-1 two layers of halite are sandwiched between Kimmeridgian-Tithonian and Lower-Upper Berriasian mudstones (Appendix 7). It is unlikely that the halite is Upper Jurassic-Lower Cretaceous in age and is probably Permian Zechstein salt which has diapirically moved up to higher stratigraphical levels. This may be due to differential loading and/or extension.

8.4.2.2 Syn-Rift Rocks

The Triassic to Lower Jurassic syn-rift extension primarily inherited NE-SW trending Caledonian structural fabrics. These rocks have only been encountered in the NPB (well 26/22-1A) due to their relative shallowness. The Triassic sequences represent massive sandstone units overlain by evaporite-bearing shale sequences (Appendix 7). Shales, occasional siltstones and interbedded limestones, overlie these.

Most of the drilled wells encounter Mid Jurassic strata, which rests unconformably on older strata (Appendix 7). In well 34/15-1, Middle Jurassic aged sequences rest

unconformably above Stephanian-Autunian sediments. This shows that the adjacent ~ NNE-SSW trending fault was reactivated during Jurassic times and has led to part of the succession being faulted down, preserving a relic Carboniferous basin margin succession in the footwall. Similar Mesozoic reactivation appears to have occurred on E-W trending faults on the southern margin of the NPB. In this case, Middle Jurassic sequences unconformably overlie Westpahlian-Stephanian rocks. Stratigraphical and petrophysical evidence also indicates severe erosion of Lower Jurassic sequences in the NPB. In the NPB and MPB, the erosion is pre-Bajocian. However, regional stratigraphic evidence from the Slyne and Herbrides basins indicates a Toarcian age (Morton, 1987) and represents 'Mid Cimmerian' tectonism.

During Mid-Jurassic times, the extension direction changed from a NE-SW to E-W trend. This led to a re-organisation of structural trends (Shannon, 1991a) and commenced the typical N-S trend that characterises the steer head profile (figure 8.14). Mid-Jurassic strata are widespread in the Porcupine basins with thick Middle-Upper Jurassic sequences preserved in the NPB (Tate, 1993). The rocks are primarily composed of Bathonian to Callovian aged sequences of thin sandstones, siltstones and mudstones with fining upward channel sandstones and fresh-water ostracods. These sequences are particularly thick and shalier in wells 35/2-1 and 34/15-1, indicating more rapid subsidence with less clastic input (Appendix 7).

In Oxfordian-Tithonian times, regional eustatic rise led to a northward propagating diachronous transgressive facies. In the centre of the basin, conglomerates and sandstones from well 35/8-2 contain a range of sediment features indicative of submarine fan deposition. In the north and east, thin sandstone sequences occur in wells 26/28-1 (Tithonian) and 35/19-1 (Berriasan). This is believed to be due to denudation of the Ruadan Ridge (26/28-1) and other upstanding blocks (Tate 1993). Most of the uplifted blocks were completely submerged by Kimmeridgian times and contemporaneous deposition of continental to transitional facies in well 34/15-1 during the Kimmeridgian indicates an uplifted marginal setting (Appendix 7).

Hence, syn-sedimentary growth faults occurred primarily along the basin margins during Tithonian times in response to further rifting (e.g. Appendix 8, line 5). These faults are associated with shallow marine fans and scarp deposits. This is in marked contrast to the basin centre where pulses of sand-rich mass flow deposits interdigitate with deep-water hemipelagic shales.

8.4.2.3 Post-Rift Thermal Subsidence

The beginning of the Cretaceous heralded the onset of post-rift thermal relaxation. Basal Cretaceous units onlap and overstep a basin-wide unconformity that overlies Jurassic fault-rotated blocks. This unconformity is restricted mostly to the basin margins and forms a disconformity in the deeper parts of the basin. Faulting was generally minor during Cretaceous times, albeit, localised alluvial fans towards the basin margins were being deposited due to continued local uplift as a result of on-going 'Cimmerian' tectonics (Croker & Shannon, 1987). In general, Cretaceous sedimentation is strongly transgressive with the exception of a Middle Cretaceous regression, which drowned the supply of siliciclastics.

The onset of sea-floor spreading along the Grand Banks-Iberian and Iberian-Armorican ridges is contemporaneous with a final Aptian-Albian rift phase in the northern part of the MPB. This is manifested as regional unconformities where Mid-Aptian strata are generally absent (Appendix 8). The unconformity has a wide distribution in NW Europe (Tate 1993). The rifting event also coincides with a regressive phase and is responsible for the production of local sand-rich deltas and associated beach complexes.

Late Aptian-Albian regression resulted in southward delta progradation into the NPB and the northern fringe of the MPB. Prodelta siltstones and claystones pass upward to form delta-front sheeted sandstones, typical of high-energy tidal environments. Distributary-channel sandstones in some areas subsequently overlie these sequences, whereas, stacked beach and regressive barrier-island sandstones occur in other areas.

Upper deltaic-plain sequences occur in the NPB with areas of swamp, marsh and distributary channels making up the delta-top sequences. In the MPB, on the other hand, sediments of lower-delta plain inter-distributary bay affinities comprise the delta-top sequences. This is overlain by thick coarsening upward sandstones with transgressive barriers, beach and shoreface sandstones that resulted from deeper marine levels encroaching from the south during late Albian times (Shannon *et al.*, 1993).

Major global transgression (i.e. Haq *et al.,* 1987) commenced in the Upper Cretaceous (Cenomanian), with some re-working of Cretaceous deltaic complexes (Croker & Shannon, 1987). In most of the wells, the Upper Cretaceous-Lower Palaeocene chalk facies appears to have been deposited basinwide (Appendix 7). Up to 500m of Cretaceous chalk was drilled in the NE of the basin (wells 35/8-1 and 35/8-2) and similar amounts locally developed in the NPB (Croker & Shannon, 1987), and seismic evidence suggests up to 1km may occur in the centre of the basin (Appendix 8). The chalk is partially truncated and condensed towards the basin margins, with condensed stratigraphy being deposited on topographic highs. In well 36/16-1, Lower Cretaceous sequences overstep the margins of the Jurassic rift basin and a condensed Cretaceous stratigraphy unconformably rests upon Westphalian C-Stephanian rocks of the Clare basin (e.g. Appendix 8, line5). Seismic lines also show that Late Cretaceous sequences diachronously onlap syn-rift Jurassic strata and overstep the older pre-rift stratigraphy (Appendix 8, line5).

In the north and east of the MPB, chalk depositon is severely attenuated, e.g. Cretaceous chalks are ~6m thick in well 26/28-1. This erosional event is predominantly post-early Cenomian and pre-late Campian and is fairly widespread on the Anglo-Irish seaboard. For example, regional stratigraphic extent shows that the unconformity is similar to that seen in the Western Approaches and Goban Spur basins and the drilled Biscay continental margin (Tate 1993) but is not present in the Donegal and Celtic Sea basins (chapter 1).

8.4.2.4 Tertiary Rocks

Chalk deposition continued into Early Palaeogene (Danian) until a major regression rejuvenated the provenance areas on the basin margins. This in essence instigated a 5-fold increase in sedimentation rates (Tate 1993). In wells 35/13-1 and 35/29-1, thick Tertiary sequences of 2,445m and 2,100m respectively were encountered (Appendix 7), although, seismic evidence implies up to 4,000m may occur down the axis of the MPB (figure.8.15).

Most of the wells in the MPB overlie Danian chalk facies with a marked hiatus. For example, a conglomerate occurs at the boundary between the upper Danian and lower Thanetian in well 35/13-1 (Appendix 7). The break in deposition coincides with a major regressive phase and considerable regional volcanic activity, i.e. Antrim basalts in the Ulster basin (chapter 1). The igneous activity may have produced elevated basal heat flow. But, Green *et al.*, (1999) found no evidence from wells adjacent to the Antrim basalts.

In well 35/15-1, a number of basaltic sills/lavas intrude/cover the relatively condensed Upper Cretaceous Campanian-Maastrichtian strata (Appendix 7). Available lithological data appears to imply sub-aerial weathering has occurred, and hence, differential uplift of this area can be inferred to be lower Palaeocene in age (Roberstons technical report, 1997). The igneous rocks are probably associated with the Brendan Igneous centre to the NW. Further west in well 35/8-1, there is a very thick (174m) Tertiary (*Phillips composite well*) doleritic sill at 3km depth (Appendix 7). This intrudes earlier Aptian-Albian volcangenic ash falls (top) and siltstones (bottom) and produces a strong reflection event on (Appendix 8, line6. Earlier re-worked Barremian volcanogenic deposits also occur in this well (Appendix 7).

8.4.2.5 Palaeogene Deltaic Complexes

The chalk sequences are succeeded by a marly and shaly series and are subsequently over-stepped by a series of major prograding alluvial fans and deltas during the Upper Palaeocene-Eocene. Well 35/13-1 encountered three deltaic complexes of late Palaeocene, early Eocene and mid-to-late Eocene age (Appendix 7) and have been described in detail elsewhere (Tate 1993). The cyclicity has been attributed by many workers (i.e. Croker & Shannon, 1987; Tate, 1993) as various combinations of eustatic changes, uplift of the hinterland and tectonic controls of basin subsidence. These 3 complexes represent significant important influxes of siliciclastics (e.g. Appendix 8, line4).

8.4.3 Late Palaeogene-Neogene Unconformities

In the NPB, the Upper Palaeocene and Lower Eocene are separated by an unconformity that developed in response to major transpressional inversion of the basin axis (Tate, 1993). A basin-wide unconformity occurs at the Eocene-Oligocene boundary, e.g. in well 35/13-1, an unconformity occurs at Unit A (early-lower Miocene) and fresh basaltic lithoclasts were recovered from a conglomerate at this level (Tate, 1990). Previous workers have invoked deep circulation of Arctic waters as a possible mechanism (Tate & Dobson, 1989; Tate 1990; Tate, 1993). This unconformity is hummocky in character and is subsequently onlapped thick successions of deep-water shales and associated channelised sandstones (Appendix 8, lines 3& 7).

8.4.3.1 Syn-Sedimentary Slumps

Deep marine conditions persisted throughout Neogene times as subsidence outpaced sedimentation rates. Submarine canyons developed during the Oligocene (Naylor & Anstey, 1987) and syn-sedimentary slumping (thin-skinned tectonics) along a basinward dipping décollment surface occurred during the Miocene (Moore & Shannon, 1991;

Shannon *et al.,* 1993). The slumps follow a bathymetric gradient, primarily gravity driven and initiated possibly by seismic events (see section 8.4.6).

8.4.4 Magnetic Basement

Aeromagnetic data for the Porcupine basin was interpolated on an existing seismic grid at the offices of Total Oil Marine plc in Aberdeen. The original survey included 62,279km of aeromagnetic data that was flown in 1995 (released by Ark Geophysics Ltd). The flying height was 120m (asl) and data sampling at 0.1 seconds. The levelled magnetic anomaly data was gridded at a pitch of 200m using a continuous curvature spline gridding method and was subsequently reduced-to-pole. The data was acquired in a 500m (E-W) by 200m (N-S) grid and was merged with 9,589km of Texaco data over the Slyne Trough.

Figure 8.16 shows the aeromagnetic map of the area of study, the MPB. Due to the deep waters, the magnetic anomalies are of lower frequency in comparison with the aeromagnetics of the Kish basin (chapter 3). The aeromagnetic anomaly map depicts the general N-S trend of the basin. The negative anomaly increases in intensity towards the south and relatively positive high frequencies occur to the north, east and west. In general, this pattern indicates the depth of magnetic basement, i.e. the areas of positive anomaly depict shallow basement and the negative anomaly represents thick sedimentary sequences. The basin becomes very narrow towards the north (i.e. < 10 km, in vicinity of well 35/18-1 – figure 8.16). The western basin bounding faults show higher gradients (~N-S) than the eastern margin, where the trend changes to ~ENE-WSW and overlies a zone where magnetic basement is relatively shallower, i.e. between wells 35/29-1, 35/19-1 and 35/18-1.

8.4.5 Two-Way Travel Time Maps

Appendix 9 shows a series of two-way travel time maps of the Eocene-Oligocene unconformity (EOU), Top Chalk (unconformity) (TC), the Mid-Aptian unconformity

(MAU) and the base Cretaceous unconformity (BCU). In essence, the reflectors interpreted as being these unconformities are deepest towards the SSE and progressively shallow towards the north, and towards the east and west main basin-bounding faults. In conceptual terms, the geometry mimics the configuration of the magnetic basement (figure 8.16). For example, the central-eastern part of the MPB is distinctly asymmetrical with Mesozoic-Tertiary sequences at shallower depths on a broad platform of ~30km, i.e. between wells 35/18-1 and 35/19-1. This suggests that pre-rift rocks are relatively shallower under this area.

In general, the unconformities are deeper adjacent the eastern basin bounding faults, in comparison with those in the west. For example, the BCU is relatively shallow towards the western margin of the MPB, where it is at depths ranging from ~900 to 2000ms over a distance of ~1.5km. On the eastern and southeastern margin, the BCU is at depths >2000ms adjacent the main basin bounding fault. This suggests either greater deposition in this area or inversion has occurred on the western margin in post-Jurassic times. Tertiary deltaic sediments are reportedly thickest on the eastern margin (c.1400m – Dobson *et al.*, 1991) and therefore, the greater depths of unconformities are due to greater Cenozoic deposition in this part of the basin, implying that the Palaeogene deltaic complexes are sourced from the N. Where coverage is available, the top chalk reflector oversteps the main basin bounding faults and underlies Tertiary sequences at a depth of ~800 to 1800ms, i.e. the NE part of the MPB.

8.4.6 Seismic Reflection Lines

The major faults in the Porcupine basin are mostly oriented ~N-S (McCann *et al.,* 1995). Therefore, those seismic lines oriented E-W tends to show the most faults. Whereas, N-S oriented lines only show small ~E-W faults, which have been described by previous workers as linkage faults (Tate, 1993; McCann *et al.,* 1995).

All the seismic lines show that faulting was extensive during the main rift phases (Upper Jurassic-Lower Cretaceous) with large faults being the most dominant. McCann *et al.*,

(1995) has shown that these syn-tectonic faults form the largest category of faults. A number of the main basin bounding faults display clastic aprons on the tip-lines and a number of the Jurassic faults display reflectors with sigmoidal geometry (Appendix 8, line 4). Many of these Jurassic aged faults conform to the 'soft-domino' model, with rotated Jurassic fault blocks evident on most of the seismic lines.

These rotated Jurassic fault blocks produced palaeotopography, which was onlapped by Lower Cretaceous stratigraphy. This in most cases results in the deposition of a condensed Lower Cretaceous stratigraphy on top of the elevated block (e.g. Appendix 8, line 2, *sp* 11250-11350). During the late Cretaceous, this topography had very little effect on deposition patterns, as the chalk displays relatively uniform thickness over these former palaeo-highs.

Above the top Chalk horizon, there is a fairly uniform package of similar seismic character which on lines 2 and 3 (Appendix 8) attains maximum thickness of ~700ms[TWT]. Based on well data (Appendix 7), this package is likely to represent shales, claystones and siltstones – delta plain facies. A regressional phase produces a relatively strong reflector above this package and heralds the onset of major Palaeocene-Eocene deltaic prograding clinoforms (e.g. Appendix 8, line 2).

The Palaeocene-Eocene deltas comprise of sigmoidal, laterally continuous reflectors that dip basinwards. On line 4 (Appendix 8), 3 deltaic complexes can be seen prograding and thinning out southwards. The Eocene-Oligocene interface forms a disconformity in the south and an angular unconformity in the north. The reflector characteristics are believed to represent a change in depositional environments, from proximal sand-rich prograding deltaic sequences towards more distal mud-rich pro-delta to basinal type. These are superseded by a series of higher amplitude and relatively flat-lying reflectors and correspond with delta-top sequences. On most lines, the deltaic complexes are truncated by the Eocene-Oligocene unconformity, which is hummocky in nature (Appendix 8, line 2).

The Eocene-Oligocene unconformity (Appendices 8 & 9) correlates with the onset of current-controlled sedimentation and hence many previous workers have suggested that this erosion (drift formation) is due to the release of cold Arctic bottom waters (Masson & Kidd, 1986; Tate, 1990). Vigorous bottom water circulation has been cited as the cause of the early Lower Miocene unconformity in the well 35/13-1 (Appendix 7).

Above this unconformity, turbidites and contourite deposition is followed by a number of Neogene mass slump features. These have flowed down Oligocene canyon systems (e.g. Appendix 8, lines 2 and 4) and translate towards the ESE (e.g. Moore & Shannon, 1991, Shannon *et al.,* 1993). These syn-sedimentary slump structures occur above a décollment surface, which propagates southwards. The slump head regions are characterised by extensional features such as tilted blocks whereas the toe regions display listric basinward-dipping faults e.g. Appendix 8, line 4. The slumps tend to occur immediately above a strong reflector. This reflector has an easterly dipping listric geometry beneath the head regions and represents a basal décollement surface (Appendix 8, line 4). A number of slumps appear to be associated with faults (Appendix 8, lines 2, 3, 4 and 7) and McCann *et al.*, (1995) has suggest that minor seismic events on these structures may have acted as triggering mechanisms, a hypothesis which is supported here.

These deposits are subsequently buried by a series of continuous reflectors of probable deep marine facies origin (Appendix 8). Two mounds occur on the seabed on line 4 (Appendix 8). These features are mostly likely to be carbonate mud-mounds as described by Hovland *et al.*, (1995). The seismic character of the reflectors beneath the mounds supports this interpretation, which show velocity pull-up typical of low velocity deposits.

Figure 8.17 shows that the ~N-S extensional faulting was most extensive during Maastrichtian-Danian times. A large number of ~N-S faults were also reactivated during Oligocene times although these mostly occur in the north of the MPB. Likewise, faulting during the Late Aptian is mostly restricted to the north MPB.

The seismic lines (Appendix 8) show that most of the brittle faulting is confined to the Eocene horizon (line 2). McCann *et al.,* (1995) suggested that local stresses probably built up after the cessation of syn-rift faulting and these deviatoric stresses were further exasperated by a combination of thermal subsidence, regional downwarp flexuring and an increase in differential lithostatic stesses. Hence, late-stage brittle faulting relieved the stress. Most of the faults are normal, but some ~E-W linkage structures show some evidence of wrenching (Tate, 1993).

8.5 Tertiary – Sediment Budget

In chapter 7, it was shown that an average of 2,150m of denudation had occurred over SE Ireland during the Tertiary (based on the Laslett *et al.*, (1987) annealing model). This is comparable to a mean of 3,165m for the entire country (figure 8.18). The lowest total denudation occurs in NE Ulster, the Central Midlands and the SW (Counties Cork & Kerry) of the country. The low values over the Ulster basin fit well with the fact that it is the largest part of the country where Mesozoic-Tertiary rocks are preserved. The low denudation values in the Central Midlands coincide with a concentration of small Tertiary deposits derived from boreholes (chapter 1). In essence, the areas of maximum denudation are mostly restricted to the periphery of the country where relief is highest. The total denudation map is also consistent with the VR estimate of ~1.5km of post-chalk denudation from the Ballydeenlea outlier (section 1.2.5).

8.5.1 Denudation Efflux

The denudation rates and sediment volume discharge per 1Myr increment are shown on figure 8.19. These are based on the AFT studies of section 7.4.1 using a time-dependent palaeogeothermal gradient. The total area of denudation in Ireland has varied through time. Therefore, the total cumulative area is integrated with denudation rates to derive the total sediment discharge.

The long-term pattern of denudation rates and volume discharge are moderate in the Jurassic (figures 8.19a & 8.19b), following to a low during the Cretaceous and then progressively increasing throughout the Tertiary. The final part on the denudation curve should be interpreted with caution however due to the problems of the Laslett *et al.*, (1987) annealing model at relatively low-temperatures.

During the Early to Middle Jurassic, denudation rates are ~12m Myr^{-1} and sediment discharge is ~40 x $10^4 km^3$ Myr^{-1} (figure 8.19). Although, higher frequency events (peaks) occur on these background values with denudation rates reaching maximums of 15m Myr^{-1} and sediment discharges of ~55 x $10^4 km^3$ Myr^{-1} occurring in Mid Jurassic times. The Late Jurassic to Early Cretaceous was a period of generally decreasing denudation rates and volume discharges with values of <5m Myr^{-1} and <11 x 10^4 km^3 Myr^{-1} respectively. Although, a relatively high frequency but short-lived event occurs in the Early Cretaceous with denudation rates and volume discharges of ~10m Myr^{-1} and ~ 20 x $10^4 km^3$ Myr^{-1} respectively.

Denudation rates and volume discharges begin to steadily rise through the Late Cretaceous, with a high frequency event in the Maastrichtian-Danian, with values similar to those of the Early Cretaceous peak (figure 8.19). Throughout the Tertiary, denudation rates and volume discharge progressively rise with high frequency events occurring in the Eocene and Oligocene, i.e. maximum denudation rates and sediment discharges of ~32m Myr^{-1} and ~68 x 10^4 km^3 Myr^{-1} respectively. This trend of increasing denudation sediment discharge continues throughout the Tertiary to the present-day, with maximum denudation rates of ~70m Myr^{-1} and sediment discharges of ~130 x 10^4 km^3 Myr^{-1}. Although, the rate of denudation and discharge is an order of magnitude lower for those results based on the Gallagher (*in prep)* annealing model (figure 8.19b), i.e. denudation rates of ~27m Myr^{-1} during late Neogene times.

The low rates of denudation during much of the Cretaceous are due to maximum sea levels at this time. This probably led to the deposition of a chalk mantle over much of the Irish mainland in similar fashion to the observed offshore. This cover was subsequently

removed by Tertiary exhumation (with the exception of the Ulster basin and the Ballydeenlea chalk outlier in Co. Kerry) with insoluble pieces of Cretaceous flint spread across the whole island. In terms of sediment budget analysis, the erosion of chalk does not need to be accounted for in sink areas and vice versa. Denudation peaks in the upper-Early Cretaceous may correspond with a brief regression in the Porcupine basin at this time (Tate 1993).

The main peaks in the denudation rates and volume discharges of sediment occur in the Middle Jurassic, Early Cretaceous, Late Cretaceous-Early Palaeocene, Eocene and Oligocene. These events correlate reasonably well with known unconformities and periods of high siliciclastic input in the Porcupine basin (section 8.4). High rates of denudation during the Tertiary may partly explain the development of thick deltaic complexes. Relatively high rates during the Eocene and Oligocene may explain the development of the Eocene-Oligocene unconformity and the subsequent incision of the Oligocene canyon system that later funnelled mass slumps during Miocene time (Appendices 7 & 8). During the latter part of the Neogene subsidence rates began to outpace sedimentation. Therefore, the influence of the Irish landmass as a provenance has progressively diminished.

8.5.2 Cenozoic Sediment – Porcupine Basin

The total volume of Tertiary solid sediment in the Porcupine basin is estimated to be 54,900±6,300km^3 (Jones unpubl). As figure 8.19 shows, the average denudation rate of Ireland during this time is ~ 40m Myr^{-1}. With a present-day area of ~8,344km^2, this gives a total sediment value of ~ 22,000km^3, about a factor of 3 smaller than the solid volume occupying the Porcupine basin. This is not accounting for the volume of material, which would also have been siphoned off to other basins such as the Rockall, Slyne and Erris Troughs, and the Donegal and Hatton and the North Celtic Sea basins.

Hypothetically, if the volume of Tertiary sediment in the Porcupine basin were solely derived from the Irish mainland, then this would require denudation rates of about 100m

Myr^{-1}, and implies cooling rates of 3-4°C Myr^{-1} for a 30°C km^{-1} palaeogeothermal gradient. All samples would be at temperatures >110±10°C (total annealing) between 30-40Ma. However, none of the samples have apparent AFT central ages of this age (figure 8.3a). Therefore, it is not possible to invoke the current Irish mainland as the sole source region for the Tertiary sediments of the Porcupine basin, particularly since the discharge of clastic sediments will be even smaller than the estimates above due to material being apportioned to other basins (chapter 1).

The time correlation between denudation and deposition therefore needs to be carefully considered in order to refine the spatial links between source areas and sediment delivery. For example, the Early Cretaceous denuded material may have been subsequently drowned, during Late Cretaceous transgression, whilst the clastic load was still being transported to the Porcupine and other basins on the Atlantic seaboard. Hence, when seas regressed at the end of the Cretaceous, this material would then have been re-mobilised to produce Palaeogene deltaic complexes, e.g. the Porcupine basin. Whilst this may go someway in explaining the very large discrepancy in the sediment budget, other source areas are also required.

This leads to another key problem and that is the delineation of catchments feeding the Porcupine and indeed the Rockall, Hatton, Donegal, Slyne and Erris basins during the Tertiary. This is particularly acute because well and seismic data (Appendices 7 & 8) show that the clastic influx was transported in to the system from the north. Hence, it will also be necessary to undertake detailed provenance studies from Tertiary aged cores.

8.6 Palaeotopography Reconstruction

One way to reconstruct and delineate ancient sediment transport systems is to reconstruct palaeotopography. As illustrated in section 7.5, small amounts of tectonic uplift, particularly with pre-existing relief will produce differential erosion. The unloading of the crust results in an isostatic response that produces a positive feedback mechanism with a time-dependent diminishing rate, i.e. the isostatic contribution to total denudation

derived by an initial pulse of tectonic uplift is a factor of 6 greater in magnitude. AFT cooling may be due to a fall in the geothermal gradient or exhumation of overburden. Assuming a time-constant geotherm, unloading or denudation may be set in motion by tectonic or non-tectonic processes. Non-tectonic processes were discussed in section 7.5, e.g. changes in base level, climatic fluctuations etc. Notwithstanding, these external variables should be averaged out for large spatial and temporal areas such as Ireland throughout the Tertiary.

8.6.1 Reconstruction of Tectonics - Boundary Conditions

Palaeotopography reconstructions for the Early Tertiary are based on derived AFT denudation from the Laslett *et al.* (1989) annealing model. A digital elevation model of Ireland, with a cell-size of $1km^2$, represents a smoothed version of the present-day topography. AFT denudation estimates for 66Ma to 10Ma are added back to the topography. The denudation contribution to the topography is subsequently adjusted for isostacy. Eustatic control is derived from the Haq *et al.* (1987) sea-level chart for the Early Tertiary and Late Cretaceous. An estimate of tectonic uplift, which occurred at the beginning of the Palaeogene, is then estimated in order to reduce the landmass below the sea before the regression of Cretaceous seas.

Tectonic uplift can be deduced from denudation by accounting for both isostacy and eustacy. In section 7.5, eustacy was not accounted for in the tectonic uplift model. Haq's global sea-level curve shows, on average, that during the Early Tertiary the sea-level was on average ~220m higher than the present-day. Instead of subtracting this from the tectonic uplift values (i.e. Chadwick's equation), it is more desirable to build in known boundary conditions and further constrain the model, i.e. the present-day topography and the geological record.

Figure 8.20 is a digital elevation model that shows a subdued topography at $1km^2$, which is used below, to model palaeotopography. The present-day topography is a known quantity. The modelled values of total denudation (based on the AFT results) for the

Tertiary has been added back to the topography and isostatically compensated for the extra load.

8.6.2 Isostacy & Eustacy

Figure 8.21 is an estimate of palaeotopography of Ireland for Early Tertiary times (not withstanding the fact that parts of the offshore would also be above sea level). There are a few areas depicted below the present-day sea level without incorporating eustatic sea level changes which were ~220m lower than the present-day. These occur under samples N-1442 (borehole on the Balbriggan block, Co. Meath) and sample SB1 (western margin of Slieve Bloom, Co. Galway). Sample N-1442 is presently at 205m below the surface. Therefore, raising the sample to the present sea level can easily eliminate the area of water. However, sample SB1 appears to have simply undergone net subsidence throughout the Tertiary and hence lowers the palaeotopography below present-day sea levels.

8.6.3 Palaeotopography & Palaeobathymetry

Figure 8.22 shows the effect of incorporating Early Tertiary sea levels based on Haq's *et al.* (1987) global sea-level curve (+220m above present-day sea level) and shows a first-order approximation of what the palaeotopography may have been like during Early Tertiary times as seas were regressing. The topography in Co. Down is too high because the Mourne granites were not emplaced into the crust at this time, and the previous palaeotopography of this area is an unknown quantity. Therefore, areas that are incompatible with the geological record need to be accounted for by invoking tectonic movements. For example, in the Ulster basin, sea-levels appear to be too high because Palaeocene basalts were subaerially erupted on to an eroded karstified chalky limestone topography and were followed by deposition of non-marine Oligocene sediments. Therefore, this area must have subsided in recent times otherwise elevation would be higher to fit with geological constraints.

CHAPTER 9 – SUMMARY OF CONCLUSIONS

9.1 Introduction

Where Mesozoic-Tertiary rocks and deposits occur, there is considerable evidence for periods of uplift and subsidence. This work has shown that this tectonism has affected most of the island, with the exception of the Central Midlands. Periods of denudation represent tectonic events. Early and Late Tertiary denudational events are most likely due to tectonism with NW-SE to NNW-SSE horizontal compression.

9.2 Dextral Transform Hypothesis

The original aim of this thesis was to test a dextral transform model. This model is partly based on an E-W demarcation extending through Dublin and Galway Bays, which marks the northern limits of the offshore extensional basins of the Irish Sea and the Porcupine Trough. Reactivation of Caledonian/Hercynian fractures was predicted and the central part of eastern Ireland was initially selected as a study area.

A review of the existing geological and geophysical literature for central eastern Ireland showed that the major onshore crustal structures consisted of Caledonian folds and shear zones which trend almost E-W at the coast and swing to a NE-SW trend inland. A major gravity high extending from Malahide, north of Dublin, through county Kildare, represents up-folded Precambrian basement plus local centres of Ordovician basaltic volcanic rocks. Hercynian folds and shear zones have an identical orientation to those of the Caledonian basement rock. Clearly Hercynian deformation reactivated the older basement structures. The principal Hercynian structures consist of open-close folds with a wavelength of about 3km with zones of more intense tight chevron folding plus local cleavage adjacent to strike parallel and strike orthogonal Hercynian shear zones. Dextral ductile shearing is characteristic of the strike parallel shear zones and sinistral ductile shear for the orthogonal ones which range in strike from N-S in the east to NW-SE in the

west. Offshore the major structural features have been up to 3km of denudation of the Irish Sea region, which may be due to magmatic underplating producing a dome over the eastern Irish Sea region. Major denudation occurred Early Palaeogene times leaving eroded remnants of Mesozoic extensional basins of the southern Irish Sea area. This was followed by Neogene subsidence of the Irish Sea.

Detailed structural mapping adjacent to the ENE-WSW trending Balscadden Bay fault at Howth showed that the minor folds and anticlockwise transecting cleavage are typical Hercynian ductile structures. They intensify and their strike swings clockwise towards the fault indicating that it had a significant dextral displacement during the Hercynian orogeny. Thin section examination of the fault breccia showed that quartz grains show undulose extinction towards the margins of breccia fragments indicating low temperature cataclastic deformation. Palaeotemperature and geothermal gradient data from the Dublin Basin show that this must be the effect of post-Hercynian re-activation of the fault. East of the prominent fault line escarpment, the fault truncates a westerly draining valley system whose rock sides are red-stained. On the south side of the Howth peninsula, Cambrian greywacke and siltstones are locally weathered to soft red clay beneath a prominent erosion surface. These weathering products have clearly never been deeply buried and are interpreted as the products of Tertiary lateritic weathering. Reactivation of the Balscadden Bay fault is inferred to be of Tertiary age.

Examination of the ENE-WSW trending Southern Boundary fault to the Dublin Basin, near Rathcoole, indicates that the fault shows evidence of syn-depostional displacement during the Visean followed by ductile Hercynian deformation which formed an N-S sinistral shear zone displacing the fault. Post-Hercynian dextral reactivation of the fault is shown by normal (down to the east) displacement on the N-S jog at Rathcoole. Faulting was extensive enough to create secondary porosity in the bedrock with deep water circulation producing low-geothermal springs.

The structures along the northern margin of the Leinster batholith are also compatible with NW-SE compression and NE-SW extension. Cataclastic structures and fault

breccias along this margin shows strained quartz and little to no polygonisation. These fabrics are clearly brittle in nature, and as noted above, this is inconsistent with known palaeotemperatures in the Dublin basin during Hercynian times. The post-Hercynian palaeostress system however coincides with known Hercynian stress systems. Hence, post-Hercynian palaeostress is inferred from strained quartz grains and the lack of polygonisation. This postulate is supported by regional correlation with structural studies in NE Ireland which show that there was a phase of NW-SE compression with NE-SW extension in the Ulster Basin and is contemporaneous with dyke emplacement.

When traced westwards, the ENE-WSW trending Tertiary dextral reverse faults of the Dublin area swing to a NW trend and terminate in horsetail structures where the basement strike changes to a NE-SW trend. Known warm springs are concentrated in this area, where normal displacement would be concentrated. Elevation of bedrock data from boreholes shows considerable variation in this area, however the data is insufficient to establish whether this is due to small down-faulted blocks, karstic weathering or buried river channels.

9.3 Offshore Correlation

Correlation with the Kish basin shows that normal displacement on the Dalkey fault is incompatible with the dextral-reverse movement on the SBF. This indicates that the simple transform model cannot be extended along the northern margin of the Kish basin. A more probable model is a 'trapdoor' pull-apart graben generated on a relay structure within an overall zone of NW-SE dextral strike slip faulting related to the Oligocene-recent Newry – Sticklepath shear system. This relates to NNW-SSE horizontal compression and ENE-WSW horizontal extension which correlates with the youngest shears that cut onshore outcrop at Sorrento Point.

The truncation of the Mesozoic-Tertiary stratigraphy shows that post-Liassic uplift and deformation produced significant denudation. This is most likely to have been related to footwall uplift on major faults, e.g. the NNW-SSE Bray fault displaces the Cambrian by

over 6km. Vitrinite and AFT data indicate that this event probably occurred during the Early Tertiary and may be related to the "Irish Sea Dome". This is supported by the presence of a young palaeo-channel flowing east to west. The onshore projection of the channel correlates with a topographic low (Glencree) or it may possibly be a dextral offset to the Dublin Bay Liffey. The Wicklow High structure was probably conjugate to the Codling Fault zone with a sinistral transpression.

9.4 Onshore Correlation with Geomorphology

Two strands of the Wicklow High fault correlate with the Callowhill and Southeastern Boundary faults onshore. These produce a positive flower structure and sinistral shearing of the Carrig Mountain. Both faults link up with the ECDZ to the south.

The Vartry area is made up of a series of down-faulted tilt-blocks defined by the Vartry and Djouce faults, which parallel the Bray fault. The parallel Kilruddery fault also appears to have a dextral offset with Caledonian strike-swing. Drainage over the tilt-blocks shows marked rejuvenation across the scarps, which is compatible with Neogene movement. The northern boundary of the Vartry block is controlled by sub-parallel NW-SE trending dextral faults with local uplift of the Sugar Loaf-Bray Head block along a restraining bend. The possible onshore continuation of the palaeo-channel from the Kish basin is probably structurally controlled by these faults.

The ECDZ produces a broad zone of uplift in the Bunclody area and forms a postive flower structure. SSE flowing streams draining the Wicklow Massif once crossed the ECDZ and have since reversed and now remain as wind-gaps. The only exception to this is the main Slaney River, which follows a NW-SE trending fault where it cuts a rock gorge through the Tullow Lowland and the Blackstairs Massif and it shows a marked decline in sinuosity. This indicates that the river has had enough power to adjust its course and incision rate in response to recent uplift of the ridge.

The highest mountain in the Blackstairs Massif, Mount Leinster, is clearly not a product of differential erosion because the more resistant inner aureole schists form lower ground than the more erodible granite, which is similar in composition to the granite that underlies the Tullow Lowland. The Tullow Lowland represents an etchplain that has cut across both granite and Lower Carboniferous rocks. Core-stones and tors in the granite and de-dolomites, hums and dolines in the limestones represent features typical of Tertiary weathering. The age of this surface is indicated by the presence of late Miocene to early Pliocene clays in a karstic depression in the limestones at Hollywood. The stream-bed adjustment of the River Slaney as it flows across this surface indicates that there was uplift of the Blackstairs ridge as recently as the Pliocene.

A spectacular WNW-ESE trending escarpment marks the northern margin of the Tullow Lowland. As with the Blackstairs ridge the Baltinglass escarpment shows evidence of uplift over a broad zone in which less powerful south flowing streams have been truncated leaving a series of wind-gaps transecting the ridge. This has resulted in the River Slaney capturing the head-water of these streams to give it sufficient power to cut a rock gorge through the ridge. A reverse dextral sense of slip is inferred for this structure with north side-up. The ridge itself could also be the product of a positive flower structure. The WNW-ESE trending Glen of Imail fault shows similar kinematics to the Baltinglass escarpment. The scooped shape valley of the Glen of Imail is explained by a NNE trending normal fault.

In all three areas of study, detailed topographic analysis of digital terrain models and bedrock geology shows that differential erosion has not been a significant geomorphic factor in the formation of the present-day landscape.

Analysis of LANDSAT lineament patterns confirms the major structural features of the Leinster Mountain chain and suggests a termination of the NW end of the NW-SE trending Glenmalure fracture zone. Measures of entropy and intersection density correlated well with areas of outcrop and strong relief.

9.5 AFT Results – SE Ireland

Detailed analysis of a ~NNE-SSW geological profile and of apatite fission track data along the axis of the Wicklow Massif shows that the surface samples passed through the PAZ during the Early to Mid Tertiary as a coherent block. However, there is evidence of subsequent block faulting on known NW-SE fractures such as the Lough Dan structure. The largest displacement occurs across the Baltinglass escarpment with downthrow to the south. The quantification of denudation along the profile shows that to the south of the Lough Dan fault, the usual situation occurs of relief being positively correlated with erosion. North of the fault, the higher levels of erosion are associated with the lowest elevations. This can be explained by the greater density of fractures in this area probably representing a combination of faulting and higher rates of erosion.

9.6 Regional Implications

In SE Ireland as a whole, AFT data shows that there were 4 major episodes of denudation during Mid-Jurassic, Early Cretaceous, Palaeogene and Neogene times. The same cooling events occur throughout Ireland, with the exception of the Central Midlands plain, which displays weak subsidence during the Tertiary. Much of the Central Midlands plain forms a NNE-SSW axis of old central ages, short MTL, extends across Ireland with an orthogonal axis extending from Wicklow to South Mayo. This probably represents areas of deeper MOHO where the crust has been more stable during the Mesozoic and Tertiary. This may also explain the low relief of the area and hence low denudation rates.

In essence, the cooling events of SE Ireland occurred across the entire landmass and have a reasonable correlation with unconformities, i.e. the Palaeogene in the Ulster Basin, and the Mid-Jurassic (occurs in nearly all the offshore basins), Early Cretaceous, Palaeogene and Neogene unconformities in the Porcupine basin. In the Main Porcupine basin, major periods of extension occurred on N-S faults during the Triassic to Lower Jurassic, Late Jurassic to Early Cretaceous and Aptian-Albian. Post-rift, brittle reactivation of major

basin-bounding faults occurred during the Palaeogene and was followed during the Miocene by major slump structures.

The main periods of denudation onshore and in the Irish Sea region coincides with periods of major clastic input, i.e. delta progradation in the Porcupine basin and Rockall Trough during Late Palaeocene to Mid Eocene related to thermal subsidence of the basins. Sediment discharge from Ireland and adjacent areas has gradually diminished during the latter part of the Tertiary (i.e. Neogene times) as subsidence began to outpace deposition, leading to the present-day bathymetric deep (e.g. the Porcupine Seagbight). The Palaeogene probably represents a first-order regional uplift event resulting in high denudation in areas of moderate to high relief. Subsequent block faulting then occurred in the Neogene, e.g. the Leinster Mountain chain. The lack of denudation of the Central Midlands plain is due to thicker crust and low relief. This area probably acted as a major sediment transport route from east to west across the landmass.

9.7 Sediment Budget Analysis

An apparent mismatch in the Tertiary sediment budget from onshore Ireland to the Porcupine and other basins (particularly the Rockall) implies that the material being transported has to have come from within and beyond the Irish landmass (e.g. the Irish Sea dome). Early Tertiary uplift of the Erris and Slyne Troughs may also have contributed to this. Part of the mismatch may relate to sediment re-mobilisation from earlier periods of denudation, i.e. Mesozoic denudation may have become trapped in the system by the Late Cretaceous global transgression.

9.8 Geodynamics

The major outstanding issue to address is the driving mechanism that created the Tertiary stress systems and uplift and denudation of the crust. The simplest model is that underplating of the crust drove vertical movements by basic magma derived from the Iceland plume. The lesser uplift of NE Ireland could be the result of magma reaching the

surface using the major Caledonian fracture systems as conduits. Neogene subsidence of the Irish Sea could be the result of cooling and increased density of the underplated material. A further product of this would be to cause flexural uplift of the coastal areas such as the Leinster and Welsh Massifs (i.e. rift margins). Similarly, post-Miocene subsidence of the Porcupine Basin and Slyne and Erris Troughs could have caused flexural uplift in Connemara, Mayo and Donegal. This model does not however explain the NW-SE to NNW-SSE horizontal maximum compressions during the Tertiary. This could be the result of ridge-push and/or the effect of horizontal compression developing at the eastern tip of a mushroom shaped top to the Iceland plume. Other more speculative mechanisms could involve the effect of aspirates below the lithosphere, which are suggested by Ireland lying on a positive anomaly of the geoid.

FURTHER WORK

In chapter 5 it was shown that knickpoints are important indicators of changes in base-level. For example, consider an abrupt lowering of baselevel along a river in equilibrium. A wave of incision will propagate upstream from the locus of baselevel change. The adjustment timescale t_a reflects the time necessary for this wave to reach the upstream reaches of the catchment. For times $t < t_a$, the river will appear to be out of equilibrium; a knickpoint will separate reaches of the river that have equilibrated (through incision) from those that have not. For $t > t_a$, the river will be in equilibrium with its new boundary conditions. The presence of knickpoints in the catchments draining the Vartry plateau argues that the most recent baselevel fall must have occurred less than t_a years ago, and the spatial correspondence between the knickpoints and the escarpment implies that the knickpoints have not yet migrated significant distances upstream. However, further work is required to determine t_a, for the Leinster Mountain chain during the past 30 to 60 Myr, i.e. the time lag between uplift and fluvial incision rate. Ideally, this needs to account for climate and eustatic changes, glaciation, and a quantifiable erodibility index for the various lithologies (including other factors, particularly foliation patterns, within the same lithology).

Further work is also required for constraining the low-temperature thermal history of SE Ireland. One potential application is the (U-Th)/He dating of apatite separates. This method has a low temperature sensitivity of 40-75°C. Wolf *et al.*, (1997) has demonstrated that apatite (U-Th)/He ages in the San Jacinto Mountains record geologically useful information (Helium ages are strongly correlated with elevation) and is particularly suited to samples that have cooled slowly.

Finally, the models put forward in this thesis require testing by applying to other areas of moderate topography such as Connemara, Donegal and Munster. Are the same stress systems in SE Ireland also operating in these other areas? What are the relationships to the offshore structures?

REFERENCES

ALLEN, P., CORCORAN, D. & CLAYTON, G. 1999. Conference on Ireland Since the Carboniferous.

ALLEN, P.A. and ALLEN, J.R. 1990. Basin Analysis: Principles and Applications. Blackwell Science, Oxford, 461.

ANGELIER, J. 1989. From orientation to magnitudes in palaeostress determinations using fault slip data. *Journal of Structural Geology*, **11**, 37-50.

ANGELIER, J. 1991. Inversion directe et recherche 4-D, comparaison physique et mathématique de deux modes de détermination des tensuers des paléocontraintes en tectonique de failes. *Comptes Rendus de l'Académie des Sciences, Paris*, **312**, Série II, 1213-1218.

ANDREW, C.J. & ASHTON, J.H. 1982. Mineral textures; metal zoning and ore environment of the Navan Orebody, Co. Meath, Ireland. In: BROWN, A.G. & PYNE, J. (Eds). Mineral Exploration in Ireland Progress and Developments 1971-1981. *Irish Association Economic Geology, Dublin*, 35-46.

ANDREWS, C.J. 1992. Basin development chronology of the lower most Carboniferous strata in the north-Central Midlands. In: BOWDEN, A., EARLS, G.V., O'CONNOR, P. & PAYNE, J. (eds). Irish Association for Economic Geology, Dublin, 143-169.

ANDREW, C. J. & ASHTON, J. H. 1982. Mineral textures; metal zoning and ore environment of the Navan ore body, Co. Meath, Ireland. In: Brown, A. G. (ed), Irish Association for Economic Geology, Dublin, Ireland); *Papers; Mineral exploration in Ireland; progress and developments 1971-1981*, 35-46.

ASHBY, M.F., & VERRALL, R.A. 1973. Diffusion accommodated flow and superplasticity: *Acta Metallurgia et Materialia*, **21**, 149-163.

BALL, V. 1888. On the probable mode of transport of the fragments of granite and other rocks which are found imbedded in the Carboniferous limestone of the neighbourhood of Dublin. *Quarterly Journal of the Geological Society, London, **44***, 371-374.

BARKER, C.E. & PAWLEWICZ, M.J. 1986. The correlation of vitrinite reflectance with maximum temperaute in humic organic matter. In: BUNTERBARTH, G., & STEGENA, L. (eds), Lecture Notes in Earth Sciences, 5, Palaeogeothermics: Berlin, Springer-Verlag, 79-93.

BARKER, A.J. 1998. Introduction to metamorphic textures and microstructures. Second Edition. Stanley Thornes (Publishers) Ltd.

BARR, F.T. 1966. Upper Cretaceous foraminifera from the Ballydeenlea chalk, County Kerry, Ireland. *Palaeonotology*, **9(3)**, p492-510.

BARR, K. W, COLTER, V. S., YOUNG, R. 1981. The geology of the Cardigan Bay-St George's channel basin. In: ILLING, L. V., HOBSON, G. D.(eds). *Petroleum geology of the continental shelf of North-West Europe; Proceedings of the second conference*, 432-443.

BEESE, A. P., BRUECK, P. M., FEEHAN, J., MURPHY, T. 1983. A silica deposit of possible Tertiary age in the Carboniferous Limestone near Birr, County Offaly, Ireland. *Geological Magazin*e, **120**, 331-340.

BOTT, M. H. P. 1964. Gravity measurements in the north-eastern part of the Irish Sea. *Quaterly J of the Geol Soc of Lon,* **v120**, p369-396.

BOTT, M. H. P. & YOUNG, D. G. G. 1971. Gravity measurements in the North Irish Sea. *Quarterly Journal of the Geological Society of London*, v**126**, 413-434.

BOTT, M.H.P. & SMITH, R.A. 1958. The estimation of the limiting depth of gravitating bodies. *Geophysical Prospecting*, **VI**, 1-10.

BRAY, R.J., GREEN, P.F. & DUDDY, I.R. 1992. Thermal history reconstruction using apatite fission track analysis and vitrinite reflectance: a case study from the UK East Midlands and the Southern North Sea. In: HARDMAN, R.F.P. (ed), Exploration Britain: Geological Insights for the Next Decade. *Geological Society of London Special Publication*, **No.67**, 3-25.

BRENCHLEY, JP.J., HARPER, J.C. & SKEVINGTON, D. 1967. Lower Ordovician shelly and graptolitic faunas from south-eastern Ireland. *Proceedings of the Royal Irish Academy*, **65B**, 385-390.

BREWER, J. A., MATHEWS, D. H., WARNER, M. R., HALL, J., SMYTHE, D. K. & WHITTINGTON, R. J. 1983. BIRPS deep seismic reflection studies of the British caledonides. *Nature*, **v305**, 206-210

BRIGGS, D.J. 1991. CORINE; a European environmental information system and its relevance to Quaternary science. Quaternary Research Association annual discussion meeting, *Quaternary Newsletter*, **63**, 8.

BRINDLEY, J.C. 1954a. Some cataclastic features of the Leinster Granite and their mechanical significance. *The Science Proceedings of the Royal Dublin Society*. **v26**.

BRINDLEY, J.C 1954b. *Prooceedings of the Royal Irish Acadamy*, **56B**, 159.

BRINDLEY, J.C. 1956. The geology of the northern end of the Leinster Granite: Part II – Structural features of the country rocks. *Proceedings of the Royal Irish Academy*. **v58**,

BRINDLEY, J.C. 1957. The Blackrock Granite-Breccia, Co.Dulbin – an interpretation. *The Science Proceedings of the Royal Dublin Society.* v27.

BRINDLEY, J.C. & CONNOR, B.P. 1972. The minor acid intrusions of the Aughrim-Ballinaclash area, Co. Dublin. *Proceedings of the Royal Irish Academy*, **72B**, 165-183.

BRINDLEY, J.C., MCARDLE,P., SCHIENER, E.J. (1973). The Lower Palaeozoic volcanic rocks of SE Leinster, Ireland. *Scientific Proc. R. Dublin Society, 4A,* pp431-438.

BRODIE, J. & WHITE, N. 1995. The link between sedimentary basin inversion and igneous underplating. In: BUCHANAN, J.G. & BUCHANAN, P.G. (Eds). Basin Inversion. *Geological Society of London Special Publication*, **No.88**, 21-38.

BROUGHAN, F.M., NAYLOR, D., ANSTLEY, N.A. 1989. Jurassic rocks in the Kish Bank Basin. *Irish J of Earth Sciences,* **v10**, 99-106.

BROWN, C. & BROCK, A. 1983. A computer based study of the regional gravity and magnetic fields in Ireland and their relationship to areas of possible geothermal interest. *A.G.R.* **83/4**. *Report Series.* Applied Geophysics Unit, University College Galway.

BROWN, C., WILLIAMS, B. 1985. A gravity and magnetic interpetation of the structure of the Irish Midlands and its relation to ore genesis. *Journal of Geological Society of London,* **v142**, 1059-1075.

BROWN, C. 1991. Backstacking apatite fission track stratigraphy: a method for resolving the erosional and isostatic rebound components of tectonic uplift histories. *Geology*, **19**. 74-77.

BROWN, R. W., SUMMERFIELD, M.A., GLEADOW, A. J.W. 1994. Apatite fission track analysis: it's potential for the estimation of denudation rates and implications for models of long-term landscape development. *Process Models and Theoretical Geomorphology*, 24-53.

BRÜCK, P.M. & O'CONNOR, P.J. 1977. The Leinster batholith: geology and geochemistry of the northern units. *Geological Survey of Ireland Bulletin,* **v2**, 107-141.

BRÜCK, P.M. 1968. The geology of the Leinster Granite in the Enniskerry-Lough Dan area, Co. Wicklow. *Proceedings of the Royal Irish Academy*, **65B**, 53-70.

BRÜCK, P.M. 1972. Stratigraphic and sedimentology of the Lower Palaeozoic greywacke formations in Counties Kildare and west Wicklow, *Proceedings of the Royal Irish Academy*, **72B**, 25-54.

BRÜCK, P.M. 1974. Granite varieties and structures of the Northern and Upper Liffey Valley units of the Leinster batholith. *Geological Syurvey of Ireland Bulletin*, **1**, 381-393.

BRÜCK, P.M., POTTER, T.L., & DOWNIE, C. 1974. The Lower Palaeozoic stratigraphy of the northern part of the Leinster Massif. *Proceedings of the Royal Irish Academy*, **74 B**, 75-84.

BRÜCK, P.M. & O'CONNOR, P.J. 1977. The Leinster batholith: geology and geochemistry of the northern units. *Geological Survey of Ireland Bulletin*, **2**, 107-141.

BRÜCK, P.M. & O'CONNOR, P.J. 1980. Major transverse and other linears in the Leinster Granite. *Geological Survey of Ireland Bulletin*, **2**, 349-370.

BRÜCK, P.M. & O'CONNOR, P.J. 1981. Relationship of hydrothermal phenomena within the Leinster Granite to crustal fractures delineated from Landsat imagery. *Photogrammeria*, **37**, 151-159.

BRÜCK, P.M., POTTER, T.L. & DOWNIE, C. 1974. The Lower Palaeozoic stratigraphy of the northern part of the Leinster Massif. Proceedings of the Royal Irish Academy, **74, SectB**, 73-84

BRÜCK, P.M. & REEVES, T.J. 1976. Stratigraphy, sedimentology and structure of the Bray Group in Co. Wicklow and South Co. Dublin. *Proceedings of the Royal Irish Acadamey*, **76 B**, 53-79.

BRÜCK, P.M. & REEVES, T.J. 1983. The geology of the Lugnaquillia pluton of the Leisnter batholith. *Geological Survey of Ireland Bulletin*, **3**, 97-106.

BRÜCK, P.M. COLHURST, J.R.J., FEELY, M., GARDINER, P.R., PENNY, S.R., REEVES, T.J., SHANNON, P.M., SMITH, D.G. & VANGUESTAINE, M. (1979). South-East Ireland: Lower Palaeozoic stratigraphy and depositional history. In: HARRIS, A.L. , HOLLAND, C.H. & LEAKE, B.E. (Eds). The Caledonides of the British Isles - reviewed. *Geological Society of London Special Publication*, **8**, 533-544.

BRÜCK, P.M. & REEVES, T.J. 1983. The geology of the Lugnaquilla pluton of the Leinster batholith. *Geological Survey of Ireland Bulletin*, **3**, 97-106.

BULAT, J. & STOKER, S.J. 1987. Uplift determination from interval velocity studies, UK, southern North Sea. *In:* BROOKS, J. & GLENNIE, K.W. (Eds), *Petroleum Geology of Northwest Europe*. Graham & Trotman, London, 293-305.

BURBANK, D.W., MEIGS, A. & BROZOVIC, N. 1996. Interactions of growing folds and coeval depositional systems. *Basin Research*, **8**, 199-224.

BURDON, D.J. & BURNS, D.J. 1983. Final Report of the Irish Geothermal Project, Phase 1. Unpublished. Minerex Limited.

BURNHAM, A. K.& SWEENEY, J.J. 1989. A chemical kinetic model of vitrinite maturation and reflectance. *Geochimica et Cosmochimica Acta,* **53**, 2649-2657.

BUTTERWORTH, P., HOLBA, A., HERTIG, S., HUGHES, W. & ATKINSON, C. 1999. Jurassic non-marine source rocks and oils of the Porcupine Basin and other North Atlantic margin basins. *In*: FLEET, A.J. & BOLDY, S.A.R (eds). *Petroleum Geology of Northwest Europe: Proceedings of the 5th Conference*, 471-486. Geological Society, London.

BYERLEE, J.D. 1978. Friction of rocks: Pure and Applied. *Geophysics*, **116**, p615-626.

CAPEWELL, J.G. 1956. The stratigraphy, structure and sedimentation of the Old Red Sandstone of the Comeragh Mountains and adjacent areas, Co. Waterford, Ireland. *Quarterly Journal of the Geological Society, London*, **112**, 393-412.

CHARLESWORTH, J.K. 1953. Historical geology of Ireland. Olivor & Boyd, Edinburgh, 565.

CARLSON, W.D. 1990. Mechanisms and kinetics of apatite fission track annealing. *Am. Mineral*, **78**, 213-215.

CARRUTHERS, R.M., CORNWELL, J.D., TURNBULL, G., WALKER, A.S.D. & BENNETT, J.R.P. 1987. Interpretation of the Bouguer gravity anomaly data for Northern Ireland. *Regional Geophysics Research Group, British Geological Survey,* **No. RG 87/5**.

CARTER, N.L., CHRISTIE, J.M. & GRIGGS, D.T. 1964. Experimental deformation and re-crystallisation of quartz. *Journal of Structural Geology*, **72**, 687-733.

CHADWICK, R.A. 1985. Permian, Mesozoic and Cenozoic structural evolution of England and Wales in relation to the principles of extension and inversion tectonics. In: WHITTAKER, A. (ed), Atlas of onshroe sedimentary basins in England and Wales: Post Carboniferous tectonics and stratigraphy, 9-25. Blackie, London.

CLAYTON, G., SEVASTOPULO, G.D. & SLEEMAN, A.G. 1986. Carboniferous (Dinantian and Sileisan) and Permo-Triassic rocks in south County Wexford, Ireland. *Geological Journal*, **21**, 355-374.

CLAYTON, G., HAUGHEY, N., SEVASTOPULO, G.D. & BURNETT, R.D. 1989. Thermal maturation levels in the Devonian and Carboniferous rocks in Ireland. *Special Publication of the Geological Survey of Ireland*, 36.

CLIFT, P.D., CARTER, A. & HURFORD, A.J. 1998. The erosional and uplift history of NE Atlantic passive margins: constraints on a passing plume. *Journal of the Geological Society, London*, **155**, 787-800.

COHEN, J. M. 1979. Deltaic sedimentation in glacial Lake Blessington, County Wicklow, Ireland. In: SCHLUECHTER, C. (ed). Moraines and varves; origin, genesis, classification. 357-367.

COLE, G.A.J. 1922. Some features of the Armorican (Hercynian) folding in Southern Ireland. *Report of the Thirteenth International Geological Congress*, Belgium, 423-433.

COLE, G.A.J, & HALLISSY, T. 1924. The Wexford gravels and their bearing on interglacial geology. *Geological Magazine*., N.S., Dec, 6, **1**, 498-509.

COLLER, D.W. 1984. Variscan structures in the Upper Palaeozoic rocks of west central Ireland. In: HUTTON, D.W. & SANDERSON, D.J. (eds). Variscan Tectonics of the North Atlantic Region. *Geological Society of London Special Publication*, **14**, 185-194.

COOK, D.R. 1987. The Goban Spur. Exploration in a deep water frontier basin. In: BROOKS, J. & GLENNIE, K.W. (Eds), *Petroleum Geology of North West Europe*. Graham & Trotman, London, 623-632.

COPE, J.C.W. 1994. A latest Cretaceous hotspot and the southeasterly tilt of Britain. *Journal of the Geological Society, London*, **151**, 905-908.

COPE, J.C.W. 1998. The Mesozoic and Tertiary history of the Irish Sea. In: MEADOWS, N.S., TRUEBLOOD, S.P., HARDIMAN, M. & COWAN, G. (eds). Petroleum Geology of the Irish Sea and Adjacent Areas. In:, *Geological Society Special Publication* **124**, 47-59.

CORCORAN, D. & CLAYTON, G. 1999. Interpretation of vitrinite reflectance profiles in sedimentary basins onshore and offshore Ireland. In: CROKER, P.F. & O'LOUGHLIN, O. (Eds), Petroleum Exploration of Ireland's Offshore Basins. *Extended Abstracts from Conference*, 8-11.

CORRIGAN, J. 1991. Inversion of fission track data for thermal history information. *Journal of Geophysical Research*, **96**, 10347-60.

COULOMB, C.A. 1773. Sur une application des regles de maximus et minimis a quelques problemes de statique relatifs a l'architecture. *Academie Royale des Sciences, Memoires de Mathematique et de Phsique par divers Savants*, **7**, p343-382.

COUPEZ, Y. 1984. Structural analysis of Lower Carboniferous rocks of Malahide and Howth harbour and study of north County Dublin (Eire) by remote sensing. Unpublished Ph.D. thesis, University of Dublin, Trinity College & Universite Libre de Bruxelles.

COWAN, D. R. & COWAN, S. 1993. Separation filtering applied to aeromagnetic data. In: ODINS, J. A. & FACER, R. A. (eds). *Conference papers from the ASEG 10th geophysical conference and exhibition*, Exploration Geophysics, **24**, 429-436.

COX, A., and HART, R. 1986. Plate tectonics; how it works: Blackwell Scientific Publications, London, 392.

COXON, P., FLEGG, A. 1985. A middle Pleistocene interglacial deposit from Ballyline, Co. Kilkenny. *Proceedings of the Royal Irish Academy, Section B: Biological, Geological and Chemical Science.* **85**, 107-120.

COXON, P. and COXON, C. 1997. A pre-Pliocene or Pliocene land surface in County Galway, Ireland. In: Widdowson, M. (ed.). Palaeosurfaces: Recognition, Reconstruction and Palaeoenvironmental Interpretation. *Geological Society Spec. Pub* **No. 120**, 37-55.

CROKER, P. & SHANNON, P.M. 1987. The evolution and hydrocarbon prospectivity of the Porcupine Basin, Offshore Ireland. In: BROOKS, J. & GLENNIE, K. (eds). *Petroleum Geology of North West Europe.* 633-642.

CROKER, P. 1995. New images of the Codling fault. Abstracts from Irish Geological Research Meeting.

CROKER, P. 1997. Lough Beltra Cruise Report – Irish Sea Investigations 14th-16th April 1997. Petroleum Affairs Division, Dublin.

CROKER, P. 1995. New images of the Codling fault. Abstracts from Irish Geological Research Meeting.

CROKER, P. & SHANNON, P.M. 1995. The Petroleum of Ireland's Offshore basins. In: CROKER, P.F. & SHANNON, P.M. (Eds), The Petroleum Geology of Ireland's Offshore Basins. *Geological Society Special Publication* **No.93**, 1-7.

DAVIES, G.L. 1960. The age and origin of the Leinster mountain chain: a study of the evolution of south-eastern Ireland from the Upper Palaeozoic to the Later Tartiary. *Proceedings of the Irish Royal Academy*, **v61**, 79-107.

DAVIES, G.L. 1966. Cyclic surfaces in the Roundwood Basin, county Wicklow. *Irish Geographer*, **5**, 150-160.

DAVIES, G.L. 1970. The enigma of the Irish Tertiary. *In:* STEPHENS, N. & GLASSCOCK, R.E. (Eds) *Irish Geographical Studies*. Belfast, Queen's University, 1-16.

DAVIES, H.D. & REYNOLDS, S.J. 1996. Structural Geology of Rocks and Regions. Second Edition. John Wiley & Sons, Inc, 241.

DAVIES, G.L. & STEPHENS, N. 1978. Ireland. Methuen, London.

DEWEY, J.F. & MCKERROW, W.S. 1968. Geomorphology of NW Galway. *Geological Magazine*, **100**, 260-275.

DEWEY, J.F. & WINDLEY, B.F. 1988. Palaeocene-Oligocene tectonics of NW Europe. In: MORTON, A.C. & PARSON, L.M. (eds). Early Tertiary Volcanism and the Opening of the NE Atlantic. *Geological Society of London Special Paper,* **No.39**, 25-31.

DEWEY, J.F. 2000. Cenozoic tectonics of western Ireland. *Proceedings of the Geologists Association*, **111**, 291-306.

DICKEN, A.P. 1988. The North Atlantic Tertiary Province. In: MACDOUGALL, J.D. (ed). Continental Flood Basalts, 111-149.

DOBSON, M.R. 1977. The history of the Irish Sea Basins. In: KIDSON, C & TOOLEY, M.J. (eds). The Quaternary history of the Irish Sea. Geological Journal Special Issue, No.7. Seel House Press, Liverpool, 93-98.

DOBSON, M.R., WHITTINGTON, R.J. 1979. The Geology of the Kish Bank Basin. *Journal of the Geological Society, London,* **136**, 243-249.

DOBSON, M.R., HAYNES, J.R., BANNISTER, A.D., LEVENE, D.G. PERIE, H.S. & WOODBRIDGE, R.A. 1991. Early Tertiary palaeoenvironments and sedimentation in the NE Main Porcupine Basin (well 35/13-1), offshore western Ireland – evidence for global change in the Tertiary. *Basin Research,* **3**, 99-117.

DORÉ, A.G., LUNDIN, E.R., JENSEN, L.N., BIRKELAND, Ø., ELIASSEN, P.E. & FICHLER, C. 1999. Principal tectonic events in the evolution of the northwest European Atlantic margin. *In*: FLEET, A.J. & BOLDY, S.A.R (eds*). Petroleum Geology of Northwest Europe: Proceedings of the 5th Conference*, 41-61. Geological Society, London.

DRAFT DEVELOPMENT PLAN REVIEW 1990. Dun Laoghaire Corporation (1:5,000).

DREW, D.P. 1982. Observations on the origin of the Newcastle 'channel' and its infill material. Unpublished Report for AMI.

DREW, D.P. & JONES, G.Ll. 2000. Post-Carboniferous pre-Quaternary karstification in Ireland. *Proceedings of the Geological Association.* **111**, 345-353.

ELLIS, M.A., DENSMORE, A.L. & ANDERSON, R.S. 1999. Development of mountainous topography in the Basin Ranges, U.S.A. *Basin Research*, **11**, 21-41.

ETU-EFEUTOR, J.D. 1976. Geology of the Kish Bank Basin. *Journal of the Geological Society, London,* **132**, 708.

EVANS, A. & CLAYTON, G. 1998. The geological history of the Ballydeenlea Chalk Breccia, County Kerry, Ireland. *Marine and Petroleum Geology*, **15**, 299-307.

FARRINGTON, A. 1926. The topographical features of the granite-schist juncion in the Leinster chain. *Proceedings of the Royal Irish Academy*, **XXXVVII**, 181-192.

FARRINGTON, A. 1934. The Glaciation of the Wicklow Mountains. *Proceedings of the Royal Irish Academy*, **XLII**, 173-209.

FARRINGTON, A. & MITCHELL, G.F. 1973. *Irish Geographer*, 6, 543-560.

FERNANDES, P. M. C. 2000. Investigation of the stratigraphy, maturation and source-rock potential of Carboniferous black shales in the Dublin basin. Unpublished thesis, University of Dublin.

FITZGERALD, P.B., SORKHABI, R.B., REDFIELD, T.F., STUMP, E. 1995. Uplift and denudation of the central Alaska Range: a case study in the use of apatite fission track thermochronology in determine absolute uplift parameters. *Journal Geophysical Research*, **70**, 1497-502.

FLEGG, A.M. & O'CONNOR, P.J. 1995. Kildare-Wicklow – Sheet 16. Geological Survey of Ireland, 1:100,000 solid bedrock series.

FLETCHER, T.P. 1977. Lithostratigraphy of the Chalk (Ulster White Limestone Formation) in Northern Ireland. *Report, Institute of Geological Sciences, London,* 77/24.

FREEMAN, T.W. 1960. Ireland. 2nd Editon, London.

GALBRAITH, R.F., LASLETT, G.M. 1993. Statistical models for mixed fission track ages. *Nuclear Tracks*, **21**, 459-470.

GALLAGHER, K., HAWKESWORTH, C.J. & MANTOVANI, M.S.M. 1994 Denudation, fission track analysis and the long-term evolution of passive margin topography: application to the southeast Brazilian margin. *Journal of South American Earth Sciences*, **8**, 65-77.

GALLAGHER, K. 1995. Evolving temperature histories from apatite fission-track data. *Earth and Planetary Science Letters*, **136**, 421-435.

GALLAGHER, K., BROWN ,R. & JOHNSON, C. 1998. Fission track analysis and its applications to geological problems. Annual Reviews Earth Planet Science, 519-571.

GAMBLE, J.A., WYSOCZANSKI, R.J. & MEIGHAN, I.G. 1999. *Journal of the Geological Society, London*, **156**, 291-299.

GARDINER, P.R.R. & VISSCHER, H. 1971. The Permian-Triassic sequence at Kingscourt, Ireland. *Nature*, **299**, 209-210.

GERRARD, A.J. 1988. Rocks and landforms. Unwin Hyman Ltd, London.

GEOFFROY, L., BERGERAT, F. & ANGELIER, J. 1996. Brittle tectonism in relation to the Palaeogene evolution of the Thulean/NE Atlantic domain: a study in Ulster. *Geological Journal*, **31**, 259-269.

GEORGE, T.N. 1967. Landform and structure in Ulster. *Scottish Journal of Geology*, **3**, 413-448.

GIBSON, D., MCCORMICK AG., MEIGHAN R.D,I. And HALLIDAY, A.N. 1987. The British Tertiary Igneous Province: young Rb-Sr ages for the Mourne Mountain granites. *Scottish Journal of Geology*, **23**, 221-225

GIBSON, D., LUX, D. R. & MEIGHAN, I.G. 1995. New $^{40}Ar/^{39}Ar$ ages for the Mourne Mountians Granites, North East Ireland. *Journal of the Geological Society, London*, **149**, 93-106.

GILL, W.D. 1962. The Variscan fold belt in Ireland. In: COE, K. (Ed.), *Some Aspects of the Variscan Fold Belt*. Manchester University Press, 49-64.

GLEADOW, A.J.W., DUDDY, I.R., GREEN, P.F., LOVERING, J.F. 1986. Confined track lengths in apatite: a diagnostic tool for thermal history analysis. *Contributions to Mineralogy and Petrology*, **94**, 405-15.

GLENNIE, K. W. 1990. Introduction to the petroleum geology of the North Sea. *3rd Edition*.

GREEN, P.F. 1988. The relationship between track shortening and fiision track age reduction in apatite: combined influences of inherent instability, annealing anisotropy, length bias and system calibration. *Earth and Planetary Science Letters*, **89**, 335-352.

GREEN, P.F. 1989. Thermal and tectonic history of the East Midlands Shelf (onshore UK) and surrounding regions assessed by apatite fission track analysis. *Journal of the Geological Society, London*, **146**, 755-773.

GREEN, P.F., DUDDY, I.R., BRAY, R.J. & LEWIS, C.L.E. 1993. Elevated palaeotemperatures prior to Early Tertiary cooling throughout the UK region: implications for hydrocarbon generation. In: PARKER,J.R (Ed), *Petroleum Geology of NW Europe. Proceedings of the 4th Conference.* Geological Society of London, 1067-1074.

GREEN, P.F., DUDDY, I.R., BRAY, R.J. 1997. Variation in thermal history styles around the Irish Sea and adjacent areas: implications for hydrocarbon occurrence and tectonic evolution. In: Meadows, N.S., Trueblood, S.P., Hardman, M. & Cowan, G. (eds). Petroleum geology of the Irish Sea and adjacent area. *Geological Society Special Publication* **No. 124**, 73-93.

GREEN, P.F., DUDDY, I.R., HEGARTY, K.A. & BRAY, R.J. 1999. Early Tertiary heat flow along the UK Atlantic margin and adjacent areas. In: FLEET, A.J. & BOLDY, S.A.R. (eds), *Petroleum Geology of Northwest Europe: Proceedings of the 5th Conference*, 349-357.

GRIFFITH, A.E., LEGG, I.C. & MITCHELL, W.I. 1987. Mineral Resources. In: BUCHANAN, R.H. & WALKER, B.M. (eds). *Province, City and People: Belfast and its Region,* 43-58. Greystone Books, Belfast.

HALL, J., BREWER, J., MATHEWS, D. & WARNER, M. 1984. Crustal structure across the Caledonides from the 'WINCH' seismic reflection profile: influences on the evolution of the Midland Valley of Scotland. *Transactions of the Royal Society of Edinburgh: Earth Sciences,* **75**, 97-109.

HARLAND, W. B., 1971. *Tectonic transpression in Caledonian Spitsbergen. Geological Magazine*, **108**, 27-41.

HAQ, B. U., HARDENBOL, J., VAIL, P. R. 1987. Chronology of fluctuating sea levels since the Triassic, Science, **235**, 1156-1167.

HAUGHEY, N. 1987. Vitrinite reflectance data from the Upper Palaeozoic rocks of Ireland, with particular reference to the Silesian coalfields. Unpublished Ph.D. thesis, University of Dublin.

HIGGS, K., BEESE, A. P. 1986. A Jurassic microflora from the Colbond Clay of Cloyne, County Cork. *Irish Journal of Earth Sciences*, **7**, 99-109.

HIGGS, K.T. and JONES, G.Ll. 1998. Palynological evidence for Mesozoic karst at Piltown, County Kilkenny. In: *Ireland Since the Carboniferous: A 300 Million Year Enigma*, Handbook, Conference at Ulster Museum, Belfast, 9-10 September 1998.

HILLIS, R.R. 1991. Chalk porosity and Tertiary uplift, Western Approaches Trough, SW UK and NW French continental shelves. *Journal of the Geological Society, London.* **148**, 669-671.

HILLIS, R R. 1992. A two-layer lithospheric compressional model for the Tertiary uplift of the southern United Kingdom. *Geophysical Research Letters*, **19**, 573-576.

HILLIS, R.R. 1995. Regional Tertiary exhumation in and around the United Kingdom. In: BUCHANAN, J.G. & BUCHANAN, P.G. (Eds). Basin Inversion. *Geological Society of London Special Publication*, **No.88**, 167-190.

HITZMAN, M. W. 1992. Bedrock geological map of the Carboniferous of Central Ireland. 1:100,000 scale map series, sheet 15. Chevron Mineral Corporation of Ireland and Ivernia West plc.

HOLLAND C. 1972. The Geology of Ireland. Scottish Academic Press, Edinburgh.

HOVLAND, M., CROKER, P.F., MARTIN, M. 1995. Fault-associated seabed mounds (carbonate knolls?) off western Ireland and north-west Australia. *Marine and Petroleum Geology*, **11**, 232-246.

HULL, E. 1878. The physical geology and geography of Ireland. London.

HURFORD, A.J. 1990a. International Union of Geological Sciences Subcommission on Geochronology recommendation for the standardization of fission track dating calibration and data reporting. *Nuclear Tracks,* **17**, 233-36.

HURFORD, A.J. 1990b. Stanrdization of fission-track dating calibration: recommendation by the Fission Track Working Group of the IUGS Subcommission on Geochronology. *Chemical Geology*, **80**, 171-178.

HUTCHINSON,M.F. 1988. Calculation of hydrologically sound digital elevation models. Third International Symposium on Spatial Data Handling, Sydney. Columbus, Ohio: International Geographical Union.

HUTCHINSON,M.F. 1989. A new procedure for gridding elevation and stream line data with automatic removal of spurious pits. *Journal of Hydrology*, **106**, 211-232.

HUTTON, D.H.W., REAVY, R.J. 1992. Strike-slip tectonics and granite petrogenesis. *Tectonics,* **v11**, 960-67.

ILLING, L.V. & GRIFFITH, A.E. 1986. Gas prospects in the Midland Valley of Northern Ireland. In: BROOKS, J., GOFF, J.C., & VAN HOORN. (eds). Habitant of Palaeozoic Gas in NW Europe. *Geological Society of London Special Publication*, **No.23**, 73-84.

ISACKS, B., OLIVER, J., AND SYKES, L.R., 1968. Seismology and the new global plate tectonics. *Journal of Geophysical Research,* **73**, 5855-5899.

JACKSON, J S. 1965. The upper Carboniferous (Namurian and Westphalian) of Kingscourt, Ireland. *The Scientific Proceedings of the Royal Dublin Society. Series A*, **2** 131-152.

JACOB, A.W.B., KAMINSKI, W., MURPHY, T., PHILIPS, W.E.A., PRODEHL, C. 1985. A crustal model for a NE/SW profile through Ireland. *Tectonophysics,* **113**, 75-103.

JAPSEN, P. 1993. Influence of lithology and Neogene uplift on seismic velocities in Denmark: implications for depth conversion of maps. *American Association of Petroleum Geologists Bulletin*, **77**, 194-211.

JAPSEN, P. 1997. Regional Neogene exhumation of Britain and the western North Sea. *Journal of the Geological Society, London*, **154**, 239-247.

JARVIS, G.T. & MCKENZIE, D.P. 1980. Sedimentary basin formation with finite extension rates. *Earth & Planetary Science Letters*, **48**, 42-52.

JENNER, J.K. 1981. The structure and stratigraphy of the Kish Bank Basin. In: Illing, L.V. and Hobson, G.D. (eds). Petroleum Geology of the Continental Shelf of NW Europe. Heydon, London, 426-431.

JOHNSTON, J.D., COLLER, D., MILLAR, G. & CRITCHLEY, F. 1996. Basement structural controls on Carboniferous-hosted base metal mineral deposits in Ireland. In: STORGEN, P., SOMERVILLE, I.D. & JONES, G.L (eds). Recent advances in Lower Carboniferous geology. *Geological Society Special Publication* **No. 107**, 1-21.

JONES, G.L.I. & HURLEY, H.R. 1983. Preliminary progest report P.L.s 1602, 5, 6, 9 & 1610, Clane, Cos Kildare & Dublin. Unpublished report for AMI.

JONES, R.R., HOLDSWORTH, R.E. & BAILEY, W. 1997. Lateral extrusion in transpression zones: the importance of boundary conditions. *Journal of Structural Geology*, **19**, 1201-1217.

JUKES, J.B. 1862. On the mode of formation of some of the river valleys in the south of Ireland. *Quarterly Journal of the Geological Society, London,* **18**, 378-403.

JUKES, J.B. & DU NOYER, G.V. 1869. Explanations to accompany sheets 121 and 130 of the maps of the geological survey of Ireland. Department of Agriculture and technical instruction for Ireland, HMSO, Dublin.

KEAREY, P. & BROOKS, M. 1984. An introduction to geophysical exploration, 2nd Edition, p.201. Blackwell Science.

KEELEY, M.L., LEWIS, C.J., SEVASTOPULO, G.D., CLAYTON, G. & BLACKMORE, R. 1993. Apatite fission track data from southeast Ireland: implications for post-Variscan burial history. *Geological Magazine*, **130**, 171-176.

KEELEY, M.L. 1995. New evidence of Permo-Triassic rifting, onshore southern Ireland, and its implications for Variscan structural inheritence. In: BOLDY, S.A.R. (Ed.), Permian and Triassic rifting in NW Europe. *Geological Society Special Publication* **91**, 239-253.

KEELEY, M.L. 1996. The Irish Variscides: problems, perspectives and some solutions. Terra Nova, 8, 259-269-.

KENNAN, P. S., PHILLIPS, W. E. A., STROGEN, P. 1979. Pre-Caledonian basement to the paratectonic Caledonides in Ireland. HARRIS, A. L., HOLLAND, C. H. & LEAKE, B. E. (eds). The Caledonides of the British Isles; reviewed. *Geological Society of London Special Publication* **No. 8**, 157-161.

KERR, I. 1987. Basement/cover structural relationships in the North Antrim area, Ireland. Unpublished Ph.D. thesis, Queens University Belfast.

KERRICH, R., BECKINSALE, R.D. & DURHAM, J.J. 1977. The transition between deformation regimes dominated by intercrystalline diffusion and intracrystalline creep evaluated by oxygen isotope thermometry. *Tectonophysics*, **38**, 241-257.

KING, G. & ELLIS, M. 1990. The origin of large local uplift in extensional regions. *Nature*, **348**, 20-27.

KNIPE, R.J. 1989. Deformation mechanisms; recognition from natural tectonites. *Journal of Structural Geology*, **11**, 127-146.

LAMPLUGH, G.W., KILROE, J.R., MCHENRY, A., SEYMOUR, H.J. & WRIGHT, W.B. 1903. The geology of the country around Dublin. *Memoir of the Geological Society of Ireland*, **112**, 160.

LASLETT, G.M., GREEN, P.F., DUDDY, I.R. & GLEADOW, A.J.W. 1987. Thermal annealing of fission tracks in apatite, 2: A quantitative analysis. *Chemical Geology*, **65**, 1-13.

LEE, M.J., PHARAOH, T.C., SOPER, N.J. 1990. Structural trends in Central Britain from images of gravity and aeromagnetic fields. *Journal of the Geological Society, London,* **147**, 241-255.

LEEDER, M.R. 1982. Upper Palaeozoic basins of the British Isles Caledonide inheritance verus Hercynian plate margin processess. *Journal of the Geological Society, London,* **139**, 471-91.

LEWIS, C.L.E., GREEN, P.F., CARTER, A., HURFORD, A.J. 1992. Elevated K/T palaeotemperatures throughout NW England: 3km of Tertiary origin? *Earth and Planetary Science Letters,* **112**, 131-145.

LUTZ, T.M. & OMAR, G.I. 1991. An inverse method of modelling thermal histories from apatite fission-track data. *Earth Planet Scince Letters*, **104**, 181-95.

MACDONALD, H., ALLAN, P.M. & LOVELL, J.P.B. 1987. Geology of oil accumulation in Block 26/28, Porcupine Basin, Offshore Ireland. In: BROOKS, J. & GLENNIE, K. (eds). *Petroleum Geology of North West Europe*, 643-651.

MAKRIS, J., GINZBURG, A., SHANNON, P.M., JACOB, A.W.B., BEAN, C.J. & LIEBE, T. 1991. A new look at the Rockall Region, offshore Ireland. *Marine and Petroleum Geology*, **8**, 410-416.

MANCKTELOW, N.S., GRASEMANN, B. 1997. Time dependent effects of heat advection and topography on cooling histories during erosion. *Tectonophysics*, **270**, 167-95.

MASSON,D.G. & KIDD, R.B. 1986. Revised Tertiary seismic stratigraphy of the Southern Rockall Trough. *Inst. Rep. Deep-sea drill progr,* **48**, 1117-1126.

MAX, M.D. & INAMDAR, D.D. 1983. Detailed compilation magnetic map of Ireland and a summary of its deep geology. *Geological Survey of Ireland Report Series* **83/1**.

MAX, M.D., RYAN, P.D. & INAMDAR, D.D. 1983. A magnetic deep structural geology interpretation of Ireland. *Tectonics*, **2**, 431-451.

MAX, M.D., BARBER, A.J. AND MARTINEZ, J. 1990. Terrane assemblage of the Leinster Massif, SE Ireland, during the Lower Palaeozoic. *Journal of the Geological Society of London.* **v147**, 1035-1050.

MCCABE, A.M. 1985. Glacial Geomorphology. In: EDWARDS, K.J. & WARREN, W.P (eds). The Quaternary History of Ireland, 67-93. Academic Press Inc. (London).

MCARDLE, P. & KENNEDY, M.J. 1985. The East Carlow Deformation Zone and its regional implications. *Geological Survey of Ireland Bulletin*, **3**, 237-255.

MCARDLE, P., GARDINER, P.R.R., FEELY, N. & COLTHURST, J.R.J. 1987. A possible eastern extension of the East Carlow Deformation Zone: a preliminary note. *Geological Survey of Ireland Bulletin*, **4**, 63-66.

MCCAFFREY, R.J. & MCCANN, N. 1992. Post-Permian basin history of northeast Ireland. In: PARNELL, J. (Ed), The Petroleum Geology of Ireland's Offshore Basins. *Geological Society Special Publication* **No.62**, 277-290.

MCALISTER, J.J. & SMITH, B.J. 1997. Geochemical trends in Early Tertiary palaeosols from northeast Ireland: a statistical approach to assess element behaviour during weathering. In: WIDDOWSON, M. (ed): Palaeosurfaces: recognition,

reconstruction and palaeoenvironment intrpretation. *Geological Society Special Publication* **No. 120**, 57-66.

MCCANN, N. 1988. An assessment of the subsurface geology between Magilligan Point and Fair Head. Northern Ireland. *Irish Journal of Earth Sciences,* **9**, 71-78.

MCCANN, N. 1990. The subsurface geology between Belfast and Larne, Northern Ireland. *Irish Journal of Earth Sciences,* **10**, 157-173.

MCCANN, T., SHANNON, P.M. & MOORE, J.G. 1995. Fault styles in the Porcupine Basin, offshore Ireland: tectonic and sedimentary controls. In: CROKER, P.F. & SHANNON, P.M. (Eds), The Petroleum Geology of Ireland's Offshore Basins. *Geological Society Special Publication* **No.93**, 371-383.

MCCONNELL, B., PHILCOX, M.E., MACDERMOT, C.V. & SLEEMAN, A.G. 1995. Geology of Kildare-Dublin, Sheet 16, 1:100,000 scale map series. Geological Survey of Ireland.

MCCULLOCH, A.A. 1993. Apatite fission track results from Ireland and the Porcupine basin and their significance for the evolution of the North Atlantic. *Marine and Petroleum Geology*, **10**, 572-590.

MCCULLOCH, A.A. 1994. Low temperature thermal history of eastern Ireland: effects of fluid flow. *Marine and Petroleum Geology*, **11**, 389-399.

MCGEARY, S., CHEADLE, M.J., WARNER, M.R. & BLUNDELL, D.J. 1987. Crustal structure of the continental shelf around Britain derived from BIRPS deep seismic profiling. In: BROOKS, J. & GLENNIE, K.W. (eds). *Petroleum Geology of North West Europe*. Graham & Trotman Ltd., London, 33-41.

MCKENZIE, D. 1978. Some remarks on the development of sedimentary basins. *Earth & Planetary Science Letters*, **40**, 25-32.

MEIGHAN, I.G., GIBSON, D., GAMBLE, J.A. & GRAHAM, I.J. 1988. Rb-Sr isotopic determinations and the timing of Tertiary Cenbtral Complex magmatism in NE Ireland. In: MORTON, A.C. & PARSON, L.M. (eds). Early Tertiary Volcanism and the opening of the NE Atlantic. *Geological Society, London, Special Publications*, **39**, 349-360.

MEIGHAN, I.G., GAMBLE, J.A. & WYSOCZANSKI, R.J. 1999. New U-Pb (SHRIMP) zircon ages for Tertiary igneous rocks. Abstracts: *The North Atlantic Igneous Province: Magmatic Controls on Sedimentation, London*, 23.

MENPES, R.J. & HILLS, R.R. 1995. Quantification of Tertiary exhumation from sonic velocity data, Celtic Sea/Southwestern approaches. In: CROKER, P.F. & SHANNON, P.M. (Eds), The Petroleum Geology of Ireland's Offshore Basins. *Geological Society Special Publication* **93**, 321-322.

MENZIES, M., GALLAGHER, K., YELLAND, A. & HURFORD, A. J. 1997. Volcanic and nonvolcanic rifted margins of the Red Sea and Gulf of Aden: crustal cooling and margin evolution in Yemen. *Geochimca et Cosmochimica Acta*, **61**, 2511-2527.

MILLER, G. 1990. Fracturing in the NW Carboniferous basin, Ireland. Unpublished Ph.D. thesis, Queens University Belfast.

MILLSON, J.A. 1987. The Jurassic evolution of the Celtic Sea basins. In: BROOKS, J. & GLENNIE, K.W. (eds). *Petroleum Geology of North West Europe*. Graham & Trotman Ltd., London, 599-610.

MITCHELL, G. F. 1977. Periglacial Ireland. *Philosophical Transactions of the Royal Society of London, Series B: Biological Sciences,* **280**, 199-209.

MITCHELL, G.F. 1980. The search for Tertiary Ireland. *Journal of Earth Science, Royal Dublin Society*, **3**, 13-33.

MITCHELL, G.F. 1981. In: HOLLAND, C.H. (ed), The Geology of Ireland, 231-272. Scottish Academic Press, Edinburgh.

MITCHELL, G.F. 1985. The preglacial landscape. In: EDWARDS, K.J. & WARREN, W.P (eds). The Quaternary History of Ireland, 18-37. Academic Press Inc. (London).

MITCHELL, G.F. & RYAN, M. 1997. Reading the Irish Landscape. Dublin, Town House.

MOHR, O.C. 1900. Welche Umstande bedingen die Elastizitatsgrenze und den Bruch eines Materials. *Zeitschrift der Vereines Deutscher Ingenieure*, **44**, 1524-1530 and 1572-1577.

MONTGOMERY, H.B.S. 1864-1867. On a new locality of granite in limestone near Rathfranham. *Journal of the Royal Geological Society, Ireland*, **1**. 15-16.

MOORE, J.G. & SHANNON, P.M. 1991. Slump structures in the Late Tertiary of the Porcupine Basin, offshore Ireland. *Marine and Petroleum Geology*, **8**, 184-197.

MORRIS, P. & MAX, M.D. 1995. Magnetic crustal character in Central Ireland. *Geological Journal,* **30**, 49-67.

MORLEY, C.K. 1995. Developments in the structural geology of rifts over the last decade and their impact on hydrocarbon explotation. In: Lambiase, J.J (Ed.). Hydrocarbon habitat in rift basins. *Geological Society Special Publication* **No. 80.** 1-32.

MORTON, N. 1987. Jurassic subsidence history in the Hebrides, NW Scotland. *Marine and Petroleum Geology,* **4**, 226-242.

MURDOCH, L.M., MUSGROVE, F.W., & PERRY, J.S. 1995. Tertiary uplift and inversion history in the North Celtic Sea basin and its influence on source rock maturity. In: CROKER, P.F. & SHANNON, P.M. (Eds), The Petroleum Geology of Ireland's Offshore Basins. *Geological Society Special Publication* **93**, 297-320

MURPHY, T. 1952. Measurement of gravity in Ireland – gravity study of Central Ireland. *Dublin Institute of Advanced Studies, Memoirs*, **3**, 31.

MURPHY, T. 1974. Gravity anomaly map of Ireland. *Communications of the Dublin Institute for Advanced Studies, Bulletin*, **32**.

MURPHY, T. 1962. Some Unusual Low Bouguer Anomalies of Small Extent in Central Ireland and Their Connection with Geological Structure. *Geophysical Prospecting,* **vX**

MURPHY, T. 1989. Gravity Anomaly Map. Communications of the Dublin Institute for Advanced Studies, Series D, *Geophysical Bulletin No.38.*

MURPHY, N.J., SAUER, M.J. & ARMSTRONG, J.P. 1995. Toarcian source rock potential in the North Celtic Sea Basin, offshore Ireland. In: CROKER, P.F. & SHANNON, P.M. (eds), The Petroleum Geology of Ireland's Offshore Basins. *Geological Society Special Publication* **No.93**, 193-207.

MUSGROVE, F.W., & MITCHENER, B. 1996. Analysis of the pre-Tertiary rifting history of the Rockall Trough. *Petroleum Geoscience*, **2**, 353-360.

MUSSET, A.E., DAGLEY, P. & SKELHORN, R.R. 1988. Time and duration of activity in the British Tertiary Igneous Province. In: MORTON, A.C. & PARSON, L.M. (eds). Early Tertiary Volcanism and the Opening of the NE Atlantic. *Geological Society of London Special Publication,* **No.39**, 337-348.

NAYLOR, D. 1992. Post-Variscan history of Ireland. In: PARNELL,J.R. (Ed.), Basins of the Atlantic Seaboard: Petroleum Geology, Sedimentology and Basin Evolution. *Geological Society of London Special Publication*, **62**, 255-275.

NAYLOR, D. & ANSTEY, N.A. 1987. A reflection seismic study of the Porcupine Basin, offshore west Ireland. *Irish Journal of Earth Science*, **8**, 187-210.

NAYLOR, D., HAUGHEY, N., CLAYTON, G. & GRAHAM, J.R. 1993. The Kish Bank Basin, offshore Ireland. In: PARKER,J.R (Ed), *Petroleum Geology of NW Europe. Proceedings of the 4th Conference.* Geological Society of London, 845-855.

NAYLOR, D. & SHANNON, P.M.1982. The geology of offshore Ireland and west Britain. *Graham & Trotman Ltd*, London.

NICHOLSON, G. E. 1986. Wrench model for east side of southern San Joaquin Valley. *AAPG Bulletin*, **70**, 475

NOLAN, S.C. 1986. The Carboniferous geology of the Dublin area. Unpublished Ph.D. thesis, University of Dublin, Trinity College.

O'CONNOR, P.J. & BRÜCK, P.M. 1978. Age and origin of the Leinster granite. *Journal of Earth Science, Royal Dublin Society*, **1**, 105-113.

O'CONNOR, P.J, KENNAN, P.S. & AFTALION, M.A. 1988. New Rb-Sr and U-Pb ages for the Carnsore Grantie and their bearing on the antiquity of the Rosslare Complex, southeastern Ireland. *Geological Magazine*, **125**, 25-29.

O'CONNER, P.J., AFTALION, M. & KENNAN, P.S. 1989. Isotopic U-Pb ages of zircon and monazite from the Leinster Granite, southeast Ireland. *Geological Magazine*. **126**, 725-728.

O'DRISCOLL, D., HOLCOMBE, B.B., ROSE, P.T. & JONES, D.J. 1995. Cretaceous and Tertiary unconformities in the Atlantic Margin basins. In: CROKER, P.F. & SHANNON, P.M. (Eds), The Petroleum Geology of Ireland's Offshore Basins. *Geological Society Special Publication* **No.93**, 341-342.

O'REILLY, B.M., SHANNON, P.M. & VOGT, U. 1991. Seismic studies in the North Celtic Sea Basin: implications for basin development. *Journal of the Geological Society, London,* **148**, 191-195.

O'REILLY, B.M., READMAN, P.W. & MURPHY, T. 1996. The gravity signature of Caledonian and Variscan tectonics in Ireland. *Physical Chemical Earth*, **21**, 299-304.

O'SULLIVAN, P.B. & PARRISH, R.R. 1995. The importance of apatite compositon and single-grain ages when intrpreting fission track data from plutonic rocks; a case study from the Coast Ranges, British Columbia. *Earth Planet Sci. Lett,* **132**, 213-24.

OHMORI, H. 1983. A three-dimensional model for the erosional development of mountain on the basis of relief structure, *Japanese Geomorphological Union*, **4**, 107-120.

OUCHI, S. 1985. Response of alluvial rivers to slow active tectonic movements. *Geological Society of America Bulletin*, **96**, 504-515.

PARKES, M.A. & PALMER, D.C. 1994. The stratigraphy and palaeontology of the Lower Palaeozoic Kildare Inlier, Co. Kildare, Ireland. *Irish Journal of Earth Science.*

PARNELL, J., SHUKLA, B. & MEIGHAN, I.G. 1988. The lignite and associated sediments of the Tertiary Lough Neagh Basin. *Irish Journal of Earth Science*, **10**, 67-88.

PENN, I.E. 1981. Larne No. 2 Geological well completion report. *Report of the Institute of Geological Sciences, London*, 81/6.

PETRIE, S.H., BROWN, J.R., GRANGER, P.J. & LOVELL, J.P.B. 1989. Mesozoic History of the Celtic Sea basins. In: TANKARD, A.J. & BALKWILL, H.R. (eds). Extensional tectonics and stratigraphy of the North Atlantic margins. *American Association of Petroleum Geologists, Memoir,* **46**, 433-444.

PHILLIPS, W.E.A., STILLMAN, C.J. & MURPHY, T. 1976. A Caledonian plate tectonic model. *Journal of the Geological Society, London,* **132**, 579-609.

PHILLIPS, W.E.A. & HOLLAND, C.H. 1981 Late Caledonian deformation. In: HOLLAND, C.H. (ed). The geology of Ireland, 147-172. Scottish Academic Press, Edinburgh.

PRICE, L. C. 1983. Geologic time as a parameter in organic metamorphism and vitrinite reflectance as an absolute paleogeothermometer, *Journal of Petroleum Geology*, **6**, 5-38.

READMAN, P.W., O'REILLY, B.M. & SANKEY, M.J. 1995. A gravity map of Ireland and surrounding waters. In: CROKER, P.F. & SHANNON, P.M. (Eds), The Petroleum Geology of Ireland's Offshore Basins. *Geological Society Special Publication* **93**, 9-16.

READMAN, P.W., O'REILLY, B.M. & MURPHY, T. 1997. Gravity gradients and upper-crustal tectonic fabrics, Ireland. *Journal of the Geological Society, London*, **154**, 817-828.

REYNOLDS, G. 1980. The influence of glacial overburden on geo-electrical prospecting in Ireland. *Trans. Instn Min. Metall.*, **89**, B44-B49.

REID, R.E.H. 1971. The Cretaceous rocks of North-Eastern Ireland. *Irish Naturalists Journal*, **7**, 105-139.

RINGROSE, P.S. & MIGON, P. 1997. Analysis of digital elevation data for the Scottish Highlands and recognition of pre-Quaternary elevated surfaces. In: WIDDOWSON, M.

(ed): Palaeosurfaces: recognition, reconstruction and palaeoenvironment interpretation. *Geological Society Special Publication* **No. 120**, 25-35.

ROBERT, P. 1980. The optical evolution of kerogen and geothermal histories applied to oil and gas exploration. *Kerogen; insoluble organic matter from sedimentary rocks*, 385-414.

ROBERTS, D.G., GINZBURG, A., NUNN, K. & MCQUILLIN, R. 1988. The structure of the Rockall Trough from seismic refraction and wide-angle reflection measurements. Nature, 332, 632-634.

ROBERTS, D.G. 1989. Basin inversion in and around the British Isles. In: COOPER, M.A. & WILLIAMS, G.D. (Eds), Inversion Tectonics, *Geological Society Special Publication* **44**, 131-150.

ROHRMAN, M. & VAN DER BEEK, P. 1996. Cenozoic postrift domal uplift of North Atlantic margins: an asthenospheric diapirism model. *Geology*, **24**, 901-904.

ROHRMAN, M., VAN DER BEEK, P., ANDRIESSEN, P. & CLOETINGH, S. 1995. Meso-Cenozoic morphotectonic evolution of southern Norway: Neogene domal uplift inferred from apatite fission-track thermochronology. *Tectonics*, **14**, 704-718.

ROTHERY, D.A. & PHILLIPS, W.E.A. 1983. A report on the structure of the Clane block of licenses (P.L.s 1602, 5, 6, 9, 10), Co. Dublin.

ROTHERY, E. 1988. Transpression in the Variscan foreland: a study in East-Central Ireland. *Irish Journal of Earth Science*, **10**, 1-12.

ROWELL, P. 1995. Tectono-stratigraphy of the North Celtic Sea Basin. In: CROKER, P.F. & SHANNON, P.M. (Eds), The Petroleum Geology of Ireland's Offshore Basins. *Geological Society Special Publication* **No.93**, p101-137.

ROWLEY, E. & WHITE, N. 1998. Inverse modelling of extension and denudation in the East Irish Sea and surrounding areas. *Earth and Planetary Science Letters*, **161**, 57-71.

SANDERSON, D.J., ANDREWS, J.R., PHILLIPS, W.E.A. & HUTTON, D.H.W. 1980. Deformation studies in the Irish Caledonides. *Journal of the Geological Society, London*, **137**, 289-302.

SANDERSON, D.J., MARCHINI, W.R.D. 1984. Transpression. *Journal of Structural Geology*, **v6**, 449-458.

SANDWELL, D.T. & SMITH, H.F. 1995. Marine gravity anomaly from satellite altimetry, version 2. The geological data center, Scripps Institute of Oceanography, La Jolla, CA 92093. Anonymous FTP: baltica.ucsd.edu.

SCHUMM, S.A. & CHORLEY, R.J. 1966. Talus weathering and scarp recession in the Colorado Plateaus. *Geomorphology*, **10**, 11-36.

SCHUMM, S.A. 1986. Alluvial river response to active tectonics. In: *Studies in Geophysics: Active Tectonics*. Washington, National Academy Press, 80-94.

SCOTCHMAN, I. C. & THOMAS, J. R. W. 1995. Maturity and hydrocarbon generation in the Slyne Trough, northwest Ireland. In: CROKER, P.F. & SHANNON, P.M. (Eds), The Petroleum Geology of Ireland's Offshore Basins. *Geological Society Special Publication* **93**, 385-412.

SEVASTOPULO, G.D. 1981. Lower Carboniferous. In: HOLLAND, C.H. (ed). The geology of Ireland, 147-172. Scottish Academic Press, Edinburgh.

SIMMS, M.J. 1998. Sub-basalt paaeokarst and its implications for the Tertiary history of northeast Ireland. In: *Ireland Since the Carboniferous: A 300 Million Year Enigma*, Handbook, Conference at Ulster Museum, Belfast, 9-10 September 1998.

SHANNON, P.M. 1991a. The development of Irish offshore sedimentary basins. *Journal of the Geology Society, London*, **148**, 181-189.

SHANNON, P.M. 1991b. Tectonic framework and petroleum potential of the Celtic Sea, Ireland. *First Break*, 9, p107-122.

SHANNON, P.M., JACOB, A.W.B., MAKRIS, B., O'REILLY, B., HAUSER, F. & VOGT, U. 1995. Basin development and petroleum prospectivity of the Rockall and Hatton region. In: CROKER, P.F. & SHANNON, P.M. (Eds), The Petroleum Geology of Ireland's Offshore Basins. *Geological Society Special Publication* **93**, 435-457.

SHANNON, P.M., MOORE, J.G., JACOB, A.W.B. & MAKRIS, B. 1993. Cretaceous and Tertiary basin development west of Ireland. In: PARKER, J.R. (Ed.), Petroleum Geology of Northwest Europe: Proceedings of the 4th Conference. The Geological Society, London, 1057-1066.

SINCLAIR, I.K., SHANNON, P.M., WILLIAMS, B.P.J., HARKER, S.D. & MOORE, J.G. 1994. Tectonic control on sedimentary evolution of three North Atlantic borderland Mesozoic basins. *Basin Research*, **6**, 193-217.

SMITH, I.F. & EDWARDS, J.W.F. 1997. Colour shaded relief gravity anomaly map of Britain, Ireland and adjacent areas. British Geological Survey, 1: 1 500 000 series.

SMITH, R.A. 1986. Permo-Triassic and Dinantian rocks of the Belfast Harbour Borehole. *Report of the British Geological Survey*, **18**, No. 6.

SMITHSON, F. 1928. Geological studies in the Dublin district: II. The problem of Carrickgollogan. *Geological Magazine*, **65**, 78-87.

SMITHSON, F. 1932. The petrography of the Northern portion of the Leinster granite. *Geological Magazine*, **69**, 465-474.

SMYTH, D. 1989. Rockall Trough - Cretaceous or Late Palaeozoic? *Scottish Journal of Geology*, **25**, p5-43.

SOLLAS, W.J. 1889. *Proc. Geol. Assn.*, **13**, 91.

SOLLAS, W.J., 1889. *Trans. Royal Irish Acadam*, **29**, 427.

SRIVASTAVA, S.P. & VERHOEFF, J. 1992. Evolution of Mesozoic sedimentary basins around the North Central Atlantic: a preliminary plate kinematic solution. In: PARNELL,J.R. (Ed.), Basins of the Atlantic Seaboard: Petroleum Geology, Sedimentology and Basin Evolution. *Geological Society of London Special Publication*, **No.62**, 397-420.

STAMP, L.D. 1949. Britains structure and scenery. London.

STEPHENS, W.E. 1988. Granitod plutonism in the Caledonian orogen of Europe. In: Harris, A.L. and Fetteer, D.J. (eds). The Caledonian-Appalachian orogen. *Geological Society London Special Publication* **38**, 389-403.

STEWART, J.H. 1978. Basin-Range Structure in western North America. In: SMITH, R.B. and EATON, G.P: (eds). Cenozoic Tectonics and Regional Geophysics of the Western Cordillera. *Geological Society of American Memoir,* **v152**, 1- 32.

STILLMAN, C.J., BRÜCK, P.M., GARDINER, P.R.R., MAX, M.D. 1978. Field guide to the Caledonian and Pre-Caledonian rocks of SE Ireland. *Geological Survey of Ireland, Guide Series No.2.*

STROGEN, P. 1973. Brecciated lavas from Co. Limerick, Ireland, and their signficance. *Geol. Mag,* **v110**, 351-64.

STOKER, M.S. 1997. Mid- to late-Cenozoic sedimentation on the continental margin off NW Britain. *Journal of the Geological Society, London*, **154**, 509-515.

SUMMERFIELD, M. 1991. Global Geomorphology. Longman Scientific & Technical.

SWEENEY, J. & BURNHAM, A.K. 1990. Evaluation of a simple model of vitrinite reflectance based on chemical kinetics. *AAPG Bulletin*, **74**, 1559-1570.

SWEETMAN, T.M. 1987. The geochemistry of the Blackstairs unit of the Leinster granite, Ireland. *Journal of the geological society, London*, **144**, 971-984.

SYNGE, F.M. 1979. In: MCNABE (ed). Field guide to East Central Ireland, 40-48. *Quaternary Research Association, Dublin.*

TATE, M.P. 1990. Structural framework and tectono-stratigraphic evolution of the Porcupine Seabight Bsin, offshore western Ireland. PhD thesis, University ofAberystwyth.

TATE, M.P. 1993. Structural framework and tectono-stratigraphic evolution of the Porcupine Seabight Basin, offshore western Ireland. *Marine and Petroleum Geology*, **10**, 95-123.

TATE, M.P. & DOBSON, M.R. 1989. Late Permian to early Mesozoic rifting and sedimentation offshore NW Ireland. *Marine and Petroleum Geology*, **6**, p49-59.

TCHALENKO, J.S. 1970. Similarities between shear zones of different magnitudes. *Geological Society of America Bulletin*, **81**, 1625-1639.

THOMPSON, S.J. 1979. Preliminary report of the Ballymacilroy No. 1 borehole, Ahoghill, Co. Antrim. *Geological Survey of Northern Ireland, Open File Report* **63**.

THOMPSON, P. 1985. Dating the British Tertiary Igneous Province in Ireland by the $^{40}Ar/^{39}Ar$ stepwise degassing method. *Unpublished PhD Thesis*, University of Liverpool.

TRUEBLOOD, S. 1992. Petroleum geology of the Slyne Trough and adjacent basins. In: PARNELL,J.R. (Ed.), Basins of the Atlantic Seaboard: Petroleum Geology, Sedimentology and Basin Evolution. *Geological Society of London Special Publication*, **No.62**, 315-326.

TRUEBLOOD, S. & MORTON, N. 1991. Comparative sequence stratigraphy and structural styles of the Slyne Trough and Herbrides Basin. *Journal of the Geological Society, London*, **148**, 197-201.

TUCKER, R.M. & ARTER, G. 1987. The tectonic evolution of the North Celtic Sea and Cardigan Bay basins with special reference to basin inversion. *Tectonophysics*, **137**, 291-307.

TURNER, J.P. 1997. Strike-slip reactivation in the Cardigan Bay basin. . *Journal of the Geological Society, London*, **154**, 5-8.

TURNER, J.P. & PHILLIP, D.W. 1998. Tertiary exhumation of the Irish Sea Basins: results from sonic velocities. Tectonic Studies Group Conference, University of St Andrews, 84.

VAIL, P.R., MITCHUM, JR, R.M., TODD, R.G., WIDMIER, J.M., THOMPSON, S., SANGREE, J.B., BUBB, J.N., & HATFIELD, W.G. 1977. Seismic stratigraphy: application to hydrocarbon exploration. *AmericanAssociation of Petroleum Geologists Memoir*, **26**, 42-212.

VAN LUNSEN, H.A. & MAX, M.D. 1975. The geology of Howth and Ireland's Eye, Co. Dublin. *Geological Journal*. **v10**, 35-58.

VERMEULEN, N.J., SHANNON, P.M., MASSON, F. & LANDES, M. 1999. Mesozoic-Cenozoic reactivation of Caledonian and Variscan basement structures onshore and offshore southern Ireland. In: CROKER, P.F. & O'LOUGHLIN, O. (Eds), Petroleum Exploration of Ireland's Offshore Basins. *Extended Abstracts from Conference*, 46-48.

VOGT, U. 1995. The transition between the Erris and the Rockall basins: new evidence from wide-angle seismic data. *Tectonophysics*, **241**, 143-163.

VORJLIK, P., DONELICK, R.A., QUENG, J. & CLOOS, M. 1992. Testing models of fission track annealing in apatite in a simple thermal setting: site 800, leg 129. *Proceedings of Ocean Drilling Program, Scientific results.* Ed. R. LARSON, Y., LANCELOT, A., FISHER, L. ABRAMS, R., 129, 169-76. College Station, TX: Ocean Drill Prog.

WAGNER, G.A., JAGER, E. 1977. Cooling ages derived by apatite fission track, mica Rb-Sr and K-Ar dating: the uplift and cooling hisotry of the Central Alps. *Mem. Inst. Geol. Mineral Univ.* Padova, **30**, 1-27.

WALLACE, R. E. 1978. Geometry and rates of change of fault-generated range fronts, North-central Nevada, *Journal of Research of the U. S. Geological Survey,* **6**, 637-649.

WALSH, P.T. 1966. Cretaceous outliers in South West Irealnd and their implications for Cretaceous palaeogeography. *Quarterly Journal of the Geological Society of London,* **122**, 63-84.

WARREN, W.P. 1985. Stratigraphy. In: EDWARDS, K.J. & WARREN, W.P (eds). The Quaternary History of Ireland, 18-37. Academic Press Inc. (London).

WATSON, D.F. and PHILIP, G.M. 1985. A refinement of inverse distance weighted interpolation. *Geo-Processing* **2**, 315-327.

WHITE, N. & LOVELL, B. 1997. Measuring the pulse of a plume from the sedimentary record. *Nature*, **387**, 888-891.

WHITE, R.S. 1988. A hot-spot model for early Tertiary volcanism in the N. Atlantic. In Early Tertiary Volcanism and the Opening of the NE Atlantic. In: MORTON, A.C. & PARSON, L.M. (Eds), *Geological Society Special Publication* No.**39**, 3-13.

WHITE, N., TATE, M. & CONROY, J.J. 1992. Lithospheric stretching in the Porcupine Basin, west of Ireland [abstract]. In: PARNELL, J. (ed), Basins on the Atlantic Seaboard: Petroleum Geology, Sedimentology and Basin Evolution. *Special Publication Geological Societry London,* No **62**, 327-331.

WHITTINGTON, R. J., CROKER, P. F., DOBSON, M. R. 1981. Aspects of the geology of the South Irish Sea. *Geological Journal*, **16**, 85-88.

WILKINSON, G.C., BAZLEY, R.A.B & BOULTER, M.C. 1980. The geology and palynology of the Oligocene Lough Neagh Clays, Northern Ireland. *Journal of the Geological Society, London,* **137**, 65-75.

WILLIAMS, B & BROWN, C. 1986. A model for the gensis of zinc-lead deposits in Ireland. In: ANDREW, C.J., CROWE, R.W.A., FINLAY, S., PENNELL, W.M. & PYRNE, J.F. (eds). Geology and genesis of mineral deposits in Ireland. *Irish Association Economic Geology*, Dublin, 579-590.

WILLS, L.J. 1951. A palaeogeographical atlas of the British Isles and adjacent parts of Europe. London and Glasgow.

WILSON, H.E. 1972. Regional geology of Northern Ireland. H.M.S.O., Belfast.

WILSON, H.E. & MANNING, P.I. 1978. Geology of the Causeway coast, *Geological Survey of Northern Ireland*, **v2**.

WOLF, R.A., FARLEY, K.A., SILVER, L.T. 1997. Assessment of (U-Th)/He thermochronometry: the low termperature history of the San Jacinto mountains, California. *Geology*, **25**, 65-68.

WOODCOCK, N H., FISCHER, M, 1986. Strike-slip duplexes. *Journal of Structural Geology*, **8**, 725-735.

WOODCOCK, N. H. & SCHUBERT, C. 1994. Continental strike-slip tectonics. In: HANCOCK, P.L. (ed), Continental deformation. 251-263.

WOODHAM, C.R. & BARtON, K.J. 1992. Developments in regional and reconnaissance geophysical techniques in exploration with reference to the Irish Midlands. The Irish Minerals Industry 1980-1990. 369-381.

WOODLAND, A.W. 1971. The Llambedr (Michras Farm) borehole. *Report of the Institute of Geological Sciences*, 71/18.

WYNE, A.B. 1857. On the Tertiary Clay and Liginite at Ballymacadam. *Report of the Bristish Association, Dublin*, 94-95.

YOUNG, D.G.G. 1965. Unpublished Ph.D. Dublin Institute for Advance Studies, Geophysics Section, 5 Merrion Square, Dublin.

YOUNG, A. 1972. Slopes. Oliver & Boyd, Edinburgh.

YOUNG, D.G.G. 1976. A geophysical interpretation of the structural development of the Kingscourt graben. *Proceedings of the Royal Irish Acadamy,* **76**, p43-52.

YOUNG, E.M., MYERS, A.T., MUNSON, E.L. & CLONKIN, N.M. 1969. Mineralogy and geochemistry of fluroapatite from Cerro de Mercado, Durango, Mexico. *US Geol. Surv. Prof. Pap.* **650-D**, 84-93.

ZIEGLER, P.A. 1982. Geological Atlas of Western and Central Europe. Shell Internationale Petroleum Maatschappij B.V.

ZIEGLER, P.A. 1987. Manx-Furness Basin. *Tectonophysics, **v137**, p389-440.*

ZIEGLER, P.A. 1989. Evolution of the Arctic-North Atlantic and the western Tethys. *American Association of Petroleum Geologists, Memoir*, **43**, 1-198.

ZIEGLER, P.A. 1989. Geodynamic model for Alpine intra-plate compressional deformation in Western and Central Europe. In: Cooper, M.A. & Williams, G.D. (eds). Inversion Tectonics. *Geological Society of London Special Publication* **No.44**, 63-85.